Fatigue prediction for strands and wire ropes in tension and bent over sheave wheel

by

Christian Wokem

A thesis submitted in partial fulfillment of the requirements for the degree of

Doctor of Philosophy

in

Structural Engineering

Department of Civil and Environmental Engineering
University of Alberta

ABSTRACT

Strands and wire ropes are widely used in many civil and mining engineering applications, such as encountered in cable stays for bridges, suspension bridge elements, mooring structures, cranes, ropes for shovels, draglines, and for elevators and mine shaft cages and skips. These ropes are broadly classified as stationary and running ropes depending on whether they are subjected to predominantly tensile loads or both tension and bending, over a sheave. The primary reason for failure in such strands and wire ropes subjected solely to tension are fretting fatigue scenarios, manifest as individual wires rubbing against each other as a load is cyclically applied. For strands and wire ropes also bent over sheaves, the failure is invariably identified at the top of the sheave where the rope comes into maximum contact with the sheave. To this date, research based prediction of fretting induced fatigue life reduction of strands and wire rope has partially but not wholly been investigated.

Feyrer (2007) performed milestone direction work in proposing regression models, established through regression coefficients, that could be used to calculate the anticipated fatigue life of strands and wire ropes for tension only, and tension plus bending over sheave specific configuration cases. The collection of regression coefficients established by Feyrer were limited to the cases he proposed, such that the current research here extends that knowledge base, through investigating the effect of sheave to rope diameter ratio, D/d, applied load, S, sheave contact length of rope, l, and sheave groove radius, r. These results were analyzed in a parametric study generating regression coefficients to permit additional strands and wire rope types not included in Feyrer`s original investigation. Specifically 7, 19, 91 and 92-wire strands in tension, independent wire rope core (IWRC) and 6×19 Seale-IWRC wire rope (usually called 6×19 Seale wire rope) in tension were analyzed, and subsequently their predicted cyclic tension fatigue life is obtained using a stress based approach. The behaviour of 7 and 19-wire ropes subjected to both tension and bending over sheaves fatigue were also investigated. In all cases investigated, S-N fatigue regression models were proposed. Since the stress based method used for fatigue life prediction is dependent on a stress concentration factor or stress correction factor, both prediction routes have been compared with subsequent recommendations for practical application. Finite element analysis of the strand or wire rope models yielded the stress concentration and correction factors necessary for the fatigue life prediction.

ACKNOWLEDGEMENTS

This research was funded by the National Sciences and Engineering Research Council of Canada. I appreciate the supervision, encouragement and financial support from my supervisors, Dr. G. Y. Grondin, Dr. Tim Joseph and Dr. Samer Adeeb. I am also grateful to the Faculty of Graduate Studies and Research, and the Department of Civil and Environmental engineering of the University of Alberta for the support given to me over several years. I sincerely appreciate the effort and support of the examining committee. I am also grateful to Dr. David S. Nobes for his advice and assistance in providing the SolidWorks software used in this research. The author is also grateful for the computing resources provided by Compute Canada (WestGrid).

I also extend my gratitude to my loving family, especially my wife, Nyema, and our twins (Gabriel and Michael) for being there for me through my program, and finally my sincere thanks goes to my friends, David Akinmoluwa, Nawaz and Jishnu Subedi for their friendly support.

TABLE OF CONTENTS

LIST OF TABLES

List of Figures

List of Symbols and nomenclatures

a_1 to a_5	Feyrer regression coefficient for cables in tension
b_1 to b_6	Feyrer regression coefficient for cables bent over sheave
$CF_{\text{int}.stress}$	Stress correction factor
C_s	Modification for size (diameter) of wire material
C_{sc}	Modification factor for stress concentration and notch sensitivity
C_{sf}	Modification factor for wire surface finish
d	Diameter of cable (strand or wire rope)
D/d	Diameter of sheave wheel to the diameter of cable
E	Modulus of elasticity of the material
K_t	Stress concentration factor
K_f	Fatigue notch factor
l	Length of the cable in contact with sheave
N	Fatigue life
N_e	Endurance limit for wire or cable
N_f	Fully reversed fatigue life for a single wire
N_{nom}	Fatigue life obtained using nominal stress concentration factor
$N_{\text{int}.stress}$	Fatigue life obtained using stress correction factor
m	$= r_{sh} / (r_{dh} \tan \alpha_{dh} \cos \alpha_{sh})$
r	Groove radius
r_{dh}	Double helix radius measured from the central wire rope axis
r_{sh}	Single helix strand radius measured from the central wire rope axis
S	Tensile force or load
S_a	Force or load amplitude
S_{amp}	Stress amplitude
S_f	fully reversed stress range for a single wire
S_e	Fatigue limit stress range for the cable

S_{eq}	Equivalent stress amplitude obtained using the Modified Goodman equation
S_{lower}	Mean force less the force amplitude
S_m	Mean stress
S_N	Stress amplitude for a fatigue life of N
$S_{\min}$	Minimum stress range
$S_{\max}$	Maximum stress range
S_{920}	Equivalent stress amplitude for a mean stress of 920 MPa
S_o	Fatigue limit stress range for single wire
S_r	Stress range for which fatigue life is desired
SCF_{nom}	Nominal stress concentration factor
R_0	Nominal tensile strength
q	Notch sensitivity factor
z	Number of wires in the cable
σ_{app}	Applied stress (Applied load divided by area)
α_{dh}	Double helix lay angle
α_{sh}	Single helix lay angle
σ_{mv}	Maximum von Mises stress
σ_{nom}	Nominal stress (Applied force or reaction force divided by the area)
θ	Free angle rotated about the rope axis
θ_{sh} , t	$= \theta_{sh0} + \theta$
θ_{sh0}	Single helix phase angle
θ_{dh}	$= \theta_{dh0} + m\theta_{sh}$
θ_{dh0}	Double helix phase angle
ρ	Characteristic length
$\sigma_{\text{int}.stress}$	Maximum wire axial stress
UTS	Ultimate tensile strength
IWRC	Independent wire rope core

BOS	Bent over sheave

CHAPTER 1

INTRODUCTION

1.1 GENERAL BACKGROUND

1.1.1 DEFINITIONS FOR TERMINOLOGIES USED FOR STRANDS AND WIRE ROPES

Wire ropes are used in many civil engineering structures such as bridges, mooring lines, elevators and others. They are also used in mine hoist equipment such as shaft systems draglines and electric rope shovels. The choice of using wire ropes is attributed to high axial strength, bending flexibility and redundancy, generated by the failure of one wire in a wire rope not necessarily leading to the failure of the entire wire rope system. Such an eventuality might be the case for elements such as chains, where failure of one link would lead to failure of the entire chain. Wire rope systems can be either static or dynamic. A typical example of a static stationary rope would be a cable stay used for a suspension bridge. Dynamic (running) ropes are those that run over pulleys or sheaves and are commonly used in both civil and mining hoist applications such as those encountered with rope shovels or cranes. Running ropes experience cyclic loads as they run over a sheave. The main concern with running ropes is the high degree of fretting and interaction between wires that make up the whole cable (wire rope or individual strands) arrangement, and the associated interaction between the cable and the sheave, compared to the experience with stationary cables.

Wire ropes are made of strands that are wrapped helically around a central strand to form a wire rope. Each of the individual strands that make up the wire rope has wires that are wrapped around a central wire to form a strand. The wind direction of the helical wires or strands determines whether the wire rope is a Regular or Lang lay. A Lang lay is developed when the wires in the strand and the strands themselves are laid in the same direction. A Regular or Ordinary lay is developed when the wires in the strand are in the opposite direction to the direction of the strands. The number of wires and their relationship to each other determine the construction of the strand or wire rope. For example, one of the simplest form of strands used today is the 1×7 strand (7-wire strand) this is the basic component strand of most cables, also

used as a prestressing strand. Figure 1-1 shows the cross section of a 7-wire strand. Correspondingly, a 1×19 (19-wire strand) describes a strand made up of 19 wires where the cross section of this strand arrangement is shown in Figure 1-2. Other strands such as the $1\times$ 37, 1×91 and 1×92 arrangements are formed by adding several layers of wires to the 7-wire strand. Figure 1-3 shows the cross section of the 6×7 wire rope, typically known as an independent wire rope core (IWRC), which has six strands with seven wires in each of these strands wrapped helically around a central strand with seven wires. Although wire rope may have a core made of different materials, only wire ropes with steel core will be investigated in this research. Figure 1-4 shows the 6×19 Seale wire rope which comprises a central IWRC and six strands of 19 wires each around the IWRC.

Wire ropes that run over sheaves are subjected to a significant amount of cyclic loading, which after time develops degradation of the wire rope due primarily to fretting fatigue, as both the wire rope runs over the sheave and due to wire-wire contact. Much research has been conducted on wire ropes, but research on running ropes has primarily been performed by manufacturers, where such findings remain proprietary and undisclosed through research dissemination.

1.1.2 WIRE MANUFACTURING PROCESS AND ITS PROPERTIES

Steel wires are made of high strength non-alloy carbon steel with carbon content between 0.4 and 0.95%. Other elements used in the manufacturing of such wires include Si at 0.1-0.3%, P and S at <0.035%, Mo at <0.05%, Mn at 0.5-0.8%, Cr at < 0.15%, Ni at < 0.2% , Cu at < 0.25% and Al at <0.01%. A patenting process (essentially a heating process) is used on the steel wires, prior to reduction in diameter by cold drawing (Feyrer, 2007). Before the steel wire strands or wire ropes are assembled, the wires are galvanized with zinc to protect against corrosion. It is pertinent to mention that, although corrosion fatigue can occur in cables, this phenomenon was not investigated, also the effect of methods of galvanising on the fatigue life was also not included in the current research The standard nominal strength of these wires has been reported by Feyrer (2007) at 1370 MPa to 2450 MPa.

1.1.3 TYPES OF TERMINATIONS OR SOCKETS

Wire rope and strand terminations will not be specifically investigated in this current research, but it is pertinent to provide some information on the types of termination typically used for cables in civil and mining applications. In all applications it is expected that failure of the termination, joint or connection should not occur, hence connections or terminations are designed for a high duty capacity, depending on function. Swaged or poured sockets are frequently used. Figure 1-5 shows a swaged termination, which is effected by squeezing the cable hydraulically into a pendent. A poured socket consist of placing the cable in the socket orifice and pouring molten epoxy resin or Zn-Cu alloy socketing material into the orifice to affix the cable and socket together. Papanikolas (1995) provides greater detail on the various types and performance of socketing materials.

1.2 STATEMENT OF PROBLEM

To date research on the fatigue of cables has focused on failure, terminations, stress-strain range and relationships, but little on the prediction of the fatigue life of strands and wire ropes under cyclic loading activity. Almost nothing is reported on the interaction between a sheave and cable.

Wire fracture in a cable is the most significant event in overall cable life. If the onset and progression to loss of functionality of the cable, as an expression of time, is known then preventive maintenance condition based monitoring strategies can be established to circumvent overall catastrophic failure of the cable system. A fatigue model was proposed by Feyrer (2007) for some strands and wire ropes subjected to cyclic tension and in bending over a sheave. Regression coefficients related to this model were presented by Feyrer for these strands and wire ropes. However, fatigue regression models or coefficients for typical strands in industrial use, such as the 7-wire and 19-wire strands were not investigated at that time by Feyrer (2007). The same was true for 6× 7 wire ropes, and 6× 19 Seale wire ropes with IWRC in cyclic tension fatigue.

The primary focus of the research encompassed in this thesis seeks to advance the work of Knapp (2004), Raoof (1990), Hobbs and Raoof (1996), and Feyrer (2007) to predict the fatigue life of strands and wire ropes subjected to tensile and bending loads through modeling;

by considering the behaviour of the constituent wires and strands. Verification of the models developed has been performed using the physical and previous modeling results of Raoof (1990) and others. The typical application of this research will be to predict the fatigue life of mining shovel hoist ropes, as used by the P&H 4100 BOSS ultra-class mining shovel, a schematic of which is illustrated in Figure 1-6.

There are two different types of wire ropes employed in such mining shovels (ignoring the variety of low load crowd mechanisms employed); suspension ropes, and hoist ropes. Suspension ropes do not run over sheaves and act as main stays supporting the weight of the boom and ground engaging attachments. Failure rarely occurs in such cables, as they are only subjected to incremental cyclic tensile loads. Failures more typically take place in the bending length of the hoist rope that runs off and on over the sheave wheel at the top of the boom. These ropes take the cyclic brunt of the digging effort impacted by both operational function and the geological resistance of the active mining face material being excavated.

1.3 OBJECTIVES AND SCOPE OF WORK

The objective of this research is to develop a design model to predict the fatigue behaviour of stands and wire ropes subjected to tension and bending over a sheave wheel, generating fatigue. The work will consider the range of parameters needed to describe the behaviour of a range of wires, strands and wire rope configurations.

The model developed will account for variations in parameters affecting the fatigue inducing tension and bending events experienced by the cable in contact with the sheave wheel for the life of a cable of set configuration. To achieve this goal, a stress based approach similar to that used by Raoof (1990), Hobbs and Raoof (1996), and Knapp (2004) that shows good correlation with experimental results will be used.

The key objectives targeted are:

1. Review of the current literature on cables subjected to static tension, cyclic tension fatigue, bending over sheave wheels fatigue, and also a review of previous research on prediction of the fatigue life of cables, failure of cables including terminations will be conducted.
2. Validate a stress based approach that was previously proposed by Raoof (1990), Hobbs and Raoof (1996), and Knapp (2004) for tension and bending over a sheave wheel

generating fatigue of cables. This will involve comparison with the predicted fatigue life and fatigue test results from different test programs reported in the literature.

3. Modify the former approach as seen appropriate.
4. Apply the validated modified approach to investigate the effect of diameter of strand or wire rope (d) and load or stress range on the fatigue life of 7, 19, 91 and 92-wire strands, IWRC and 6×19 Seale wire rope in cyclic tension. Implicitly, the effect of the lay length on the fatigue life of strands will be investigated.
5. Apply the validated modified approach to consider bending of cables over sheaves, investigating the effect of
    a. diameter of cable,
    b. diameter of sheave wheel to the diameter of the cable (D/d ratio),
    c. groove size, r ,
    d. load or stress amplitude, and
    e. the lay length and the bending length (l)

    on the fatigue life of a 7 and 19-wire strands.
6. The stress based approach for fatigue life prediction is complicated for design use, so by using the parametric study results obtained in the present research, multiple linear regression analysis will be carried out to obtain design regression coefficients based on the fatigue model proposed by Feyrer (2007) for cables in cyclic tension and bending over sheave.

    Figure 1-7 shows the flow chart for the methodology used in achieving the objective outlined above, as well as the scope of work covered.

1.4 THESIS ORGANISATION

In Chapter 2, the literature related to research on cables will be reviewed, with a focus on tension and bending of cables over sheave arrangements leading to fatigue.

In Chapter 3, the development of the user defined content required for the finite element models used in this research will be explained. This chapter will also include a comparison of the numerical strand stiffness and a theoretical or measured stiffness, and an explanation of the proposed stress based approach for the determination of the fatigue life for strands and wire ropes.

Chapter 4 will provide details of the finite element analysis results for strands and wire ropes subjected to tension only, and provide a discussion of the fatigue analysis results. The effect of parameters such as strand diameter, and strand or rope load on fatigue resistance will be investigated. Validations via statistical comparison between the literature reported fatigue test results and the modeled fatigue results developed here will be discussed. A regression analysis of the predicted fatigue life will be carried out, to establish regression coefficients that may then be applied to the Feyrer model for strands and wire ropes in tension.

The finite element results of strands in bending over sheaves will be discussed in Chapter 5. This will include a discussion of the multiple effects and impact of the diameter of sheave to the diameter of the cable, D/d ratio, bending length, groove size, lay length and load level on the overall fatigue life of the cable will be investigated using the stress results obtained from the finite element model used. Comparisons will be made between the literature reported fatigue test results and modeled fatigue analysis results discerned from the model outcomes. Incorporation of the effects of the targeted parameters investigated into the Feyrer's equation will be investigated in Chapter 5. Such parameters will be evaluated via the establishment of regression coefficients for the cables in combined tension and bending over a sheave.

The summary of the research conducted, conclusion and recommendations for future work are presented in Chapter 6.

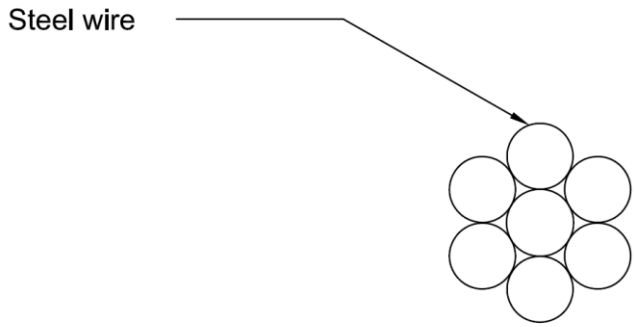

Figure 1-1: Cross section of a 7-wire strand

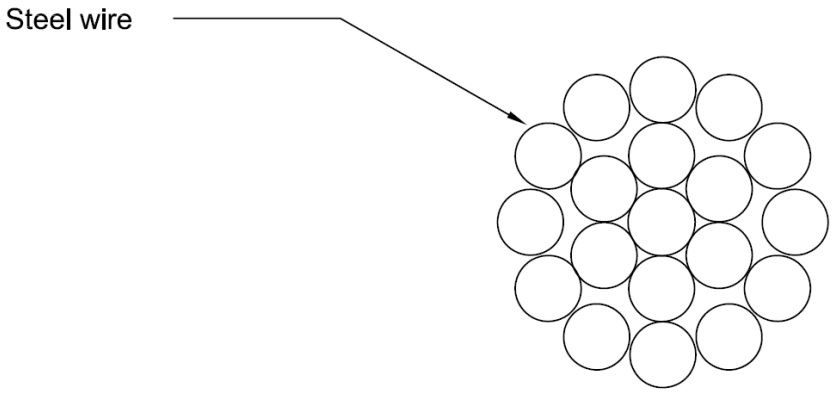

Figure 1-2: Cross section of a 19-wire strand

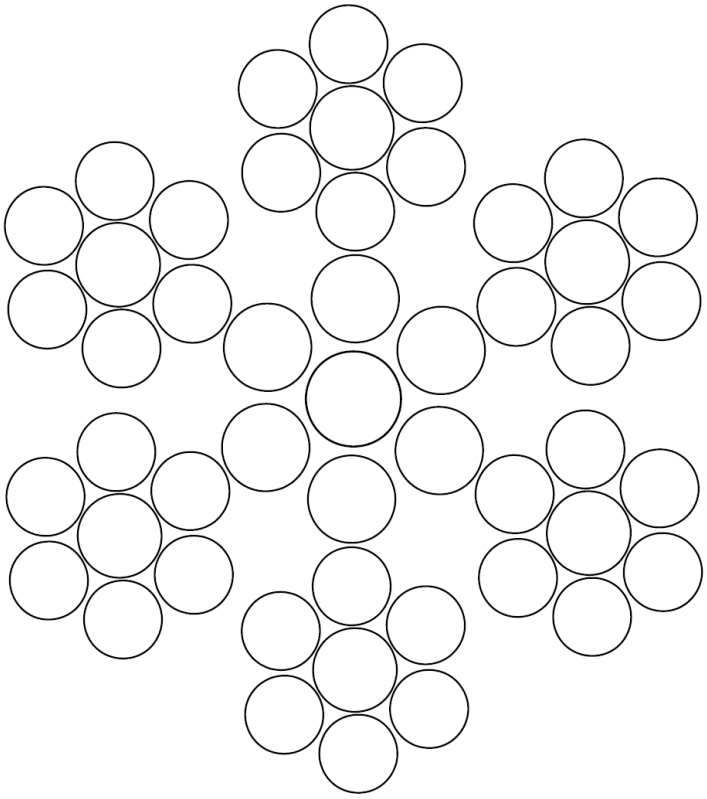

Figure 1-3: Cross section of an IWRC

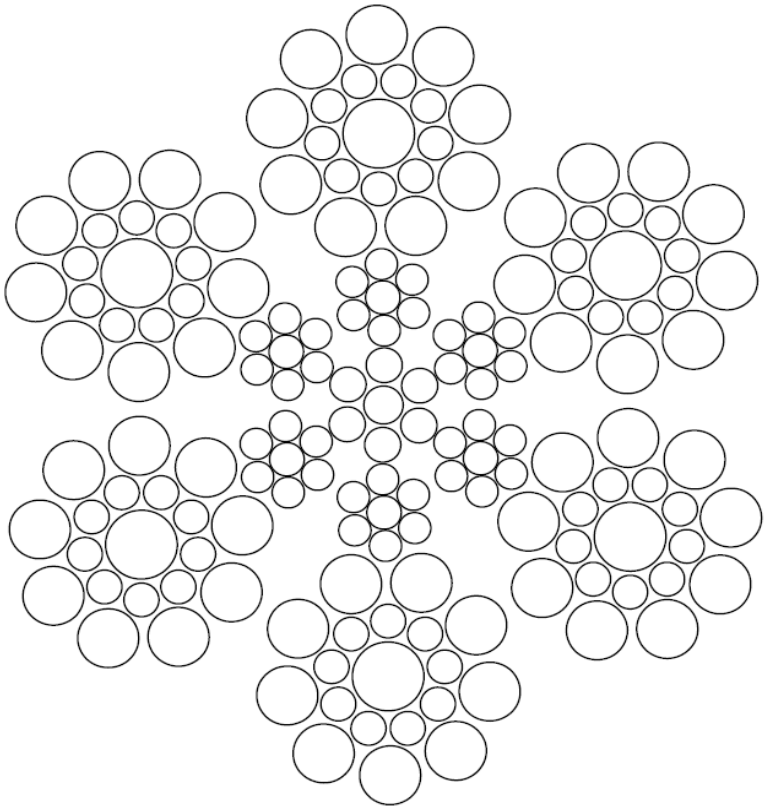

Figure 1-4: Cross section of a 6×19 Seale wire rope

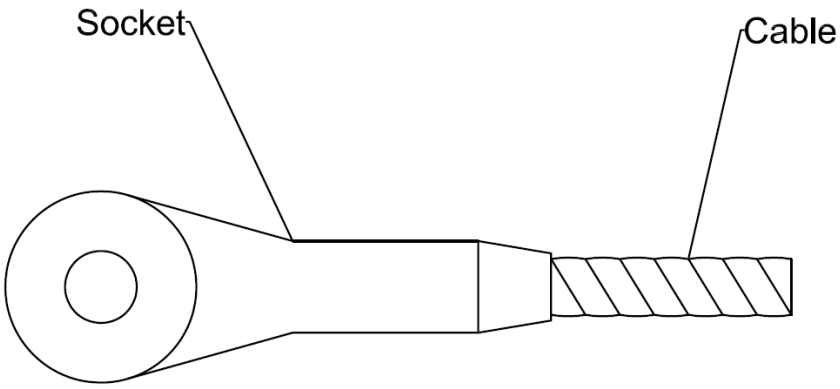

Figure 1-5: Swaged termination

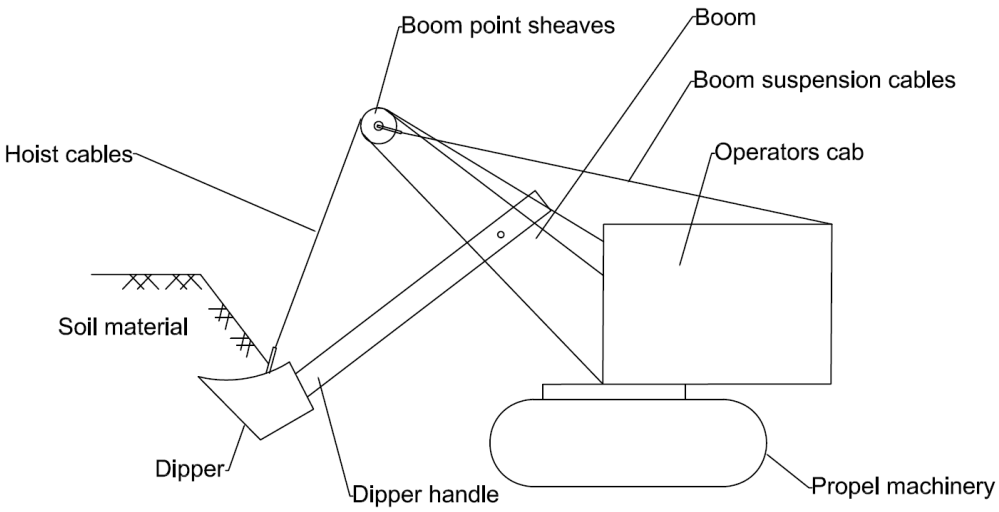

Figure 1-6: Schematics of a shovel showing hoist and suspension cables

CHAPTER 2

LITERATURE REVIEW

2.1 INTRODUCTION

Extensive research exists on the static behaviour of wire ropes, where such investigations have primarily focused on failure analyses of wire ropes subjected to tensile loads. The applications for these previously reported loading cases are considered primarily hoisting type applications in the absence of a sheave. These applications were simple scenarios such as employed in cable stay bridges and mooring lines, although it is recognized that some degree of bending and fatigue loading would be present.

The effect of parameters such as wire rope diameter, nominal wire rope strength and length of rope was primarily investigated by Feyrer (2007) amongst other researchers. The behaviour and fatigue resistance of wire rope is significantly affected when a rope is bent over a sheave, and compounded when subjected to cyclic loading as evident in the active hoist ropes used for mining draglines, rope shovels and construction cranes.

Little research has focused on finding a unified approach to predict the fatigue life of wire ropes subjected to cyclic tension and bending over a sheave. This chapter thus focuses on the research focused on these two areas.

2.2 TENSION BEHAVIOUR OF WIRES, STRANDS AND WIRE ROPES

2.2.1 TENSION BEHAVIOUR OF WIRES AND STRANDS

Zhang *et al*. (2003) investigated the effect of fretting wear on the fatigue life of individual steel wires used in hoisting rope application. They investigated the effect of contact forces and the wear mechanisms between steel wires. The steel wires used in their work were obtained from 6×19 ropes, where each wire was 1 mm in diameter. In order to simulate fretting, two wires were aligned at 90 degrees to each other. The tests were conducted at a frequency of 3.3 Hz and amplitude of 75 μm, where the contact force was varied from 14 N to 40 N. Fatigue tests were also conducted in a pull-pull loading mode, with tensions fluctuating between 200 and 1000 N at

a frequency of 9 Hz. They observed that as the contact force increases the friction coefficient between the wires decreases, but attained a stable value after the contact loads reach a certain value. They concluded that the wear depth depends on the contact stresses and the fretting time, and that both had a directly proportional relationship. Fretting wear notching was found to lead to stress concentrations and accelerated crack initiation, reducing fatigue resistance.

Thorpe and Rance (1983) studied the fatigue behaviour of zinc coated wires used to manufacture 40 mm diameter wire ropes, with individual wires of diameter ranging from 1.8 to 2.3 mm. Some of the wires were galvanised using a hot dip method, while others were galvanised by electro deposition. The experiments conducted involved four target criteria: corrosion, fatigue in air, fretting fatigue and corrosion fatigue. The effectiveness of the zinc coating was validated by immersing single wires in natural seawater at 5 to 10 ^{o}C for 6 months. The wires were then examined for corrosion impacts. All wires were tension tested before and after immersion. They did not observe any visual signs of corrosion but some zinc coating was lost, evaluated by measuring the remaining thickness of the coating. They also did not observe any deterioration in the mechanical properties of the wire after it was removed from the seawater. Fatigue testing in air was carried out on the wires galvanised using the two methods outlined above. The frequency of the fatigue testing was set at 4 Hz, and the mean tensile stress set at 915 MPa or 366 MPa (representative of 50 or 20% of UTS, respectively). The ends of the wires were cast into cylindrical blocks of cold setting epoxy resin with carbon fibre added to minimize epoxy cracking during testing. They observed that fatigue endurance strongly depended on stress range, but the mean stress had a negligible effect on the endurance. Electro galvanised wires were shown to exhibit slightly longer life. Corrosion-fatigue testing was carried out in almost the same manner as described previously, but the gauge length of the wire was surrounded by a Perspex cell, through which seawater at 5 to 10 ^{o}C was permitted to flow. Two loading frequencies were evaluated at 4 Hz and 0.1 Hz, for both types of galvanised wire tested. Additional tests were carried out at low frequencies on bare ungalvanized wires and with wires subjected to half the thickness of galvanized coating. They observed that, the fatigue endurance of a fully coated, hot-dipped wire during corrosion-fatigue was lower than fatigue in air, and that the corrosion-fatigue endurance decreased with increasing mean stress and decreasing test frequency. A decrease in fatigue life was observed when the thickness of the zinc coating was reduced by half at a loading frequency of 0.1 Hz. The bare ungalvanized wire showed a decrease

in the fatigue life at higher stress ranges. The fatigue endurance of electro galvanised and hot-dipped galvanized wires were seen to be similar. They investigated fretting fatigue using a scale physical simulation, in which one vertical wire was placed in contact with two horizontal wires. The fretting fatigue test was carried out in air at 4 Hz, on each of fully coated, hot-dipped and electro galvanised wires. It was concluded that the action of fretting had the most negative effect on the fatigue life of wires compared to all other imposed conditions.

Cappa (1988) examined accumulated wire strain for undamaged and damaged steel strands subjected to tensile loads. The effect of severing a number of external wires on a strand on the developed strain in a wire rope, subjected to static and quasi-static loading was examined experimentally. A 7-wire strand was cut from a new piece of rope and examined. The wires in the strand were seen to be bright and unlubricated, and had external wires with a diameter of 3.0 mm and internal wires with diameter 3.2 mm. The equivalent overall diameter was measured as 9.2 mm. The Lay length was for the assembly was measured at 136 mm for an overall length of sample of 1258 mm. The tensile static breaking load for the sample was recorded at 71.2 kN The strands were loaded and unloaded about 100 times prior to commencing the tests. Measurements were taken at six static load levels up to a load of 29.4 kN, with readings taken at 20 minute intervals for each load level. Their test was repeated 10 times. Strain results measured via 6 independent strain gauges showed unequal load sharing between nominal identical wires, which decreased with increase in applied quasi-static loads from 0 to 29.4 kN. Comparing the results of the quasi-static to the static loading conditions, they observed that in the quasi-static case unequal load sharing was increased. It also observed that for nominally identical wires that the load sharing between wires was not related to the wire position. For a test repeated with a severed wire it was concluded that the higher strained wires are not the ones closest to the interrupted severed unit.

Raoof (1990a) carried out a series of axial and torsional tests on newly manufactured 41 mm strands as a comparison to the behaviour of an older established 39 mm strands (fully ‘bedded-in’). The 41 mm strand had three layers with 24, 18 and 12 wires in the first, second and third layers, respectively. Within the innermost third layer, a central core comprising a single straight wire surrounded by six helical wires was present. The lay types were LH, RH and LH for the first, second and third layers, respectively. He concluded that newly manufactured strands

may need a very long time to become fully ‘bedded-in’ and stable, such that within this period there is a change in hysteresis behaviour. They also suggested that, before the strand became fully ‘bedded-in’ any results obtained from hysteresis measurements could not be considered representative of the behaviour of a strand in long term service. In older fully ‘bedded-in’ specimens, a fluctuating load did not cause a substantial increase in cable hysteresis. Raoof also noted that the torsional and full-slip axial stiffness are not sensitive to time in service or ‘bedding-in’ state. They also suggested that the strains in the free length of the cable and at the sockets were not significantly different.

Utting and Jones (1985) investigated the tensile behaviour of a seven-wire strand. An instrument that measured both strand extension and rotation simultaneously was used, with a strain gauge load cell used to monitor the tensile load and torque. Five strands with seven wire construction were used in their work. Strands I, II and III were cut from the same length, having lay lengths of 115 mm, and core wires with helical wire diameters of 3.94 and 3.73 mm, respectively. The wire had a minimum breaking stress of 1.77 GPa. The wires were ‘bright’ and not lubricated. Strand IV was cut from a different length of rope but having the same construction as the other strands described previously. Strand V comprised of seven galvanized wires and all the wires were lubricated. The core wire diameter and the helical wire diameter were 3.91 mm and 3.73 mm, respectively. Strand V did not have the wire grade specified. Polyester based resin with silica filling was chosen for securing the strands in the socketing arrangements. The test machine used had a limited test length of 527 mm. Strain gauges were attached at common comparable locations of the five sample strands tested. The resulting strain measurements showed that the helical wires share load unequally, particularly when close to the end grips. It was noticed that as the load increased, most of the failures took place at the end grips by pulling the wires from the epoxy and socket. Other samples had complete fracture of all wires in the strands and hence these researchers suggested that further termination techniques should be investigated.

Llorca *et al*. (1989) presented a model for analysis of the fatigue behaviour of a strand or cable, where they assumed that the behaviour can be derived from the behaviour of individual wires using fracture mechanics. The results of their model were compared with dynamic tests on wires and ropes. The cable (strand) sizes compared were 12.7 mm and 15.2 mm, where the wires

had diameters of 3, 5, and 7 mm. The free length between grips for the wires and the ropes tested were between 600 and 960 mm, and the loading test frequency was set between 4 and 15 Hz. They applied a sinusoidal load to specimens between 60% and 70% of the actual strength of the specimen for the first series; and if after 2×10^6 cycles no rupture had occurred then the maximum load is increased to 80% of its strength until fracture testing was continued. The second series of tests were done between 70 and 80% of the actual strength; the minimum load was reduced to 60% of the strength, if no rupture occurred after 2×10^6 cycles. Epoxy resin mortar was used for socketing. After testing, they observed the fracture surfaces of the wires in a profile projector to obtain the geometry of the crack that ultimately led to the final rupture, in some cases the surfaces were observed with scanning electron microscope. They concluded that (i) the fatigue life for thinner wires is shorter than that of thicker wires, but the same endurance limit was observed for both sizes; and that (ii) the spin angle below 20^o had negligible effect on the fatigue behaviour, and fatigue life decreases with increasing spin angle.

Hobbs and Smith (1983) investigated the effect of stress fluctuation on the safe working life of socketed cable systems. They examined the influence of fatigue loading on guy insulators. A series of in-line fluctuating tension tests were conducted on a 16 mm diameter strands with 19 wires. A standard Amsler tensile testing machine with a 50-tonne capacity was used to test these strands at constant amplitude loading. The length of the specimens was set at 740 mm. Two batches of 6 specimens were tested, with most testing performed at 4.4 Hz except for some at lower amplitudes where the frequency was increased to 8.8 Hz to save testing time. A smaller number of tests were conducted on much longer 38 mm strand specimens (92 wire semi-balanced constructions). These were carried out to investigate extrapolating the behaviour of large diameter strands predicted from smaller diameter strands at a loading frequency of 4.4 Hz, where in-line test lengths were set at 6 m and transverse test lengths at 8.5 m. The sockets for these tests were filled with zinc metal. Amongst other findings, they found that fatigue failure of socketed cables occurs in the socket interface for both in-line (axial) and transverse fluctuating (flexural) loading conditions. In the in-line test, the fatigue life seemed to be independent of the mean value of tension applied. A pull out of the strands from the sockets occurred for cases in which the socket jaw fractured. Hobbs and Smith proposed a method to evaluate fatigue performance of 38 mm compared to other diameter cables, but stated that further tests on other cable sizes needed to be carried out before such methods would be confidently acceptable.

Papanikolas (1995) investigated the fatigue behaviour of multilayered strands in tension only. The strands investigated were a 19 and 91-wire strand configuration with diameters of 25 and 45 mm respectively. Papanikolas studied the effect of stress range, strand make-up and the length to diameter ratio on fatigue life. Fatigue tests were conducted on both types of strand and the stress range and strand make-up were found to have significant impact on fatigue life. From fractographic inspection of some specimens it was concluded that wire fracture was due to fretting fatigue. Fatigue S-N curves was proposed for both types of strand.

Fisher and Viest (1961) presented S-N curves based on fatigue testing of 18 specimens on suspension bridge materials of 3/8 inch diameter prestressing strands. Their test was conducted in conjunction with AASHO, leading to a linear plot of the logarithm of fatigue life versus minimum stress or the stress range, which generated a mathematical model. 120 test results on 7/16 inch diameter prestressing strands were presented by Warner and Hulsbos (1966), consisting of 69 constant cycle tests and 51 cumulative damage tests. For the 69 constant cycle tests, premature failure of the termination took place in the strand weldment.

Cullimore (1972) conducted several tests on 15.2 mm diameter prestressing strands, while studying hangers for suspension bridges. A total of 59 specimens were tested, with a mean stress of 550 MPa, and a stress range as low as 220 MPa. He concluded that an endurance limit does not exist for the stress levels investigated when the strand life is less than 10 million cycles. Muller and Zeller (1975) continued this work and presented the results of 41 fatigue tests on 12.4 mm and 15.2 mm prestressing strands, where the specimens were tested at different stress levels.

Paulson *et al*. (1983) investigated the fatigue behaviour of prestressing strands. They carried out fatigue tests on 11.1 mm (Grade 250) diameter prestressing strands. The strands were tested using two stress ranges, to 326.1 or 465.4 MPa. They also presented previous fatigue test results from Fisher and Viest (1961), Muller and Zeller (1975), Cullimore (1972), and Warner and Hulsbos (1966); and other researchers who had conducted tests on different ASTM A416 prestressing strands; to generate a single S-N curve. The diameter of the ASTM A416 prestressing strands that were used were 9.5, 11.1, 12.7 and 15.2 mm.

Heller (2003) investigated the fatigue response of prestressing concrete beams and fatigue tests were conducted on 7-wire ASTM A416 prestressing strands with diameters of

12.7 mm; where the minimum tensile strength was 1860 MPa. The effect of stress range was investigated. The fatigue behaviour was found to be similar to that of Paulson *et al.* (1983), with their test results falling within the S-N data reported by Paulson *et al*. (1983).

2.2.2 TENSION BEHAVIOUR OF WIRE ROPES

Suh and Chang (2000) conducted fatigue tests on steel cables to investigate the axial fatigue behaviour of wire ropes used as hangers for suspension bridges. The wire rope construction investigated was 6×19 with IWRC, Warrington, RHO, and zinc coated. The rope had a diameter and cross-sectional area of 12.75 mm and 78 mm^2, respectively, and the test specimen lay length was 88.8 mm. The nominal tensile strength and actual breaking strength for the wire ropes were 1572 MPa and 122.6 MPa, respectively. An initial overload of 80% of the rope's ultimate tensile strength (UTS) was applied to affix the specimen to the socket. The frequency of the testing was set at 2.5 Hz to 4 Hz. They reported that the locations of wire break were distributed between the free length and the anchor point of the wire rope and mostly in the outer wires of the outer strands. The failure criterion used in these tests was a 10% loss in stiffness. Suh and Chang investigated the effect of specimen length, mean stress and stress range. They observed that the fatigue life increases with increase in specimen length, although they suspected that the shorter life observed in shorter specimens might have been due to the effect of terminations, and hence they recommended further investigation to confirm this trend. They observed that as the mean stress increased, the fatigue life decreased especially at a mean stress of 65% of UTS, even though this was not very significant for a mean stress of 15 to 40% of UTS. As they expected, the stress range was found to be the most significant parameter affecting fatigue life.

Evans *et al*. 2001 investigated the effect of cyclic tension loading on the load transfer length (defined as the length from a break point where the load is carried in full); measured via local strain measured close to the breaking point. They did not know where the breaking points will occur; so the strain gauges were distributed uniformly along the specimen length. They extended the investigation to the variation in load transfer length comparing ordinary and Lang's lay rope configurations. The effect of individual wire breakage on the stress shedding to other wires within the same cross section was also investigated. They investigated two rope

constructions: a 19mm Seale 6×19 (9/9/1) RHO rope with IWRC, and an equivalent right-hand Lang lay rope. They kept the length of the rope constant at 1.1m, and the ropes were instrumented with 12 strain gauges to monitor the strain in the outer wires as a function of the wire rope load. All fatigue tests were conducted at a load range of 10 to 25% of the rope tensile breaking strength at a frequency of 0.8 Hz. Resin sockets were used to terminate the rope specimens. The tests conducted on ordinary lay ropes indicated that a rope with a broken wire takes up its complete load creating a transfer length at about two rope lay lengths from the break point immediately after the break occurs and extends to 3 rope lay lengths after 20,000 cycles. They attributed this behaviour to inter-wire slippage under cyclic loading. For the Lang lay rope, it was seen that the transfer length occurred at one lay length from the breakage. They concluded that the difference observed between the two ropes were due to the greater inter-layer forces in the Lang lay rope. Wire breakage effectively caused a decrease in strain in the wires on the opposite side of the rope; this was attributed to localized bending of the rope resulting from wire breakage. However, only external wire breaks were observed using the strain gauges and no knowledge was discerned concerning wires within the cross section structure.

Casey and Waters (1988) carried out tensile fatigue tests on three sizes of steel wire rope to investigate the change in stiffness and transfer length, where stiffness values were obtained from plots of load and test machine crosshead displacement. A 6×41 wire ropes, comprising of 6×7 IWRC at three sizes; 40, 70, and 127 mm diameter ropes with test lengths of 3.75, 3.6, and 7 m, respectively, were tested. The minimum breaking strength was noted at 1.01 MN, 3.30 MN, and 9.71 MN, respectively as specified by the manufacturer. The ropes were sinusoidal loaded to 20 ± 15% of the manufacturer's minimum breaking load, at a frequency of 0.3 Hz, chosen to avoid overheating of the largest 127 mm rope during testing. Prior to testing each specimen was loaded statically to a maximum fatigue load five times. Plots of load and crosshead displacement during static loading to maximum fatigue loading were obtained by interrupting the fatigue test. The rope had silica-filled polyester resin inside steel cylindrical sockets used for its termination. It was shown by these authors that, by a plot of stiffness versus elongation there is a relationship between the point at which stiffness starts to decrease and rope endurance, identified at 25 to 35% of the rope life, where wire breaks were considered the explanation for a change in rope stiffness. They also found out that outer strand breakage occurs late in the life of a rope subjected to tensile fatigue, as sections taken from ropes that failed prematurely provided no visual

evidence of wire breakage in outer strands. They concluded that an accurate indication of the overall condition of the rope cannot be known by visual examination of ropes only. IWRC breakage was suspected to be a viable explanation for this kind of failure mechanism.

Casey *et al*. (1988) evaluated wire breaks in a 40 mm diameter rope using an acoustic emission wire break detector. The ropes were of 6×41 construction surrounding an IWRC of 7× 7 strand construction. The length of each specimen of 3.75 m, and each rope had end terminations consisting of steel cylindrical sockets with silica-filled polyester resin. They conducted axial fatigue testing in a 1 MN testing machine. Out of 12 specimen tested, seven of the ropes failed either due to rope unwinding as a result of rotation at the terminations or at one of the terminations, four failed away from the ends, and one specimen was tested to a high endurance and so the test was stopped. Their major finding was that wire breaks start at the IWRC, and that the outer strand starts to accumulate wire breaks at later stages of the wire rope life.

Casey and Lee (1989) described the degradation of large diameter six strand wire ropes subjected to constant amplitude tension fatigue. The wire ropes investigated were a 6 × 41 with a diameter of 40 mm and 70 mm, and a 6 × 49 with a diameter of 127 mm also having an ordinary lay and 6× 7 IWRC with a Lang lay. Considering contact as either being continuous or discrete, they described that for a 40 mm diameter rope specimen, majority of wire breaks took place in the IWRC. These wire breaks were shown to have an effect on the stiffness, hysteresis and elongation. They observed that for a 40mm diameter rope at the early stages of rope life deterioration, elongation and stiffness were found to initially increase with a corresponding decrease in hysteresis; this was followed by the stiffness and hysteresis remaining unchanged while elongation increased. At about 50% of rope life the stiffness then started to decrease and the hysteresis increased, and this trend continued until 15% of the rope life remained. At that point the properties changed relationship such that elongation and hysteresis in the wire rope increased while the stiffness decreased, maintaining this trend until failure. They suggested that the change in stiffness and hysteresis that occurred at approximately 50% of the rope life was as a result of fracture of wires in the IWRC. Final rupture of outer wires was observed at 85% of the fatigue life.

Hanzawa *et al*. (1981) used a wire-breakage detection system to investigate the factors that influence the tensile fatigue strength of 50 mm wire ropes. The fatigue performance of socketing polyester, Zn/Cu or epoxy resin material was also investigated. One specimen had a length of 1810 mm; two specimens had lengths of 800 mm, while all others had lengths of 700 mm. The fatigue life was defined as complete when wire breakage rates reached 5%.They observed that the larger the diameter, the greater the fatigue strength, and that the fatigue strength of large diameter wire ropes can be evaluated from the information from 50 mm wire ropes. They showed that the fatigue strength decreases with the wire ability to rotate, and increases with an increase in wire diameter and wire strength. Fatigue wire breakage was observed to occur in the outer strands and inner/core strands at low and high stress ranges respectively. Epoxy resins were concluded by the researchers to be the best socketing material. Zn/Cu was shown to be unsatisfactory.

Smith *et al*. (1978) reviewed the effect of periodic overloads and salt water on the endurance of wire ropes investigated by the Naval Research Laboratory. Their work comprised of two pendants in parallel connected by load equalizing gussets. Each pendant had an eye splice at both ends formed around galvanized steel thimbles. They used an electro-hydraulic mechanical testing machine loading to 89 kN in a closed-loop, applied sinusoidally with a stress ratio (R) close to zero, at a loading frequency of 1 Hz. Six types of wire rope were investigated. Type A Rope (6×19 IWRC, IPS, right regular lay (RRL)) tested, had a diameter of 6.4 mm, an overload of 62% of the breaking strength was applied at 43% and 24% of service loading respectively. These tests produced a recorded overload ratio of 1.44 and 2.60, respectively, where a decrease in wire breakage was observed. For Type B Rope (Aircraft Rescue Hoist, 19×7 IWRC, SS) of diameter 4.8 mm tested at load levels of 25%, 50% and 75% were applied to effect partial damage studies. They observed that when wire-break density was plotted versus decreasing applied load proportion, a peak was observed at 50% load level. A plot of breakage density and static breaking load versus percentage endurance showed that wire breakage is insignificant up to 50% of rope life. The results indicated a relationship between number of breaks and the remaining static breaking strength. Any scatter in the data was deemed likely to be due to the weakness of the eye splice. For Types C, D, E, and F Ropes of 6.4 mm diameter; where ropes C, D, E, and F were respectively 6×19 IWRC IPS, 6×7 FC Iron, 6×19 FC IPS, and 6×19 IWRC EIPS, all four ropes were RRL. Plots of break density versus load fraction were

plotted generating different peaks. No breaks were observed in the soft iron rope. For all tests performed, loading was conducted for 5000 cycles at a 30% load factor. Varying endurance was observed for different overload ratios. An overload ratio of 2.5 times the base load (75% of ultimate) seems to have a beneficial effect on the endurance of higher strength ropes, attributed to a peak overload ratio initiating yield in the rope. The iron rope yielding was found to occur at a ratio of 1.5 times 30% of the base load or 45% of the ultimate load. They concluded that there is an increase in fatigue life of a wire rope with an increase in overload, until yielding commences, and then any beneficial effect of overload begins to decrease. An increase in fatigue life was attributed due to a combination of two processes: crack growth retardation and readjustment of stresses due to changes in contact points between wires. By introducing an aqueous 3.5% solution of sodium chloride with Type A ropes, it was observed that a decrease in endurance in salt water was insignificant compared to that in air, but more dependent on load cycle and duration. Under a scanning electron microscope evaluation, it was observed that there were portions of the wires showing evidence of fretting. It was also observed that wire breaks were not significant until 50% of the rope life was used up, and that failure of individual wires occurred as a result of subcritical fatigue crack growth.

Stonesifer and Smith (1979) continued the research of the Smith *et al.* (1978) on 4.8 mm diameter wire rope pendants. They focused on the effect of an initial overload or periodic overload on the fatigue life of a wire rope, performing tests on galvanized steel wire rope pendants with eye splice pendants at both ends. The length of the free rope between compression sleeves was 0.44 m. A cyclic load of 89 kN closed-loop was applied in a sinusoidal load-time pattern at frequency of 1 to 5 Hz. It was noted from the earlier work (Smith *et al.,* 1978) that for one type of rope, most wire break-up occurs after 50% of the wire rope life has been expended. It was also observed that a relationship between break density and static breaking strength of fatigue damaged ropes exists. Consequently, they loaded two specimens for a predetermined number of cycles at a load level less than the expected life to investigate this phenomenon, where on stopping the test a wire count was performed in one specimen, while the other one was tested to destruction in tension. They concluded that only using wire break count is not the best as a sole replacement criterion. This evaluation was extended to include the effect of applying a mean load, to which it was concluded that overloading generally increases the fatigue life of a wire rope, where the maximum life is attained by repeated periodic overloads that are large enough to

cause yielding of the rope. They suggested that this loading had both the benefits of lower compliance (higher stiffness) and maximum crack retardation, and that a single initial overload applied to a pendant was expressed as being almost as beneficial as periodic overloads and may be more practical. They also concluded that increasing the mean load was observed to increase the fatigue life to a maximum up to the ultimate tensile strength, but working-in a new pendant at lower loads has no advantage in increasing cyclic tension fatigue life.

2.2.3 PREVIOUS WORK ON TENSION FATIGUE LIFE PREDICTION FOR STRANDS AND WIRE ROPES

Using a regression analysis applied to previous fatigue tests on strands, Feyrer (2007) developed a fatigue prediction model from the investigations of other researchers via the effect of tensile strength on the fatigue life of wire ropes. Feyrer (2007) proposed an empirical model that predicts fatigue life of strands subjected to tension as shown in Equation 2-1, written in a slightly different form:

$$LogN = a_0 + a_1 \log \frac{2S_a}{d^2} + a_2 \frac{S_{lower}}{d^2} + a_3 \left(\frac{S_{lower}}{d^2} \right)^2 + a_4 \log d \qquad (2\text{-}1)$$

where, S_a is the force amplitude in Newtons (N), S_{lower} is the mean force minus the force amplitude in Newtons, d is the strand or wire rope diameter in mm, and a_i are regression coefficients. N is the number of cycles experienced to strand or wire rope breakage. For strands and wire rope in tension, taking into account the number of wires, Feyrer (2007) proposed the following equation; again the model was written in a slightly different form:

$$LogN = a_0 + a_1 \log \frac{2S_a}{d^2} + a_2 \frac{S_{lower}}{d^2} + a_3 \left(\frac{S_{lower}}{d^2} \right)^2 + a_4 \log d + a_5 \log z \qquad (2\text{-}2)$$

where, z is the number of wires in the strand. Regression coefficients for Equation 2-2 were obtained for spiral strands with 37 to 292 wires and strand diameters ranging from 4 to 127 mm.

Knapp (1987) proposed a model that predicts the fatigue life of cables under fluctuating axial tension. In this model the contact stress obtained analytically, was taken to behave like a

notch permitting a stress concentration factor to be obtained. The endurance stress was computed using the Goodman equation (Stephens *et al*., 2001), to obtain the failure stress and fatigue life.

Raoof (1990) also looked at the prediction of fatigue life for multilayered strands in tension only. In his work a stress based approach was used to estimate the fatigue life of 19, 92 and 139 wire strands having diameters of 16.4, 39 and 51 mm, respectively. The method involved obtaining stress concentration factors using an analytical approach and then using this stress concentration factor, and fatigue test stress results for single wires, evaluate the fatigue life of strands via adjusting the S-N relationship for a single wire.

Wang *et al*. (2013) used a finite element method to investigate the state of stress and strain in a multi layered 6×19 wire rope with 19 wire strands in 3 layers. The behaviour of a strand in tension was compared to Costello's theory (Costello, 1997) with good correlation. Fretting fatigue behaviour of the wires was investigated by studying the evolution of wear and models were proposed for estimating the crack growth in a cable solely under tension.

2.3 BENDING BEHAVIOUR OF STRANDS AND WIRE ROPES

2.3.1 BENDING BEHAVIOUR OF STRANDS

Feyrer (1981a) and Feyrer (1981b) focused his studies on alternating bending in a 16 mm diameter rope over a sheave of 400 mm diameter. The tension applied on the wire rope at 30. 42, and 60 kN, generated a bending zone of 22.5^{o} (360 mm), a contact angle of 165^{o} within a groove radius of 8.5 mm. Tests were carried out on standard ropes with fibre inserts and parallel lay ropes; divided into 6- and 8-strand standard ropes and 8- and 9-strand non-standard ropes. One group with a 6-stranded Warrington-Seale rope and other parallel ropes were also tested. Fracture of at least one strand was taken at the end of a bending test, where a bend reversal was considered to be the process of transitioning from a straight configuration into a bend and back into a straight configuration. Feyrer's work was completely statistical which concluded that the number of bending reversals sustained by wire ropes follows a normal logarithmic distribution, and that the dispersion in such a distribution is relatively small when only one rope construction is repeatedly tested. For several rope constructions the dispersion was larger. Feyrer also observed that in all cases Lang lay ropes exhibited longer service life than ordinary lay ropes,

where ropes containing 8 strands performed better in terms of service life than ropes with 6 strands. They also observed that as long as the same tensile stress was applied to a rope with a steel or fibre insert under bending, the fibre insert configuration would have a longer service life. However if the diameter of the wire ropes tested was the same, subjected to the same tension, then the service life would be approximately the same. Considerations such as construction would create a difference as a function of tension applied.

2.3.2 BENDING BEHAVIOUR OF WIRE ROPES

Gorbatov *et al*. (2007) conducted flexure fatigue strength tests on wire ropes. The two wire ropes tested had a diameter of 16 mm and the same construction (Warrington Seale 6×36 steel wire ropes). However the wire ropes differed by core design: One had an E-1 oil-impregnated hemp core and the other an ASKM-impregnated jute core. They observed that the ASKM-impregnated jute core developed a longer service life of higher quality than the E-1 oil-impregnated hemp core.

Waters (1985) mainly presented a review of work performed on large diameter wire ropes in bending over sheaves (BOS) fatigue testing. The study presented a plot of load range as a percentage of breaking load versus the number of cycles to failure in direct tension fatigue, from tests conducted by other researchers, and a plot of bending pressure ratio versus number of cycles to failure from a series of BOS fatigue tests for different diameters of steel wire ropes, also conducted by other researchers. It was shown that it was difficult to predict fatigue performance of large diameter wire ropes from smaller diameter ropes. The theoretical assessment of the performance of a wire rope was concluded as complex.

Ridge *et al*. (2001) evaluated the influence of manner of rope degradation and impaired quality on fatigue endurance of wire ropes subjected to a repeated bending at constant tension, with prediction of fatigue endurance using such experimental results. Two rope constructions were tested, namely (i) a 6×25F (12/6+6F/1) + IWRC 6(6/1) with right hand lay (RHL) and 1960 MPa wire grade, and (ii) a 34×7 with Left regular lay (LR) deformed multistrand (16/6+6/6) with wire steel core (WSC) and 1960 MPa wire grade. Ultimate breaking load (UBL) and bending fatigue performance was measured for these new ropes, followed by quality impairment BOS fatigue testing under artificially induced degradation. Specimens had constant

bending lengths of 150 mm, described as the length which ran on and off the sheave. Each test had a D/d ratio of 18, a constant rope tension of 20% UBL, a frequency of cycling at 0.097 Hz and a sample length of 1.7 m established with cast resin cone sockets. The artificially induced degradation and impairments introduced into the specimens were:

1. External wire breaks within the bending zone introduced to the 6 strand Lang lay rope and internal wire breaks introduced to multi-strand wire ropes.
2. Abrasion wear introduced by grinding to simulate running rope applications.
3. Plastic wear caused by sliding during contact with the sheave
4. Corrosion introduced by opening the wires and degreasing to produce a stiffer wire.
5. Slack wires or strands.
6. Torsional imbalance.

They observed that under BOS fatigue, the endurance of the ropes were minor, indicating that the type of damage did not affect the endurance of the wire rope as much as the D/d ratio, which they suggested, is due to wire curvature. Feyrer's equation was used to predict the endurance of these ropes, where the difference between the predicted and test results were about 61% for the 6×25F wire rope, and 5% for the 34×7 wire rope.

Fatigue testing of a 109 mm diameter (large diameter) wire rope was carried out by Vennemann *et al*. (2008). The wire rope was subjected to tensile loads ranging from 50 to 330 tonnes (i.e. loads up to 33% of MBL at 1000 tonnes). NDT magnetic flux tests were frequently carried out during fatigue testing to obtain information about the wire rope deterioration over its life. The wire ropes used in these bending fatigue tests were low torque multi-strand ropes having either compacted or uncompacted strands, where in both cases the lengths of the specimens were 11.75 m. The wire ropes pass over sheaves of diameter 2200 mm with a D/d ratio of 20. Single cycles were established within 8 to 20 second periods. ISO 4309 discard criteria was used which indicated that the wire rope must be discarded when the number of visible broken wires exceeds 2 over a rope length of 6d or if the number of broken wires is more than 4 over 30d., Testing proceeded until significant rope elongation due to increased wire failures was detected or it became clear that one or more strands were broken and the wire rope became imbalanced. Water cooling was applied to the bend zones of some test specimens, while others did not have such cooling. They observed that, 1) most wire failures occur internally, with

little visible damage on the rope surface, 2) Magnetic flux or any NDT should be used with the ISO 4309 discard criteria, 3) High temperature could result in a reduction in wire rope life and application of active cooling to wire ropes can increase the lifetime of these wire ropes by 50%.

Urchegui *et al*. (2008) identified predominant wear patterns for polymer-covered stranded rope and wear evolution as fatigue life proceeded. They also analysed the effect of sheave size on the wearing of ropes. Three different wear patterns were identified for the rope: 1) "Linear wear scars", which they identified was "due to the contact of the central wire of strands with wires in the inner layer and the contacts of adjacent wires within the same layer", 2) "Nick type A", which they defined as "wear scars caused by inter-strand point contacts due to interaction of the wires of the outer layer of strands with wires of the outer layer of the core", and 3) "Nick type B", which they defined as "wear scars caused by inter-strand point contacts due to the interaction with the outer layer of adjacent strands". The 7×19 strand steel wire rope was covered with a polymeric sheath and had minimum breaking load of 22.5 kN. The metallic part of the rope was 5.0 mm and the total diameter including the cover was 6.5 mm. flash brass-plated wires were used and had diameters between 0.22 to 0.45 mm. Warrington right lay strand was the core, with the rope outer layer consisting of 6 Seale strands wrapped around the core in a right regular lay pattern. The wires had a tensile strength that was over 2,800 MPa and was made of cold-drawn eutectoid carbon steel (0.8% C). A 200 mm diameter traction sheave was used for the test, and the 200mm tension sheave applied a tensile load of 3 kN. Three different sheave sizes were used, 200 mm (D/d of 40), 150 mm (D/d of 30), and 100 mm (D/d of 20). The ropes tested were subjected to a velocity of 3.2 m/s at a wrap angle of 180 degrees. They observed that the most severe wear pattern experienced corresponded to Nick-Type A with a maximum scar depth of 40μm, and Nick-Type B at 23 μm. They expected that Nick Type B would have produced the most severe wear state, and suggested that due to the presence of the polymeric cover, contact was prevented for some time and delayed the formation of Nick-type B. They also observed that reduction in D/d ratio from 40 to 30 doubled the volumetric wear rate, and a reduction in D/d from 40 to 20 caused a 2200% increase in volumetric wear rate. The wear pattern in all cases was measured via planimetric wear and wear scar depth, the latter described by the authors as "the maximum difference between the worn profile and the profile of a new

wire along its axis", and the former was defined as "the area enclosed between the new and worn profiles", determined numerically.

Giglio and Manes (2005) applied a number of analytical formulations to estimate the state of stress for inner and external wires of a rope. This was compared with experimental data defining modulus of elasticity, fatigue and rope bending states. A MIL-W-83140 specification type I wire rope was tested which had 19×7 stainless steel. The diameter of the rope was 4.76 mm. It consisted of a core of seven strands of seven wires each, and had a left Lang laid configuration. The outer layer had 12 strands of seven wires each, and this had a right regular lay configuration. Using MTS 10 kN electro-mechanical machine, three tests were conducted on three lengths without terminals. The three specimens were; 1) core strand, 2) core strand with the first layer of strands and 3) the entire rope consisting of one core strand and two layers of strands. Modulus of elasticity was determined at a maximum load of 20% of ultimate tensile load using thimble terminations, since this was used to measure loss of strength. A pulsating cyclic traction test with loads varying from 1330 N to 2660 N was used for the whole wire rope, representing a hoist cycle. The other two specimens had a pulsating load which was calculated from an analytical model of axial load. Strains were obtained via an extensometer mounted on the specimens and hence Young's modulus can be obtained from the cyclic stress-strain plot. To estimate the ultimate tensile strength of the material (obtained at about an average of 1714 MPa) static tests were carried out on single wires. A comparison was made for the modulus of elasticity obtained from the analytical program and the cyclic traction test, with the three specimens, having Young's moduli of 149,630, 76,810 and 74,700 MPa, respectively. The wire material had a Young's modulus of 159,300 MPa. It was evident from their model, which had assumed no friction between the wires and small displacements, that high oscillation angles greater than 35^{o} to 40^{o} may cause premature inner and non visible failures. 28^{o} of oscillation was established as the limit of alternating bending fatigue. Fatigue limit stress amplitude of 285 MPa divided by the maximum Von Mises stress in the external strand for 28^{o} alternate bending fatigue was recommended as the design coefficient by the authors.

Ridge *et al*. (2000) presented strain gauge measurements of cyclic bending strain in wires of a six strand steel wire rope with right-handed Lang's lay construction running on and off a pulley. The test consists of two samples, both made from the same coil of rope; a 6 strand rope

with RHL and IWRC of construction 6×25 F. The rope diameter used is 19 mm. It had outer strand diameter of 6.2 mm and outer strand outer wire diameter of 1.2 mm. The lay angle of each strand was 25^{o} and a rope lay length 125 mm. An ultimate breaking load of 273 kN was measured, for a sample length of 1.7 m. A total of ten strain gauges were mounted on the test sample. Rope test loads were applied to 20% of ultimate breaking load for tests cycled at a test frequency of 0.097 Hz. The terminations were made of cast polyester with 70% talc powder filling. They observed that the test on the first sample ended with the rope failing at 82,577 cycles. One cycle defined as straight-bent-straight. Only one strain gauge remained intact to the rope failure. In the second test, they observed that three gauges survived to failure. In monitoring cyclic bending strain as a function of time, they observed that the strain developed a characteristic peak value as the rope contacted and then left the pulley. They also observed that the amplitude of these peaks had a significant impact on the bending fatigue endurance of a rope. They suggested that these peaks may be due to a local reaction to shear forces associated with the changing moment as the rope approached the pulley. Lubrication and wire sliding movements were considered the reason for small fluctuations in waveforms. Some of their conclusions were that, degradation and imperfection had limited effect on the fatigue life in cyclic bending. They observed that the predicted cyclic strains were consistent with the measured cyclic bending strains. That also the cyclic strain amplitude is highly dependent on the diameter ratio of the pulleys to wires, axial position of the wires with regards to the bending motion, and the relative location of the wire in the rope.

Chen and Gage (1981) qualified the degree of improved endurance for wire ropes reacting with nylon sheaves compared to steel sheaves in a lifting device. The wire rope specimen was obtained from a single 305 m spool of 3/4 inch 6×25 FW PRF RRL EIPS IWRC wire rope. The ultimate tensile strength of three specimens averaged 290 kN. Nylon sheaves were monomer cast anionic polymerized caprolactam, while steel sheaves were machined and hardened. The sheave – rope pitch diameters used were 18/1 and 24/1 with rope grooves and a contact angle of 140^{o}. Cast nylon and a steel sheave were simultaneously installed at each end of the test machine for comparison. The load applied used design factors of 10, 5, and 3.5 for the 24/1 sheave ratio and 3.5 for the 18/1 sheave ratio. They stopped the test at defined periods for evaluation of wear, deformation and wire breaks until a replacement point was established, at a stress level of 10% of the rope breaking strength where 6 strands were retired from the steel

sheave contact and one from the nylon sheave contact. At 20% breaking strength, 5 and 2 ropes were retired from steel and nylon sheave contacts respectively. At 28.6% breaking strength, the same observation was obtained at both ratios. At 10%, 20%, and 28.6 % breaking strength for D/d ratios of 24 and 18, the wire rope endurance life for the nylon sheave interaction was recorded as 4.5, 2.2, 1.9, and 1.3 times that for the steel sheave interaction respectively. Chen and Gage (1981) observed more scatter in the plot for the steel sheave interactions. Using a stress factor and fatigue factor they were able to establish the remaining strength of a rope, where the degree of stress in a wire rope decreases as the sheave ratio and the design factor increases. Tests were considered complete when a combined total of seven ropes were removed from both sheave interaction sides. The ropes in removal were subjected to tensile tests to failure to determine the remaining strength. Visible breaks were classified as crown break and tangential break due to rope/sheave and strand/strand contacts respectively. The lack of abrasion and improved rope support they observed was considered to have reduced the incidents of crown break in the nylon sheave.

Giglio and Manes (2003) completed bending fatigue tests for cyclic free swinging motions over guide sheaves, evaluating angular wrap variation below which rope damage would not occur. Mil-W-83140 Type I, 19×7 stainless, preformed, non-rotating wire rope was used for the tests. The core of the rope consisted of seven strands of seven wires each, and the outer layer of the rope having 12 strands of seven wires each. The inner core was a left lang lay, while the outer layer was a regular right lay. The wire rope had a diameter of 4.76 mm, and a length of 1000 mm. Fatigue testing were also carried out on parts of the ropes that was close to the terminal; to observe the effect of angular variation developed rotation imposed on the rope terminals by the support, and thereby on the fatigue life. An applied preload of 98.1 N was used and a test frequency of 0.5 Hz to a maximum angular variation of 180 degrees. The failure condition was assessed at complete breakage of an entire strand on the outer surface of the rope, per the UNI ISO 4309 standard, performed by visual inspection. Little temperature increase due to overheating as a result of the test frequency was observed. Giglio and Manes (2003) confirmed that when a rope is allowed to swing when wrapped around sheave wheels, damage of the rope can occur where the fatigue life increases with reduction in test angle. Below 28^{o} no damage is expected to take place in the rope.

Nabijou and Hobbs (1994) focused on investigating whether a change in sheave size, generating D/d ratios between 12 and 20, and the ratio of rope breaking load to the working load, generally referred to as the factor of safety, SF, will drastically affect the fatigue life of a wire rope. Wire rope diameters of 28 mm and 35 mm for a 6×36 construction rope were tested in a rig consisting of a sheave and jack frame assembly. The sheave frame transmitted a lateral pull to 1 MN. The failure criteria used in this study were based on ISO 3601 which states that failure has occurred when the number of broken wires equals to 5% of the total number of outer wires in a rope of length five times the rope diameter. Nabijou and Hobbs (1994) concluded that the fatigue life decreased with a decrease in D/d ratio and an increase in line tension, The IWRC rope tested displayed a better fatigue performance than the FC (Fibre core) wire rope tested. The comparison of IWRC wire ropes indicated that the smaller the diameter, the more resilient the fatigue life within the stress range considered. Nabijou and Hobbs (1994) also observed that galvanizing seriously reduced the fatigue life within the stress range studied. The effect of microscopic details on the sheave surface was observed to affect fatigue performance. Foreign contaminant soil particles such as sand and mud were seen to reduce fatigue performance, where frequent re-lubrication and cleaning actions were recommended under severe operating conditions.

Feyrer (1981c) studied the effect of bending length on the fatigue life of a wire rope. He described the bending length as the length of the wire rope that is subjected to bending and as this length becomes larger; there is an increased probability of failure in the stressed portion. Feyrer (1981c) considered both fatigue tests carried out on a wire and on a wire rope. For the wire, of diameter 0.75 mm, the test was performed in a crank-driven testing machine, where the wire moved to and fro over a pulley of diameter 115.75 mm. The maximum bending and tensile stresses were 1300 and 400 MPa respectively, reaching a breaking strength of 1701 MPa (nominal strength 1570 MPa) for a bending length of 192 mm. Overall, Feyrer (1981c) carried out 13 bending tests, leading to a lognormal distribution plot of the percentage of broken wires versus endurance. For the wire rope test, the diameter of the sheave used, D, was 250 mm with a groove radius of 5.3 mm; and the diameter of the rope, d, was10 mm, The lubricated Seale rope had a (8×19+FEN, DIN 3062, ordinary lay) fibre core with a mean effective breaking strength of 1561 MPa and a nominal strength of 1370 MPa. The 13 fatigue tests were performed with bending lengths of 450 mm. Again, a lognormal distribution was obtained between the

percentage rope breakage and the number of bending cycles; where it was observed that an increase in bending length increases the probability of failure in the stressed portion.

Krause and Neumann (1984) investigated the effect of parameters such as lubrication and sheave construction material on the fatigue life of wire ropes. A test rig was designed with the goal of investigating the effect of lateral deflection angle on the fatigue life of wire ropes. Using a steel sheave, tests at a frequency of eight bending reversals per minute with a deflection angle of 4^o caused an inertia temperature of 33.4^oC. While using a PVC-coated sheave at a deflection angle of 0^o degrees generated a temperature of 39.8^oC at an ambient temperature of 21.4^oC. Krause and Neumann (1984) specified that the temperature should be limited to 50^oC. In investigating the effect of varying deflection angle, a 6×36 Warrington-Seale parallel constructed rope was used for the tests. This rope also had fibre inserts, was 200 m long, but only tested 60 m of the length, with a nominal tensile strength of 1770 MPa. The rope of diameter 20 to 34 mm, used for the tests, was made up of five different sized wires. The sheave diameters used ranged from 450 to 900 mm. The rope traction force was varied from 0 to 100 kN at a speed varied from 0 to 1.66 m/s with deflection angles from 0 to 12^o, and a constant stroke length of 2.5 m. The test length of the rope was 1500 mm. The resultant plots generated by Krause and Neumann (1984) showed an increase in the number of fractures as the deflection angle increased; indicating a rope replacement decision length of 30d.

Research on the effect of sheave diameter, D, to the diameter of a wire rope, d, via the ratio D/d, as a function of the tensile stress on fatigue life dates back to the early 1940s. Drucker and Tachau (1945) developed a factor called the dimensionless bearing-pressure variable, $B = 2T/UdD$, which relates the load, T, ultimate tensile strength, U, sheave diameter, D, and cable diameter, d, to the fatigue life of 6×19 and 6×37 ordinary lay ropes. Drucker and Tachau (1945) observed that as B decreases, the number of bends to failure increases. The effect of sheave diameter and rope tensile stress on a 16 mm, 6×19+1H construction lang lay rope was investigated by Müller (1961), who observed that the working life (bending reversals to failure) increased with D/d ratio and decreased with an increase in rope tensile stress. Müller (1961) investigated D/d ratios varying from 7.3 to 59.3 and tensile stresses up to 980.7 MPa. Chen and Gage (1981) investigated the effect of D/d ratios of 18 and 24, although primarily targeting the impact of quality of improvement using nylon versus steel sheaves. They observed that the stress

level in the wire rope was reduced by increasing the D/d ratio. Nabijou and Hobbs (1994) considered D/d ratios from 12 to 20, witnessing a decrease in fatigue life of the wire rope with a decrease in D/d ratio. Urchegui *et al*. (2008) observed wear evolution as a function of the fatigue life of a wire rope being expended for D/d ratios of 40, 30 and 20. They observed that a reduction in D/d ratio increases the volumetric wear, leading to a shorter fatigue life. Costello (1997) also reported the same trend between fatigue life and D/d ratios of 20 to 30.

Müller (1961) carried out bending tests on wire ropes with bending lengths (defined as the contact length between the sheave and the cable) from 20 to 350 mm for a sheave diameter of 400 mm (30d). The fatigue life was seen to remain initially constant, but the working life rose gradually as the bending length becomes smaller than the lay length. Feyrer (1981b) also studied the effect of bending length on fatigue life, observing that an increase in the bending length increases the chance of failure. Feyrer (2007) also presented results of fatigue tests with bending lengths up to 1000d.

The effect of the angle of wrap, also termed the angle of contact, that is the angle made by the hoist rope directly in contact with the sheave, was investigated by Scoble (1930) and Müller (1961). Both observed the same trends although with different rope constructions, diameters, and under different applied tensile stress. They observed that as the contact angle became smaller than 10^{o}, the fatigue life increased dramatically. They explained this as due to the contact angle reduction essentially produces a minimal bending stress, decreasing fatigue life with angle of wrap between about 10^{o} and 30^{o}, but increasing fatigue life with an angle of wrap from 30^{o} to 50^{o}. Finally, they observed that the fatigue life remains constant up to 180^{o}.

Wiek (1973) obtained stress curve for two wire ropes bent over sheaves using strain gauge attached to the wire ropes, showing that wire ropes that have broken wires can still carry loads beyond one lay length.

2.3.3 PREVIOUS WORK ON BENDING FATIGUE LIFE PREDICTION FOR STRANDS AND WIRE ROPES

Only a small handful of research has focused on the prediction of fatigue life of wire ropes subjected to bending over sheaves.

The most important physical parameters that affect the fatigue resistance of wire ropes were identified by Feyrer (2007) as the D/d ratio and the rope tensile force. He investigated the tensile force as a function of the square of the diameter, S/d^2, where values ranged from 20 to 540 MPa for D/d ratios of 10 to 63.

For wire ropes in bending over sheaves, Feyrer (2007) proposed the following relationship:

$$LogN = b_0 + \left(b_1 + b_4 Log\frac{D}{d}\right)\left[\log\left(\frac{S}{d^2}\right) - 0.4\log\left(\frac{R_0}{1770}\right)\right] + b_2\log\frac{D}{d} + b_3\log d + \frac{1}{b_5 + \log\frac{l}{d}} \tag{2-3}$$

where, R_0 is the nominal tensile strength of the wire rope in MPa and l is the bending length in mm. Regression coefficients b_i, were obtained for equation 2-3 for 8×19 Seale wire ropes with fibre core (FC) and IWRC, 8×19 Warrington wire ropes with FC and IWRC, $8\times(19+6F)$ Filler with FC and IWRC, and finally, 8×36 Warrington Seale wire ropes with FC and IWRC. Feyrer's equation corrected the fatigue life prediction obtained using Equation 2-3 for impacts such as rope lubrication, rope constructions of 8 strands or 6 strands, sheave groove radius, and side deflections.

Onur and Imrak (2012) investigated the fatigue life of a 6×36 Warrington Seale wire rope with IWRC and right regular lay. They investigated the effect of the load and sheave size on the fatigue life of the wire rope, concluding that the fatigue life decreases with smaller sheaves and higher tensile loads. In their work they proposed some alternative regression coefficients for Feyrer's model to predict the fatigue life of the 6×36 Warrington Seale wire rope, which they observed to give better prediction of the performance than the original Feyrer's equation, and had a difference in the predicted and test results of about 46%, for that particular type of wire rope.

Knapp (1988) also proposed a theory to predict the state of stress in a helical wire bent into a circular arc using simplifying assumptions and their results were compared with experimental results of bending and shear stresses and they obtained good predictions. A

theoretical model for state of wire stress for helical strands in bending in multi-layered and axially preloaded spiral strands was proposed by Raoof and Huang (1992).

Knapp (2004) discussed tension and bending fatigue modeling of cables by computing the stress components acting on individual helical wires and comparing these stresses to crossed-wire stresses developed between wire layers. The stress concentration in the cables was taken as an equivalent notch and it was used to obtain the fatigue life via a stress based approach. CableFATIG software was used to compute fatigue life, yielding promising results when compared with test results.

Sasaki *et al*. (2007) estimated the fatigue life of wire ropes by assuming that the fatigue life of the wire rope may be obtained from the fretting fatigue life of the individual wires that make up the rope. A model of the wire rope was created using finite element analysis and the contact pressures obtained. Using a relationship between the stress amplitude, contact force, and the fretting fatigue life obtained via fretting tests on wires, the fatigue life of the wire rope was estimated.

Jiang (2012) investigated the stress behaviour of a 7-wire strand, 11.4 mm diameter wire rope subjected to ending. Finite element analysis showed behaviour was identical to Costello's theory for a strand subjected to bending.

2.4 FAILURE AND DAMAGE RESEARCH ON STRANDS AND WIRE ROPES

Casey *et al.* (1985) described equipment used for detecting failure of wires in investigating12mm diameter rope. Denison-Mayes and Shenck testing machines were used to establish initial load and the ensuing cyclic loading experiments, with a Hitachi VC-6041 digital storage oscilloscope recording transducer signals at galvanised wire breakage. The ropes tested were 500 mm and 150 mm length 6×7 (6/1) + 1×7 (6/1) steel core construction, with a breaking load of 95 kN. Initial load and fatigue tests were carried out on short specimens, while breakage tests were performed on longer specimens. Three principal tests were conducted using signal analysis: 1) Single wires with small notches loaded to failure, where the transducer was positioned adjacent to the notch; 2) 20 notches introduced to outer wires, with the ropes then loaded to failure of a single wire, then the load was removed and repeated; 3) Rope specimens

tested between 20 and 70 kN at a frequency of 1.2 Hz, where for wire break detection, 2 sub-sets of tests a) where each was designed to determine whether only a single wire break was detected, with no other noise effect. For these tests, 16 notches were introduced into outer wires, with the rope reloaded until failure of the notched wires prior to load removal. A good correlation between number of events and number of wire breaks became evident; permitting Casey *et al.* (1985) to conclude that the set-up was suitable for detecting failure of the wires, such that noise sources may be eliminated via threshold settings for the instruments.

Yeung and Walton (1986) described an acceptable accelerated testing procedure for wire ropes using block testing. They discussed cumulative damage theories, such as Miner's law which displayed shortcomings such as linear damage accumulation. Yeung and Walton (1986) acknowledged that there are two methods to predict fatigue life under variable amplitude loading conditions: 1) by using cumulative damage theory, and 2) using variable-amplitude load testing in a laboratory, simulating conditions that represent service damage conditions. They evaluated variable-amplitude testing as either approached by random-load or block testing. Random-load testing may be carried out in a servo-controlled fatigue testing machine, through service recorded stress signal or randomised signal input. Block testing however can be directly used to verify Miner's law and also to predict the endurance of wire ropes under random loading. For block testing blocks (typically 6 to10) of constant maximum load plateaus were used to replace the load history. Yeung and Walton (1986) discussed the beneficial effect of high overloads and means of accelerating tests via a) increasing test speed with 2 Hz as an upper frequency limit to obtain valid results, or b) by testing at increasingly higher stress levels followed by extrapolation to reduce to service stresses. The latter (b) approach displayed problems in validating such extrapolations to effect a reduction in testing time, as condensed blocks with smaller numbers of load reversals may introduce errors while editing the stress history. The final approach adopted by Yeung and Walton (1986) to reduce test duration was the omission of low stress and high cycle events, given that it was assumed that low stress level contribute little to the fatigue damage.

Casey (1988) described control and data acquisition systems for monitoring changes in rope response properties as a fatigue test proceeds. Stiffness, cyclic displacement, hysteresis and elongation may be measured via load - extension data. A stiffness hysteresis plot shows that the

stiffness initially increases as a rope "beds-in" followed quickly by a hysteresis reduction, thereafter stiffness drops with hysteresis increase, marking the degradation process. Casey (1988) noted that cyclic displacement increases rapidly as the rope beds-in and rope length increases to the onset of failure.

Edward (1988) used a simulator which applied a progressively increasing tensile load to 100 kN onto a Crosby socket mounted sample housed in a salt spray cabinet constructed to ASTM B117. Samples of 0.9 m length and 25 mm diameter were tested; with the first test conducted to failure and subsequent tests carried out for shorter durations to identify the residual breaking strength. Visual examination of wires, and lubrication level through mechanical testing was noted. The Dyform 17 ropes loaded to 75% of SWL experienced failure at 229 000 cycles. At about 180,000 cycles strength loss accelerated with rapid deterioration to failure at about 215,000 cycles, with fatigue failure predominating in the inner wires and core. Fretting corrosion was noted to be less than that experienced in service. A ratio of residual breaking load divided by minimum breaking load was plotted versus service life, establishing a pair of linear regression lines for both samples that failed and those that did not fail. A comparison made between galvanised and non-galvanised ropes showed that newly galvanised ropes have greater performance than ungalvanised ropes, degrading to a lesser extent.

Hansel and Oleksy (1986) presented fatigue testing performed to obtain a relationship between calculated stress in a rope and the number of bending cycles, while considering the sources and characteristics of partial stress in a rope, based on the work of other authors. Plots of reduced stress versus fatigue life, maximum bending stress versus bending diameter, maximum stress versus fatigue life, and maximum bending stress versus angle of lap, permitted the influence of wire diameter on rope safe operating life, influence of carbon content on fatigue life and the relationship between fatigue life and wire diameter to be considered. They found that, fatigue life decreases with increasing wire diameter and an increase in carbon content was seen to effect an improvement in fatigue life.

Kuruppu *et al*. (2000) presented loss of metallic area (LMA) determined by the geometry of wearing surfaces via a loss in wire mass. This was related to a loss in breaking strength of the wire rope. The focus of this study was on abrasive wear but not plastic wear. Worn-out discarded

wire ropes were acquired from a mine drum winder at a Western Australian gold mine. The rope was made of 6 triangular flattened 6×19 fiber core strands, with a nominal diameter of 32 mm. The nominal diameter of the outer and inner strand wires were 3.35 and 0.98 mm, respectively. A core of 3 strands had wires with nominal diameter of 1.04 mm. The rope had nominal metallic cross-sectional area of 425.5 mm^2. 12 rope samples of different wear states were cut, including portions with significant wear at the drum end. Corrosion was considered insignificant. The loss of metallic area (LMA) was measured using callipers to give 1) the wear chord where it intersects imaginary lines parallel to the axis of the rope, describing a width of wear, U1; 2) chord length of worn wires U2, 3) geometry of the wire at mid section, U3, plus 4) Loss of mass of the outer wires, LM. Linear regression equations were obtained for the relationship between loss of breaking strength, LBS and each of the measured values estimating LMA.

de Silva and Fong (2002) investigated cases were external abrasive wear was introduced into a 6-strand steel wire rope, where the effect of such wear on the tensile strength of the wire rope was examined against several wear based discard criteria. They tested steel wire rope 6×37 (1-6-12-18) RRL/ IWRC with a diameter of 10 mm. Each rope had 6 strands with 37 wires each with 18 wires in the outer most layer, followed by 12 and 6 wires in the next 2 layers. The grade of the steel wire was 1960 MPa with an actual breaking load of 6750 kgf. To introduce wear, each rope sample was held in tension and rotated slowly in a lathe, while a file was moved against the outer surface to cause wear over a length of 1.5 lay lengths. The strain rate applied in a universal testing machine was set at 5 mm/min. Resin compounds secured the two ends of the rope, with an effective gauge length of 0.6 m. The samples of wire rope tested were worn by 1%, 3%, and 5% of the nominal diameter of the wire rope. For each wear extent a large number of measurements such as the maximum depth of flat (reduction in the outer wire diameter) and reduction in steel cross section were recorded. They observed that the specified breaking strength of the wire rope was always higher than the actual breaking strength, as the specified breaking strength may not account for geometric irregularities. Tensile strength versus percentage reduction in rope diameter, loss in outer wire thickness, maximum width of flat, and percentage loss in steel area was recorded for a 15% drop in tensile strength. The most indicative parameter reflected the degree of abrasive wear was shown to be the reduction in outer wire diameter, comparable with a previously suggested 33% reduction in depth of outer wires by the UK National Coal Board (NCB) indicating discard. The maximum width of external flat produced on

the outer wires by abrasive wear was used as a convenient practical assessment of the extent of reduction in tensile strength of the wire rope, given that width measurement could be performed accurately. They reported on actual wear in the field of a 38 mm diameter rope with right hand lang's lay and fibre core, such that when the percentage decrease in breaking strength was plotted versus percentage reduction in depth of outer wires for both lab measured and field data, two significant drops were evident. The first drop occurred at 12% reduction in outer wire diameter, corresponding to the onset of failure of outer wires for a service rope to meet the BS 302:1987 reverse bend test requirement, and for inner wires to meet a torsion test requirement to the same standard. The second drop represented the point where the touching of the outer wires circumferentially ceases and a reduction in outer wire diameter exceeds 50%, leading to rapid accumulation of damage.

The effect of degradation type and wear on the endurance of a wire rope has initiated parallel research activities. Ridge *et al*. (2001) evaluated the effect of various degradation processes and impaired quality on the fatigue resistance of wire ropes subjected to bending fatigue over sheaves. Plastic and abrasive wear, corrosion, wire breaks, slack strands or wires, and torsional imbalance were all investigated. They found that any degradation or damage had a similar effect on fatigue life and that the D/d ratio was the physical parameter that had the most influence on fatigue life.

Argatov *et al*. (2011) studied wear evolution using Archard's wear law based on mathematical models of fretting wear between contacting wires. This was applied to previous experimental work carried out by Urchegui *et al*. (2008) and the effect of mean and contact pressures on fretting wear of thin steel wires studied by Cruzado *et al*. (2010). Argatov *et al*. (2011) observed that for higher loads a high coefficient of wear was evident, permitting a relationship between normal force, stroke and the wear to be established. Cruzado *et al*. (2011) also investigated the effect of wire - sheave crossing angles on fretting wear of steel wires. Two scenarios were studied: the first was a variation in crossing angle while the load was held constant, and the second was the influence of crossing angle at constant pressure. In the first scenario, the contact pressure reduced with a decrease in crossing angle and hence less wear developed giving rise to a longer fatigue life. In the second scenario it was found that the fatigue life remained unchanged as the crossing angle was varied.

Velinsky and Schmidt (1988) considered a wire rope as a collection of wires helically arranged, such that equations of equilibrium were applied for bending and twisting assuming the wires to be thin rods. Constitutive relations where formulated based on wire-to-wire and wire-to-sheave contact wear, permitting them to conclude that stiffness is not a good measure of the condition of a rope, primarily as axial stiffness of the rope can increase as wearing ensues.

Cable terminations was not the subject of this work, but one of such work that discusses about the selection, inspection and replacement of various types of terminations used in cable application is by Metcalf and Matanzo (1980). They performed some testing on several termination types to evaluate their effectiveness.

2.5 SUMMARY

Research on the fatigue state of wire ropes have focused on, stress and strain, fatigue testing, failure and damage investigations, and terminations. Studies on the prediction of the fatigue life of strands and wire ropes subjected to tension and bending over sheaves is limited. Feyrer (2007) model appears to be the most comprehensive approach to the onset of the research reported in this thesis, where Feyrer (2007) used regression coefficients to calculate the fatigue life of a number of strands and wire ropes. Feyrer's model does not report regression coefficients for all strands and wire ropes, especially those widely used by hoisting dominated mining equipment in the surface mining industry. For example; the fatigue behaviour of 7-wire and 19-wire strands in tension and bending was not investigated by Feyrer (2007). Also the tension fatigue behaviour of IWRC and 6×19 Seale wire ropes with IWRC were not included in the Feyrer's regression analysis. The stress based approaches proposed by Raoof (1990) and Knapp (2004) appear to be comprehensive approaches for predicting fatigue life, but have short comings associated with complex analytical computations. One outstanding consideration with little study as yet performed is an evaluation of the number of cycles to cause outer wires to break. This period in the life of a wire rope is of great significance since it dictates the time between targeted inspection and maintenance activities. The approaches adopted by Raoof (1990) and Knapp (2004) consider fatigue life as the number of cycles to cause outer wires to break. It is this work by Raoof (1990) and Knapp (2004) and the work of Feyrer (2007)

that will be extended in this thesis to establish a more comprehensive wire performance of wire ropes used by surface mining equipment subjected to high excavation tensile forces.

CHAPTER 3

FINITE ELEMENT METHOD, VALIDATION AND THE STRESS BASED APPROACH FOR FATIGUE LIFE OF CABLES

3.1 INTRODUCTION

In this chapter the finite element models developed to investigate the effect of various parameters on the stress conditions for several cables in tension or bent over sheaves will be discussed. The results of the finite element analysis of the cables are needed to obtain the stresses or stress parameters that are pertinent to fatigue life computations. A description of the model geometries, material properties, element type, mesh type, mesh refinement, boundary conditions and loads are presented. The finite element analysis of the cable is necessary to obtain the maximum von Mises stress and maximum internal axial strain in the wires of the cable, and also to obtain the reaction force, which will be used to compute the stress concentration and correction factors. The stress based approach will be used to predict the fatigue life of cables in cyclic tension and in bending over sheaves (Chapter 4 and Chapter 5), and this requires some inputs such as the stress concentration and correction factors.

To validate the finite element modeling technique used, an investigation was conducted, which involved developing the model of a 7-wire strand using Abaqus/CAE. The 7-wire strand model was subjected to a tensile load and validated using a load versus strain prediction using the theory developed by Costello (1997). The validation of the finite element modeling technique also involved comparing the modulus of elasticity of a 7-wire, 12.7 mm diameter, ASTM A416 prestressing strand to the measured modulus of elasticity of test specimens by Heller (2003). Six prestressing ASTM A416 strands, two 19-wire strands, one 91-wire strand, one 92-wire strand, one 6×7 wire rope and one 6×19 Seale wire rope subjected to tension were modeled using techniques similar to that used for the initial 7-wire strand analysis, where the fatigue life was predicted using a similar stress based approach to that proposed by Raoof (1990) and Knapp (2004). A 7-wire strand model bent over a sheave was developed as part of the analysis. Finally, a 19-wire strand tested by Knapp (2004) was modeled. All the cables modeled were selected because of availability of essential dimensions for modeling, as well as availability of

experimental or analytical fatigue life results for comparison with the predicted fatigue life from the current research.

3.2 FINITE ELEMENT MODEL DESCRIPTION

3.2.1 MODEL GEOMETRY, MATERIAL PROPERTIES

A finite element model of a 7-wire strand with a diameter of 15.5 mm was developed to compare its load-deformation behaviour to the load-deformation for the same strand presented by Costello (1997). The dimensions of the 7-wire strand are typical of the dimensions used as prestressing strands. This same strand configuration was used later to investigate the stress conditions in strands bent over sheaves. The core (central) wire of the strand was generated by the extrusion of a circle with a diameter of 5.23 mm. The external wires were helical in shape with a diameter of 5.13 mm. A revolution command was used to generate the external wires by specifying a lay length (pitch) of 247.65 mm, direction of twist generating left or right lay, (left lay for this case), and the total revolution angle to achieve a specified model length (in this model the angle was set equal to 360 degrees, which means the strand model length was equal to the lay length). Figure 3-1 shows the cross section of the 7-wire strand and Figure 3-2 shows the geometry of the 7-wire strand one lay length long. Later effort will be made to reduce the model length so as to reduce computation time.

A finite element model for six ASTM A416 prestressing strands was generated with diameters of 6.4, 7.9, 9.5, 11.11, 12.7 and 15.24 mm. The dimensions of the ASTM A416 prestressing strands used in the modeling are provided in Table 3-1. The lay lengths of 9.5, 11.11, 12.7 and 15.24 mm 7-wire prestressing strands are as specified in the SWPC specification sheets conforming to the ASTM Standard. The lay length of the for the 6.4 and the 7.9 mm prestressing strands were chosen in the current research to conform to the range of lay length specified by the ASTM Standard.

The stress condition and fatigue behaviour of multi-layered strands are essential to understand the behaviour of larger diameter strands and wire ropes; hence a 19-wire strand presented by Raoof (1990) was also modeled. Raoof (1990) used a similar stress based approach for predicting the fatigue life for this strand configuration, as the approach used for this research.

Table 3-2 shows the dimensions of the 19-wire strand as analysed by Raoof (1990) and Figure 3-3 shows the cross section of the 19-wire strand. The core wire of this arrangement was created by generating a 3.594 mm diameter circle in the parts module of Abaqus/CAE and extruding it to a length of one sixth of the largest lay length (i.e. length of 31.83 mm). Costello (1997) and Erdönmez and İmrak (2009) presented the relationship between the lay length, lay angle and the lay radius as:

$$\tan\beta = \frac{p}{2\pi R} \tag{3-1}$$

where p is the lay length, and α is the lay angle of the strand, and β is equal to $90-\alpha$, R is the lay radius; defined as the vertical dimension between the axis of the strand or core wire to the centre of a wire in the layer under consideration. Equation 3-1 was used to compute the lay length in Table 3-2, since it was not reported by Raoof (1990). The second layer of helical wires was created by generating a circle above the core wire of diameter 3.25 mm and using the revolution command in the parts module to revolve the geometry around the central wire. A single wire created in the second layer was cloned to create five more wires around the core wire. A similar technique was used for the 12 wires in the third layer. Figure 3-4 shows the geometry of the 19-wire strand.

A 19-wire strand tested by Papanikolas (1995) was also modeled in Abaqus/CAE to predict the stress distribution and fatigue life of multi-layered strands subjected to cyclic tension. Table 3-3 shows the dimensions of the 19-wire strand tested by Papanikolas (1995) used to create the strand as based on the modeling technique described above. In Table 3-3, the Layer O.D is defined as 2 times the vertical dimension between the axis of the strand to the top of the wire in the layer under consideration.

A 92-wire strand and 91-wire strands were created using the same approach described for the 19-wire strand. The basic difference between the 92-wire and the 91-wire strands was the second layer, which consisted of 7 and 6 wires for the 92 and 91-wire strands, respectively. Both strands had six layers, starting with a central straight wire as layer 1, increasing to layer 6 with 30 wires. Table 3-4 and Table 3-5 show the dimensions used to create the model of the 92-wire and the 91-wire strands, respectively. Figure 3-5 and Figure 3-6 show the cross section and the

geometry of the 92-wire strand, respectively. The cross section and the geometry for the 91-wire strand are shown in Figure 3-7 and Figure 3-8, respectively.

For a 6×19 Seale wire rope, three strand diameters were used in a parametric study. The diameters of the wire ropes were 33, 49.53 and the 70 mm. Since only direct tension was applied to the wire rope, the dimensions of the 49.53 and 70 mm wire ropes were scaled-up versions of the 33 mm wire rope. The stress concentration and stress correction factor obtained using the finite element analysis for all three wire ropes were suspected to be the same; so only the finite element modeling of the 33 mm wire rope will be carried out. This will be verified when the plot of the von Mises stress versus the applied stress for the different 7-wire prestressing strands is carried out in Chapter 4. If a constant slope is obtained for all prestressing strands, then it can be surmised that a scaled model should have the same stress concentration or correction factor, but the size effect that takes into account a reduction in fatigue life for larger diameter components (discussed latter in this Chapter) will be applied to modify the endurance of each wire rope for the parametric study in Chapter 4. The dimensions of the 33 mm diameter 6×19 Seale wire rope are shown in Table 3-6; the geometry of which was originally presented by Velinsky (1981). Table 3-6 presents a parameter m defined by İmrak and Erdönmez (2010) as:

$$m = r_{sh} / (r_{dh} \tan\alpha_{dh} \cos\alpha_{sh}) \tag{3-2}$$

where r_{sh} is a single helix strand outer radius measured from the central wire rope axis (same as the Strand O.R. in Table 3-6), α_{sh} is a single helix lay angle and r_{dh} and α_{dh} are the respective double helix radius and lay angle, respectively. These were measured relative to the axis of the wire rope, although the double helix radius is measured from the central wire in its strand to the centre of the wire of interest. The parameter m is used to develop the 6×19 Seale wire rope, and it is used specifically to generate coordinates of the double helix wires (refer to Appendix A). Figure 3-9 shows a typical cross section for the 6×19 Seale wire rope, containing the three types of strand. Figure 3-10 shows the nomenclature used to describe strand 1, where the dimensions of H11 to H16 are the same, except for the relative position of each of the wires within the strand. Figures 3-11 and 3-12 show similar nomenclature for strands 2 and 3, respectively. The dimensions of H21 to H26 are identical. Similarly, the dimensions of H31 through H39 are the same, and the dimensions of H41 through H49 are also the same. Table 3-6 provides all

dimensions for the wire rope. Each of the wires of the Seale wire rope was generated using parametric equations in SolidWorks, as presented in Appendix A. Figure 3-13 shows the geometry of the Seale wire rope once the parts have been imported from SolidWorks and assembled in Abaqus/CAE. The SolidWorks files were converted to a STEP format and then imported into Abaqus/CAE.

The IWRC was formed by removing strands 3 of the 6×19 Seale wire rope. Figure 3-14 shows the geometry of the IWRC.

Bending over sheave fatigue behaviour of strands and ropes is of interest in the current research since hoist ropes in shovels and elevator ropes are subjected to this type of loading. The effect of the diameter of a sheave, D, to the diameter of a wire strand, d, (D/d), the tensile load (S) and the radius of the sheave groove (r) on the stress conditions was investigated using the 7-wire strand presented by Costello (1997) and the 19-wire strand tested by Knapp (2004). The strand from Costello's (1997) was a 7-wire strand as discussed previously. The Knapp (2004) test specimen was a 19-wire strand, generated using extrusion and revolution of circular cross sections as described previously. The dimensions of the 19-wire, 3.3 mm diameter strand tested by Knapp and used for the finite element model are shown in Table 3-7.

Homogenous and isotropic material properties with a Young's modulus of 200 GPa and Poisson's ratio of 0.3 were used for the wires, and a friction coefficient of 0.12 was used as; this friction coefficient was also used by Raoof (1990), considered to be representative of friction between lubricated galvanised wires over long periods by Raoof and Hobbs (1988), established by comparing theoretical and experimental data. The mass density of the steel material was specified as 7800 kg/m^3. General contact with a penalty algorithm, which is basically a contact enforcement method (refer to ABAQUS documentation), was used to simulate contact between wires and contact between wires and a sheave. In the bend-over sheave analysis the wires in the strands were considered the "slave" surfaces, and the sheave, modeled as a rigid body, was the "master" surface. This is because the "slave" surface should be the more finely meshed surface, and should be the softer material as recommended by the ABAQUS documentation. A large displacement, non-linear geometry analysis was conducted to capture the contact behaviour between the adjacent wires and between wires and the sheave.

3.2.2 INTERACTION, BOUNDARY CONDITIONS AND LOADING

All 7-wire strands that were subjected to tensile loading only, had all the nodes at each end slaved to a reference point at each end. The cross section of the wires at one end of the strand was tied to the reference point (reference point 2, RP2) using a multi-point constraint (Beam type). The beam type multi-point constraint was used to constrain the displacement and rotation of the slave nodes to the displacement and rotation of a control point (a single point, where boundary conditions or loads can be applied, and it ultimately applied this to the slave nodes), while the nodes at the other end of the strands were tied using kinematic coupling. Kinematic coupling limits the motion of the slave nodes to the rigid body motion of a reference node (reference point 1, RP1). Several alternatives were tried to model the behaviour of the strands under load; with the beam type multi-point constraint at one end of a strand and the kinematic coupling at the other end providing the best stiffness estimate output for the strand performance. RP1 for each cable was subjected to several concentrated loads, with RP2 having all degrees of freedom fixed. Loads were applied using a tabular amplitude curve, ramped up to full magnitude within a time period of 0.001 for the 7 and 19-wire strands. The loads were applied in a similar manner for the 91, 92-wire strands, the IWRC and the 6×19 Seale wire rope, but a time period of 0.01 was used for these cables. All strands and wire ropes subjected to tension only had the same boundary conditions as the 7-wire strand, and the complete details of the loads applied to each case will be presented in Chapter 4.

For the strands bent over sheaves, the cross section of the wires at both ends of the strands was tied to a reference point using the kinematic coupling constraint, and the boundary condition was applied to the reference point. The length of each strand that bends over the sheave was determined using the length of an arc formula:

$$L = \theta R \tag{3-3}$$

where R is the radius of the sheave plus the radius of the strand and θ is the angle subtended by the strand in contact with the sheave, expressed in radians. If the strand was made significantly longer than the length obtained from Equation (3-3), then the analysis became highly unstable and produced unrealistic results. This problem was suspected to be because, in a quasi-static analysis, when the downward displacement is applied to the strand, it can generates a dynamic

effect that creates an unwanted displacement in the strand as it falls and wraps around the sheave. Displacement control loading was used for loading the strands after it wraps around the sheave. Figure 3-15 shows the wire strand and the applied displacements at both ends in the downward direction; and the geometry of the 7-wire strand over the sheave is shown in Figure 3-16. The displacement applied depended on the applied tension, and the radius of the sheave involved in each analysis. The strands were free to rotate about the z-axis and also free to translate in the x-axis, as defined in Figure 3-16. All other degrees of freedom were restrained. The time period was varied between 0.12 to 0.16 seconds, as was the mass scaling factor; the latter described as a factor that scales up the mass of the model, effectively increasing the overall kinetic energy of the model in Abaqus/CAE Explicit, and hence speeds up the analysis. The mass scaling factor was only applied to the cables bent over sheave, because of computation time required to bend the cable over the sheave and apply a tension. For the 7-wire strands bent over sheave a mass scaling factor of five was used, and for 19-wire strands bent over sheave a mass scaling factor of 49 was used. Using higher values of mass scaling factor produced output that had kinetic energy greater than 5% of the internal energy, and hence the produced results were completely unreliable. Figure 3-17 shows the geometry of the 19-wire strand over a sheave before the application of a displacement, and this was the same as the geometry of the strand and sheave investigated by Knapp (2004), which had a very high (D/d) ratio at 90.9 and a groove radius of $r = 1.92d$. All sheaves had all the degrees of freedom restrained at the centre, and a coefficient of friction of zero (which can allow for free sliding of the cable over the sheave) was specified between the cable and the sheave, while the coefficient of friction between wires of the cable was set at 0.12 (as suggested by Raoof (1990)).

3.2.3 MESH REFINEMENT STUDY AND ELEMENT TYPE

Cables have complex geometry, which makes the prediction of the location of the maximum stress concentration very difficult. Therefore, the whole cable mesh must be refined to predict accurately the stress concentration.

The mesh was generated after all boundary conditions and loads were applied to the model. The mesh of the 7-wire strands was generated using a free meshing technique in Abaqus/CAE. The current research used C3D8R elements, which are 8-node linear brick,

reduced integration with hourglass control, as recommended in the ABAQUS documentation for contact and large deformation problems. A mesh refinement study was conducted to obtain the most appropriate element size. This was done using a 7-wire strand of 15.5 mm diameter as used by Costello (1997). The lay length and the length of the strand modeled was 247.65 mm.

An alternative to reduce the model size is necessary to reduce computational time. Wang *et al*. (2013) and Jiang (2012) have used a model with length of one-sixth of the lay length (short model) and they obtained satisfactory load-strain predictions, since larger cable sizes will be modeled in the current research the same will be adopted to reduce computational time. The comparison of the load-strain predicted using the short model and the full lay length model will be carried out in the current section, also a comparison of von Mises stress obtained using a short model and a long model (with length of 300 mm) of the prestressing strands will be carried out and is presented in Appendix B.

Figure 3-18 (a) shows the results of the mesh refinement study comparing the load-strain relationship for each mesh size to the predicted load-strain relationship proposed by Costello (1997). From the comparison plot it can be seen that with 1,224,132 elements the load-deformation behaviour of the finite element model was very close to that predicted by Costello's theory. The axial force versus the strand axial strain or the strand bending moment versus bending curvature predicted using Costello's theory has been used by several researchers such as Wang *et al*. (2013), Jiang (2012), İmrak and Erdönmez (2010), Erdönmez and İmrak (2009) to compare with their model axial or bending behaviour and they all found that their model load-strain relationship had less than 5% difference from the Costello's predictions, provided the material response is elastic. Figure 3-18 (b) shows the mesh refinement study based on the von Mises stress, it can be observed that although the von Mises stress seems to have converged in a coarser mesh (10250 elements), the strand is still very flexible, so it is better for such elements to observe convergence of both the stress of interest as well as the stiffness whenever it is possible, and this flexible behaviour of the C3D8R elements was also reported in the ABAQUS documentation. Therefore, a mesh size of 1,224,132 elements was selected for this strand size. Figure 3-19 shows an overall view of the mesh for the short model. For all other 7-wire strands, subjected to tension only, no further mesh study was considered necessary since the number of elements around the cross section relative to the strand diameter was kept constant. However,

later it is necessary to explore alternatives to reduce computational time and cost by reducing the overall length of the model. As the number of wires in a strand increases contact between wires becomes more complex, necessitating a significant refinement of the C3D8R elements to ensure convergence. Also, as geometric non-linearity increased these elements became significantly costly to use. To overcome such problems, C3D10M elements were used for the 19, 91 and 92-wire strands. The C3D10M element is a solid second order modified tetrahedral element known for good performance in contact and geometric non-linear problems (refer to ABAQUS documentation).

To investigate the effect of a reduction in the length of the model on the load-strain relationship, the behaviour of a 7-wire strand presented by Costello (1997) in tension only was compared to the behaviour predicted by Costello's theory for the same strand. A load of 83.67 kN in this case was applied to only one end of the strand. The model with length reduced to one sixth of its lay length as suggested and applied by Wang *et al*. (2013) and Jiang (2012) was analysed and compared to a model with length equal to one full lay of 247.65 mm. Figures 3-20 and 3-21 shows the displaced model for the long model (length of one lay length), and the short model (with a length of one sixth of the lay length), respectively. Figure 3-22 compares the load-strain results of the finite element analysis with the prediction from Costello's theory, indicating that the finite element model here accurately predicts the load-strain relationship suggested by Costello (1997) with less than 1% difference. The load-strain of the reduced length for the strand is also shown in Figure 3-22. It can be concluded that there is a reasonably good prediction of the load-strain relationship by the short or long model when compared to the load-strain predicted from Costello's theory.

Figure 3-23 shows the results of the mesh refinement study conducted on Raoof's 19-wire strand at a load of 23.4 kN. A mesh with 33,850 elements was chosen as mesh refinement beyond this did not lead to any significant difference (about 1% difference) in stress values. The selected mesh is shown in Figure 3-24. Since a similar wire size as the 19-wire strand was modeled for the 92 and 91-wire strands, the same element size was used for the 92 and 91-wire strands as shown in Figure 3-25 and Figure 3-26, respectively.

Although, the element size used for the strands may be extended to the 6×19 Seale wire rope, a mesh refinement study was carried out as shown in Figure 3-27. Figure 3-28 shows the final mesh chosen with 106,204 elements; representing the number of elements to be used if the same element size as used for the strands were used. For strands subjected to bending a different mesh size was selected. The Costello and Knapp 7 and 19-wire strand 'bending over sheave' models were given element sizes of 0.70 and 0.20 mm, respectively. An overall view of the mesh for the 7 and 19-wire strands bending over sheave are shown in Figure 3-29 and Figure 3-30, respectively.

3.2.4 STRANDS AND WIRE ROPES SUBJECTED TO TENSION ONLY

All 7-wire strands had loads up to 50% of the tensile strength applied. For the 6.4 and 7.9 mm prestressing strands, loads up to 20 and 32.25 kN, respectively were applied along the axis of the strand. A 9.5 mm ASTM A416 strand was loaded axially with a load up to 45 kN at only one end of the strand. 11.11 mm, and 12.7 mm ASTM A416 prestressing strands were loaded up to 60 kN and 83.7 kN, respectively. A 15.24 mm strand was loaded with a tensile load up to 128 kN, applied to one end of the strand. Raoof's 19-wire strand was loaded with a force up to 81.9 kN (30% of the UTS), based on the load investigated by Raoof (1990). The 19-wire strand model for the strands tested by Papanikolas (1995) was loaded up to an axial force of 150 kN.

The 91-wire strand was loaded axially with a force up to 700 kN. The loads applied to the 19 and 91-wire strands tested by Papankolas (1995) were intended to create a stress range up to 25 to 29% of the minimum ultimate tensile strength as specified by Papanikolas (1995) (UTS for the 19 and 91-wire strands was 1402 and 1409 MPa, respectively). The 92-wire strand was loaded at various load levels up to 369 kN (30% of the UTS specified by Raoof (1990)). Similarly, the 6×7 strand was subjected to an applied load up to 50 kN. The 6×19 Seale wire rope was given applied loads up to 360 kN. The loads applied to the strands and wire ropes will be discussed in Chapter 4 in the parametric study. Feyrer (2007) reported that the factor of safety for crane stay ropes and steel construction (including bridges) is 3.2 and 2.2, respectively. Tension loads were applied to all strands and wire ropes such that the fatigue life will be investigated to a maximum factor of safety within a range of 2 to 3.

3.2.5 STRANDS SUBJECTED TO BENDING OVER SHEAVE

To study the behaviour of strands bent over a sheave, two strand types were used: a 7-wire strand used by Costello (1997) and a 19-wire strand investigated by Knapp (2004). For the 7-wire strand, a parametric study was conducted, which varied the diameter of the sheave to the diameter of the strand ratio (D/d) at 12, 15, 20, 40 and 60, with corresponding varying load levels in each case. The corresponding lengths used for the above D/d ratios were 317, 391, 512, 999 and 1486 mm, respectively. These lengths were based on Equation 3-3 for a strand bent over a sheave. The diameter of the strands was considered constant at 15.5 mm for this analysis, except when the effect of the diameter of strand was investigated.

The effect of change in diameter for a 7-wire strand bent over a sheave was also investigated, where the diameter was reduced by 50% and 75% of the original diameter and loaded over a sheave; this was carried out for D/d ratios of 12 and 15. The groove radius (r) used was typically 0.53 times the diameter of the strand, this is normally the groove size used in practice (Feyrer, 2007), although the effect of the groove was also investigated for D/d ratios of 12 and 15. For the D/d ratios of 12 and 15, a groove radius of $0.53d$, $0.8d$, $1.0d$ and a flat groove (D/d of 12 only) were also investigated.

A parametric study to investigate the effect of D/d and load on stress concentration in the multi-layered 19-wire strand was carried out for D/d ratios of 10, 15, 30, 60 and 90.9. For all these cases the radius of the groove was kept constant at $0.53d$. To investigate the effect of change in strand diameter, the diameter of the 19-wire strand was increased by 50% and 100%, bent over a sheave, and then loaded for D/d ratios of 10 and 15. To observe the effect of groove radius for multilayered strands, groove radii of $0.53d$, $0.8d$ and $1.0d$ were investigated for a D/d ratio of 10.

The fatigue life of strands bent over sheaves will be obtained using the maximum von Mises stress in a strand and the nominal stress, which is expressed as the reaction force at the sheave divided by the nominal cross sectional area at the cable.

3.2.6 COMPARISON OF PREDICTED AND ACTUAL STIFFNESS

A 12.7 mm ASTM A416 prestressing strand described and tested by Heller (2003), with a Young's modulus of 202,706 MPa generated a finite element analytical solution here with a Young's modulus value of 202,614 MPa; this was generated from a plot of the strand force versus the strain in Figure 3-31. Further validations were performed as fatigue life predicted using stress based approaches are compared with fatigue test results in the following chapters. The validation of the finite element model and the validation of the stress based approach for fatigue life prediction were conducted. The latter will be treated in two parts, 1) a fatigue analysis for strands and wire ropes subjected to tension only and, 2) a fatigue analysis for strands bent over a sheave, such that the validation of the stress based approach for fatigue of strands and wire ropes will be discussed in Chapters 4 and 5.

3.3 ANALYSIS

A non-linear elastic quasi-static analysis was conducted, with an elastic stress concentration factor (SCF_{nom}) computed as the ratio of the maximum von Mises stress, σ_{mv}, to the nominal stress, σ_{nom}, as described by:

$$SCF_{nom} = \frac{\sigma_{\text{mv}}}{\sigma_{nom}} \tag{3-4}$$

The nominal stress is the applied force divided by the gross cross sectional area for the strands or wire ropes subjected to tension only. The gross cross sectional area of the cable is obtained by summing up the circular cross sectional area of all the individual wires that make up the cable. In calculating the SCF_{nom} for strands bent over sheaves, the nominal stress was defined as the reaction force at the sheave obtained from the finite element analysis divided by the sum of the nominal cross sectional area of each wire in the strand. The fatigue life will also be obtained using a stress correction factor $(CF_{\text{int}.stress})$ suggested by Raoof (1990) and given as:

$$CF_{\text{int}.stress} = \frac{\sigma_{mv}}{\sigma_{\text{int}.stress}} \tag{3-5}$$

where $\sigma_{\text{int.}stress}$ is the maximum internal wire stress. The analysis was sub-divided into two main categories: (1) tension and (2) bending over sheave analyses. In the tension analysis, 10 strand types were considered: six of which were 7-wire prestressing mono strands (ASTM A416 strands); a 19-wire strand as investigated by Raoof (1990); a 19-wire strand as tested by Papanikolas (1995); 91 and 92-wire strands, and one 6×19 Seale and one IWRC wire rope will also be analysed. In bending over sheaves, one 7-wire strand as considered by Costello (1997) and a multilayer 19-wire strand that was tested by Knapp (2004) were investigated for stress concentration, stress correction and fatigue resistance. In all cases, to obtain a quasi-static analysis, the kinetic energy in the dynamic explicit analyses was found to be less than 5% of the internal energy, this check is necessary to ensure that the loads or displacements are applied in such slow and steady manner that the impact of the dynamics of the model does not affect the results, as will be expected when the kinetic energy is greater than 5 to 10% of the internal energy (refer to ABAQUS documentation)

3.4 FATIGUE ANALYSIS

The main goal of this research is to predict the fatigue life of strands and wire ropes in cyclic tension and bending over sheaves, from fatigue test results for single galvanised wires. To predict the fatigue life of cables made of wires that are not galvanised a similar stress based approach can be used, but the fatigue S-N curve for a single wire that is not galvanised will have to be used for the fatigue life prediction for such cables. Figure 3-32 shows the schematic of a fatigue S-N curve for a single wire and the reduced fatigue S-N curve for a strand or wire rope. The endurance limit for the single wire, S_o, is modified to obtain the reduced endurance limit for a strand or wire rope, S_e, as proposed by Bannantine *et al*. (1990) as:

$$S_e = S_o C_{sf} C_{sc} C_s \tag{3-6}$$

where C_{sf} is the modification factor for wire surface finish, C_{sc} is the modification factor for a stress concentration or notch sensitivity, and C_s is the modification factor for size (in this case diameter) of the component. C_{sf} depends on the surface finish and the tensile strength and can be found from the literature (Bannantine *et al*., 1990). C_{sc} is the reciprocal of the fatigue notch

factor, where the notch sensitivity factor for fully reversed loading was previously developed by Neuber (1961) as:

$$q = \frac{1}{1+\sqrt{\rho / r_n}} \tag{3-7}$$

where ρ is the characteristic length dependant on the material and r_n is the notch root radius. The fatigue notch factor is related to the notch sensitivity factor from the equation presented in Stephens *et al*. (2001):

$$K_f = 1 + q(K_t - 1) \tag{3-8}$$

where K_t is the stress concentration factor. For steel with an ultimate tensile strength of 1725 MPa and a notch radius of 1 mm as defined by Stephens *et al*. (2001), the fatigue notch factor is about 1.0. So, the fatigue notch factor for this research analysis was assumed to be equal to the SCF_{nom} or $CF_{\text{int}.stress}$, as the notch sensitivity factor for such high strength steels used in making strands or wire rope approaches unity. C_s was presented by Bannantine *et al*. (1990) and Shigley and Mitchell (1983) as:

$$C_s = 1.189 d^{-0.097} \tag{3-9}$$

where d in the current research is the diameter of the strand or wire rope, Equation 3-9 was used if $8 \text{ mm} \le d \le 250 \text{ mm}$. For $d \le 8$ mm, C_s is 1.0. Equation 3-9 was derived from plots of actual test specimens, considering the effect of specimen size on the endurance limit for specimens under reversed bending and torsion. Although, some of the wires in the strands and wire ropes in the analysis were subjected to tension only, the geometry of the wires analysed are such that the wires are invariably subjected to twisting when in tension, so that the specimen size effect should be applied to strands and wire ropes in tension or bent over sheaves. Table 3-8 shows the typical modification factors for surface finish and size used in the current research. The SCF_{nom} or $CF_{\text{int}.stress}$ was obtained from a linear elastic finite element analysis of strands or wire ropes,

where afterwards a reduced endurance limit for a strand or wire rope was obtained, the fatigue life of the cable could be calculated using the S-N equations:

$$N = 10^{-c/b} S_N^{1/b} \tag{3-10}$$

where,

$$b = \frac{\log\left(\frac{S_f}{S_e}\right)}{\log\left(\frac{N_f}{N_e}\right)} \tag{3-11}$$

$$c = \log(S_f) - [\log(\mathrm{N}_f) / (\log \frac{N_f}{N_e})](\log \frac{S_f}{S_e}) \tag{3-12}$$

where S_f is the maximum stress amplitude for a single wire, N_f is the corresponding fatigue life for a single wire at the maximum stress amplitude, and S_N is any arbitrary stress amplitude for which a fatigue life N is being estimated. Thorpe *et al*. (1985) conducted fatigue tests on single wires such that: S_f is 644 MPa and N_f at 58,880 cycles for a mean stress of 920 MPa. S_o is the fatigue limit for a single wire and using the definition from Thorpe *et al*. (1985), it was offset at 490 MPa, as defined by Equation (3-6) and N_e, the corresponding endurance limit fatigue life for a single wire (1,020,000 cycles) is shown schematically in Figure 3-32. Figure 3-33 shows the flow chart for the process of obtaining the fatigue life for cables either in cyclic tension or bent over sheave wheels.

3.5 DISCUSSION

In this chapter, the method used for the development of the finite element models was presented for cables in tension and bent over sheave wheel. The strands models generated were seven 7-wire strands, two 19-wire strands, one 92 and one 91-wire strands, also modeled was one IWRC and one 6×19 Seale wire rope , all of these were subjected to tension only, so as to investigate the tension fatigue resistance of cables. All of the 7-wire strands investigated in the current research had dimensions that conform to ASTM A416 prestressing strands, and there

were availability of fatigue test data for most of these 7-wire prestressing strands for comparison in the following chapter. The other multi-layered strands investigated were reported by other independent researchers, such as Raoof (1990) and Papanikolas (1995), again these were standard strand types used in civil or mining applications.

The bend over sheave behaviour of cables is of great importance, since equipments such as shovels, cranes, and elevators are subjected to such loading conditions, hence two strand types; 7 and 19-wire strand at different sheave diameter to strand diameter ratios, groove sizes, and tensile load was created in a parametric form. The 19-wire strand was from the work of Knapp (2004) and hence had fatigue test results for comparison with the current research prediction. The 7 and the 19-wire strands were not investigated and presented by Feyrer (2007), but they are the fundamental strands for all other larger cables and investigating the fatigue behaviour of such strands when bent over sheave wheels will enable us to understand behaviour of larger cables bent over sheaves, since the same factors such as the load, and the diameter of sheave to the diameter of cables affects small or large cables.

Non-linear elastic model was used for all analysis to obtain elastic stresses and strains, hence elastic stress correction or concentration factors will be obtained, and since yielding was not included in the material behaviour high stresses of several magnitudes higher than the yield stress of steel should be expected. The stress-life method of fatigue prediction does not work well in low cycle fatigue where there is significant plastic deformation (Bannantine *et al*. 1990); hence the use of elastic stress correction or concentration factors with the stress based approach for cables, which will typically be subjected to high cycle fatigue in the current research is justified.

The loads applied to each cable were meant to achieve a factor of safety between the ranges of 2 to 3, which is typical of field conditions.

The fatigue life of strands will be obtained using a stress based approach that treats the stress correction or concentration factor as an equivalent notch and reduces the fatigue limit of the S-N plot for a single wire (assumed to be without any notch or stress concentration) by accounting for the stress concentration, surface finish, and size of the cable as recommended by Bannantine *et al*. (1990) and used for other types of structures.

One of the shortcomings in the present chapter is the availability of stress results to compare with the finite element model results. Costello's Theory remains the most widely used theory to check the models load-strain relationship. This theory has been used by several researchers such as Wang *et al*. (2013), Jiang (2012), İmrak and Erdönmez (2010), Erdönmez and İmrak (2009) to mention just a few, and it had resulted in good prediction of the cable strains and stiffness, with less than 5% difference between the model and Costello's predicted load-strain relationship. The other shortcoming is the fact that running large models with hundreds if not thousands of contact points in a single cable is time consuming, so in order to overcome this, a model with one-sixth of the largest lay length in the cable was adopted. The stiffness of such "short" model has been proven in the current chapter to be representative of the measured and predicted modulus and load-strain behaviour by Heller (2003) and Costello (1997), respectively. In the absence of actual or predicted von Mises or contact stress for such complex cables, we have differed further validation or justification of the short model to the following Chapters and Appendix B.

Table 3-1: Dimensions of the ASTM A416 Prestressing strands

ASTM Strand diameter (mm)	Core Wire Diameter (mm)	External Wire Diameter (mm)	Lay Length (mm)	Lay Angle (degrees)
6.4	2.150	2.130	90	8.53
7.9	2.660	2.620	110	8.53
9.5	3.220	3.160	130	8.76
11.11	3.750	3.680	165	8.05
12.7	4.290	4.210	180	8.43
15.24	5.150	5.040	205	8.88

Table 3-2: Dimensions of the 16.4 mm diameter, 19-wire strand by Raoof (1990)

Layer	No. of Wires	Lay Direction**	Wire Diameter (mm)	Lay Angle (degrees)	Lay Radius (mm)	Lay Length (mm)
1	1	—	3.594	—	—	—
2	6	LL	3.250	11.42	3.30	102.66
3	12	RL	3.250	11.91	6.41	190.98

** LL is left lay, and RL is right lay

Table 3-3: Dimensions of the 25 mm diameter, 19-wire strand tested by Papanikolas (1995)

Layer	No. of Wires	Lay Direction**	Wire Diameter (mm)	Lay Length (mm)	Layer O.D (mm) *	Lay Angle (degrees)
1	1	—	5.260	—	5.260	—
2	6	RL	5.056	161	15.43	11.44
3	12	LL	5.056	263	25.34	13.62

* O.D is outer diameter

** LL is left lay, and RL is right lay

Table 3-4: Dimensions of the 39 mm diameter, 92-wire strand by Raoof (1990)

Layer	No. of Wires	Lay Direction**	Wire Diameter (mm)	Lay Angle (degrees)	Lay Radius (mm)	Lay Length (mm)
1	1	—	5.050	—	—	—
2	7	RL	3.540	15.42	4.19	95.46
3	12	RL	3.540	14.90	7.04	166.26
4	18	LL	3.540	15.93	10.57	232.71
5	24	LL	3.540	16.45	14.10	300.09
6	30	RL	3.540	17.74	17.73	348.27

** LL is left lay, and RL is right lay

Table 3-5: Dimensions of the 45 mm diameter, 91-wire strand tested by Papanikolas (1995)

Layer	No. of Wires	Lay Direction**	Wire Diameter (mm)	Lay Length (mm)	Layer O.D (mm) *	Lay Angle (degrees)
1	1	—	4.315	—	4.315	—
2	6	RL	4.034	100	12.29	14.54
3	12	RL	4.034	206	20.16	13.82
4	18	LL	4.034	301	28.29	14.21
5	24	RL	4.034	395	36.27	14.38
6	30	LL	4.034	506	44.37	14.06

* O.D is outer diameter

** LL is left lay, and RL is right lay

Table 3-6: 6×19 Seale wire rope by Velinsky (1981) of 33 mm diameter

Strand §	Wire	No. of Wires	Lay Direction **	Wire Radius (mm)	Lay Length (mm)	Strand O.R* (mm)	Strand Lay Angle (degrees)	Double Helix Radius (mm)	*m* (Eq. 3-2)
1	H10	1	RL	0.801	—	—	—	—	—
	H11-H16	1	RL	0.735	33.02	1.536	16.30	—	—
2	H20	1	RL	0.704	77.47	4.287	19.18	—	—
	H21-H26	1	RL	0.656	77.47	4.287	19.18	1.360	1.5087
3	H30	1	LL	1.456	199.61	11.413	19.77	—	—
	H31-H39	1	LL	0.712	199.61	11.413	19.77	2.168	3.3855
	H41-H49	1	LL	1.243	199.61	11.413	19.77	3.867	3.3855

§ Refer to Figures 3-9 to 3-12

* O.R : outer radius

** LL is left lay, and RL is right lay

Table 3-7: Dimensions of the 3.3 mm strand tested by Knapp (2004)

Layer	No. of Wires	Lay Direction**	Wire Diameter (mm)	Lay Length (mm)	Strand O.D (mm)
1	1	—	0.700	—	0.700
2	6	RL	0.660	19	2.000
3	12	LL	0.640	33	3.300

** LL is left lay and RL is right lay

Table 3-8: Modification factors used for various cables

Cable type	Diameter (mm)	C_{sf}	C_s
7-wire prestressing strands	6.4	0.53	1.00
	7.9	0.53	1.00
	9.5	0.51	0.96
	11.11	0.53	0.94
	12.7	0.53	0.93
	15.24	0.53	0.91
19-wire strands	16.4	0.50*	0.91
	25	0.54**	0.87
	3.3	0.53	1.00
92-wire strand	39	0.50*	0.83
91-wire strand	45	0.54**	0.82
6×7 wire rope	12.6	0.53	0.93
6×19 Seale wire rope	33	0.53	0.85

* The value was used by the Raoof (1990)

** based on specified tensile strength of 1402 and 1409 MPa reported by Papanikolas (1995)

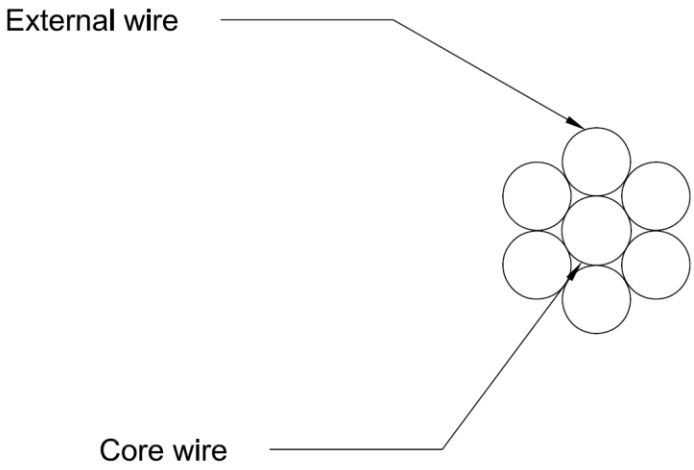

Figure 3-1: Cross section of the 7-wire strand

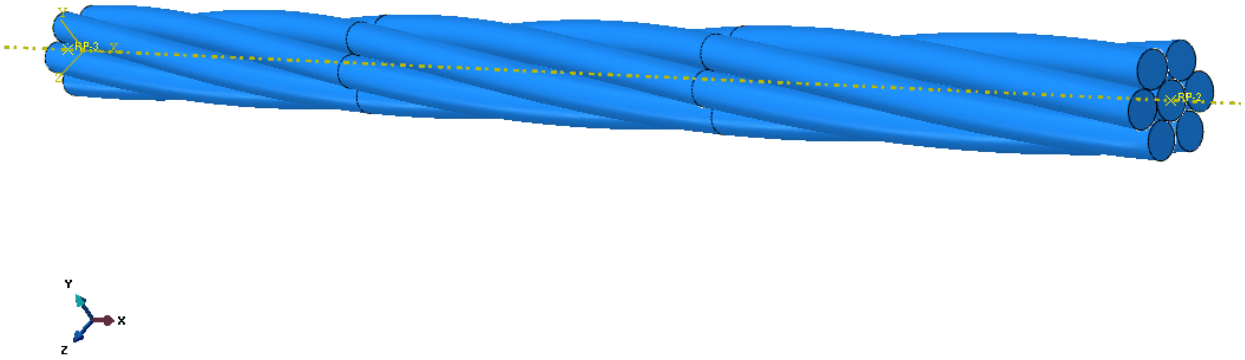

Figure 3-2: Geometry of 7-wire strand

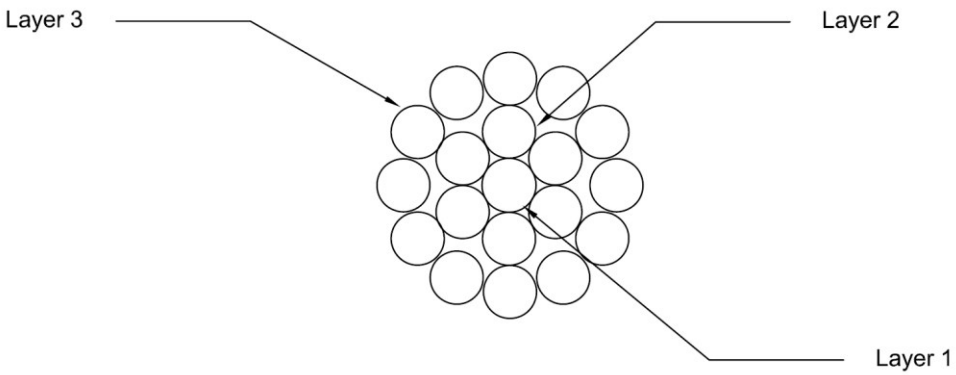

Figure 3-3: Cross section of the 19-wire multilayer strands

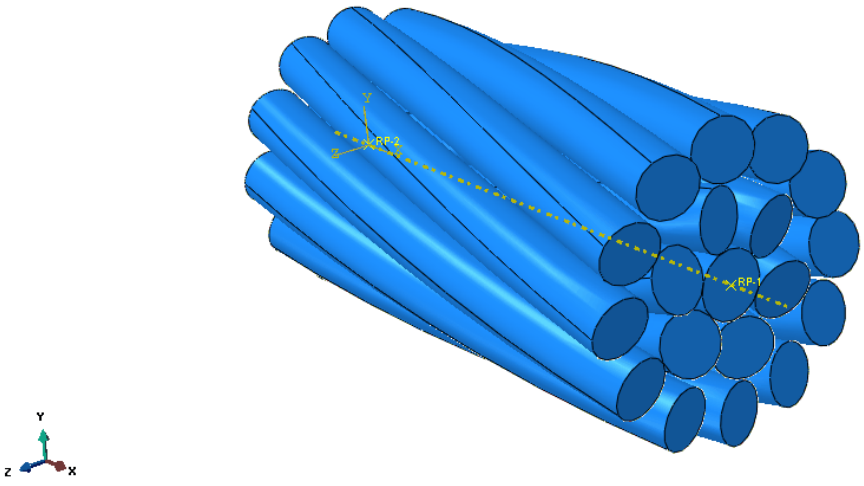

Figure 3-4: Geometry of a 19-wire strand

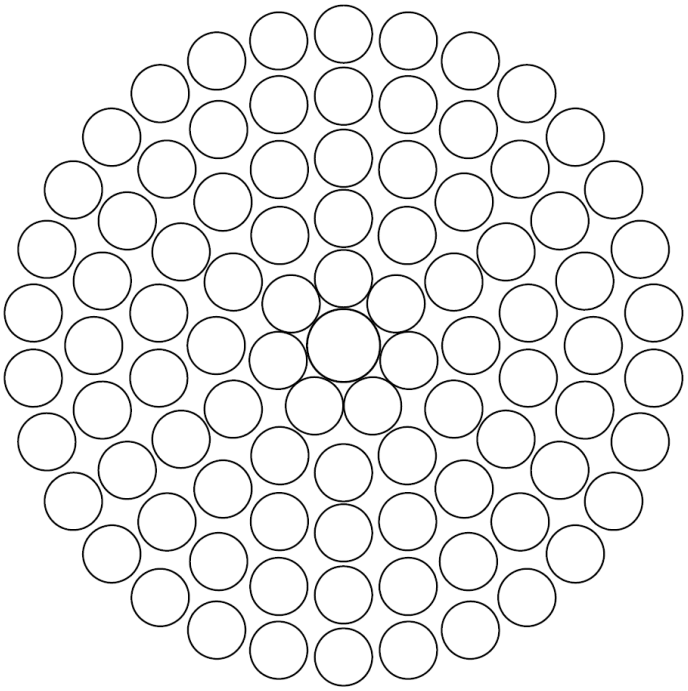

Figure 3-5: Cross section of 92-wire strand

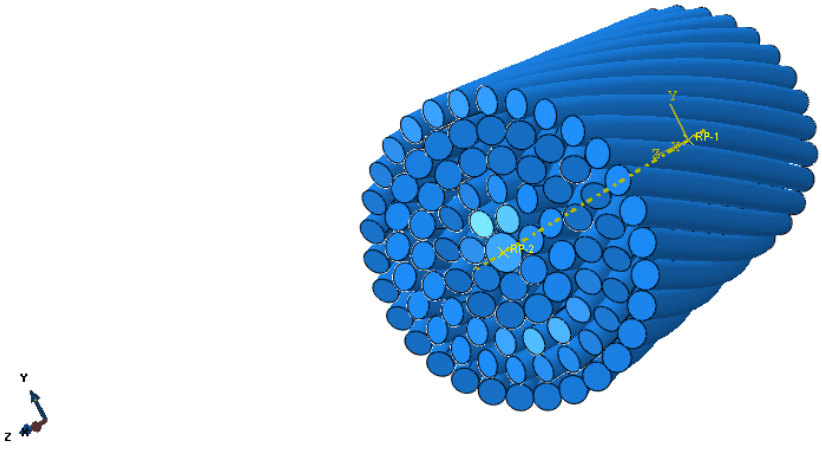

Figure 3-6: Geometry of 92-wire strand

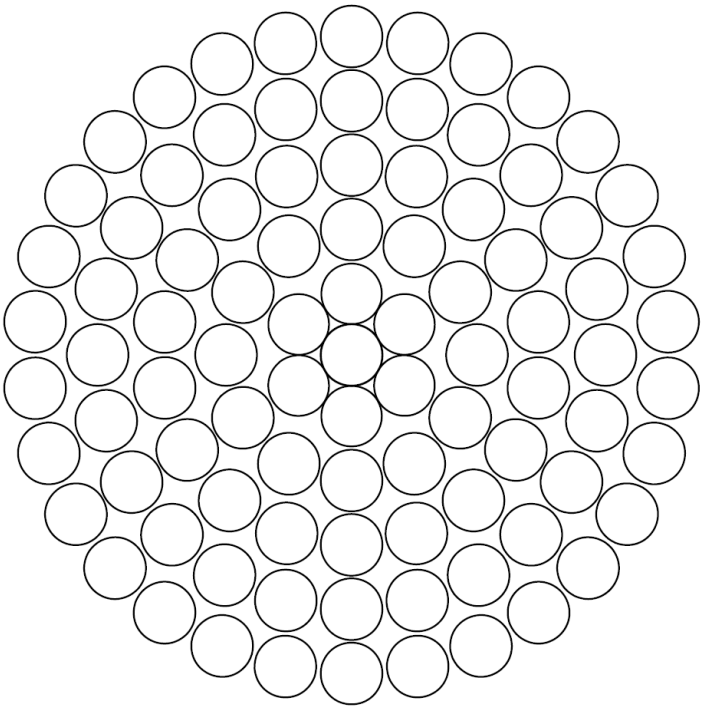

Figure 3-7: Cross section of 91-wire strand

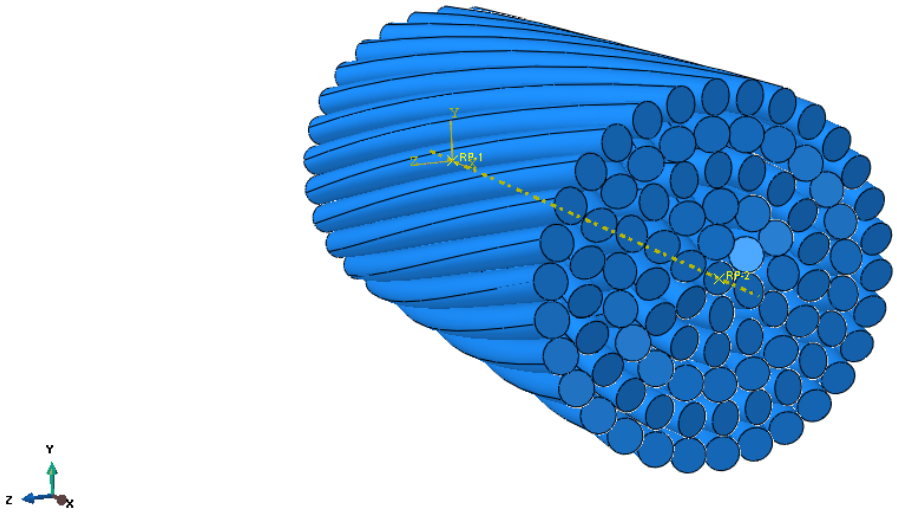

Figure 3-8: Geometry of 91-wire strand

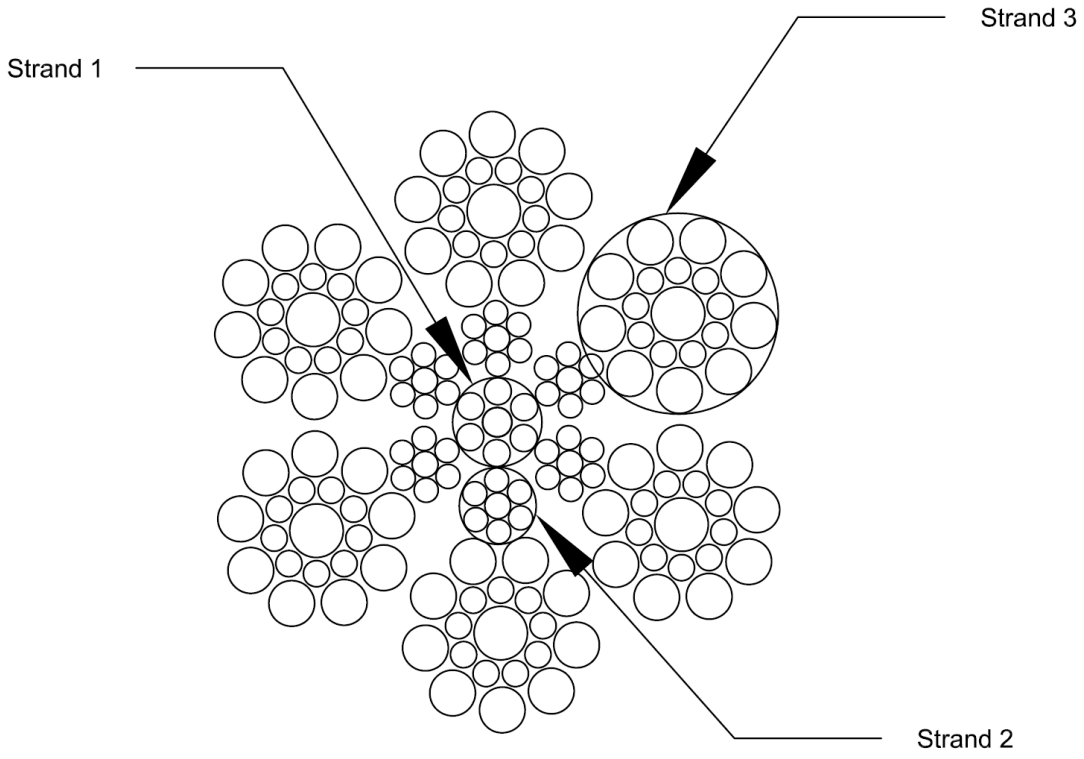

Figure 3-9: Cross section of the 6×19 Seale wire rope

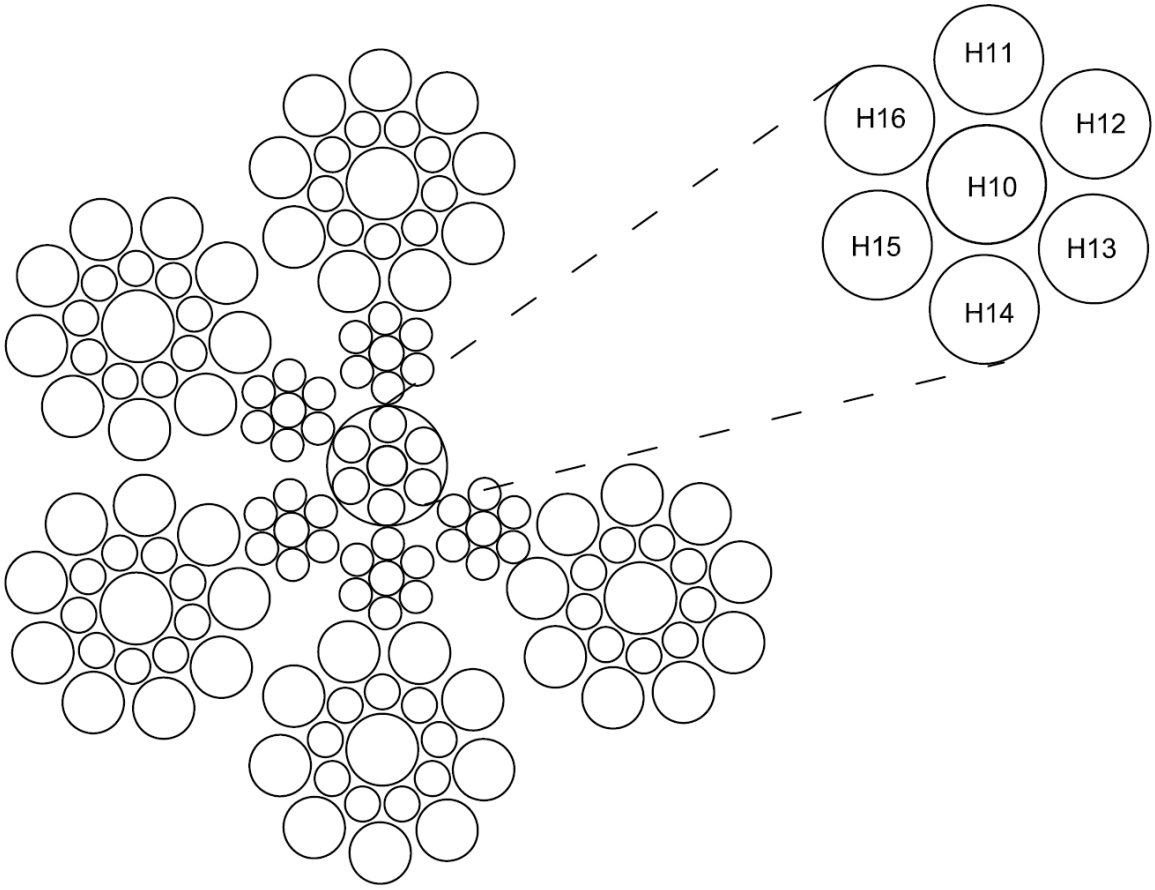

Figure 3-10: Nomenclature for the wires of strand 1 of the 6×19 Seale wire rope

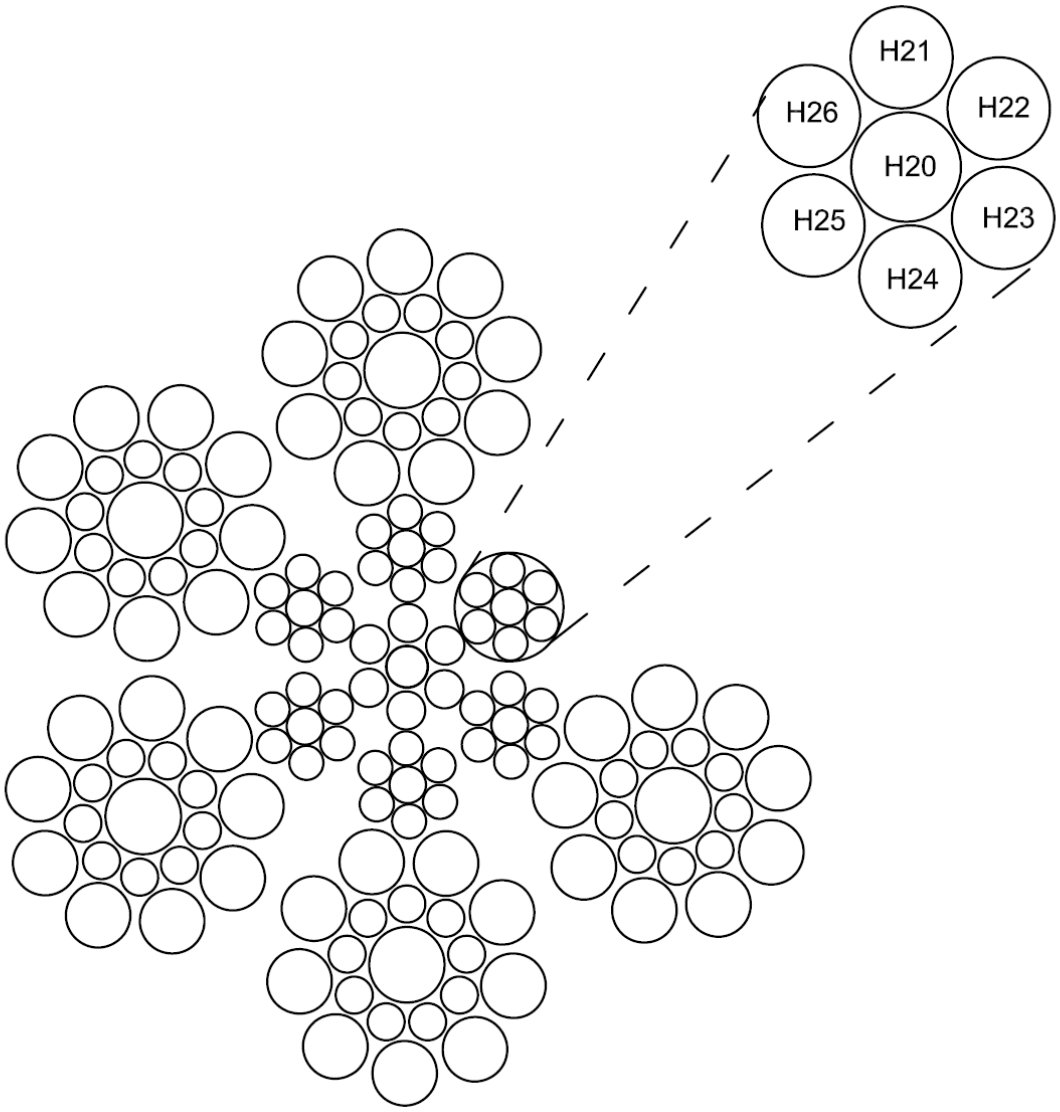

Figure 3-11: Nomenclature for the wires of strand 2 of the 6×19 Seale wire rope

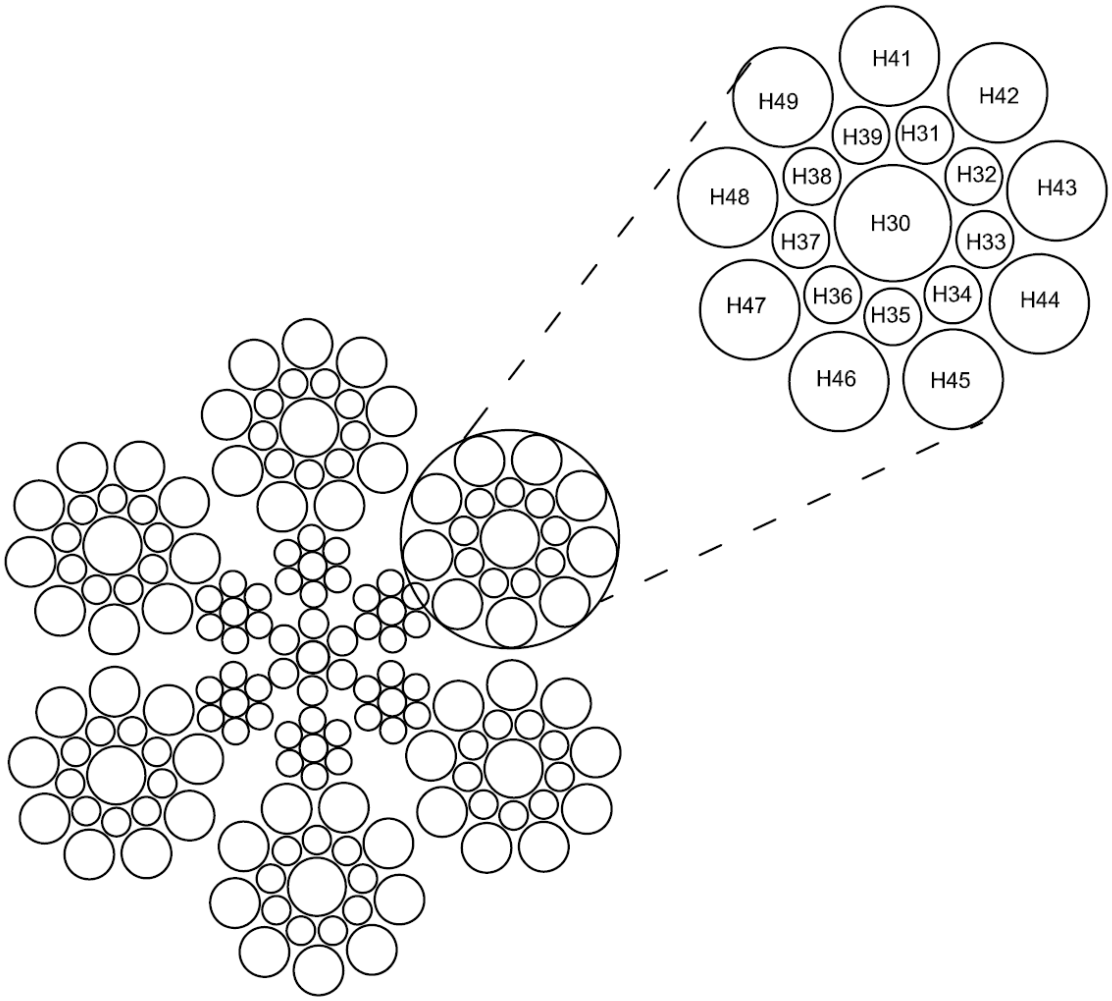

Figure 3-12: Nomenclature for the wires of strand 3 of the 6×19 Seale wire rope

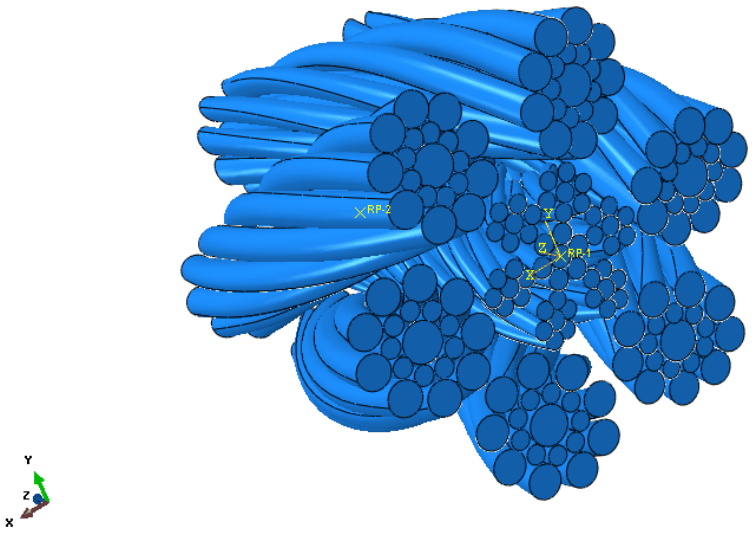

Figure 3-13: Geometry of the 6×19 Seale wire rope

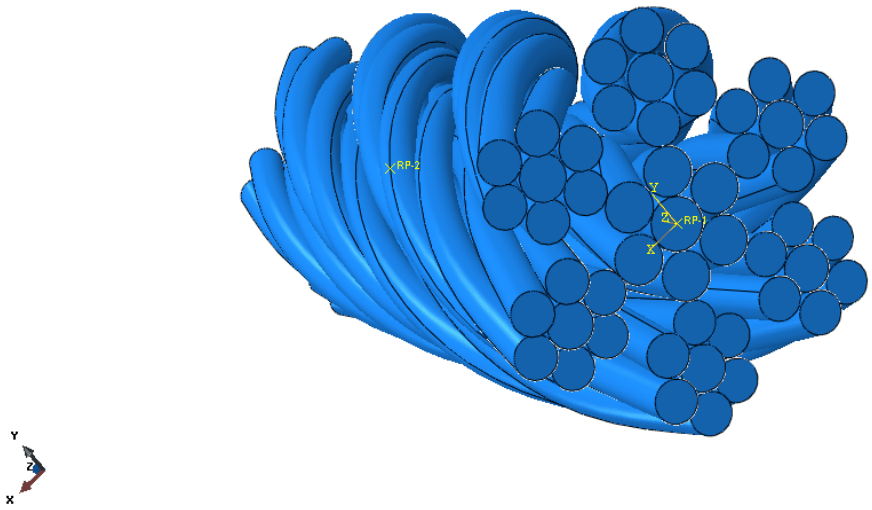

Figure 3-14: Geometry of the IWRC

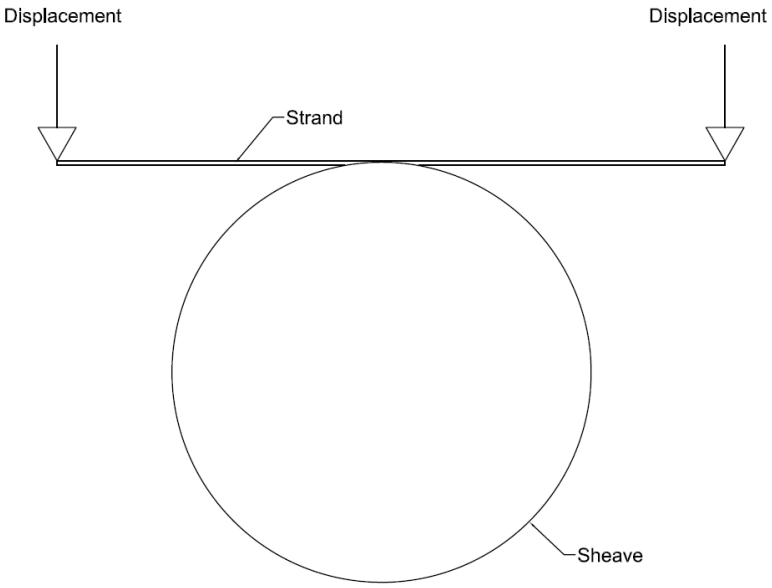

Figure 3-15: Schematics of load on wire strand to be bent over a sheave

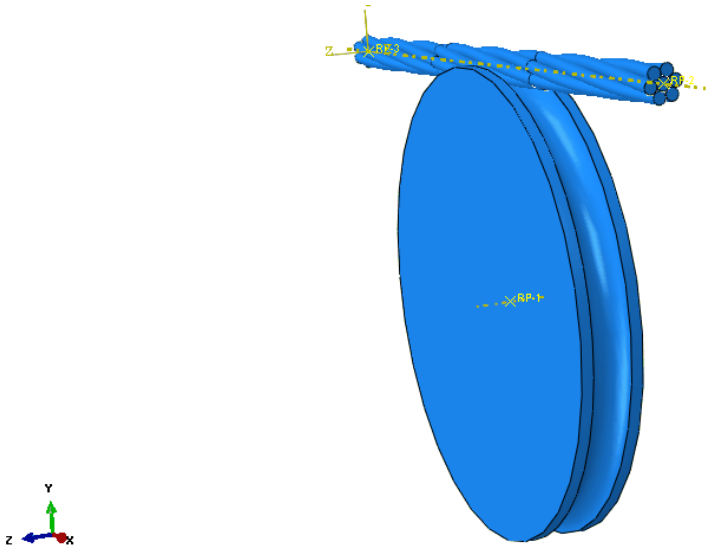

Figure 3-16: Geometry of a 7-wire strand on a sheave

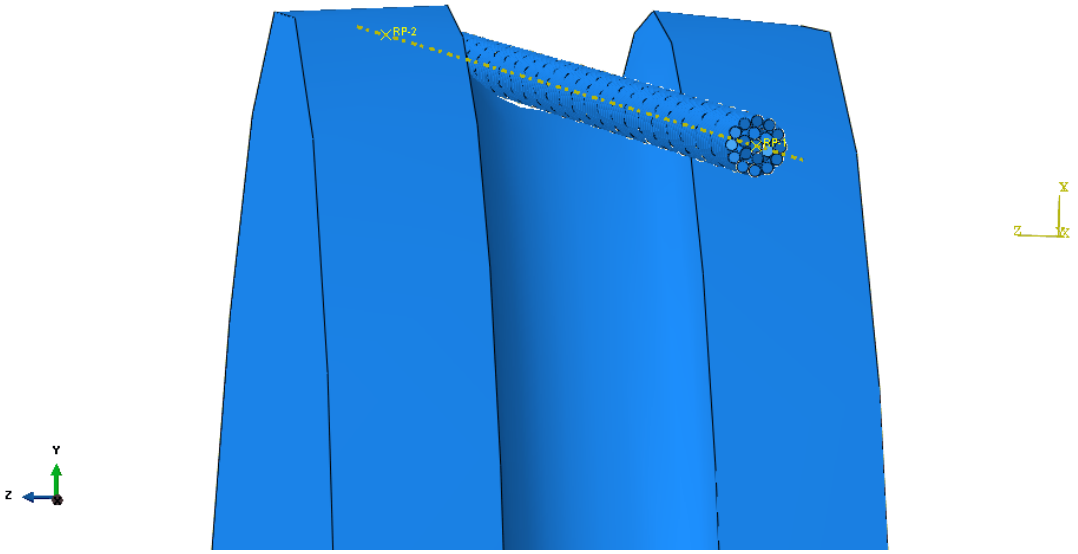

Figure 3-17: 19-wire strand on a sheave for D/d=90.9

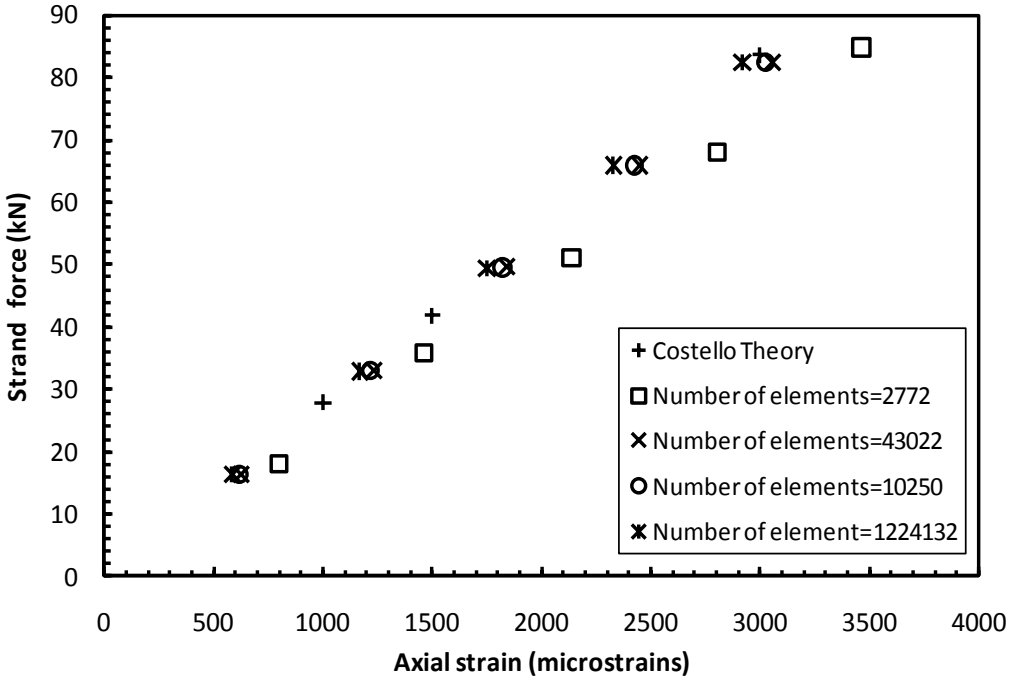

(a) Mesh refinement using the stiffness

Figure 3-18: Mesh refinement study for 7-wire strand in tension (using C3D8R elements and model of one lay length)

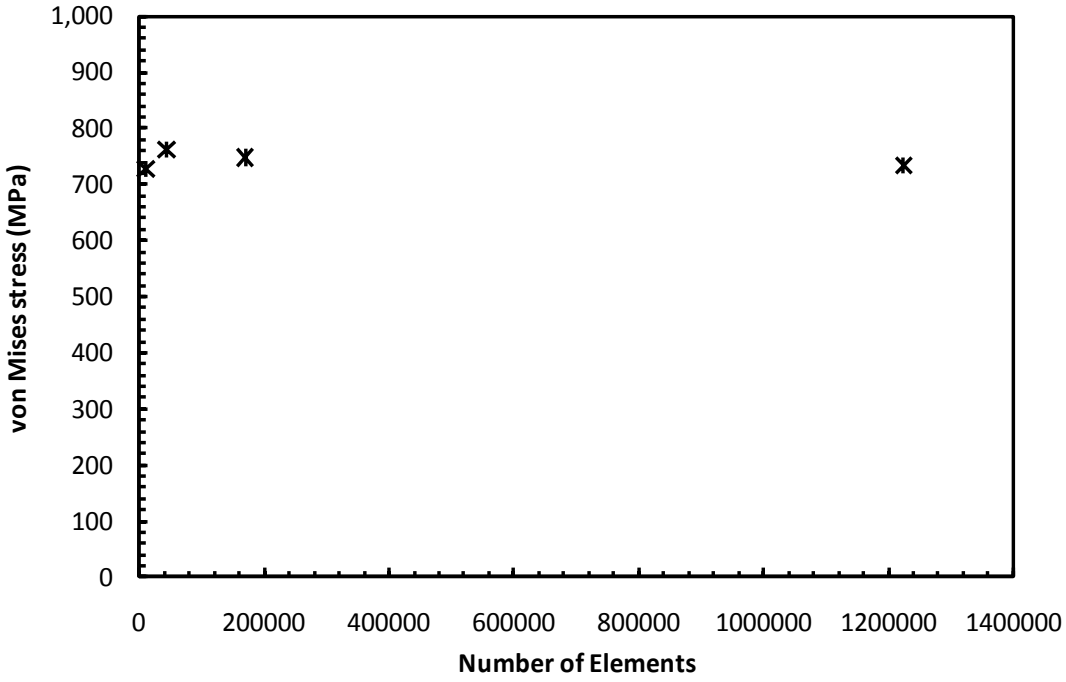

(b) Mesh refinement using the von Mises stress

Figure 3-18: (Cont'd)

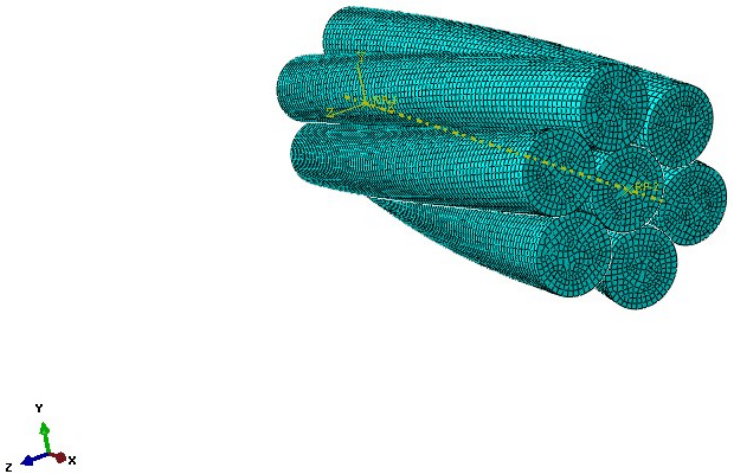

Figure 3-19: Overall view of the mesh for 7-wire strand (1,224,132 elements)

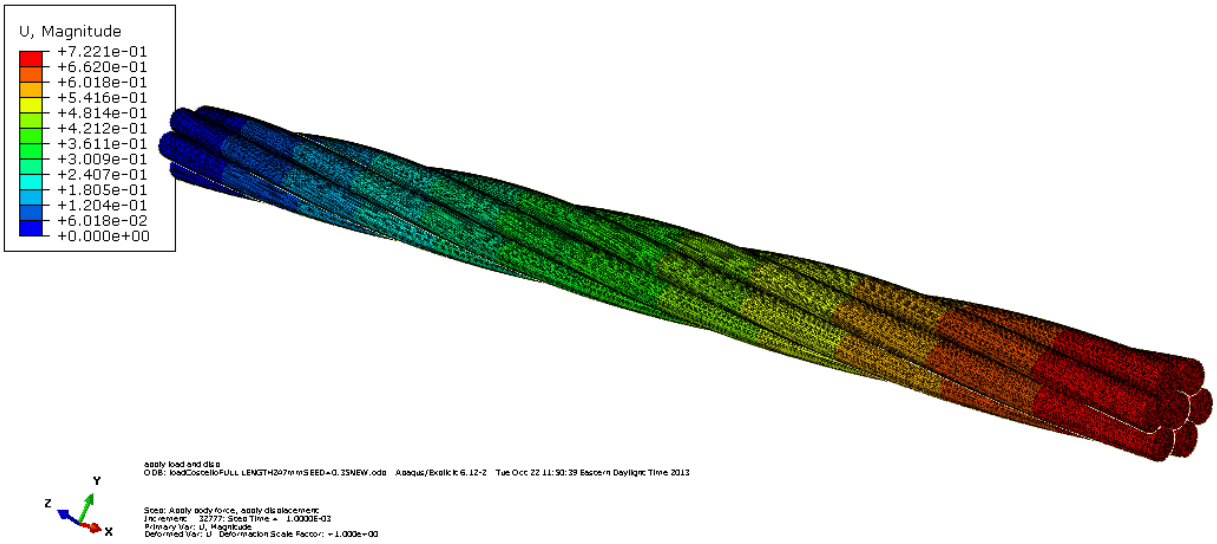

Figure 3-20: Costello 7-wire strand (length= one lay) showing the displaced strand

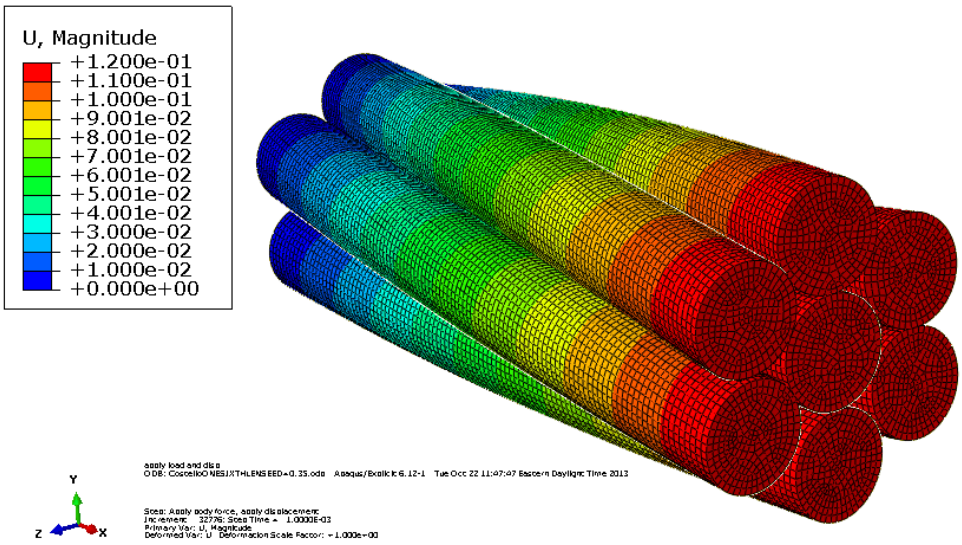

Figure 3-21: Costello 7- wire strand (length= one sixth of the lay length) showing the displaced strand

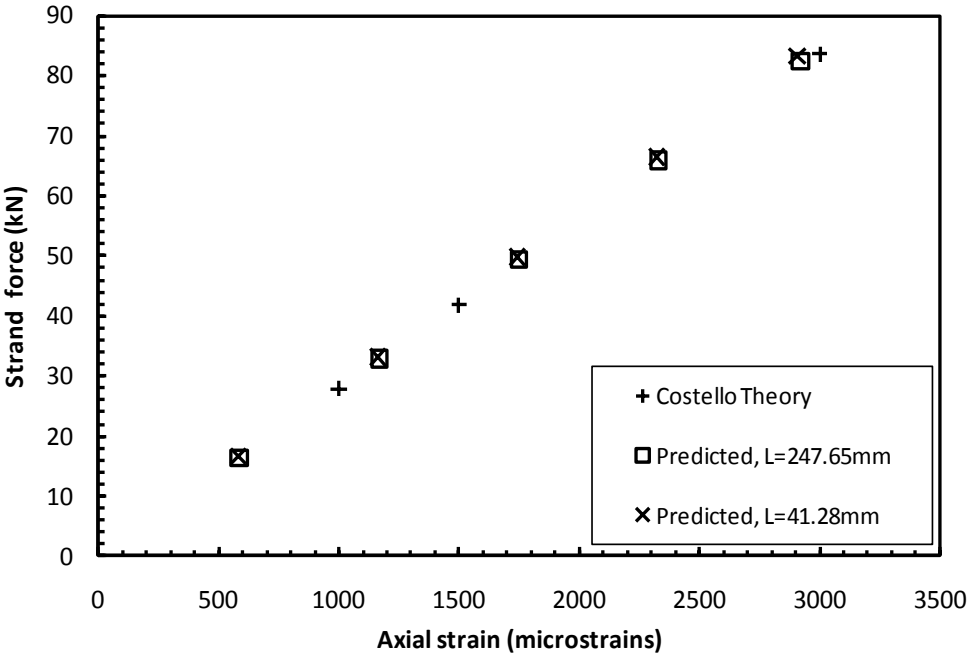

Figure 3-22: Stiffness prediction for various strand lengths

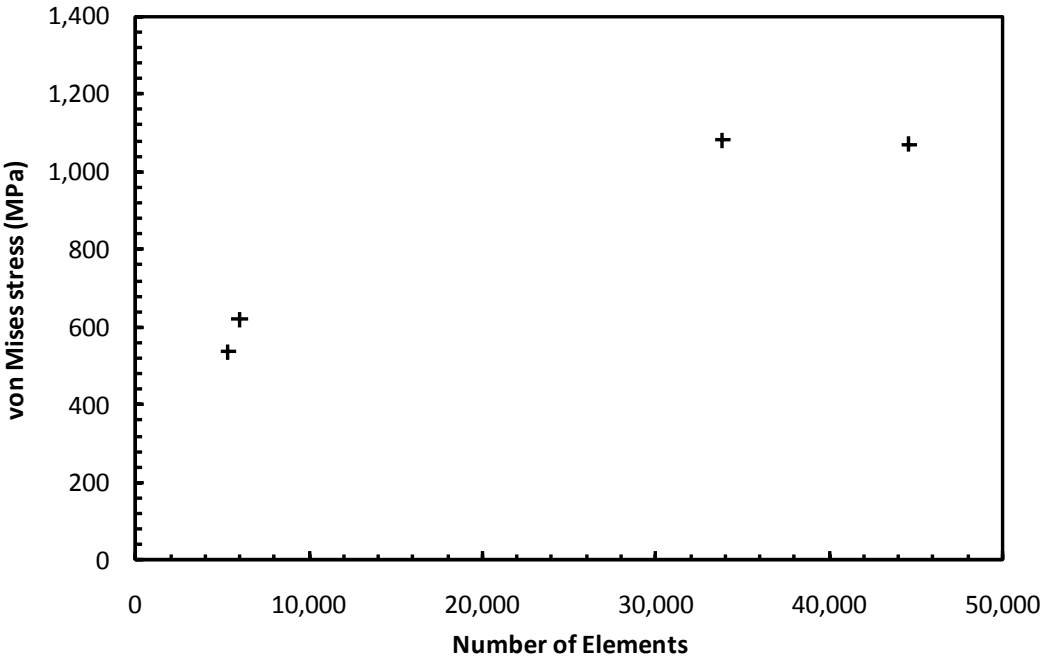

Figure 3-23: Mesh refinement study for 19-wire strand in tension (C3D10M elements)

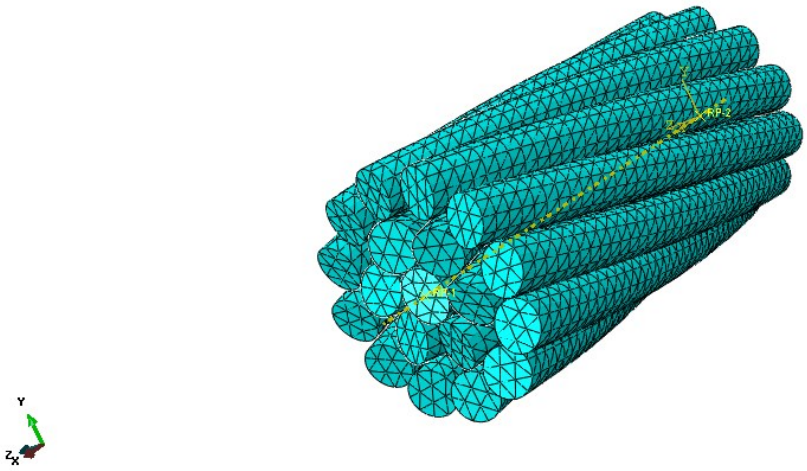

Figure 3-24: Overall view of the mesh for 19-wire strand

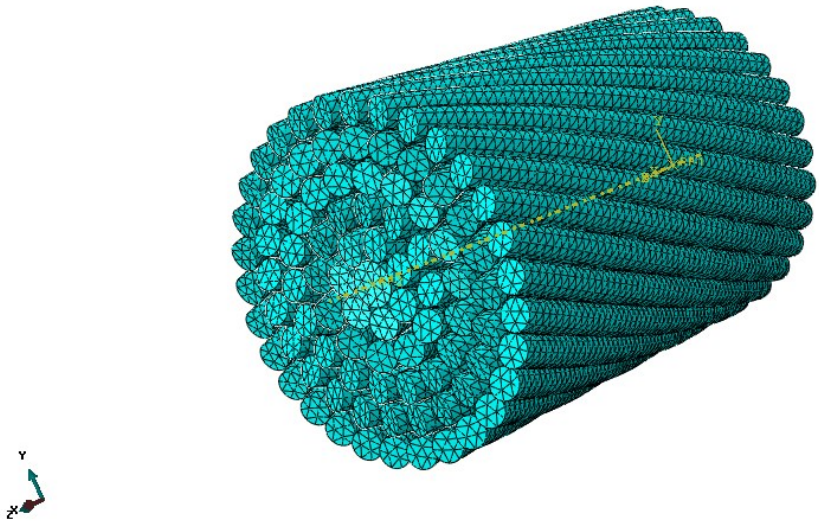

Figure 3-25: Overall view of the mesh for 92-wire strand

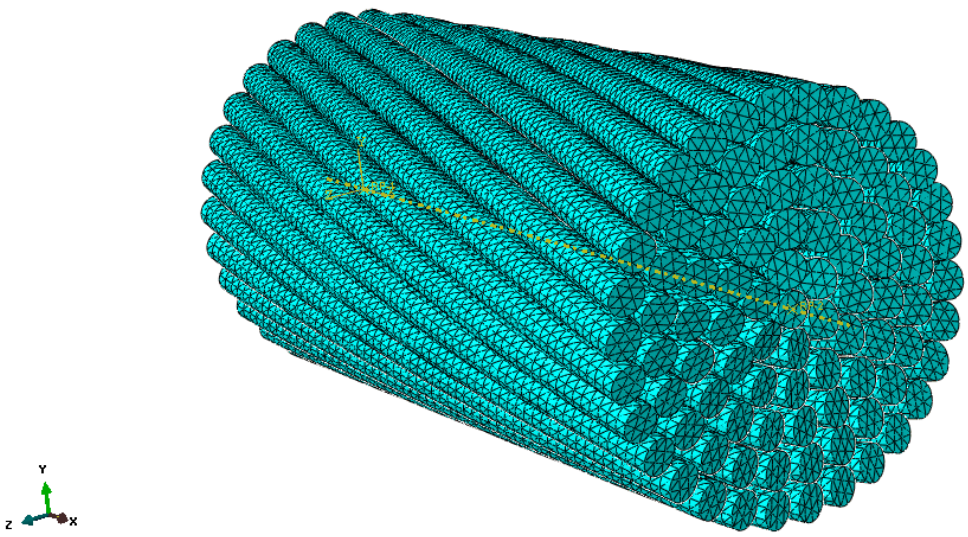

Figure 3-26: Overall view of the mesh for 91-wire strand

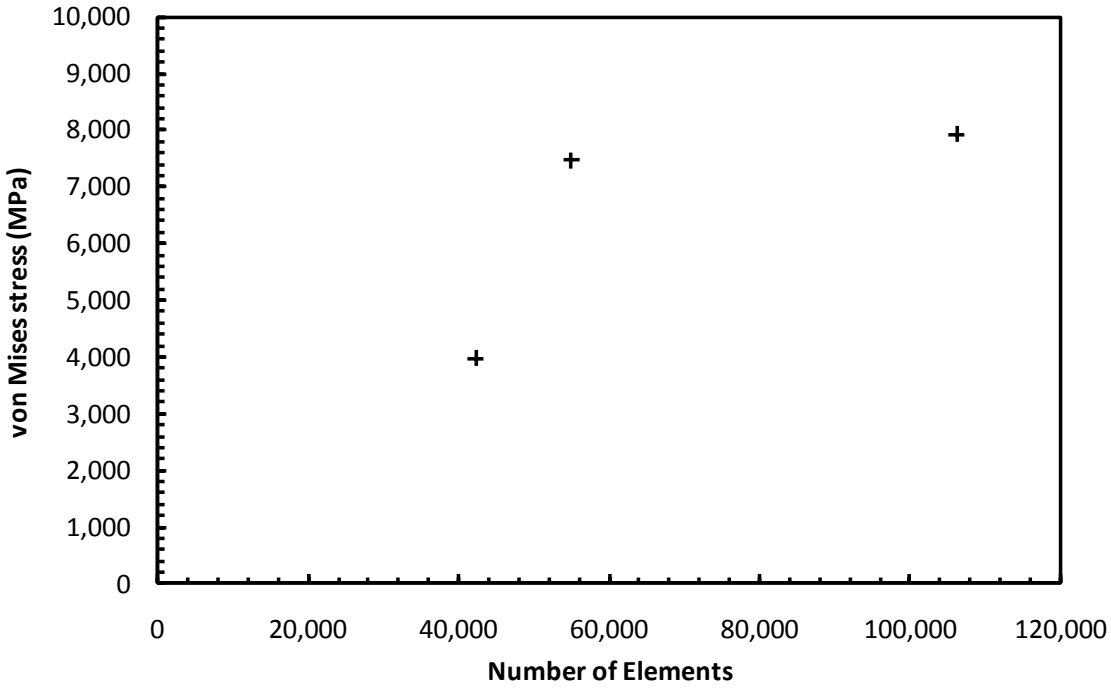

Figure 3-27: Mesh refinement study for 6×19 Seale wire strand in tension (C3D10M elements)

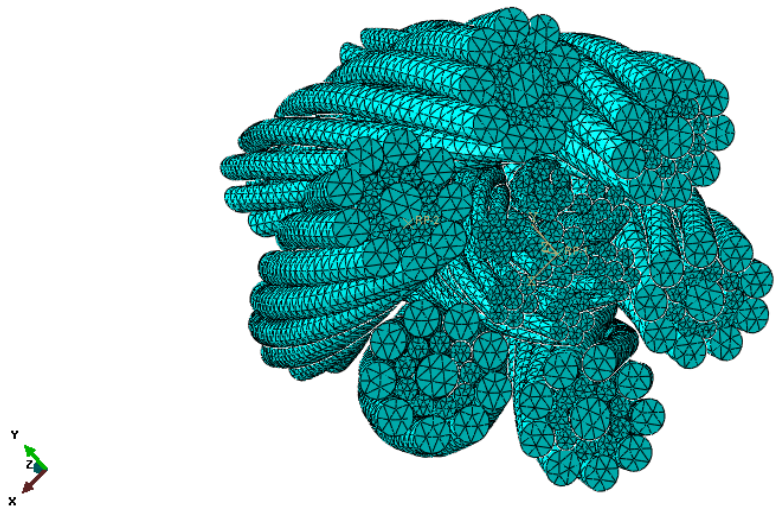

Figure 3-28: Overall view of the mesh for the 6×19 Seale wire rope

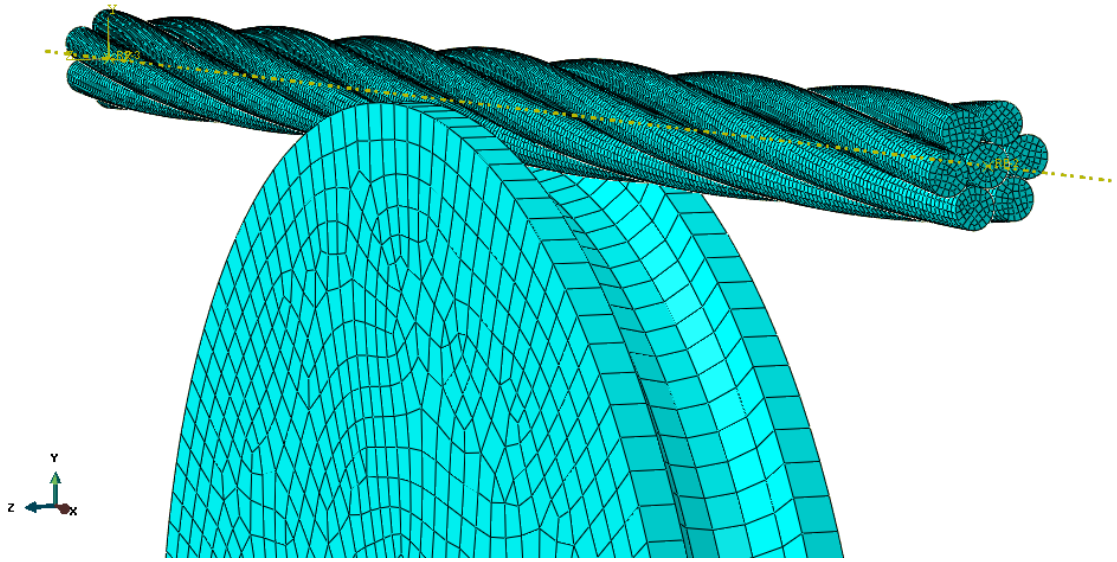

Figure 3-29: Overall view of the mesh for 7-wire strand on a sheave

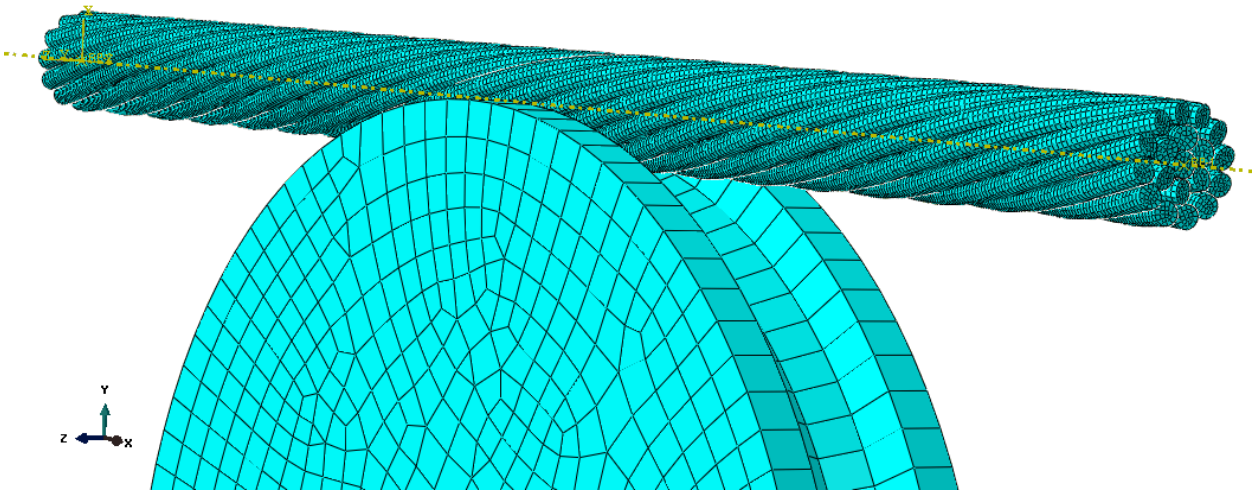

Figure 3-30: Overall view of the mesh for 19-wire strand bent on a sheave

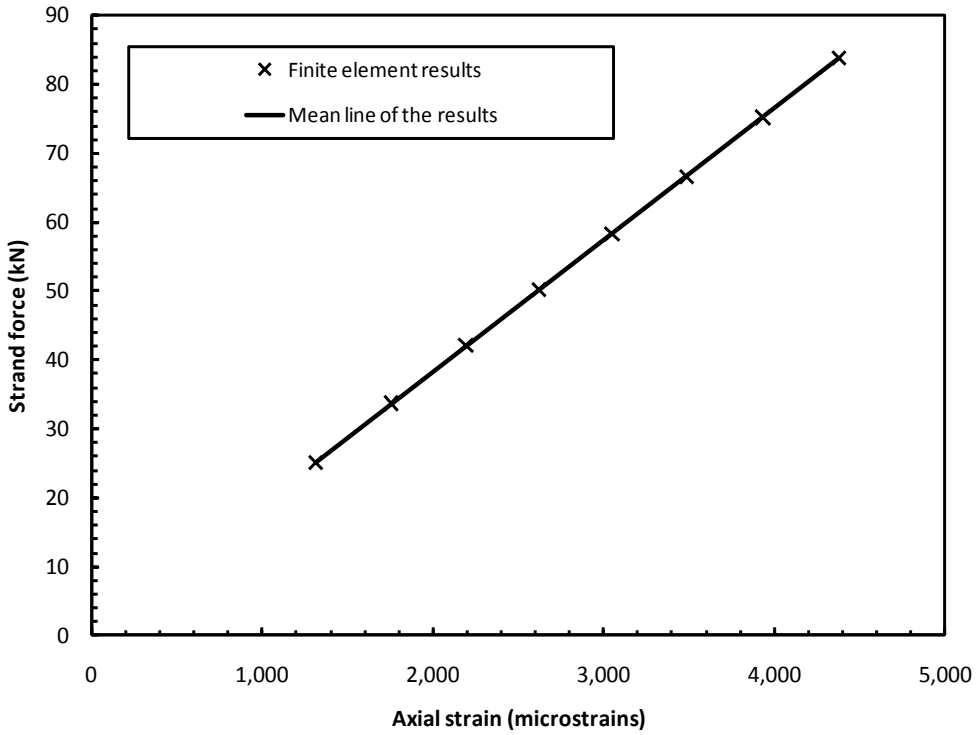

Figure 3-31: Strand force versus strain for 12.7 mm ASTM A416 prestressing strand

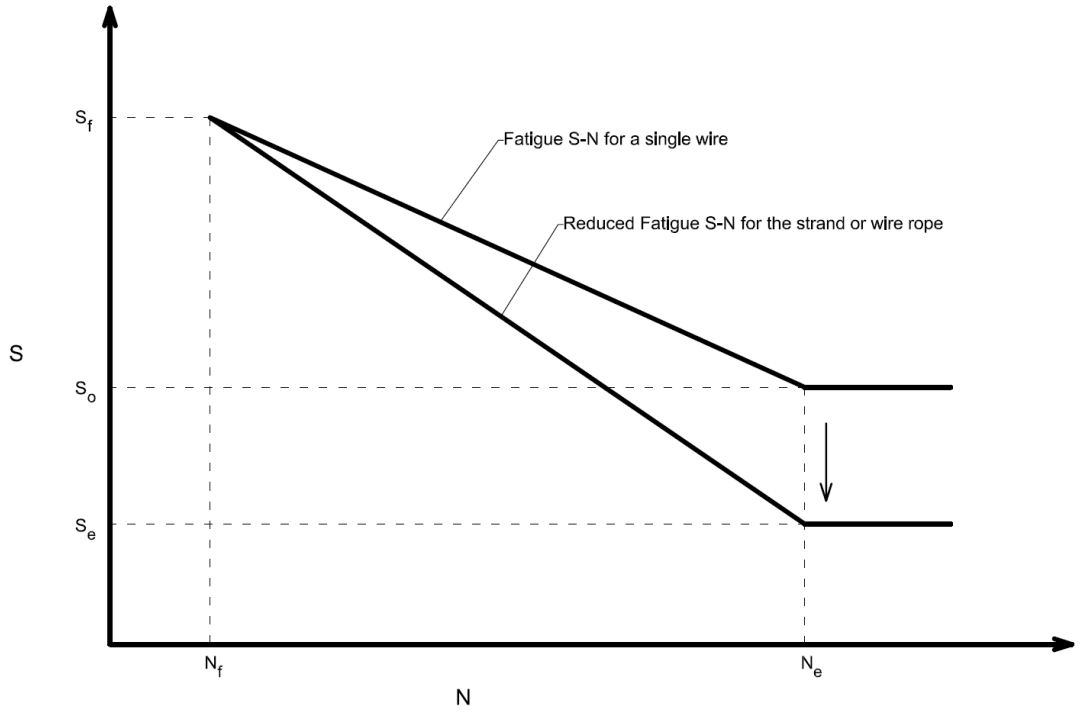

Figure 3-32: Fatigue S-N Plot

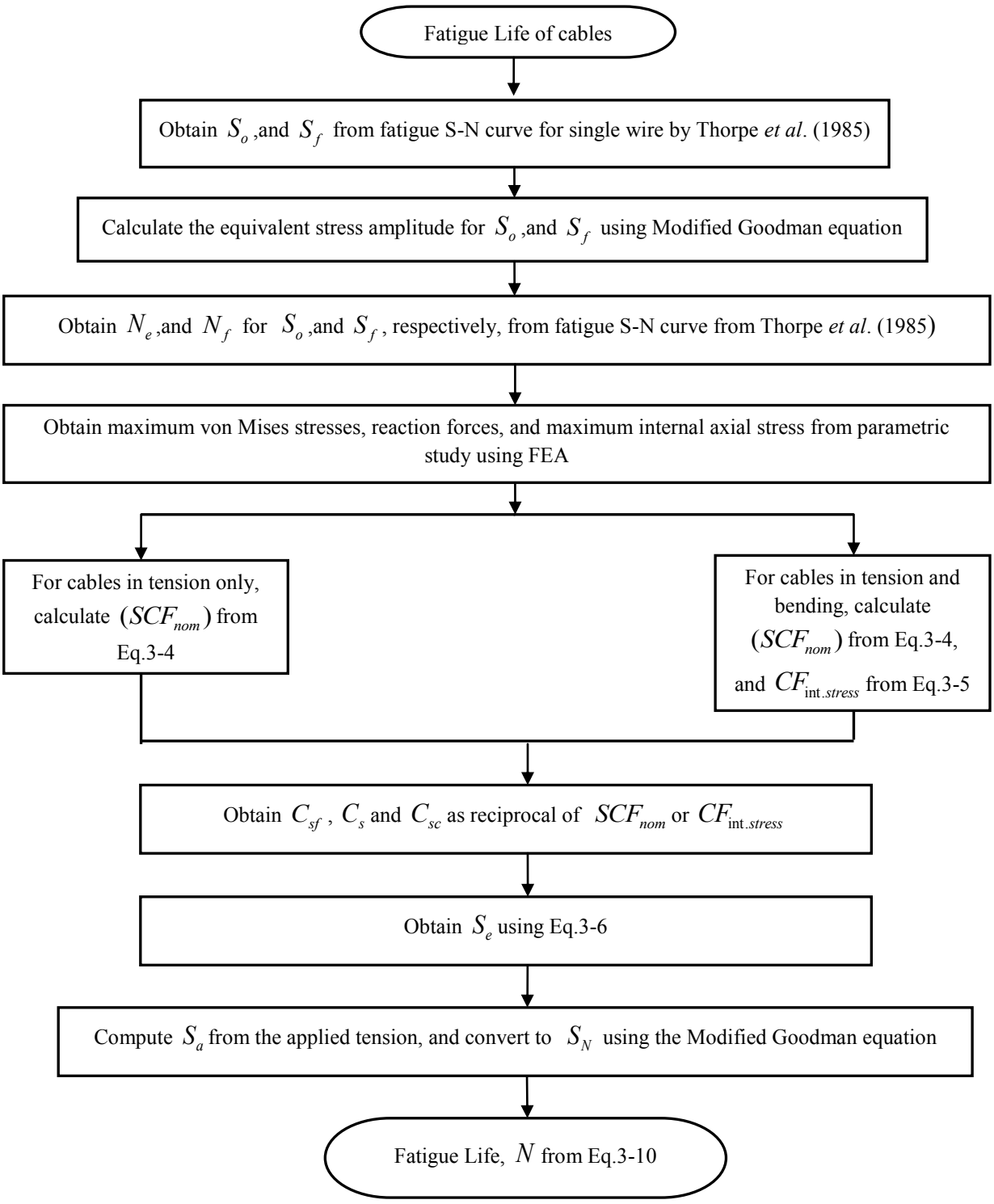

Figure 3-33: Flow chart for obtaining the fatigue life for cables

CHAPTER 4

FINITE ELEMENT RESULTS AND FATIGUE LIFE FOR TENSION ONLY CABLES

4.1 INTRODUCTION

The effects of stress amplitude, diameter of strand and lay length on stresses and fatigue resistance were investigated for a number of 7-wire ASTM A416 prestressing strands. Models of a 7-wire strand were developed using the finite element method previously described in Chapter 3. The strand models developed had diameters of 6.4, 7.9, 9.5, 11.1, 12.7 and 15.24 mm. The finite element analyses results for 19, 91, and 92-wire strands, 6×7 wire rope (IWRC) and a 6×19 Seale wire rope subjected to tension will also be presented. Applied boundary conditions and loads were previously discussed in Chapter 3. The stress concentration and the stress correction factors will be obtained from the results of the tension analysis using the finite element method. Fatigue life prediction models were then derived from fatigue S-N curve of a single wire tested by Thorpe *et al*. (1985) using a stress based approach. The effect of inter-wire friction is included in all the analyses. Only elastic stress concentration and stress correction was considered in this research work, and yielding of the cable was ignored in the analysis.

4.2 FINITE ELEMENT ANALYSIS RESULTS

Two methods have been presented for quantifying the stress intensity, through nominal stress concentration and stress correction factors. The nominal stress concentration factor (SCF_{nom}) has been arrived at via the conventional method used to calculate the stress concentration factor of parts of a structures as defined via Peterson's stress concentration factor (Pilkey, 1997), which involved dividing the maximum stress by a nominal stress. In the current research the SCF_{nom} is obtained through the use of Equation 3-4, by dividing the maximum von Mises stress by the nominal stress (applied force divided by the summation of the areas of the individual wires that make up the cable). The use of the maximum von Mises stress as the maximum stress is because, 1) Fatigue failure is a shear failure. Even if the fatigue crack initially starts as a tension crack it quickly changes it orientation to a shear crack, 2) Fretting fatigue

behaviour of a part is dependent on factors such as frictional shear stresses, amplitude of the relative motion, normal contact pressure between the surfaces in contact, the magnitude of applied mean or alternating stresses (Stephens *et al*. 2001), and von Mises stress seems to capture almost all of these factors. Using the contact stress only, is a bit simplistic for the failure condition under fretting fatigue, but the von Mises stress also includes the effect of contact stresses as well as other multi-axial stresses that are occurring in a cable. A similar approach for calculating the stress concentration factor was used by Wokem and Grondin (2010), the difference is that the maximum stress was the maximum principal stress. The alternative method, using a stress correction factor ($CF_{\text{int}.stress}$) obtained using Equation 3-5, and it uses the maximum internal axial stress obtained as the maximum internal axial strain along the axis of the strand multiplied by the modulus of elasticity of a wire, in ratio to the von Mises stress. A similar approach of using the $CF_{\text{int}.stress}$ was initially proposed by Raoof (1990) and Hobbs and Raoof (1996) for obtaining the fatigue life of strands, but their approach uses an analytical formula proposed by Thomas and Hoersh (1930) to compute the maximum von Mises contact stress under a contact surface at a depth below the surface of the cable in tension and they obtained the nominal wire axial stress using an analytical formulae. Their approach was used for strands, but could become very complicated for use in wire ropes, where the strands and wires of the wire ropes are laid in different directions and the same is true when cables are subjected to tension and bending. The current research uses a numerical method to obtain the maximum von Mises stress and the maximum internal wire stress for strands and wire rope in tension or bending over sheaves. Both factors have been used here to estimate the fatigue life of strands and wire ropes. The conventional approach for predicting the fatigue life of parts of a structures makes sole use of SCF_{nom}, but where wire ropes are concerned it may be necessary to use $CF_{\text{int}.stress}$, to account for inter-wire strains within the strand or wire rope.

4.2.1 Effect of load amplitude and strand diameter on the stresses for ASTM A416 7-wire prestressing strands

The effect of load range and strand diameter for six 7-wire ASTM A416 prestressing strands was investigated. It was shown in Chapter 3, that the stiffness of the short finite element model (length of 1/6 lay length) of the 7-wire strand was representative of the measured modulus of elasticity by Heller (2003) and the modulus predicted using Costello's Theory (Costello,

1997). A comparison between the behaviour of the short model (length of 1/6 of the lay length) and the long model (length of 300 mm) will be carried out and is shown in Appendix B. In the meantime, the finite element results of the short model are discussed in this section.

A 6.4 mm ASTM A416 prestressing strand was evaluated with a nominal tensile strength of 40 kN (ASTM A416-99). The steel cross sectional area of the strand being 23.2 mm^2. The strand was analysed in direct tension only. Table 4-1 shows the values of the stress parameters, SCF_{nom} and $CF_{\text{int}.stress}$, which have been used to compute the fatigue life of the strand. Figure 4-1 shows the maximum von Mises stress distribution in the strand, with the maximum von Mises stress equal to 1,098 MPa for a loading of 20 kN, corresponding to 50% of the minimum breaking strength of the strand. The maximum von Mises stress occurred on the outer surface of the exterior wire, while the maximum contact stress occurred at the interface between the exterior wire and the central wire. The maximum von Mises stress is expected to be maximum at the interface between wires and not at the end, hence this may be due to boundary effects which may have been as a result of using a short model, this will be analysed as the results of more strands are modeled. It should be mentioned that although the maximum von Mises stress for this strand is at the ends, the difference in the maximum von Mises stress at the ends and at the interface between the wires is about 11%. Figure 4-2 shows the contact surfaces for the 6.4 mm prestressing strand, which are elliptical due to the helical geometry of the external wires referenced to the central or core wire in the strand. The contact patches were formed as a result of the tensile force and the geometry of the individual wires as they rolled over the adjacent wires. There are also contact patches between the external wires, but these are longer surfaces than those between the external wires and the central wire. The distribution of contact patches over a length of the central wire in the strand suggested that at that load, contact has been established between some sections of the external wire and the central wire. These contact patches are considered typical of the origin of fretting fatigue wear scars which may lead to the ultimate failure of the strands under repeated loading. Casey and Lee (1989), Cruzado *et al*. (2010) and Zhang *et al*. (2003) described wear scars remarkably similar in shape to the contact patches obtained using the finite element analysis conducted here.

A 7.9 mm ASTM A416 prestressing strand was also analyzed, with a nominal breaking strength of 64.5 kN and a steel cross sectional area of 37.4 mm^2. Table 4-2 shows the values of the stress parameters and the computed SCF_{nom} and $CF_{\text{int}.stress}$ values. These values have been

used to compute the fatigue life in this chapter. Figure 4-3 shows the von Mises stress to a maximum of 1,147 MPa for a load of 32.25 kN, representing 50% of the minimum breaking strength. As with the previous strand investigated above, the maximum von Mises stress occurred in one of the external wires of a 6 wire layer.

A 9.5 mm ASTM A416 prestressing strand with a minimum breaking strength of 89 kN and cross sectional area of 54.8 mm^2 for Grade 1860; yielded SCF_{nom} and $CF_{\text{int}.stress}$ parameters used to compute the fatigue life of the strand shown in Table 4-3. Figure 4-4 shows the von Mises stresses for a load of 45 kN, as 50% of the minimum breaking strength.

An 11.11 mm ASTM A416 prestressing strand with a minimum breaking strength of 120.1 kN and area of 69.7 mm^2 for Grade 1725; yielded Table 4-4 values of SCF_{nom} and $CF_{\text{int}.stress}$ parameters that were used to compute the fatigue life, reported in the following chapter. Figure 4-5 shows the von Mises stress in the strand when it was subjected 50% of the minimum breaking load, at 60 kN.

An ASTM A416 12.7 mm prestressing strand with a minimum breaking load of 160.1 kN and area of 92.9 mm^2 for Grade 1725; yielded Table 4-5 showing SCF_{nom} and $CF_{\text{int}.stress}$ parameters. Figure 4-6 shows the von Mises stress for a load of 83.64 kN.

Finally, a 15.24 mm ASTM A416 prestressing strand with a minimum breaking load of 260.7 kN and area of 140 mm^2, was analysed in direct tension only. The stress parameters SCF_{nom} and $CF_{\text{int}.stress}$ used to compute the fatigue life later are shown in Table 4-6. Figure 4-7 shows the model von Mises stress for a load of 128 kN.

Although the von Mises stress for all 7-wire strands evaluated show a maximum at the ends of the external wires, the von Mises stress for the internal surfaces are almost the same (with a maximum difference of 11%). Since, it is suspected that the high von Mises stress at the ends of the all the 7-wire strands were due to the use of the short models, it was necessary to compare the von Mises stress for the short models to that of the long models (length of 300 mm). Appendix B has results of the locations and magnitudes of the maximum von Mises stress for the short and long models of the 7-wire prestressing strands, and also a comparison between the magnitudes of the maximum von Mises stress for both models. The major observation was that the location of the maximum von Mises stress in the long model is more representative of what is expected when theses strands are subjected to cyclic fatigue loading, that is, the maximum von

Mises stress should be between wires and not at the ends, as seen in the shorter model. Fretting fatigue cracks will initiate at the internal surfaces rather than in the external surfaces that are not in contact. The other conclusion drawn was that, the maximum difference in magnitude of the maximum von Mises stress between the short and long models was 10%. The difference in the stress results will yield a maximum difference in slope and intercept of 0.24 and 0.57 for the mean regression fatigue life equations between the long and short strand models (Refer to Appendix B). The von Mises stress was observed to be higher at the ends rather than at the wire surfaces in contact because: from Appendix B and Table 3-1, it can be observed that, the 7-wire ASTM prestressing strand has a smaller lay angle, such that there is little inter-wire contact stress because of a large contact surface area,; so it is possible that the maximum von Mises stress is not primarily due to contact, but may have other higher stresses developed at the ends. This behaviour is expected to change if the number of layers or the lay angle is varied.

Figure 4-8 shows a plot of the maximum von Mises stress versus applied force, and it can be seen that the maximum von Mises stress is directly proportional to the applied force. As explained in Chapter 3, the finite element analysis was linear elastic, and yielding of the material was not modeled. The plot of the maximum von Mises stress versus applied stress shown in Figure 4-9 reflects a linear relationship. A regression analysis of the data shows that a relationship between the maximum von Mises stress, σ_{mv} and the applied stress may be expressed as Equation 4-1:

$$\sigma_{mv} = 1.26\sigma_{app} + 50.99 \qquad (4\text{-}1)$$

where, σ_{app} is the nominal applied stress, and the coefficient of determination, R^2 for Equation 4-1, is 0.993. The effect of lay length for a 7-wire strand in tension then becomes insignificant within the lay length specified by ASTM standards (i.e. 14 to 16 times the diameter of the strand).

4.2.2 EFFECT OF LOAD AMPLITUDE AND STRAND DIAMETER ON THE STRESSES FOR 19-WIRE STRANDS

Two 19-wire strands were modeled with one of the strands from the work of Raoof (1990) and the other tested by Papanikolas (1995). The major difference in the two strands was in the lay length or lay angle. The boundary conditions and dimensions applied are as previously described in Chapter 3. The first strand, originally presented by Raoof (1990), is

16.4 mm in diameter, has an area of 159.5 mm^2, and a breaking strength of 234 kN. Figure 4-10 (a) shows the finite element results for the strand with a maximum von Mises stress of 3,395 MPa, when the strand is loaded with a tension of 81.9 kN. The maximum von Mises stress occurred in one of the wires of layer 2 (shaded) in Figure 4-10 (b). Raoof (1990) also reported that the maximum stress in the strand should occur between the 6 wire layer and the 12 wire layer, which is layer 2 and layer 3, which was also observed in this research. Figure 4-10 (c) shows the von Mises stress distribution and the point of maximum stress for the critical wire, where all the other wires of the strand were removed. The contact stress distribution and elliptical contact patches formed in the wire can clearly be seen in Figure 4-10 (d). Table 4-7 shows the stress parameters at different load levels. It was expected, based on the results that the first wire break would be in one of the wires in layer 2 since this exhibited the highest stress concentration in the strand. It can was also observed that the difference between the SCF_{nom} and $CF_{\text{int}.stress}$ is minimal. The reason for the maximum von Mises stress in layer 2 is suspected to be because the wires of that layer had the lowest lay angle giving a condition with closely contacting wires, and the direction of lay in layer 2 and layer 3 were opposite (i.e. left and right lay), creating a critical scenario for high contact stresses compared to lays in the same direction.

The second 19-wire strand modeled was from the work of Papanikolas (1995). The strand had a diameter of 25.34 mm and a minimum ultimate tensile strength of 543 kN with an actual breaking strength of 596 kN (Papanikolas, 1995). The area of the strand was reported as 387 mm^2. Table 4-8 provides the stress parameters at various loads and Figure 4-11 (a) shows the maximum von Mises stress for the strand and an overview of the von Mises stress distribution in the external wires of the strand from the finite element analysis for a load of 150 kN. The maximum von Mises stress occurred at the central straight wire (shaded) as shown in the cross section of Figure 4-11 (b). Papanikolas (1995) reported a large number of wire breaks in the external wires (layer 3) compared to breaks in wires of other layers, which does not correspond to the location of high stress indicated by the finite element analysis at that load level, but the overall location of the maximum von Mises stress as observed in Appendix B is between layer 2 and layer 3. Figures 4-11 (c) and (d) showed the stress distribution within the interior core wire with all of the exterior wires removed. Again the contact patches were seen to be elliptical but not well distributed along the length of the wires as seen in Raoof's 19-wire strand, it is likely due to the fact that the lay length for this strand was larger than the lay length

for the strand that Raoof investigated. Layer 2 had the smallest lay angle and again creates a condition with closely contacting wires compared to the wires of other layers.

From the plot of maximum von Mises stress versus applied force shown in Figure 4-12 it can be observed that the maximum von Mises stress increases with applied load. Figure 4-13 shows that the maximum von Mises stress versus applied stress is not the same for both cables, indicating that there must be at least another parameter that affects von Mises stress. As previously explained, this observed difference may be explained due to the stress concentration or stress correction factors of both strands, commensurate with the difference in the lay angle of the strands (Refer to Chapter 3 for strand dimensions). The lay angle for the Papanikolas strand was generally larger than the Raoof strand, so larger stress concentration and correction factors would be expected for the Raoof strand, hence it agrees with the notion that the lay length or lay angle has an effect on the stress and the fatigue life of a strand.

4.2.3 EFFECT OF LOAD AMPLITUDE AND NUMBER OF WIRES ON THE STRESSES FOR 91-WIRE AND 92-WIRE STRANDS

The fatigue life of strands with a large number of wires is of considerable importance as they are often used for applications under cyclic tension, but not often bending. Raoof (1990) reviewed the performance of a 92-wire strand tested in cyclic tension by Hobbs and Ghavami (1982), and similarly Papanikolas (1995) tested a 91-wire strand in cyclic tension. These two strand types were analysed and Figure 4-14 (a) shows a maximum von Mises stress of 6,962 MPa for a load of 369 kN for the 92-wire strand. The maximum stress occurred on one of the wires of layer 4, and at the interface between layers 3 and 4, as shown by the shaded wire in Figure 4-14 (b). The high stress between the wires of layers 3 and 4 compared to wires in other layers of the strand was also commented on by Raoof (1990). Figures 4-14 (c) and 4-14 (d) show a closer view of the stress at the contact surfaces of the interior critical wire when all other wires were removed. Figure 4-15 (a) shows the maximum von Mises stress (4,905 MPa) for the 91-wire strand subjected to a load of 700 kN. Figure 4-15 (b) shows the cross section of the strand showing the critical wire (shaded). The stresses around the locations of maximum stress are shown closer in Figures 4-15 (c) and 4-15 (d), where only the critical wire is shown. The maximum von Mises stress occurred in one of the wires in layer 3, and between layers 3 and 4. Papanikolas observed in his test that most wire breaks in strands were predominantly located in

layers 3 and 4 (mainly layer 3), which is the area of high stress as indicated in the finite element analysis. Again, as before, the model showed elliptical isolated contact patches as points of stress concentration in these types of strand. Tables 4-9 and 4-10 show the von Mises stress at different load levels for the 92 and 91-wire strands, respectively and the corresponding values for the SCF_{nom} and $CF_{\text{int}.stress}$ parameters. The stresses are seen to be higher in the 92-wire strand compared to the 91-wire strand. The reason for higher stresses in the 92-wire strands compared to the 91-wire strand is again considered due to the difference in the lay length between both strands, although the numbers of wires are also marginally different in both strands. The results for both 92 and 91-wire strands tend to suggest that the most critical lay is located between layers were the summation of the lay angles are minimum compared to the combination of the lay angle in other layers, and both layers are of opposite lay direction, that is the summation of the lay angles that is minimum is between layer 3 and 4 for both the 92, and 91-wire strands, provided the lay directions are in opposite directions. Layers with the same lay direction do not result in high stresses compared to layers with opposite lay direction.

4.2.4 EFFECT OF LOAD AMPLITUDE ON THE STRESSES FOR 6×7 WIRE ROPE (IWRC)

The 6×7 wire rope (IWRC) is a wire rope of 49 wires, modeled here as an independent wire rope, although its geometry and dimensions were taken as previously described for the full 33 mm diameter 6×19 Seale wire rope (by removing strand 3) in Chapter 3. For fatigue life prediction, three diameters of this wire rope were considered: 12.6, 38.1 and 70 mm wire ropes. The latter two diameters are scaled up from the 12.6 mm diameter rope, hence only the finite element analysis results for the 12.6 mm diameter wire rope were used as the basis for the fatigue analysis considered for all other rope sizes, as the same stress concentration or stress correction factors were expected in all three size cases, as evident with the 7-wire prestressing strands. A modification factor that accounts for size of the rope will be applied to the scaled models to obtain its fatigue life. Table 4-11 shows various stress parameters discerned from the analysis of these strands as the load was varied. Also, Figure 4-16 (a) shows the maximum von Mises stress at a load level of 50 kN for the 12.6 mm diameter rope. The critical wire (shaded) relative to the wire in the cross section can be seen in Figure 4-16 (b). The location of the maximum von Mises stress at the corresponding load occurred at the central straight wire. Figures 4-16 (c) and 4-16

(d) show the interior of the wire rope where all the wires wrapped around the central core wire have been removed, such that the central wire is shown. As previously observed, similar isolated elliptical patches were evident in the core wire.

4.2.5 EFFECT OF LOAD AMPLITUDE ON THE STRESSES FOR 6×19 SEALE WIRE ROPE

One of the most frequently used wire ropes is the 6×19 Seale wire rope with IWRC. This rope is primarily used for cyclic tension and bending applications, such as might be used for cyclic wire rope hoist systems on mining shovels and draglines. One 33 mm diameter rope was analysed in tension, but the fatigue life will be predicted for two scaled up wire ropes, 49.53 and 70 mm respectively, by applying a modification factor for size effect. The dimensions of the 33 mm diameter rope were described previously in Chapter 3. Table 4-12 shows the stress parameters that were used to compute the fatigue resistance of these wire ropes at different load levels. An increase in contact stress was basically observed with an increase in load range. A maximum von Mises stress of 7,934 MPa for a load of 360 kN is shown in Figure 4-17 (a) for the 33 mm diameter wire rope. From Figure 4-17 (b) it can be seen that the critical wire was located in the IWRC. The maximum von Mises stress occurred in one of the six helical wires surrounding a central straight wire. Figures 4-17 (c) and 4-17 (d) show the highly stressed wire and the isolated elliptical contact patches distributed over the length of the wire rope, where all other wires have been removed.

4.3 FATIGUE ANALYSIS RESULTS

The fatigue life of strands and wire ropes was obtained using the mean fatigue S-N regression relationship for a single wire, as tested by Thorpe *et al*. (1985) and described in Chapter 3, applying the stresses obtained via the finite element analysis. The fatigue life was obtained by two methods: the first is the fatigue life, N_{nom}, obtained using SCF_{nom}; and the second is the fatigue life $N_{\text{int}.stress}$, obtained using $CF_{\text{int}.stress}$. Depending on the proximity between wires or the extent of lay angle, these methods can prospectively yield very different fatigue life values. It must be emphasized that the current prediction considers the fatigue life to be based on "First wire fracture in the cable".

4.3.1 FATIGUE TEST ON SINGLE WIRE BY THORPE ET AL. (1985)

Thorpe *et al*. (1985) conducted fatigue tests on single wires in air and seawater. This work focuses only on fatigue tests in air. The wires investigated by Thorpe *et al*. (1985) had diameters of 2 mm. Figure 4-18 shows the mean regression for the data to two standard deviations. The mean regression was then expressed as:

$$LogN = 56.88 - 18.50 LogS_r \tag{4-2}$$

where, S_r is the stress range in MPa, and N is the number of cycles to failure. The standard error in Equation 4-2 was discerned as 0.36, as per Appendix B reflecting the test data and regression analysis. The mean regression reflected in Equation 4-2 may then be considered to derive the fatigue resistance for all other strands and wire ropes. The fatigue life was converted to a fully reversed fatigue expression via the Modified Goodman model presented in Bannantine *et al*. (1990) and given by:

$$S_N = S_{amp} / (1 - S_m / S_{ult}) \tag{4-3}$$

where S_N is the fully reversed fatigue strength, S_m is the mean stress, S_{ult} is the ultimate tensile strength of the wire, and S_{amp} is the stress amplitude. The fatigue life in all test programs and all the predicted fatigue life were converted to an equivalent fatigue life using Equation 4-3. This conversion was necessary to set a uniform approach to compare fatigue test results from previous test programs with the predicted fatigue life outlined here. The standard error used for all prestressing strands was taken as 0.23 from the previous work of Warner and Hulsbos (1966), who conducted a high volume of fatigue test at different stress ranges generating a representative variation in fatigue life estimation.

4.3.2 FATIGUE ANALYSIS RESULTS FOR ASTM A416 PRESTRESSING STRANDS

The results of the predicted fatigue life using the stress based method will be presented and discussed. Fatigue tests on prestressing strands have been conducted by previous researchers, such that here a comparison of the predicted fatigue life to the test fatigue for various sizes of strand has been assessed. Appendix C houses the test data used for this comparison and the corresponding regression analysis.

Table 4-13 reflects applied load, and fatigue life for a 6.4 mm prestressing strand, commensurate with stress amplitude and fatigue life for loads up to 20 kN. Table 4-13 also shows the predicted fatigue life for this strand using SCF_{nom} or $CF_{\text{int}.stress}$ obtained by dividing the von Mises stress by the nominal stress and the maximum internal stress, respectively. It can be seen that there is negligible difference in the fatigue life via both factors, as seen in the ratio N_{nom} to $N_{\text{int}.stress}$.

The 7.9 mm strand was loaded in tension to a maximum load of 32.25 kN as shown in Table 4-14, reflecting the stress amplitude and the corresponding fatigue life for the strand. Table 4-14 also shows the predicted fatigue life for the strand, and again there is little difference in the fatigue life estimate, obtained via using SCF_{nom} or the $CF_{\text{int}.stress}$.

No test data in the 6.4 or 7.9 mm prestressing strand category was identified to compare to a predicted fatigue life using a stress-based approach. Figures 4-19 and 4-20 show the fatigue life and mean predicted S-N regression line for 6.4 mm and 7.9 mm strands, respectively, yielding Equation 4-4:

$$LogN = 16.75 - 4.26LogS_N \tag{4-4}$$

The 9.5 mm strand exhibited an S-N relationship as presented in Table 4-15, and this indicates that the relationship between the stress amplitude and the fatigue life follows a logarithmic profile. The maximum load in this case was recorded as 45 kN. Figure 4-21 shows a fatigue life for the 9.5 mm prestressing strand, comparable to the experimental fatigue test results conducted by Fisher and Viest (1961), with a standard error of 0.23 was used to fit the 2 standard deviations line, as shown in Figure 4-21, although not all the test data fell within the band. The predicted fatigue life is more conservative than the test data. The mean predicted S-N regression line in this case is given by Equation 4-5:

$$LogN = 15.72 - 3.88LogS_N \tag{4-5}$$

For the 11.11, 12.7 and the 15.24 mm strands the predicted fatigue life is shown in Tables 4-16 through 4-19, and also shown, is the data used to obtain the fatigue life for the strands. The predicted fatigue life are for both 250 and 270 grades for the 12.7 mm strand. As

seen previously for other 7-wire strands, the fatigue life calculated using either a nominal stress or the maximum internal axial stress, gave virtually the same result.

The comparison of the predicted fatigue life and test fatigue life for an 11.11 mm strand is shown in Figure 4-22. The comparison was made to the test results of Warner and Hulsbos (1966) and Paulson *et al*. (1983), the data from which may be found in Appendix C. The mean predicted S-N regression line is then given by:

$$LogN = 15.38 - 3.77 LogS_N \tag{4-6}$$

It should be commented that almost all the data reported by Warner and Hulsbos fell within 2 standard deviations of the mean predicted fatigue life band; and only a few data fell outside the band for the test data reported by Paulson and others.

Figure 4-23 shows the predicted and the test fatigue life for the 12.7 mm strand, which exhibited an ultimate strength of 1725 MPa, where it can be seen that the test data sourced from Muller and Zeller (1975) fall within 2 standard deviations of the mean. The mean predicted S-N regression line is described by:

$$LogN = 15.56 - 3.83 LogS_N \tag{4-7}$$

A 12.7 mm strand with a tensile strength of 1860 MPa displayed a fatigue behaviour reflected in Figure 4-24, where the predicted fatigue life was compared to fatigue test data after Heller (2003). This was also shown to fall within 2 standard deviations from the mean predicted S-N regression line of,:

$$LogN = 14.93 - 3.60 LogS_N \tag{4-8}$$

Figure 4-25 shows the fatigue behaviour of 15.24 mm strands, whose predicted life was compared to test data after both Muller and Zeller (1975) and Cullimore (1972); shown to exhibit a good fit between experimental and predicted fatigue life, with only a few data external to 2 standard deviations of the mean predicted band width. The mean predicted S-N regression line here was described by:

$$LogN = 15.47 - 3.80 LogS_N \tag{4-9}$$

The results of the mean predicted S-N regression line shows that the fatigue life decrease with increase in strand diameter, and increase in load amplitude, although there seem to be very little differences in the prediction, evident in a difference in slope and intercept of the mean predicted S-N regression of 0.66, and 1.82, respectively.

4.3.3 FATIGUE ANALYSIS RESULTS FOR 19-WIRE STRANDS

Two 19-wire strands were investigated using a stress based approach. The first was a 16.4 mm diameter strand as introduced in Chapter 3. The S-N data for this strand has been presented in Table 4-20. It was noted that the fatigue life calculated using a nominal stress and that calculated using a maximum internal axial stress in the cable gave almost the same results. The analytical predictions of Raoof (1990) for 16.4 mm diameter strands with 19 wires were compared to the predicted results here. Figure 4-26 shows that the predicted mean fatigue life is almost the same as that predicted by Raoof, within 2 standard deviations (based on a standard deviation from the 19 wire strands tested by Papanikolas of 0.37). Equation 4-10 describes the mean predicted regression model:

$$LogN = 9.75 - 1.76 LogS_N \tag{4-10}$$

The second 19-wire strand was previously tested by Papanikolas (1995) and it had a diameter of 25 mm. The fatigue life for this strand seemed to be longer than for the 19-wire strand reflected in Table 4-21. For this strand it was seen that there is some difference between the predicted fatigue life using a nominal stress and that derived from using the maximum internal axial stress. This difference was attributed to the proximity of the wires to one another, such that it may be considered that the wires were not very compressed against each other. Raoof's 19-wire strand had wires that were very much in contact with each other, but Papanikolas' strand displayed some clearance between wires. This separation was very closely related to the lay length or lay angle of the wires in the strands. The test results for the 19-wire strand tested by Papanikolas (1995) were compared with the fatigue prediction conducted here, as shown in Figure 4-27. Although there seems to be a great deal of scatter in the test data reported by Papanikolas, these non-compliant results are few to justify a complete statistical analysis to make any accurate conclusions. Most of the test results fall within 2 standard deviations of a mean predicted S-Nregression line of:

$$LogN = 19.07 - 5.60 LogS_N \quad (4\text{-}11)$$

Comparing Equations 4-10 and 4-11, there exist a huge difference in slope and intercept values. This is again as previously mentioned attributed to the fact that for Raoof's model the wires were in close contact, whereas the Papanikolas strand had wires with large spacing due to lay configuration.

4.3.4 FATIGUE ANALYSIS RESULTS FOR 91/92-WIRE STRANDS

Two large multilayered strands were analysed using Abaqus/CAE. The first was a 92-wire strand with a diameter of 39 mm. This strand was initially tested by Hobbs and Ghavami (1982) and later reported by Raoof (1990), the geometry of which was described in Chapter 3. The stress amplitude and fatigue life defined using a stress based approach was presented in Table 4-22; it was observed that there is a difference between the fatigue lives obtained using nominal and maximum internal axial stress in the strand. The former is more conservative, thus recommended for such situations of greater inter-wire contact. The standard deviation (with a value of 0.21) used for the 92 and 91-wire strands were from the statistical analysis of the experiment data presented by Papanikolas (1995).The analytical and test results for the 92-wire strand presented by Raoof (1990) have been compared to the results of the analysis performed here in this research, as reflected in Figure 4-28. A mean predicted S-N regression line was established for the 92-wire strand as:

$$LogN = 9.29 - 1.54 LogS_N \quad (4\text{-}12)$$

The experimental results contained only three results and as such would not permit an accurate statistical analysis; but it can be seen that both the experimental results and analytical results here tend to fall within the 2 standard deviation lines.

The multilayered strand of 91 wires tested by Papanikolas (1995) had a diameter of 45 mm, the S-N values for which are presented in Table 4-23. The fatigue life calculated using a nominal stress again yields a more conservative estimate. Figure 4-29 shows an equivalent experimental and predicted fatigue life comparison. It should be noted that for small strands such as a 7-wire

strand, as the number of wires are small, the predicted and the experimental results are almost the same. The mean fatigue life for the 91-wire strand may be expressed as:

$$LogN = 10.42 - 2.03 LogS_N \tag{4-13}$$

Again, most of the test data falls within the 2 standard deviation band. From the plots for the 91 and 92- wire strands, it seems that the fatigue resistance for the 91-wire strand is higher than that of the 92-wire strand when a stress correction factor approach is used. But this is most likely due to an increased size (diameter) and number of contact points produced by increasing the number of wires in a 92-wire strand compared to that of a 91-wire strand.

4.3.5 FATIGUE ANALYSIS RESULTS FOR 6×7 WIRE ROPE (IWRC)

A parametric study was performed to consider the fatigue resistance of 6×7 wire ropes as the stress amplitude was increased. Three sizes of rope investigated had diameters of 12.60, 38.1 and 70 mm. Table 4-24 presents the results of the stress based approach on 12.6 mm wire rope. The S-N behaviour for this wire rope has been represented in Figure 4-30. The 38.1 and 70 mm diameter wire ropes yielded S-N data as presented in Tables 4-25 and 4-26, respectively by applying a modification for size to the finite element analysis results for the 12.6 mm diameter wire rope. It is observed from the tables that, the fatigue life calculated using a nominal stress was more conservative, again this is suspected to be because of an increased effect of lay angle or the proximity of wires in the cable.

Experimental data for IWRC and 6×19 Seale wire ropes were not available, so a proposed fatigue life estimate using finite element predicted stresses will be discussed here. For IWRC, three sizes were analysed; 12.6, 38.1 and the 70 mm diameter wire ropes. The mean regression fatigue life for the 12.6 mm wire ropes is given by Equation 4-14:

$$LogN = 11.37 - 2.36 LogS_N \tag{4-14}$$

It is evident that there is a reduction in fatigue life as the diameter reduces as reflective of the correction for size effects discussed previously in Chapter 3.

4.3.6 FATIGUE ANALYSIS RESULTS FOR 6×19 SEALE WIRE ROPE

A parametric study was carried out to investigate the impact of stress amplitude and wire rope diameter on 6×19 Seale wire ropes. The fatigue life of a 33, 49.53 and 70 mm diameter wire ropes were investigated in the study. Table 4-27 and Figure 4-31 represent the stress-life behaviour of the 33 mm diameter Seale wire rope. Tables 4-28 and 4-29 presented a stress range and corresponding fatigue life for 49.53 mm and 70 mm diameter cables.

The fatigue life of strands and wire ropes not only depend on load or stress range but also on the diameter of the cable, when subjected solely to tensile loads. In each case investigated, the fatigue life calculated using a nominal stress was seen to be more conservative than the fatigue life calculated using a maximum internal axial stress, as previously stated it is mainly because of an increased effect of lay angle or the proximity of wires in the cable.

Figure 4-31 shows the mean predicted S-N regression line for the 33 mm 6×19 Seale wire rope given by:

$$LogN = 12.08 - 2.64 LogS_N \tag{4-15}$$

4.4 FEYRER FATIGUE LIFE MODEL FOR STRANDS AND WIRE ROPES

Multiple linear regression analysis was conducted as a parametric study of the fatigue life for 7-wire, 19-wire, 91-wire and 92-wire strands, IWRC and the 6×19 Seale wire rope. The regression results may be found in Appendix D, where the variables used for the linear regression have previously been described by Feyrer (2007), for strands subjected to tension only, Equation 4-20 was suggested (Feyrer, 2007):

$$LogN = a_0 + a_1 \log \frac{2S_a}{d^2} + a_2 \frac{S_{lower}}{d^2} + a_3 \left(\frac{S_{lower}}{d^2} \right)^2 + a_4 \log d \tag{4-16}$$

Table 4-30 provides the regression coefficients obtained for each strand and wire rope case using predicted fatigue life obtained using the maximum internal axial strain. A general model that estimated the fatigue life of strands taking into account the number of wires was also presented by Feyrer (2007) as reflected by Equation 4-21:

$$LogN = a_0 + a_1 \log \frac{2S_a}{d^2} + a_2 \frac{S_{lower}}{d^2} + a_3 \left(\frac{S_{lower}}{d^2} \right)^2 + a_4 \log d + a_5 \log z \quad (4\text{-}17)$$

where, S_a is the force amplitude, S_{lower} is the mean force less the force amplitude, d is the strand or wire rope diameter, and z is the number of wires in the strand. For strands and wire ropes that are closely in contact with each other before being put into use, the fatigue life model using a nominal stress was shown to be more appropriate and more conservative; so Equation 4-16 or Equation 4-17 should be used with the regression coefficients shown in Table 4-31. It was necessary to present at least a visual comparison between the predictions in the current research and the predictions by Feyrer (2007) model; this comparison is not aimed at making definite conclusions, since the wire constructions or materials are different for both predictions. The S_{lower}/d^2 used for the following plots is zero, the specific force is defined by Feyrer (2007) is the force divided by the square of the cable diameter, S/d^2 .The plots of the predictions for 16 mm IWRC with steel (current research) and a IWRC made up of natural fibre core (Feyrer (2007)) is shown in Figure 4-32. A plot of the predicted fatigue life for a 12.5 mm diameter 6× 19 Seale wire rope using Equation 4-16 and the predicted fatigue life for the same diameter 6× 19 Warrington wire rope with IWRC using the coefficients proposed by Feyrer (2007) is shown in Figures 4-33. Figure 4-34 shows the predicted fatigue life for a 16 mm diameter 6×19 Seale wire rope with different cores (IWRC and natural fibre core (NFC)) using the current research prediction and Feyrer's model , there is very little basis for comparison as mentioned previously, since the construction or material of the wire ropes are different, and the current research predicts the failure as fracture of the first wire, while Feyrer (2007) defines failure as complete wire rope breakage. In all cases compared by visually, the fatigue predictions using both predictions are not far apart. This predictions will definitely vary as the S_{lower}/d^2 is varied amongst other factors, and as the S/d^2 is also varied. DNV-OS-E301 providing parameters for the S-N curve to be used for tension fatigue of stranded and spiral ropes. A slope of 4.0 and 4.8 is recommended for stranded and spiral strands, while and intercept parameter of 3.4×10^{14} and 1.7×10^{17}, respectively. Figures 4-35 and 4-36 show the comparison between the predicted fatigue life in the current research and the recommended by DNV-OS-E301 standard for a 7-wire strand and a stranded rope, respectively. It can be observed that the recommended fatigue life for using the

recommendations from the DNV-OS-E301 is conservative, and this may also be because the current research predicts failure as first wire break.

4.5 DISCUSSION

Till date predictive models for cables subjected to cyclic tension fatigue is very limited. Feyrer (2007) has done a milestone research work in establishing a predictive model and regression coefficients for several cables, but the prediction of the fatigue life for some industrial type cables, such as, 7 and 19-wire strands, as well as the 6×7 wire rope and 6×19 Seale wire rope subjected to cyclic tension fatigue is still pending.

In this chapter finite element analysis results were presented for six ASTM A416 prestressing strands, two 19-wire strands, one 91-wire strand, one 92-wire strand, one 6×7 wire rope and one 6×19 Seale wire rope subjected to tension. The finite element results essentially yield the maximum von Mises stress, which is used to obtain the stress concentration and stress correction factors that are required for cyclic tension fatigue predictions for these cables using a stress based approach. There was no significant difference observed in the predicted fatigue life using the stress concentration or stress correction factor for the 7-wire prestressing strands, this can be attributed to the fact that the lay angle or lay length of these strands are substantially small (less than 9 degrees), such that it looks like an almost straight wire over the core straight wire. Evidently this reduces the contact pressure, but multiple contact points, which may still produce high stress concentrations, will exist in such cases because of the reduced lay length.

It was also noticed that using the short model ($1/6^{th}$ lay length) predominantly resulted in boundary effects in these 7-wire strands. This seemed to be because of the reduced contact stresses at the internal surfaces (due to reduced lay angle), it may have been possible that the stress concentration shifted to the boundaries, although in all cases the maximum difference between the maximum von Mises stress at the ends and at the internal surface was about 11%. To further investigate the implication of using a short or a long model on the magnitude and location of the maximum von Mises stress at different load levels, six long models (length of 300 mm) were generated for all six 7-wire prestressing strands investigated in the current research. Appendix B has the results for the magnitudes and locations of the maximum von Mises stress. There is evidently a shift in the location of the maximum von Mises stress from

predominantly being at the boundaries to the internal surfaces, but overall the maximum difference in magnitude of the maximum von Mises stress was 10%, which yields a maximum difference in slope and intercept of 0.24 and 0.57 for the mean regression fatigue life equations for the long and short strand models (Refer to Appendix B).

For the 19, 92, 91-wire strands, the effect of boundary conditions were negligible, as is evident in the location of the maximum von Mises stress at all load levels completely shifting to the internal surfaces (refer to Appendix B). The stress concentration and the stress correction for the 19-wire strand from the work of Raoof (1990) shows no significant difference, this can be attributed to the reduced lay angle or reduced lay length as previously observed in the 7-wire strands. The difference between the stress concentration and the stress correction can be seen in the 19-wire strand from the work of Papanikolas (1995), the 92, and 91-wire strands, as well as the 6×7 wire rope and 6×19 Seale wire rope, at this point it was conclusive that the lay angle or lay length has an effect on the fatigue life of multi-layer cables. It can be concluded that for the fatigue life predictions for multi-layer strands or wire ropes, the summation of the lay angle at two consecutive layers gives information about the critical layer, with layers with opposite lay directions being most critical than layers with same lay directions. The higher the lay angle (or lay length) the lower the von Mises stress and the higher the fatigue life. Rather than looking at the contact surface or contact stress in isolation it is best to look at it this way; an increased lay angle means an isolated contact surface will have a higher contact stress compared to a lower lay angle, but for a lower lay angle the contact surfaces are more and hence can lead to significant increase in the overall von Mises stress.

The predicted fatigue life using the stress based approach was compared with independent test programs from different researchers, and the prediction is significantly accurate. In all, a complete parametric study was conducted to investigate the effect of stress amplitude, and size or diameter of cable on the predicted fatigue life (using the stress based approach) of cables subjected to cyclic tension. Using the results of the parametric study, regression coefficients were proposed for the Feyrer`s model for 7, 19, 92, and 91-wire strands, 6×7 wire rope and 6×19 Seale wire rope.

Although in the current work it was evident that for the 7-wire strands, the shorter model did not adequately capture the realistic location of the maximum von Mises stress, it did give representative magnitudes of the von Mises stress. It may be necessary to further investigate the effect of length on the stress results for 7-wire strands. There was absolutely scarce information on the measured dimensions for wire ropes and measured stresses to further compare with the numerical model behaviour.

Table 4-1: Effect of load magnitude on SCF_{nom} and $CF_{\text{int}.stress}$ for a 6.4 mm ASTM A416 prestressing strand

Applied Load (kN)	Maximum von Mises stress (MPa)	Reaction Force (kN)	Axial Wire Strain	SCF_{nom}	$CF_{\text{int}.stress}$
8.00	450	8.03	0.001642	1.304	1.370
10.00	556	9.99	0.002048	1.291	1.359
12.00	664	11.99	0.002457	1.284	1.351
14.00	774	14.03	0.002872	1.283	1.348
16.00	880	15.98	0.003277	1.275	1.342
18.00	989	18.01	0.003691	1.275	1.340
20.00	1,098	20.02	0.004104	1.274	1.338

Table 4-2: Effect of load magnitude on SCF_{nom} and $CF_{\text{int}.stress}$ for a 7.9 mm ASTM A416 prestressing strand

Applied Load (kN)	Maximum von Mises stress (MPa)	Reaction Force (kN)	Axial Wire Strain	SCF_{nom}	$CF_{\text{int}.stress}$
12.90	479	12.90	0.001747	1.387	1.369
16.13	588	16.13	0.002181	1.363	1.348
19.35	700	19.32	0.002613	1.353	1.340
22.58	813	22.56	0.003052	1.347	1.333
25.80	925	25.84	0.003492	1.341	1.324
29.03	1,040	29.04	0.003928	1.335	1.319
32.25	1,150	32.22	0.004361	1.330	1.315

Table 4-3: Effect of load magnitude on SCF_{nom} and $CF_{\text{int}.stress}$ for a 9.5 mm ASTM A416 prestressing strand

Applied Load (kN)	Maximum von Mises stress (MPa)	Reaction Force (kN)	Axial Wire Strain	SCF_{nom}	$CF_{\text{int}.stress}$
18.00	476	18.04	0.001681	1.449	1.416
22.50	579.6	22.52	0.002098	1.412	1.381
27.00	674.1	26.95	0.002514	1.368	1.341
31.50	775.2	31.49	0.002935	1.349	1.320
36.00	883.8	36.04	0.003359	1.345	1.315
40.50	989.4	40.53	0.003778	1.339	1.310
45.00	1,093	44.95	0.004195	1.331	1.303

Table 4-4: Effect of load magnitude on SCF_{nom} and $CF_{\text{int}.stress}$ for an 11.11 mm ASTM A416 prestressing strand

Applied Load (kN)	Max. von Mises stress (MPa)	Reaction Force (kN)	Axial Wire Strain	SCF_{nom}	$CF_{\text{int}.stress}$
18.00	373.7	18.17	0.001243	1.447	1.503
24.00	475.3	23.96	0.001643	1.380	1.446
30.00	588.9	30.06	0.002057	1.368	1.432
36.00	690.8	35.95	0.002461	1.338	1.404
42.00	802.8	42.07	0.002875	1.332	1.396
48.00	901.1	47.94	0.003281	1.309	1.373
54.00	1,008	54.05	0.003695	1.301	1.364
60.00	1,112	59.98	0.004102	1.292	1.356

Table 4-5: Effect of load magnitude on SCF_{nom} and $CF_{\text{int}.stress}$ for a 12.7 mm ASTM A416 prestressing strand

Applied Load (kN)	Max. von Mises stress (MPa)	Reaction Force (kN)	Axial Wire Strain	SCF_{nom}	$CF_{\text{int}.stress}$
25.10	378.9	25.07	0.001310	1.490	1.446
33.46	484.3	33.73	0.001755	1.429	1.380
41.82	592.4	42.09	0.002191	1.398	1.352
50.19	702.5	50.19	0.002621	1.382	1.340
58.55	814.6	58.33	0.003049	1.373	1.336
66.92	926.4	66.66	0.003487	1.367	1.329
75.28	1,042	75.25	0.003933	1.366	1.325
83.64	1,158	83.89	0.004380	1.367	1.322

Table 4-6: Effect of load magnitude on SCF_{nom} and $CF_{\text{int}.stress}$ for a 15.24 mm ASTM A416 prestressing strand

Applied Load (kN)	Max. von Mises stress (MPa)	Reaction Force (kN)	Axial Wire Strain	SCF_{nom}	$CF_{\text{int}.stress}$
42.67	452.6	42.60	0.001557	1.485	1.454
53.33	547.3	53.18	0.001945	1.437	1.407
64.00	640	63.92	0.002337	1.400	1.369
74.67	737.4	74.77	0.002730	1.383	1.351
85.33	827.1	85.49	0.003123	1.357	1.324
96.00	915.1	96.09	0.003512	1.335	1.303
106.70	1,012	106.70	0.003898	1.328	1.298
117.30	1,108	117.20	0.004287	1.322	1.292
128.00	1,205	127.90	0.004677	1.318	1.288

Table 4-7: Effect of load magnitude on SCF_{nom} and $CF_{\text{int}.stress}$ for a 19-wire strand by Raoof (1990)

Applied Load (kN)	Max. von Mises stress (MPa)	Reaction Force (kN)	Axial Wire Strain	SCF_{nom}	$CF_{\text{int}.stress}$
23.42	1,081	23.52	0.000861	7.362	6.281
46.77	2,015	46.75	0.001686	6.872	5.975
70.19	3,011	70.13	0.002510	6.842	5.998
81.90	3,395	81.90	0.002924	6.612	5.806

Table 4-8: Effect of load magnitude on SCF_{nom} and $CF_{\text{int}.stress}$ for a 19-wire strand by Papanikolas (1995)

Applied Load (kN)	Max. von Mises stress (MPa)	Reaction Force (kN)	Axial Wire Strain	SCF_{nom}	$CF_{\text{int}.stress}$
45.00	304.3	45.08	0.001235	2.617	1.232
60.00	407.3	59.89	0.001434	2.627	1.420
75.00	509.2	74.30	0.001634	2.628	1.558
90.00	593	90.25	0.001733	2.550	1.711
105.00	672.6	104.80	0.001770	2.479	1.900
120.00	791.6	119.70	0.001816	2.553	2.179
135.00	923.7	134.90	0.001869	2.648	2.471
150.00	1,048	150.00	0.001934	2.704	2.709

Table 4-9: Effect of load magnitude on SCF_{nom} and $CF_{\text{int}.stress}$ for a 39 mm strand (92 wires)

Applied Load (kN)	Max. von Mises stress (MPa)	Reaction Force (kN)	Axial Wire Strain	SCF_{nom}	$CF_{\text{int}.stress}$
61.50	2,122	61.54	0.001478	31.60	7.18
123.00	3,092	123.00	0.002784	23.02	5.55
184.50	4,179	184.60	0.003986	20.74	5.24
246.00	5,227	246.00	0.005099	19.46	5.13
307.50	5,872	307.50	0.006141	17.49	4.78
369.00	6,962	369.00	0.007173	17.28	4.85

Table 4-10: Effect of load magnitude on SCF_{nom} and $CF_{\text{int}.stress}$ for a 45 mm strand (91 wires)

Applied Load (kN)	Maximum von Mises stress (MPa)	Reaction Force (kN)	Axial Wire Strain	SCF_{nom}	$CF_{\text{int}.stress}$
140.00	2,046	139.40	0.003284	17.35	4.02
280.00	2,902	279.90	0.004977	12.30	4.77
420.00	3,430	420.00	0.005847	9.69	4.84
560.00	4,246	560.00	0.006208	9.00	5.35
700.00	4,905	700.00	0.006496	8.32	5.60

Table 4-11: Effect of load magnitude on SCF_{nom} and $CF_{\text{int}.stress}$ for a 6×7 wire rope (d=12.60 mm)

Applied Load (kN)	Max. von Mises stress (MPa)	Reaction Force (kN)	Axial Wire Strain	SCF_{nom}	$CF_{\text{int}.stress}$
10.00	2,035	9.88	0.002978	14.29	3.42
20.00	3,702	20.01	0.004842	13.00	3.82
30.00	5,115	30.02	0.006430	11.97	3.98
40.00	5,950	40.05	0.007845	10.45	3.79
50.00	6,843	50.01	0.009191	9.61	3.72

Table 4-12: Effect of load magnitude on SCF_{nom} and $CF_{\text{int}.stress}$ for a 6×19 Seale wire rope (d=33.02 mm)

Applied Load (kN)	Max. von Mises stress (MPa)	Reaction Force (kN)	Axial Wire Strain	SCF_{nom}	$CF_{\text{int}.stress}$
72.00	1,710	72.06	0.003309	11.14	2.58
144.00	3,253	144.00	0.005327	10.60	3.05
216.00	4,702	216.00	0.007127	10.21	3.30
288.00	6,001	288.00	0.008842	9.77	3.39
360.00	7,934	359.90	0.01050	10.34	3.78

Table 4-13: Predicted fatigue results for a 6.4 mm prestressing strand using finite element analysis results

Applied Load (kN)	S_N **(MPa)**	N_{nom} **(Cycles)**	$N_{\text{int}.stress}$ **(Cycles)**	$N_{nom} / N_{\text{int}.stress}$
8.00	190.24	13,382,450	10,741,060	1.25
10.00	244.11	4,591,808	3,813,594	1.20
12.00	300.92	1,825,567	1,575,489	1.16
14.00	360.91	805,635	723,145	1.11
16.00	424.35	391,620	361,064	1.08
18.00	491.57	201,122	191,069	1.05
20.00	562.9	108,859	106,147	1.03

Table 4-14: Predicted fatigue results for a 7.9 mm prestressing strand using finite element analysis results

Applied Load (kN)	S_N **(MPa)**	N_{nom} **(Cycles)**	$N_{\text{int}.stress}$ **(Cycles)**	$N_{nom} / N_{\text{int}.stress}$
12.90	190.3	10,159,036	10,736,905	0.946
16.13	244.27	3,757,823	3,907,083	0.962
19.35	301	1,566,342	1,610,596	0.973
22.58	361.12	721,543	738,261	0.977
25.80	424.49	361,158	368,106	0.981
29.03	500.77	191,366	193,709	0.988
32.25	574.82	106,277	106,893	0.994

Table 4-15: Predicted fatigue results for a 9.5 mm prestressing strand using finite element analysis results

Applied Load (kN)	S_N **(MPa)**	N_{nom} **(Cycles)**	$N_{\text{int}.stress}$ **(Cycles)**	$N_{nom} / N_{\text{int}.stress}$
18.00	180.33	9,006,909	8,712,970	1.03
22.50	231.07	3,675,788	3,558,736	1.03
27.00	284.43	1,728,103	1,675,997	1.03
31.50	340.61	846,324	827,284	1.02
36.00	399.85	434,754	428,350	1.02
40.50	462.39	237,896	235,307	1.01
45.00	528.92	136,152	135,202	1.01

Table 4-16: Predicted fatigue results for an 11.11 mm prestressing strand using finite element analysis results

Applied Load (kN)	S_N **(MPa)**	N_{nom} **(Cycles)**	$N_{\text{int}.stress}$ **(Cycles)**	$N_{nom} / N_{\text{int}.stress}$
18.00	138.87	23,105,716	19,576,995	1.18
24.00	189.94	8,141,848	6,846,933	1.19
30.00	243.71	3,060,591	2,671,340	1.15
36.00	300.41	1,384,535	1,230,915	1.13
42.00	360.29	657,814	602,787	1.09
48.00	423.61	344,714	322,377	1.07
54.00	490.68	186,644	178,788	1.04
60.00	561.84	105,608	103,291	1.02

Table 4-17 Predicted fatigue results for a 12.7 mm prestressing strand using finite element analysis results (UTS = 1860 MPa)

Applied Load (kN)	S_N **(MPa)**	N_{nom} **(Cycles)**	$N_{\text{int}.stress}$ **(Cycles)**	$N_{nom} / N_{\text{int}.stress}$
25.10	136.58	13,845,274	15,526,880	0.892
33.46	186.68	5,243,551	5,868,476	0.894
41.82	239.39	2,250,519	2,462,765	0.914
50.19	294.98	1,070,158	1,141,643	0.937
58.55	353.56	551,837	577,575	0.955
66.92	415.50	304,158	314,738	0.966
75.28	481	175,991	180,467	0.975
83.64	550.40	106,306	107,860	0.986

Table 4-18: Predicted fatigue results for a 12.7 mm prestressing strand using finite element analysis results (UTS = 1760 MPa)

Applied Load (kN)	S_N **(MPa)**	N_{nom} **(Cycles)**	$N_{\text{int}.stress}$ **(Cycles)**	$N_{nom} / N_{\text{int}.stress}$
25.10	145.8	19,164,691	16,827,198	1.14
33.46	199.62	6,549,770	5,969,409	1.10
41.82	256.45	2,548,949	2,357,124	1.08
50.19	316.61	1,107,331	1,033,111	1.07
58.55	380.25	525,464	496,621	1.06
66.92	447.83	268,225	258,059	1.04
75.28	519.58	144,478	141,490	1.02
83.64	596	81,598	81,030	1.01

Table 4-19: Predicted fatigue results for a 15.24 mm prestressing strand using finite element analysis results

Applied Load (kN)	S_N **(MPa)**	N_{nom} **(Cycles)**	$N_{\text{int}.stress}$ **(Cycles)**	$N_{nom} / N_{\text{int}.stress}$
42.67	166.15	9,320,223	10,086,682	0.924
53.33	212.46	4,118,043	4,405,719	0.935
64.00	260.99	2,005,093	2,129,058	0.942
74.67	311.88	1,028,088	1,082,636	0.950
85.33	365.24	569,941	595,330	0.957
96.00	421.37	329,133	340,167	0.968
106.70	480.61	194,147	198,397	0.979
117.30	542.43	118,985	120,548	0.987
128.00	608.26	74,625	74,945	0.996

Table 4-20: Predicted fatigue results for a 16.4 mm strand (19 wires) using finite element analysis results

Applied Load (kN)	S_N **(MPa)**	N_{nom} **(Cycles)**	$N_{\text{int}.stress}$ **(Cycles)**	$N_{nom} / N_{\text{int}.stress}$
23.40	76.5	2,176,274	2,654,642	0.820
46.80	159.3	663,718	747,680	0.888
70.20	249.9	305,061	329,152	0.927
81.90	298.4	227,863	242,550	0.939

Table 4-21: Predicted fatigue results for a 25 mm strand (19 wires) using finite element analysis results

Applied Load (kN)	S_N **(MPa)**	N_{nom} **(Cycles)**	$N_{\text{int}.stress}$ **(Cycles)**	$N_{nom} / N_{\text{int}.stress}$
45.00	60.31	28,500,597	1,280,000,000	0.0161
60.00	81.44	12,885,390	145,643,379	0.0646
75.00	103.1	6,969,708	38,504,202	0.134
90.00	125.32	4,476,251	13,613,892	0.251
105.00	148.12	3,045,707	5,731,768	0.410
120.00	171.54	1,947,759	2,651,593	0.587
135.00	195.58	1,299,815	1,453,173	0.721
150.00	220.28	927,582	925,014	0.773

Table 4-22: Predicted fatigue results for a 39 mm strand (92 wires) using finite element analysis results

Applied Load (kN)	S_N **(MPa)**	N_{nom} **(Cycles)**	$N_{\text{int}.stress}$ **(Cycles)**	$N_{nom} / N_{\text{int}.stress}$
61.50	34.2	1,597,679	7,686,512	0.207
123.00	69.7	913,954	3,289,745	0.278
184.50	106.56	573,276	1,633,114	0.351
246.00	144.88	400,747	947,444	0.423
307.50	184.74	306,498	640,056	0.479
369.00	226.22	228,607	430,104	0.532

Table 4-23: Predicted fatigue results for a 45 mm strand (91 wires) using finite element analysis results

Applied Load (kN)	S_N **(MPa)**	N_{nom} **(Cycles)**	$N_{\text{int}.stress}$ **(Cycles)**	$N_{nom} / N_{\text{int}.stress}$
140.00	61.21	1,299,499	8,132,474	0.160
280.00	127.26	609,574	1,411,235	0.432
420.00	198.73	362,048	581,780	0.622
560.00	276.32	224,340	288,629	0.777
700.00	360.87	150,629	171,978	0.876

Table 4-24: Predicted fatigue results for a 6×7 wire rope (d=12.60 mm) using finite element analysis results

Applied Load (kN)	S_N **(MPa)**	N_{nom} **(Cycles)**	$N_{\text{int}.stress}$ **(Cycles)**	$N_{nom} / N_{\text{int}.stress}$
10.00	74.07	1,280,615	9,503,141	0.135
20.00	154.36	475,935	1,438,901	0.331
30.00	241.67	255,855	509,075	0.503
40.00	336.98	161,967	252,558	0.641
50.00	441.44	108,005	138,782	0.778

Table 4-25: Predicted fatigue results for a 6×7 wire rope (d=38.1 mm) using finite element analysis results

S_N **(MPa)**	N_{nom} **(Cycles)**	$N_{\text{int}.stress}$ **(Cycles)**	$N_{nom} / N_{\text{int}.stress}$
74.07	1,171,846	7,493,072	0.156
154.36	447,428	1,247,907	0.359
241.67	244,745	463,166	0.528
336.98	156,903	236,661	0.663
441.44	105,923	133,540	0.793

Table 4-26: Predicted fatigue results for a 6×7 wire rope (d=70 mm) using finite element analysis results

S_N **(MPa)**	N_{nom} **(Cycles)**	$N_{\text{int}.stress}$ **(Cycles)**	$N_{nom} / N_{\text{int}.stress}$
74.07	1,118,466	6,636,833	0.169
154.36	433,161	1,160,093	0.373
241.67	239,117	441,247	0.542
336.98	154,318	228,909	0.674
441.44	104,851	130,933	0.801

Table 4-27: Predicted fatigue results for a 6×19 wire rope (d=33.02 mm) using finite element analysis results

Applied Load (kN)	S_N **(MPa)**	N_{nom} **(Cycles)**	$N_{\text{int}.stress}$ **(Cycles)**	$N_{nom} / N_{\text{int}.stress}$
72.00	80.1	1,312,810	12,563,148	0.105
144.00	167.5	451,214	1,445,093	0.312
216.00	263.2	231,466	459,420	0.504
288.00	368.5	140,059	209,076	0.670
360.00	484.9	90,961	107,473	0.846

Table 4-28: Predicted fatigue results for a 6×19 wire rope (d=49.53 mm) using finite element analysis results

S_N **(MPa)**	N_{nom} **(Cycles)**	$N_{\text{int}.stress}$ **(Cycles)**	$N_{nom} / N_{\text{int}.stress}$
80.10	1,263,575	11,218,869	0.113
167.50	439,888	1,357,646	0.324
263.20	227,505	441,982	0.515
368.50	138,520	204,209	0.678
484.90	90,469	107,937	0.838

Table 4-29: Predicted fatigue results for a 6×19 wire rope (d=70 mm) using finite element analysis results

S_N **(MPa)**	N_{nom} **(Cycles)**	$N_{\text{int}.stress}$ **(Cycles)**	$N_{nom} / N_{\text{int}.stress}$
80.10	1,227,277	10,305,167	0.119
167.50	431,445	1,295,326	0.333
263.20	224,532	429,278	0.523
368.50	137,358	200,615	0.685
484.90	90,095	107,050	0.842

Table 4-30: Mean fatigue life prediction regression coefficients using the maximum internal axial stress

Strand or wire rope type	a_0	a_1	a_2	a_3	a_4	a_5
7-wire	10.14	-0.99	0.012	1.32E-05	0.211	-
19-wire	-27.32	17.50	0.18	0.00044	5.20	-
7 &19-wire	3.58	2.73	0.029	3.37E-05	0.80	-1.62
7,19,91,92-wire	7.42	0.54	0.017	1.78E-05	0.52	-1.05
IWRC	11.80	-2.65	-0.0021	-1.1E-06	-0.11	-
6×19 Seale	13.64	-3.60	-0.0076	-1.3E-05	-0.12	-

Table 4-31: Mean fatigue life prediction regression coefficients using the nominal stress

Strand or wire rope type	a_0	a_1	a_2	a_3	a_4	a_5
7-wire	10.00	-0.83	0.013	1.47E-05	0.01	-
19-wire	-6.35	5.75	0.069	0.00016	3.32	-
7 &19-wire	4.21	2.58	0.027	3.12E-05	0.68	-1.94
7,19,91,92-wire	5.64	1.48	0.020	1.96E-05	0.50	-1.26
IWRC	8.38	-1.23	0.00086	1.23E-06	-0.036	-
6×19 Seale	8.80	-1.42	-2.5E-06	-7.8E-07	-0.045	-

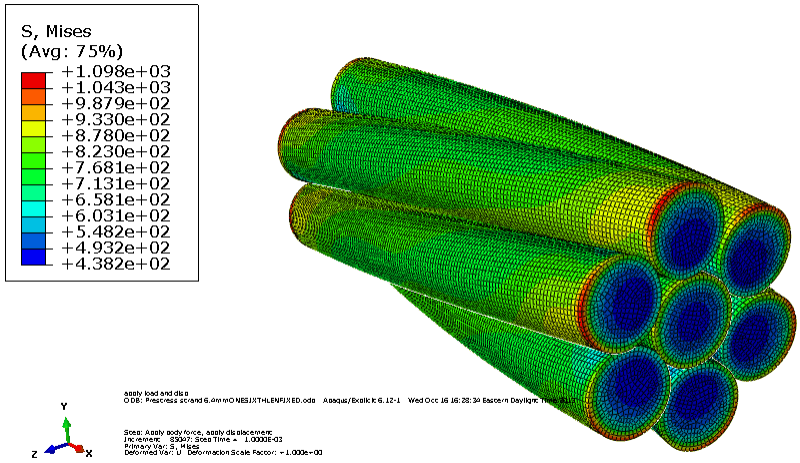

Figure 4-1: von Mises stresses in 6.4 mm ASTM A416 prestressing strand subjected to tensile force of 20 kN

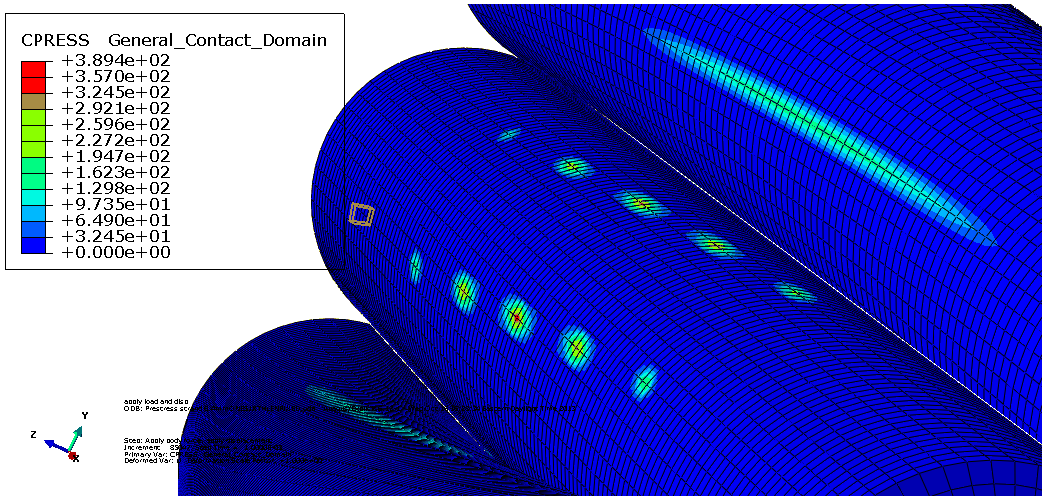

Figure 4-2: Contact stresses in 6.4 mm ASTM A416 prestressing strand subjected to a tensile force of 20 kN (1/6th lay length)

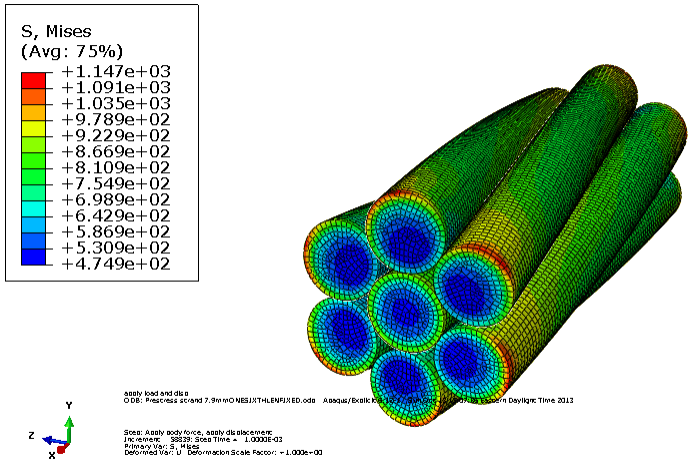

Figure 4-3: von Mises stresses in 7.9 mm ASTM A416 prestressing strand subjected to a tensile force of 32.25 kN

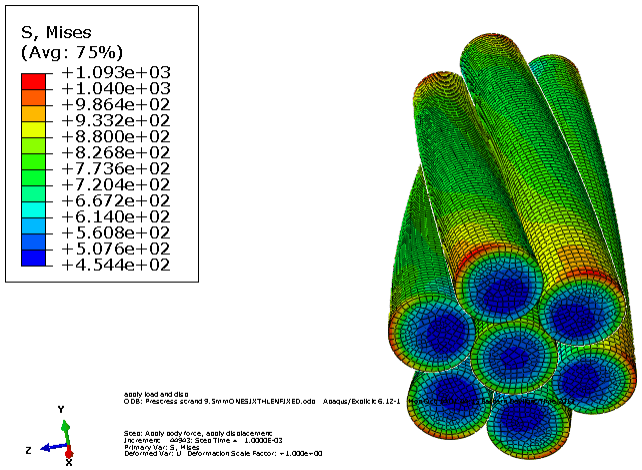

Figure 4-4: von Mises stresses in 9.5 mm ASTM A416 prestressing strand subjected to a tensile force of 45 kN

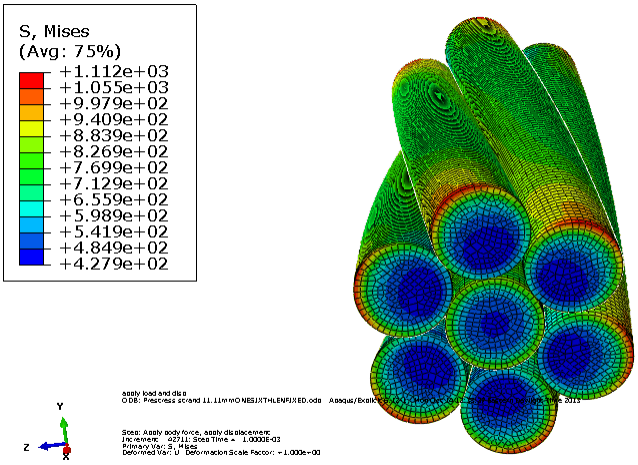

Figure 4-5: von Mises stresses in 11.11 mm ASTM A416 prestressing strand subjected to a tensile force of 60 kN

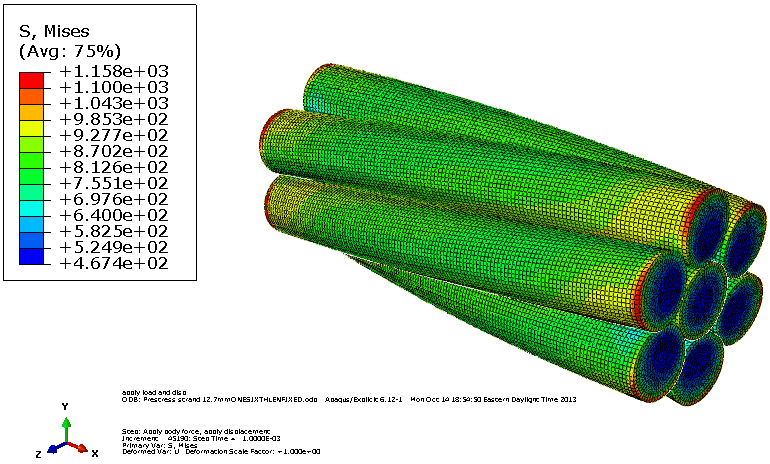

Figure 4-6: von Mises stresses in 12.7 mm ASTM A416 prestressing strand subjected to a tensile force of 83.64 kN

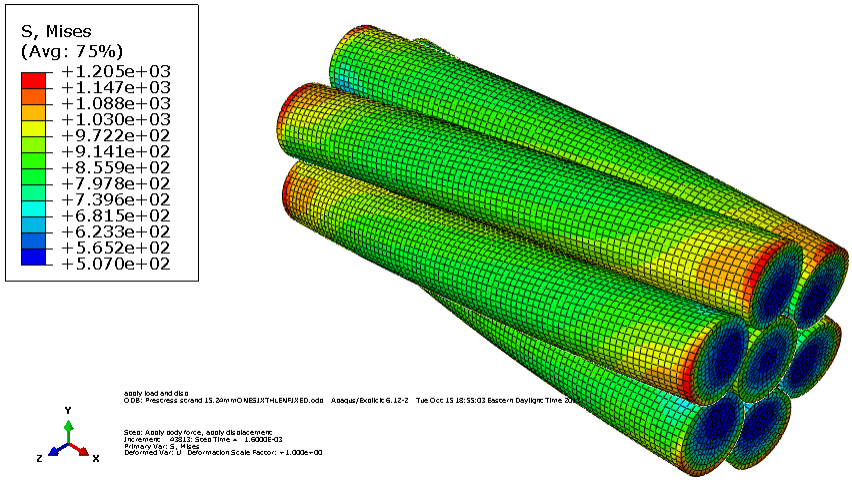

Figure 4-7: von Mises stresses in 15.24 mm ASTM A416 prestressing strand subjected to a tensile force of 128 kN

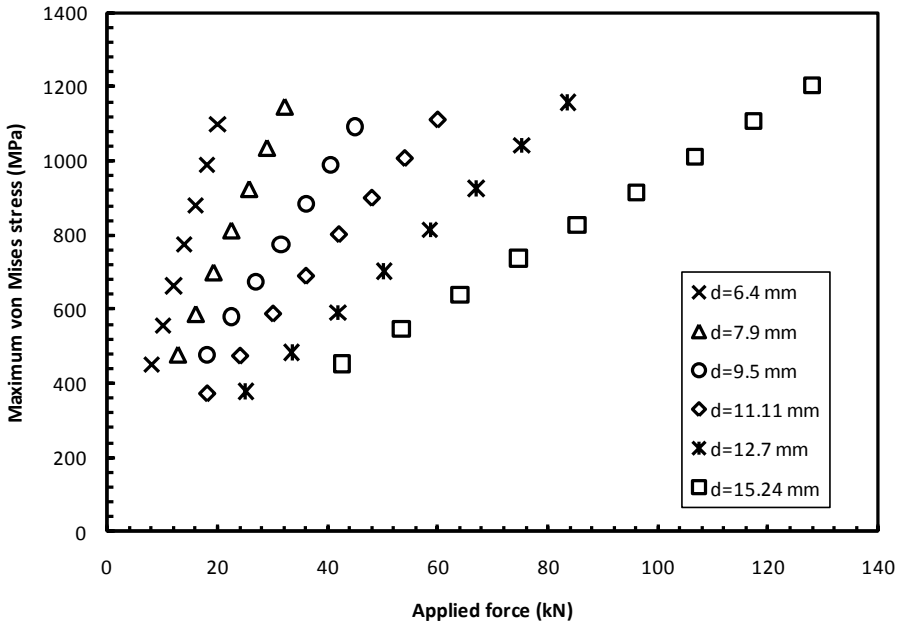

Figure 4-8: von Mises stress versus applied force for prestressing strands in tension

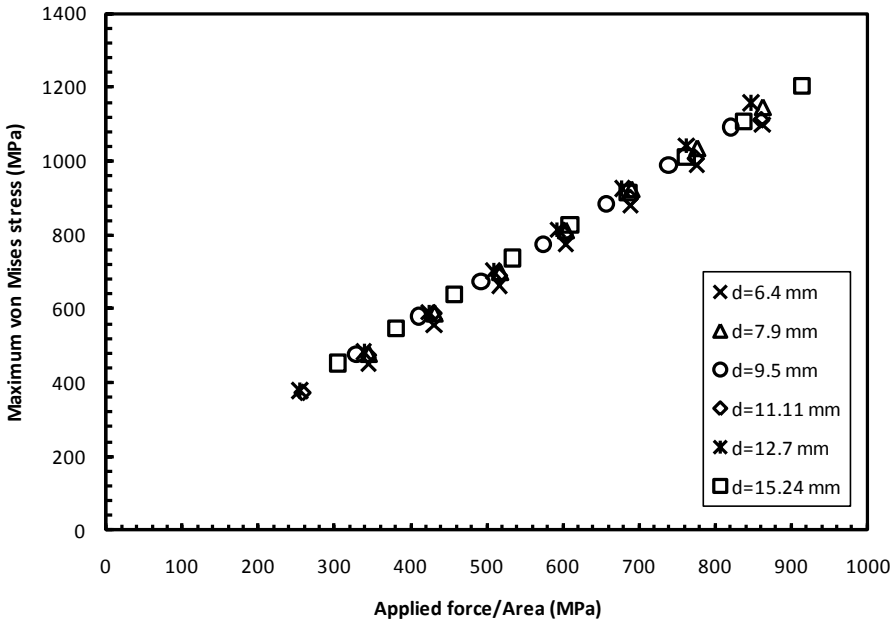

Figure 4-9: von Mises stress versus applied stress for prestressing strands subjected to tension

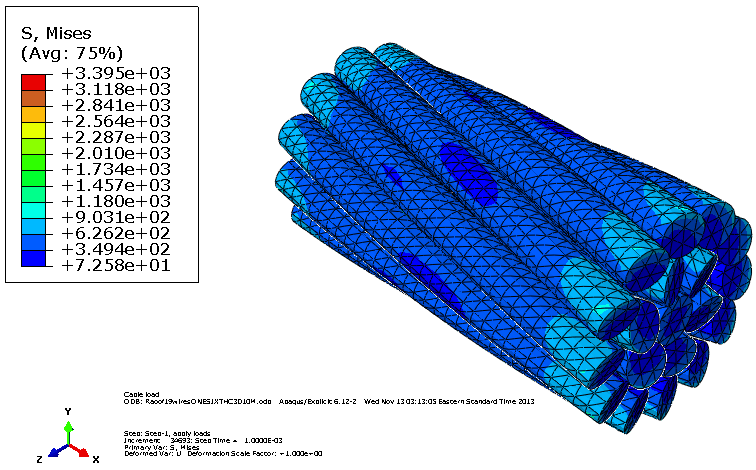

(a) von Mises stresses in 19-wire strand subjected to tension

Figure 4-10: Stresses in 19-wire strand investigated by Raoof (1990) – Tensile force applied on strand of 81.9 kN

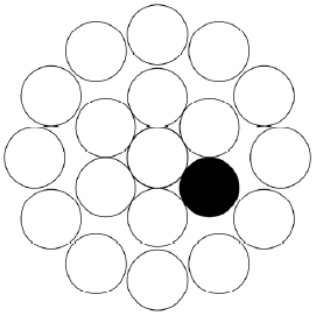

(b) Diagram of 19-wire strand cross section showing the critical wire

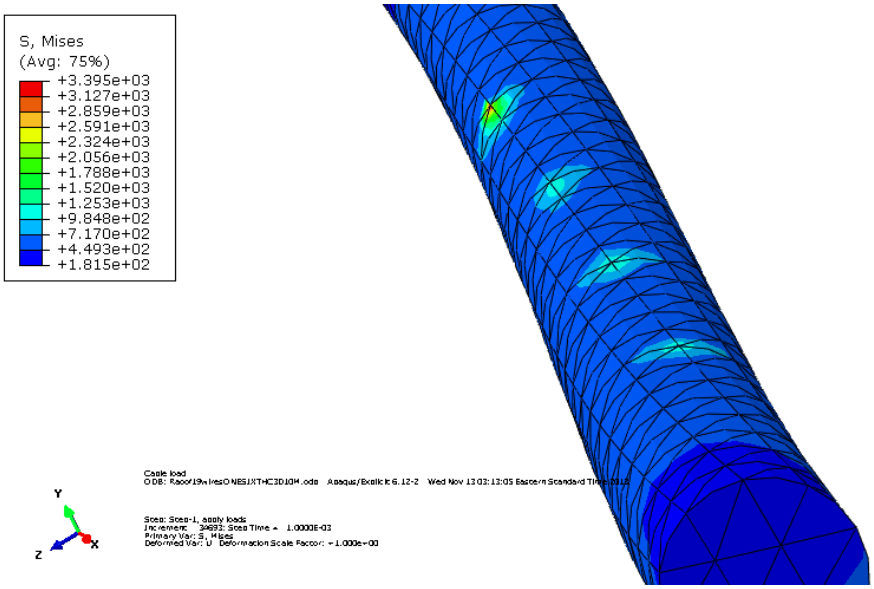

(c) Close-up of wires showing von Mises stress distribution in the 19-wire strand

Figure 4-10: (Cont'd)

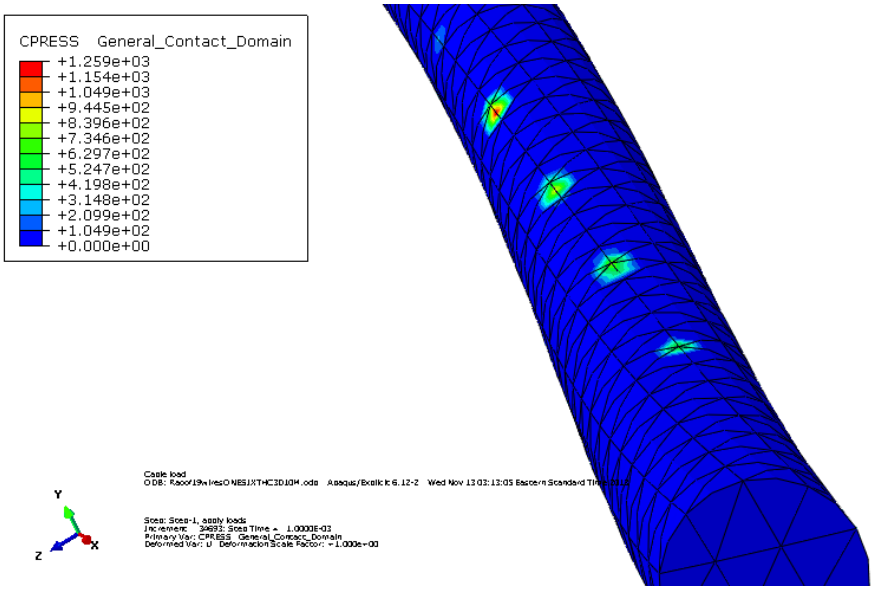

(d) Close-up of wires showing contact stress distribution in the 19-wire strand

Figure 4-10: (Cont'd)

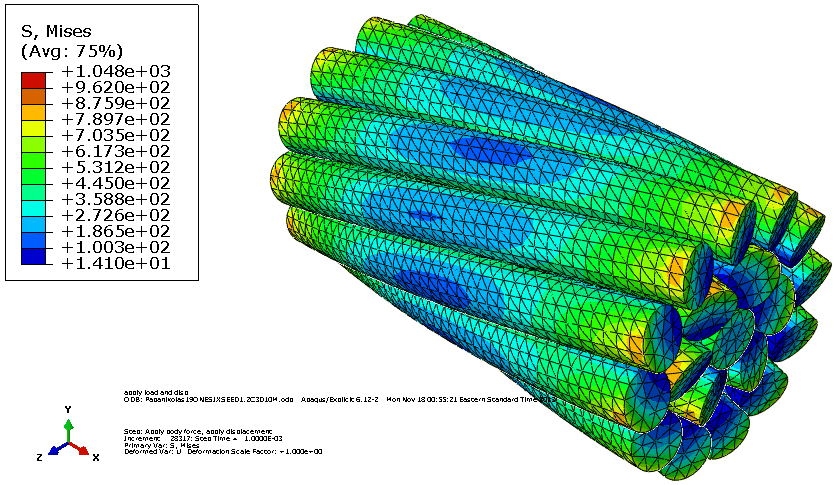

(a) von Mises stress in 19-wire strand

Figure 4-11: Stress in 19-wire strand tested by Papanikolas (1995) - Tensile force applied on strand of 150 kN

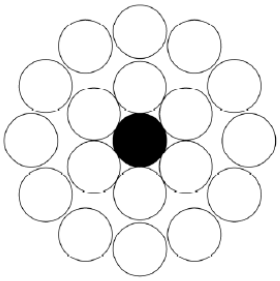

(b) Diagram of 19-wire strand cross section showing the critical wire

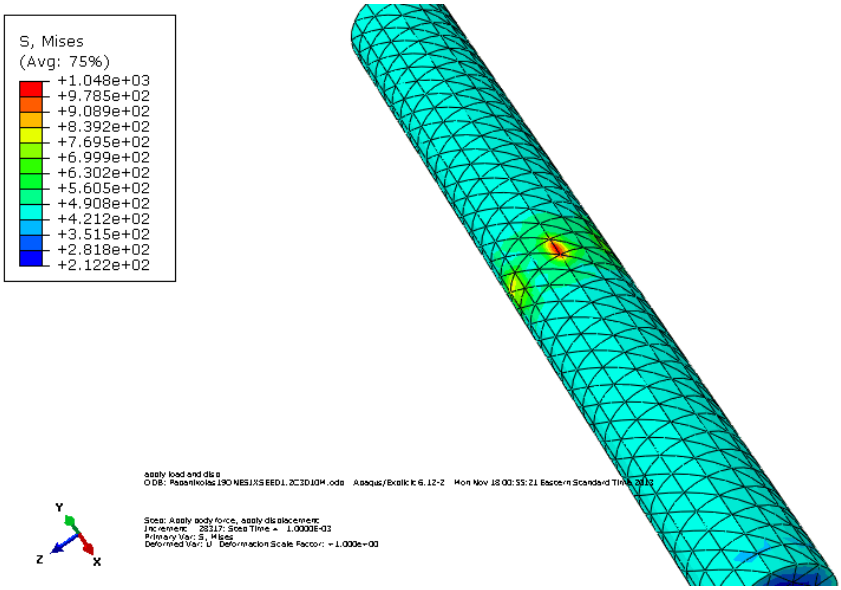

(c) Close-up of wires showing von Mises stress distribution in the 19-wire strand

Figure 4-11: (Cont'd)

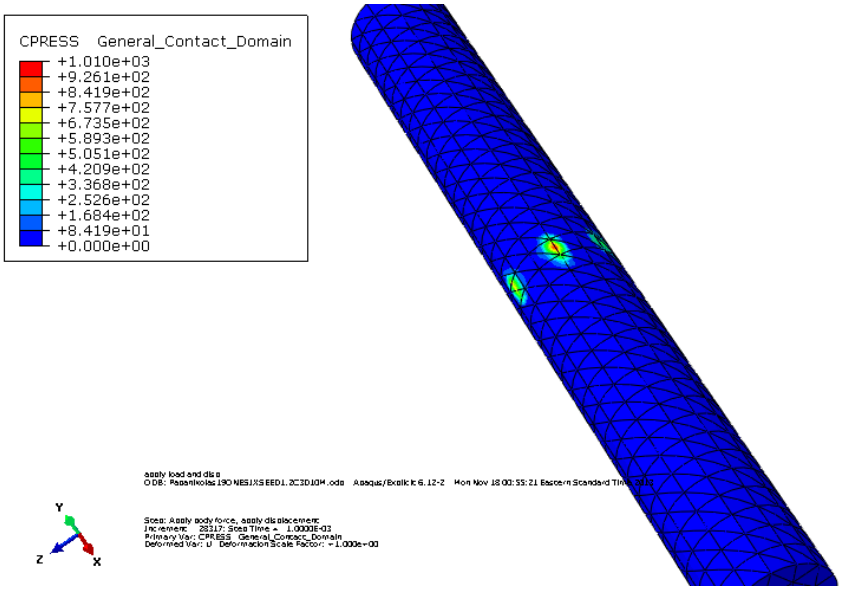

(d) Close-up of wires showing contact stress distribution in the 19-wire strand

Figure 4-11: (Cont'd)

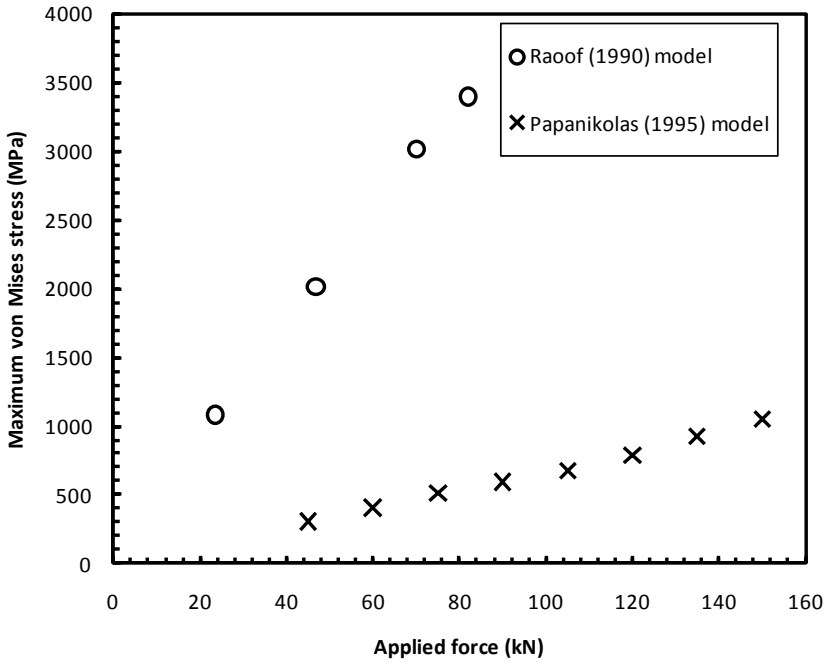

Figure 4-12: von Mises stress versus the applied force for 19-wire strand subjected to tension

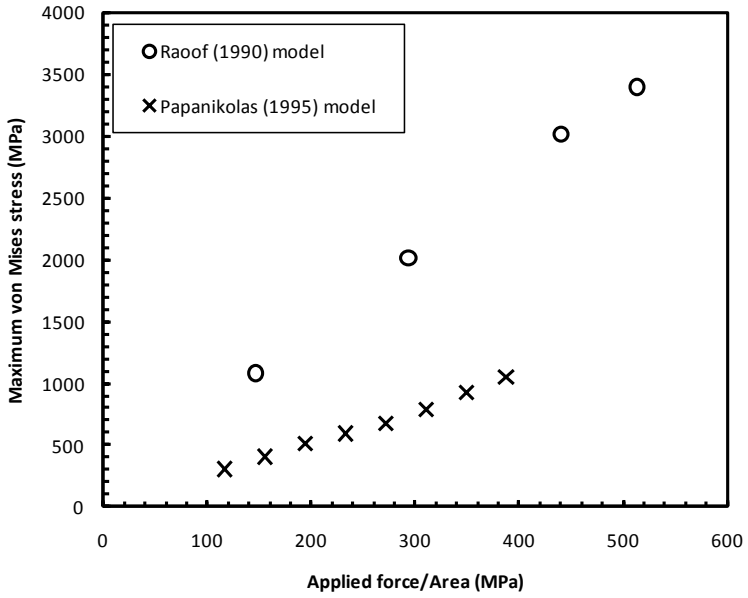

Figure 4-13: von Mises stress versus the applied stress for 19-wire strand subjected to tension

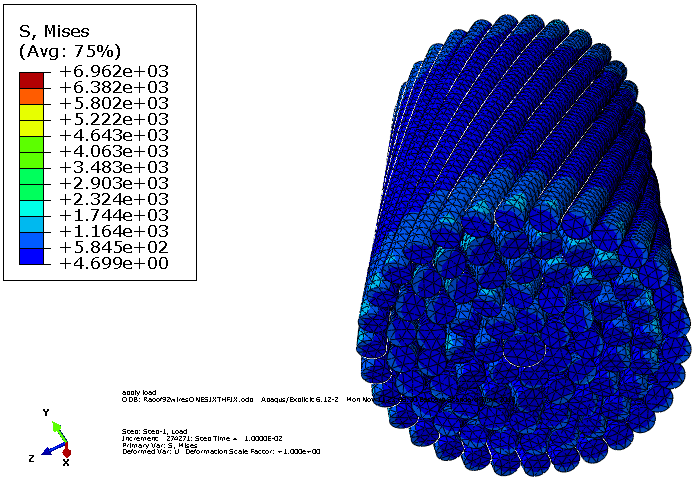

(a) von Mises stresses in 92-wire strand

Figure 4-14: Stresses in 92-wire strand subjected to a tensile force of 369 kN

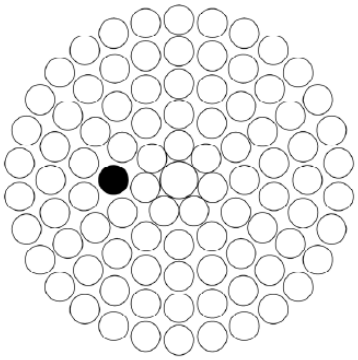

(b) Diagram of 92-wire strand cross section showing the critical wire

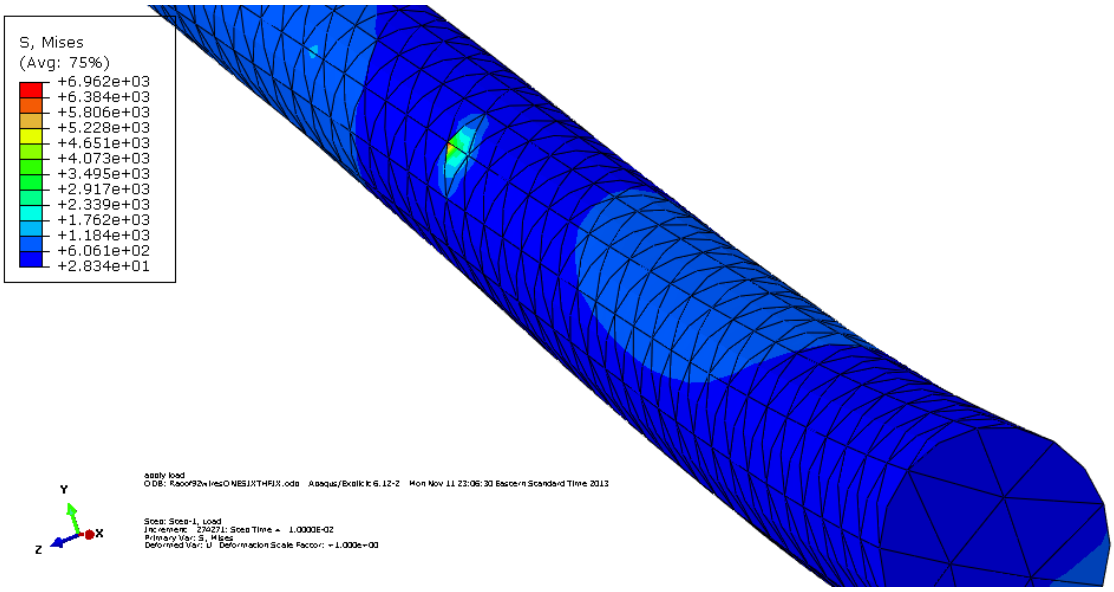

(c) Close-up of wires showing von Mises stress distribution in the 92-wire strand

Figure 4-14: (Cont'd)

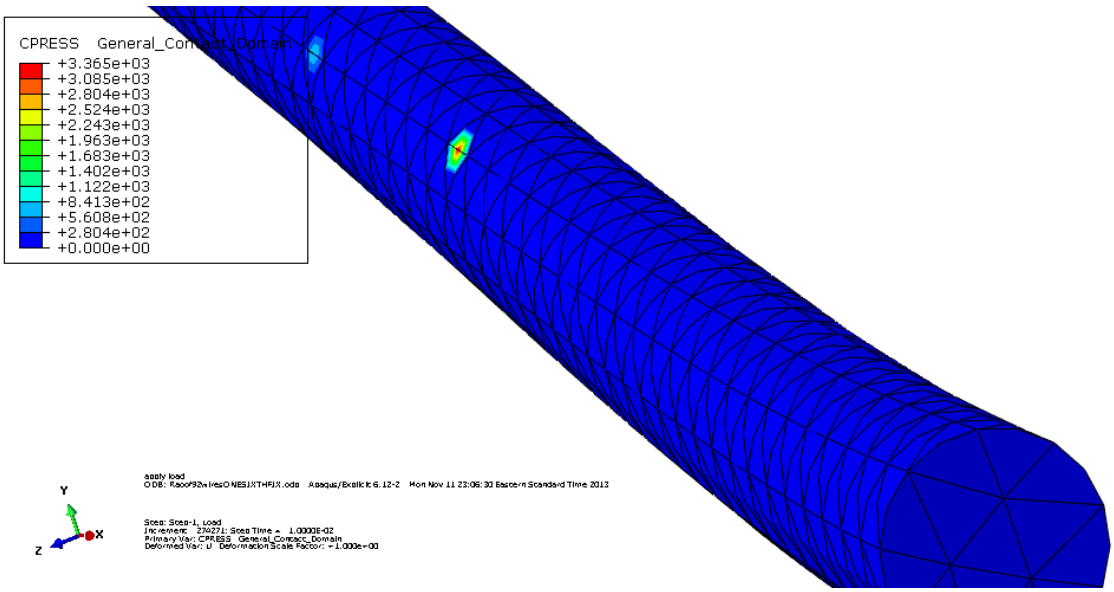

(d) Close-up of wires showing contact stress distribution in the 92-wire strand

Figure 4-14: (Cont'd)

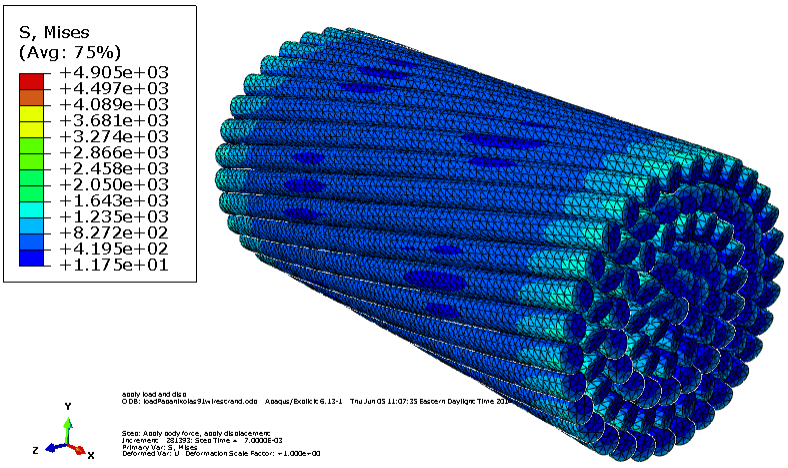

(a) von Mises Stresses in 91-wire strand

Figure 4-15: Stresses in 91-wire strand subjected to a tensile force of 700 kN

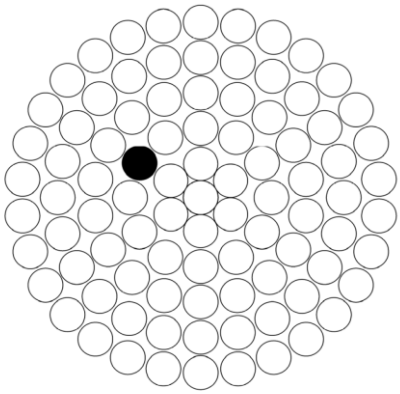

(b) Diagram of 91-wire strand cross section showing the critical wire

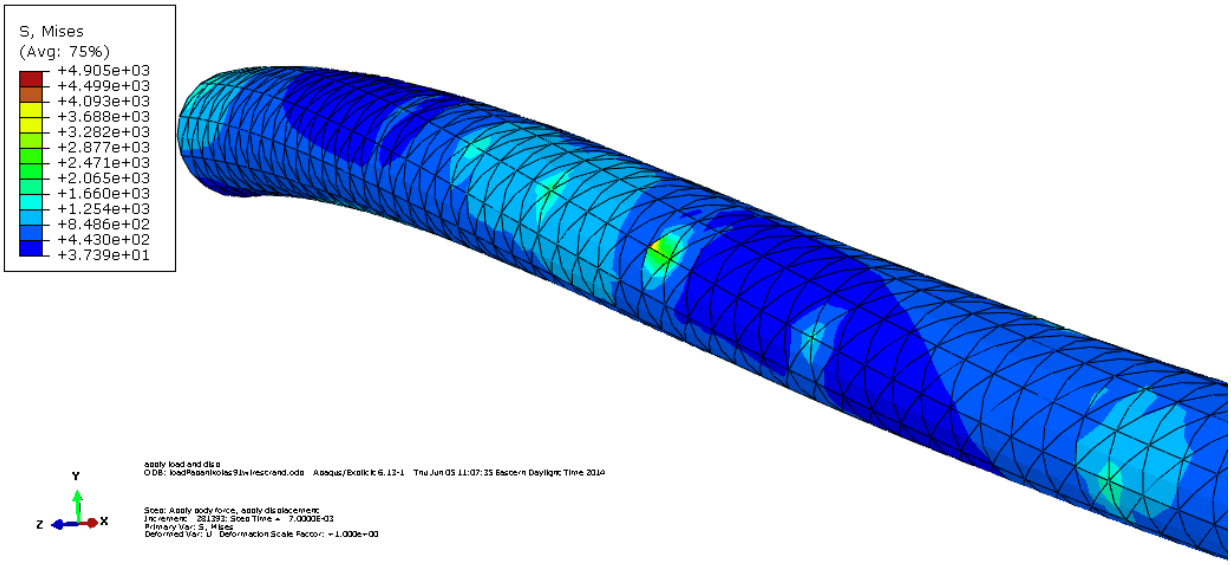

(c): Close-up of wires showing von Mises stress distribution in the 91-wire strand

Figure 4-15: (Cont'd)

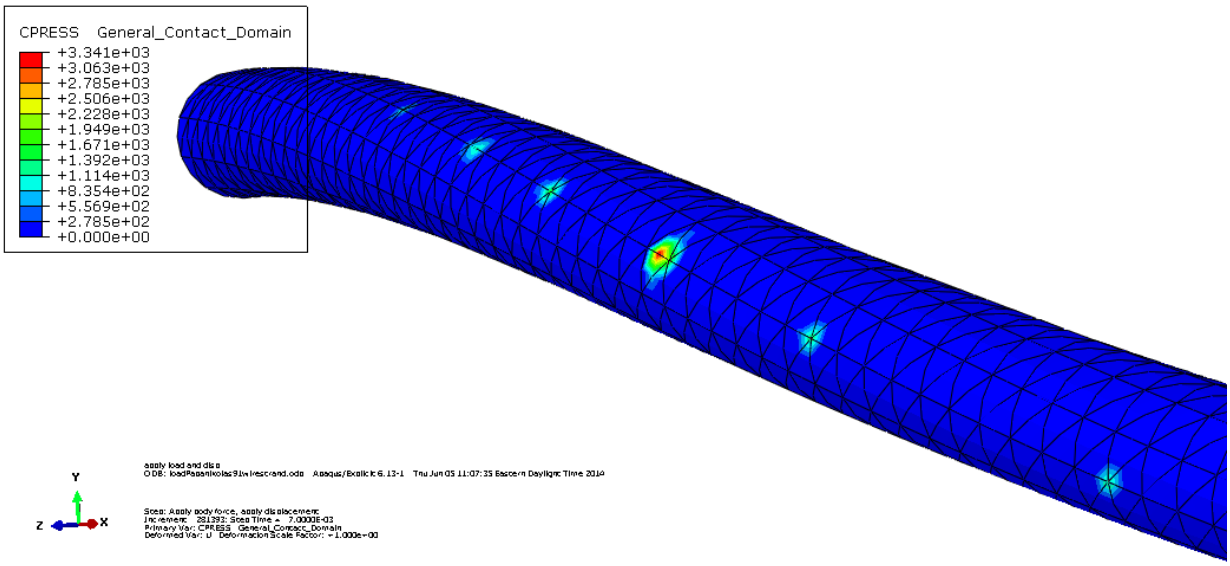

(d) Close-up of wires showing contact stress distribution in the 91-wire strand

Figure 4-15: (Cont'd)

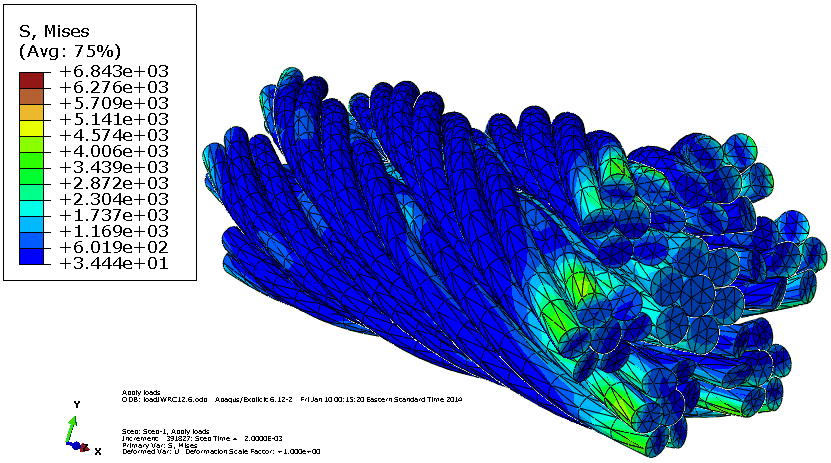

(a) von Mises Stresses in 6×7 wire rope

Figure 4-16: Stresses in 6×7 wire rope subjected to a tensile force of 50 kN (d=12.6 mm)

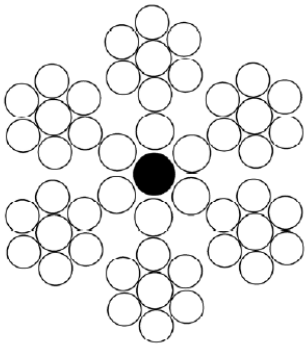

(b) Diagram of IWRC cross section showing the critical wire

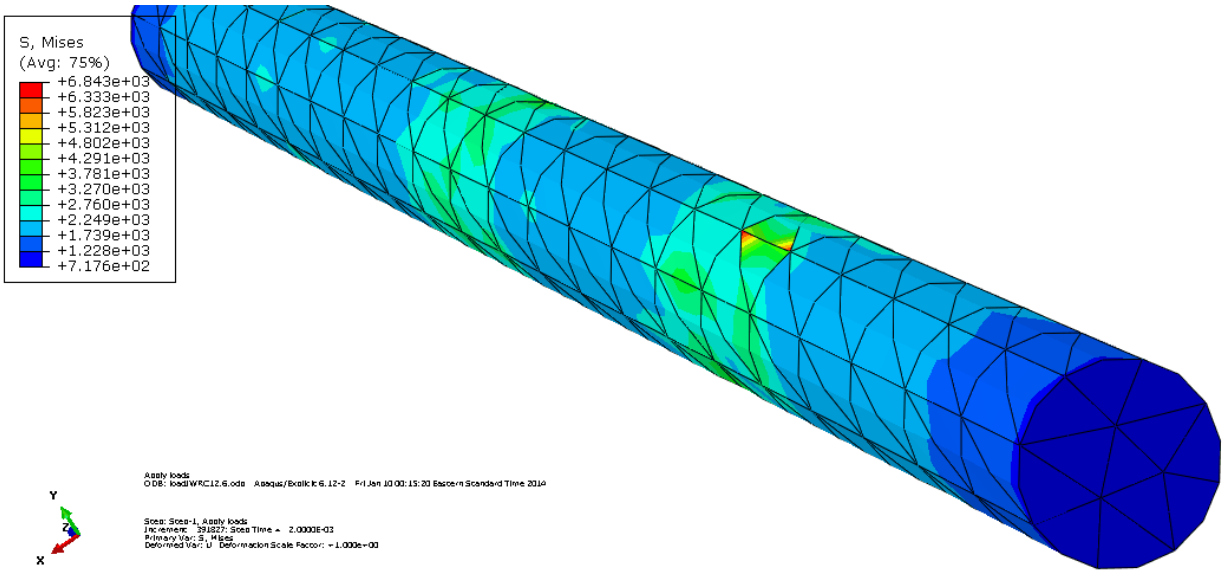

(c) Close-up of wires showing von Mises stress distribution in the 6×7 wire rope

Figure 4-16: (Cont'd)

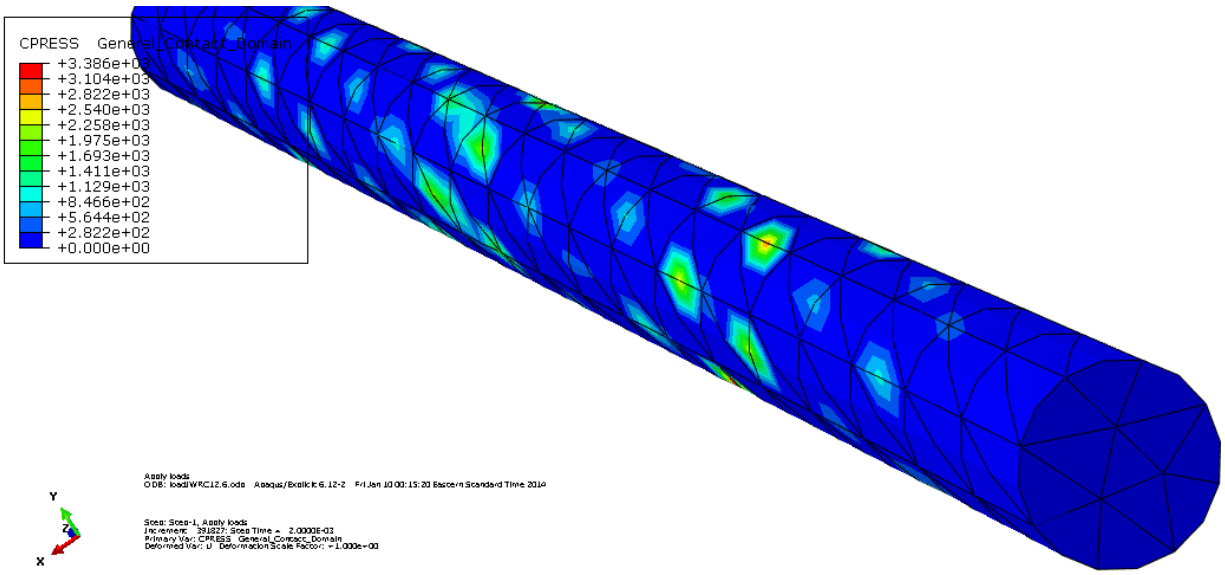

(d) Close-up of wires showing contact stress distribution in the 91-wire strand in the 6×7 wire rope

Figure 4-16: (Cont'd)

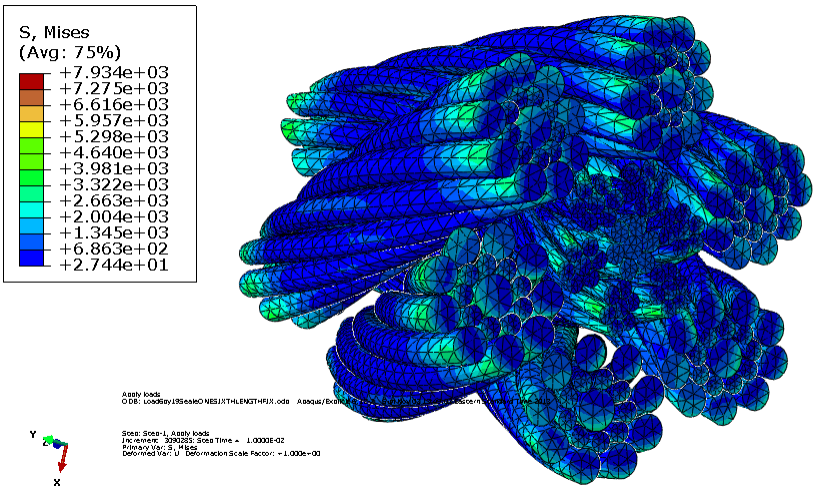

(a) von Mises Stresses in 6×19 Seale wire rope

Figure 4-17: Stresses in 6×19 Seale wire rope subjected to a tensile force of 360 kN (d=33.02 mm)

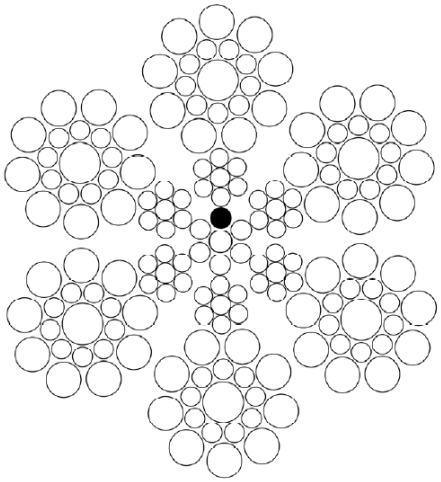

(b) Diagram of 6×19 Seale wire rope cross section showing the critical wire

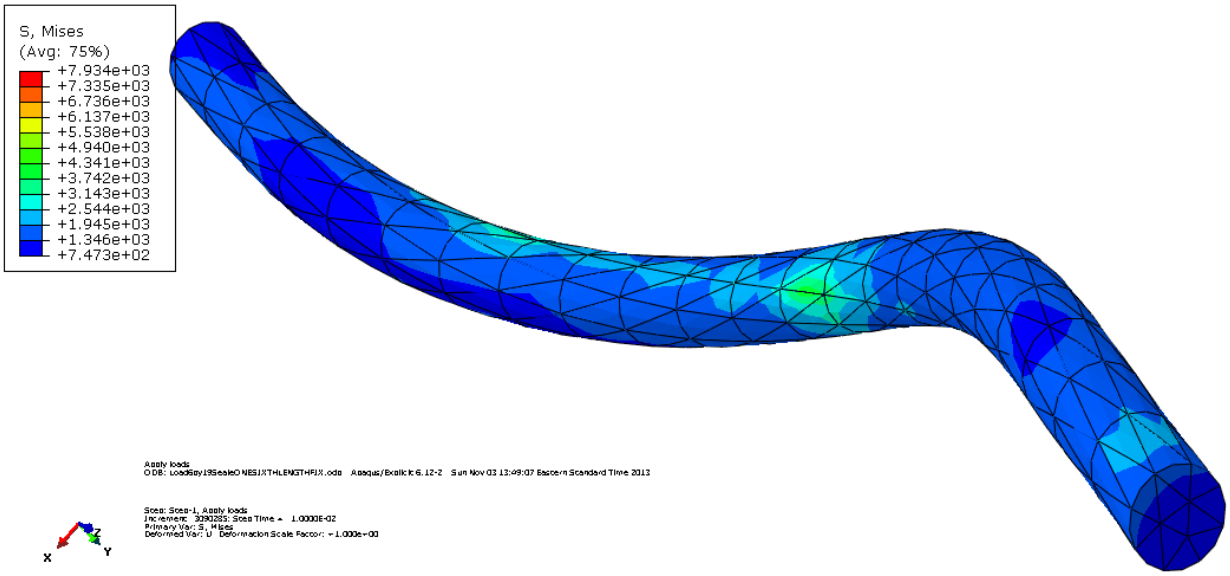

(c) Close-up of wires showing von Mises stress distribution in the 6×19 Seale wire rope

Figure 4-17: (Cont'd)

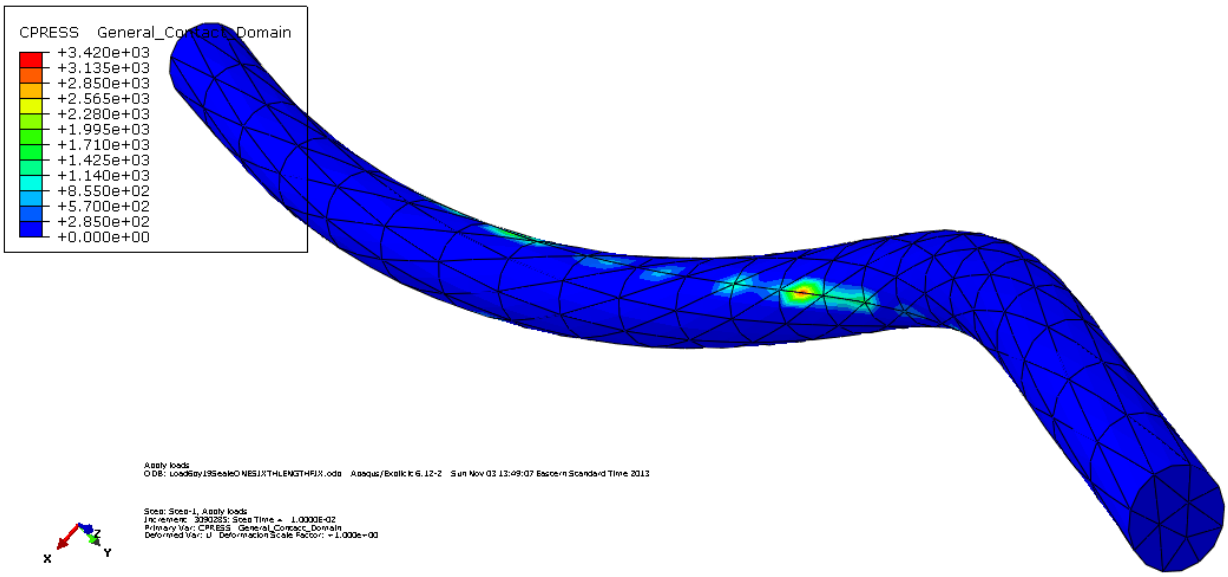

(d) Close-up of wires showing contact stress distribution in the 6×19 Seale wire rope

Figure 4-17: (Cont'd)

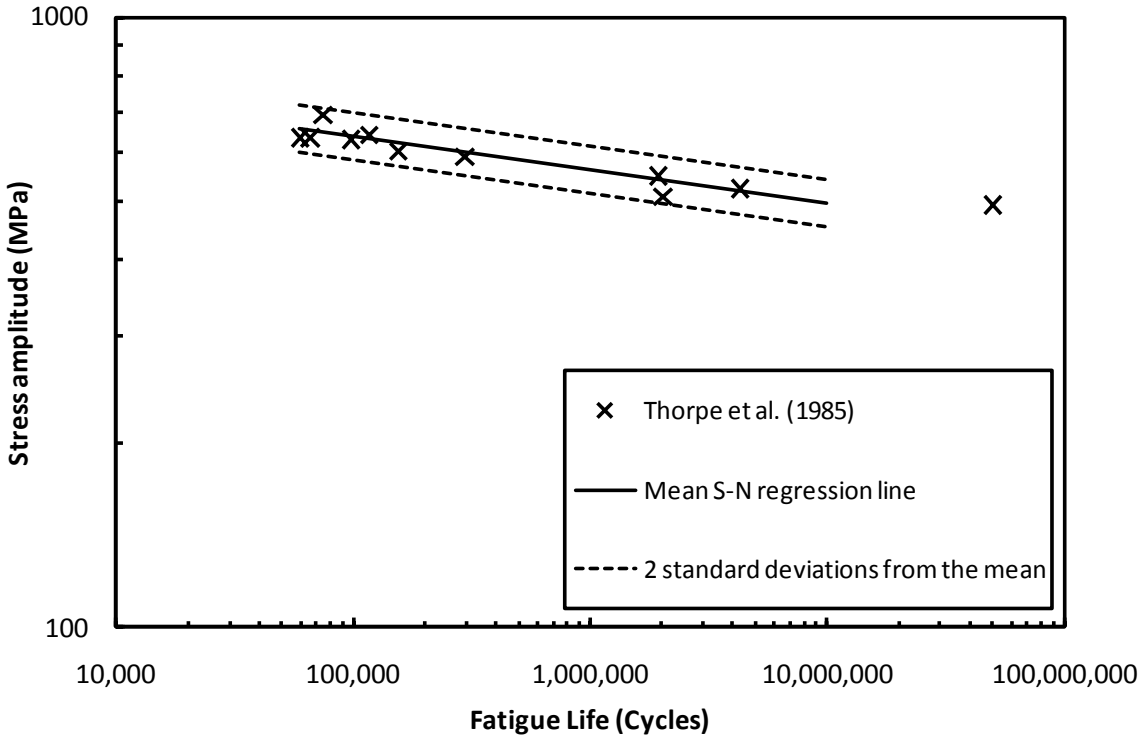

Figure 4-18: Fatigue test results and regression lines for single steel wire (Thorpe *et al.*, 1985)

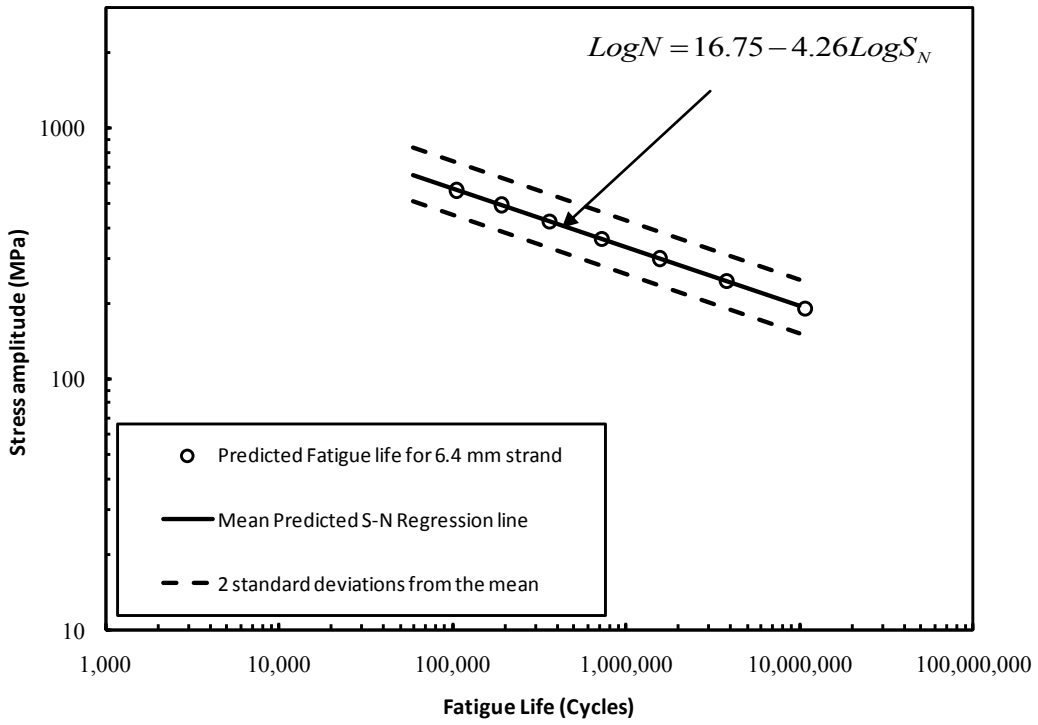

Figure 4-19: Fatigue life for 6.4 mm prestressing strand

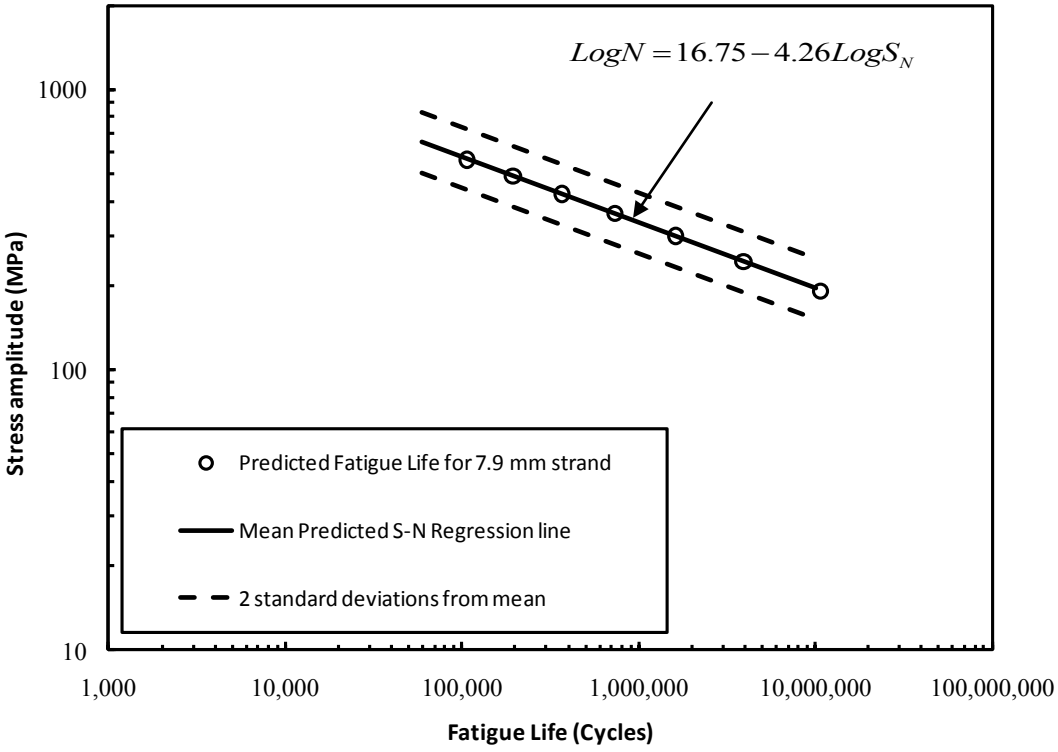

Figure 4-20: Fatigue life for 7.9 mm prestressing strand

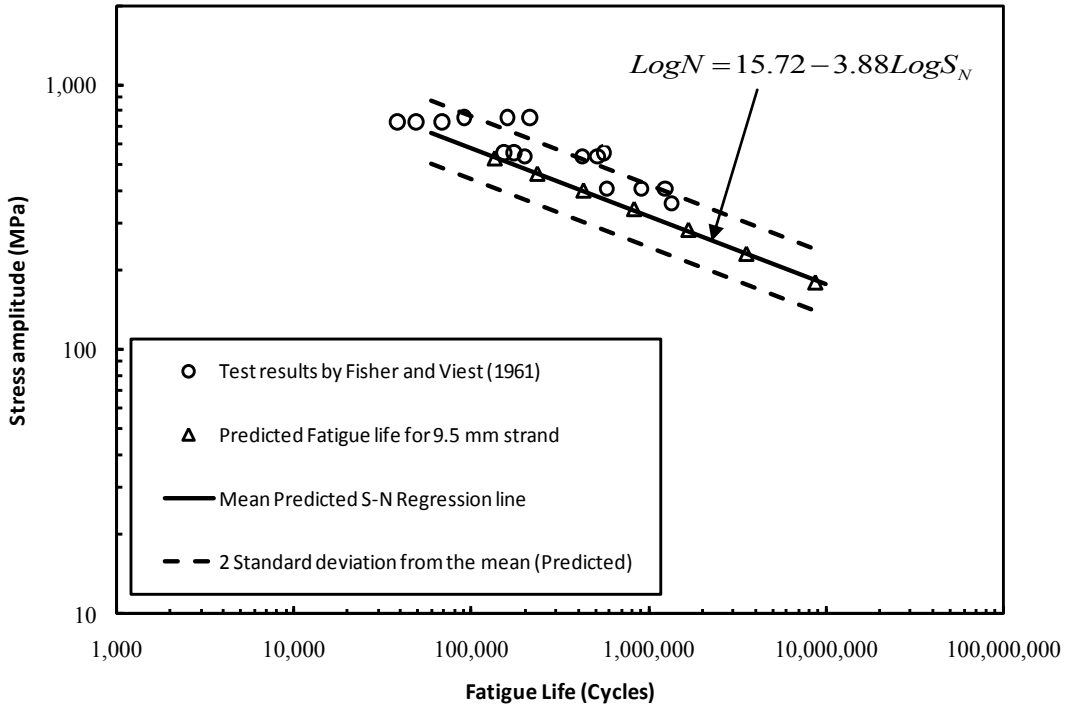

Figure 4-21: Comparison with test fatigue life for 9.5 mm prestressing strand

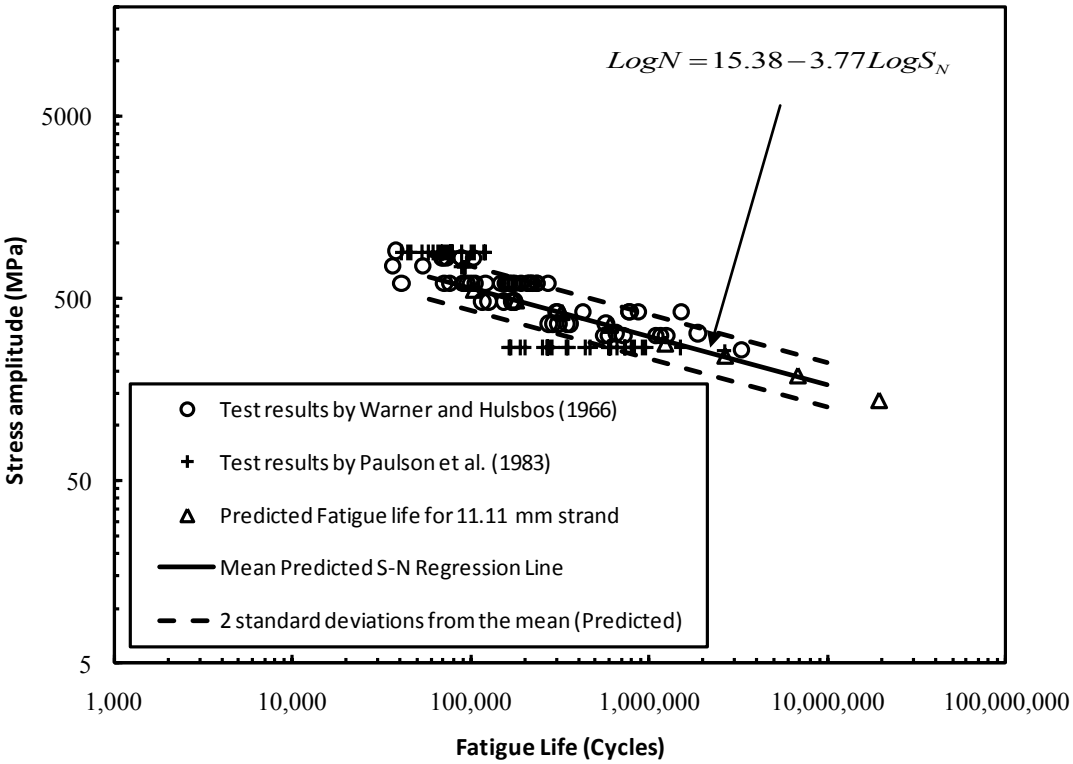

Figure 4-22: Comparison with test fatigue life for 11.11 mm prestressing strand

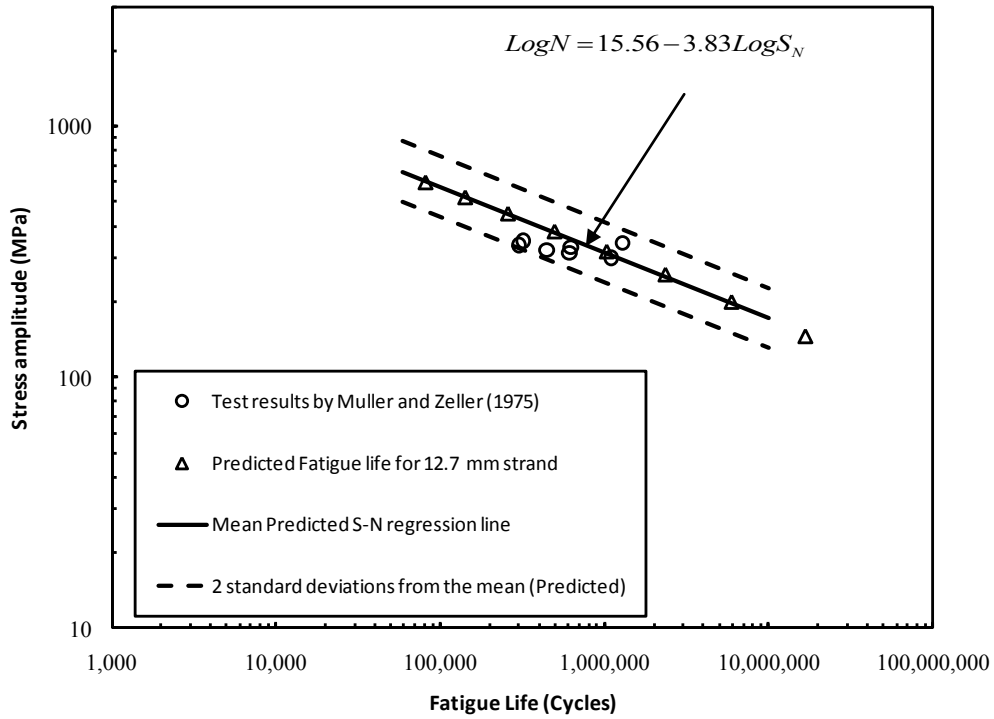

Figure 4-23: Comparison with test fatigue life for 12.7 mm prestressing strand (Grade 250)

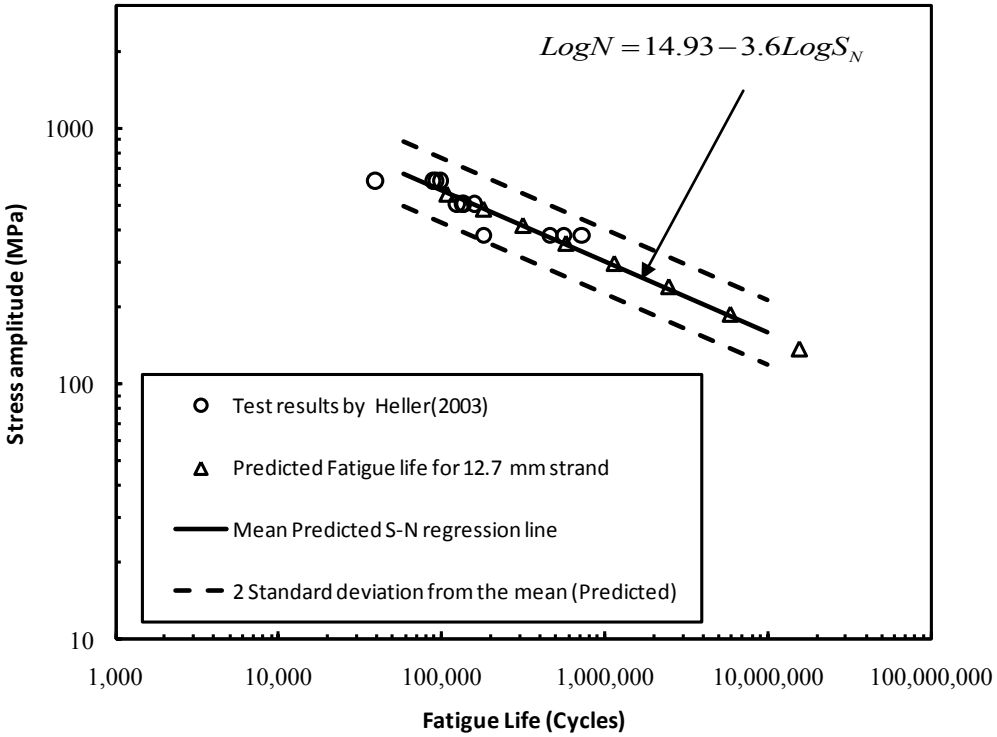

Figure 4-24: Comparison with test fatigue life for 12.7 mm prestressing strand (Grade 270)

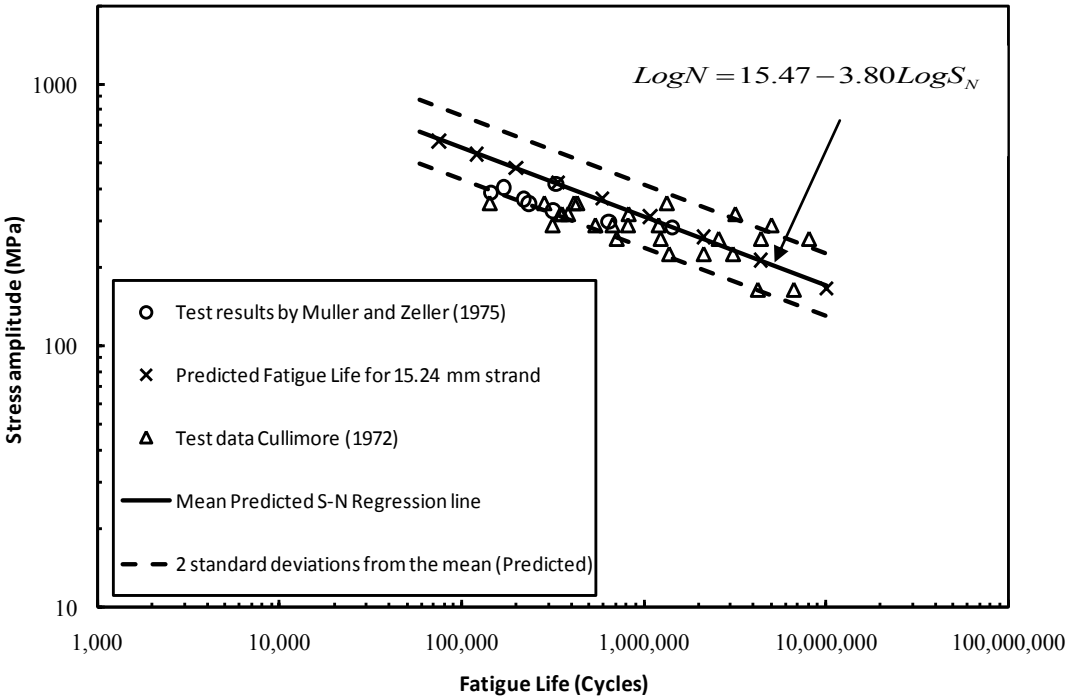

Figure 4-25: Comparison with test fatigue life for 15.24 mm prestressing strand

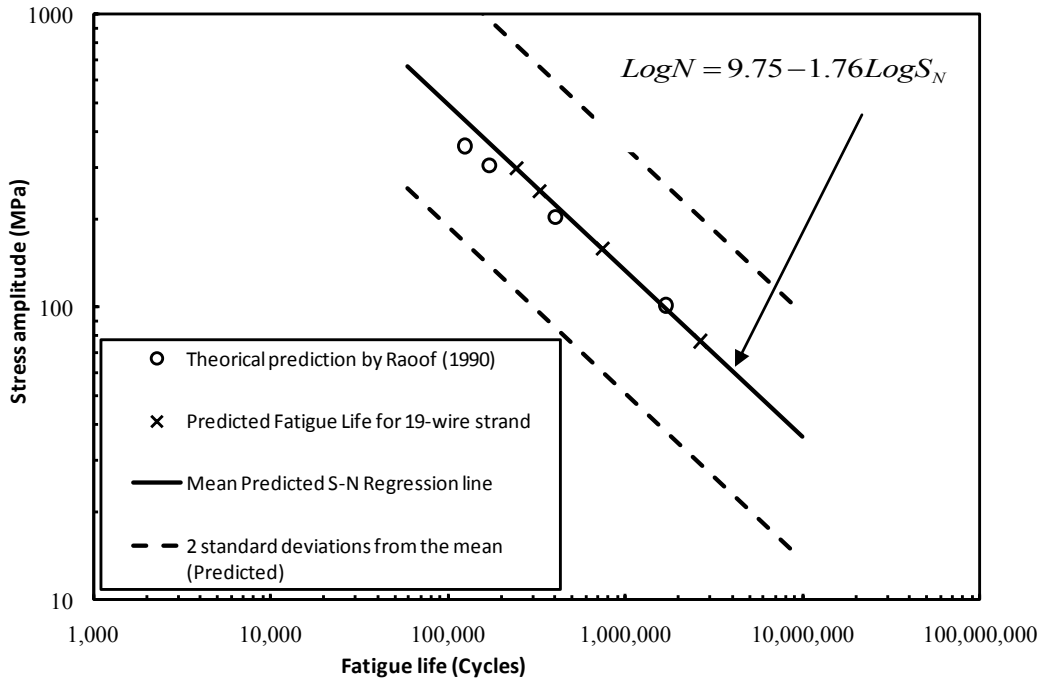

Figure 4-26: Comparison with test fatigue life for 16.4 mm strand (19 wires)

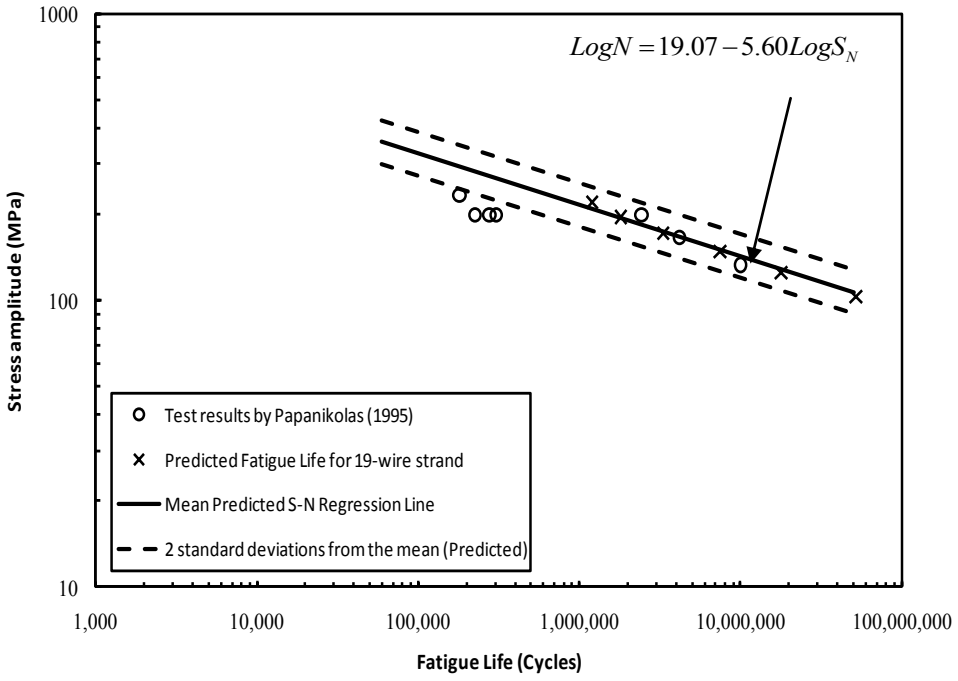

Figure 4-27: Comparison with test fatigue life for 25 mm strand (19 wires)

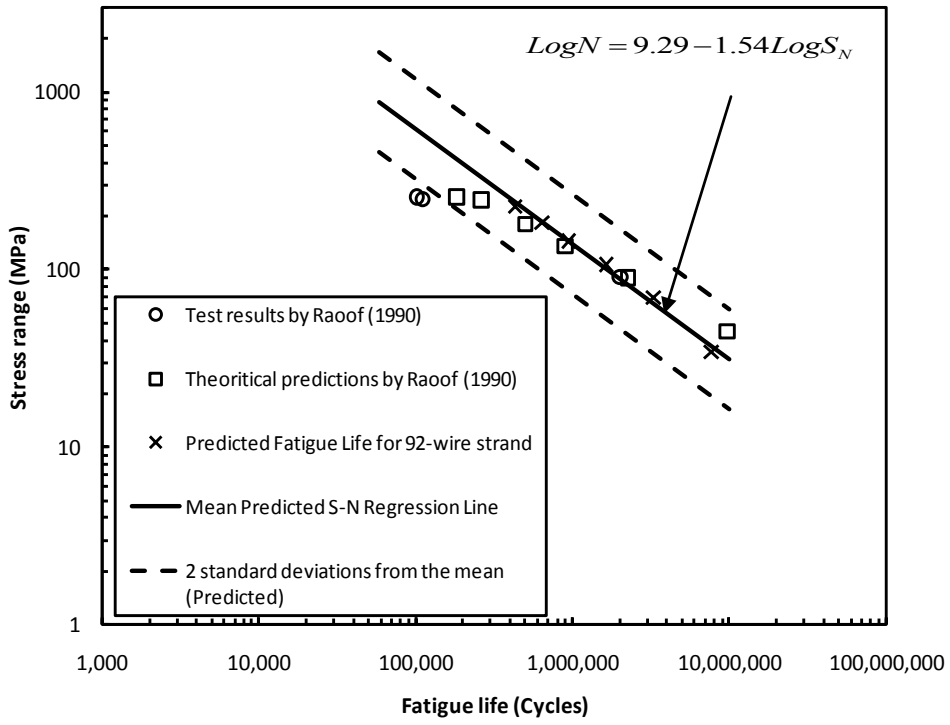

Figure 4-28: Comparison with test fatigue life for 39 mm strand (92 wires)

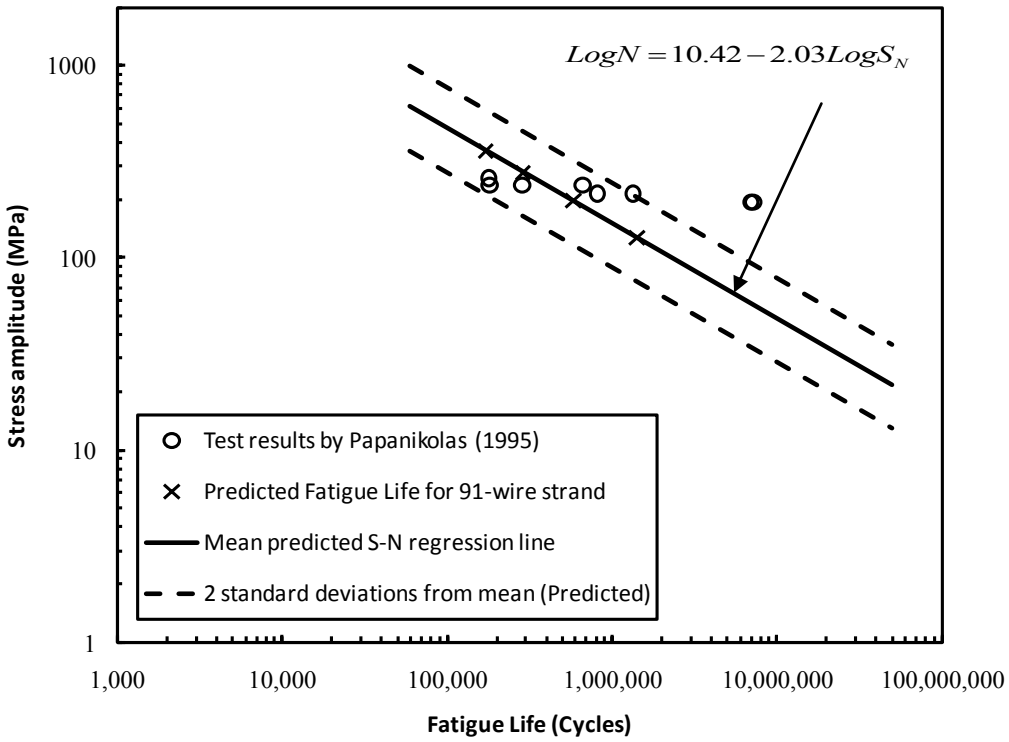

Figure 4-29: Comparison with test fatigue life for 45 mm strand (91 wires)

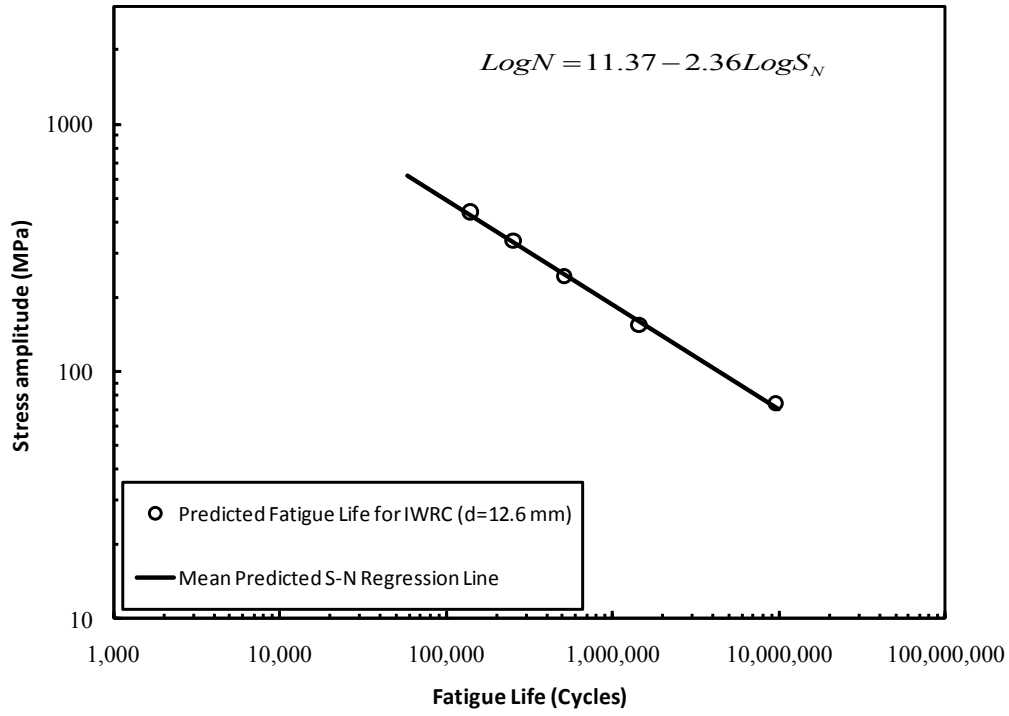

Figure 4-30: Fatigue life for IWRC (d=12.60 mm)

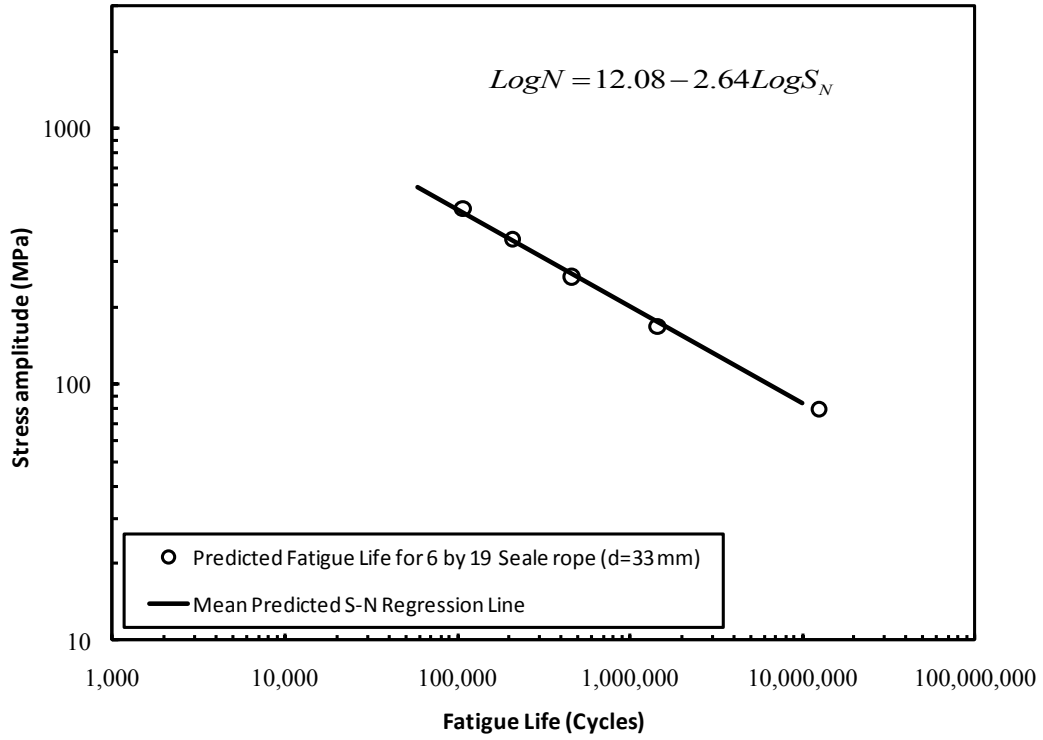

Figure 4-31: Fatigue life for 6×19 Seale wire rope (d=33 mm)

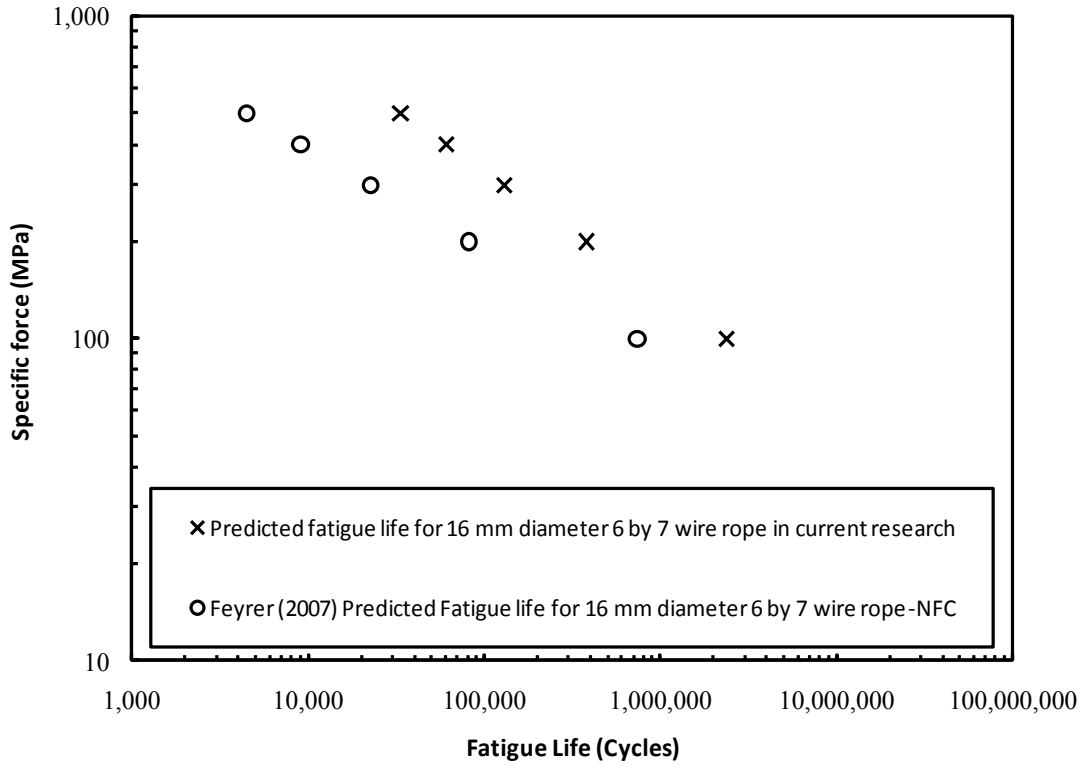

Figure 4-32: Comparison of predicted fatigue life for 6×7 ropes made of different cores

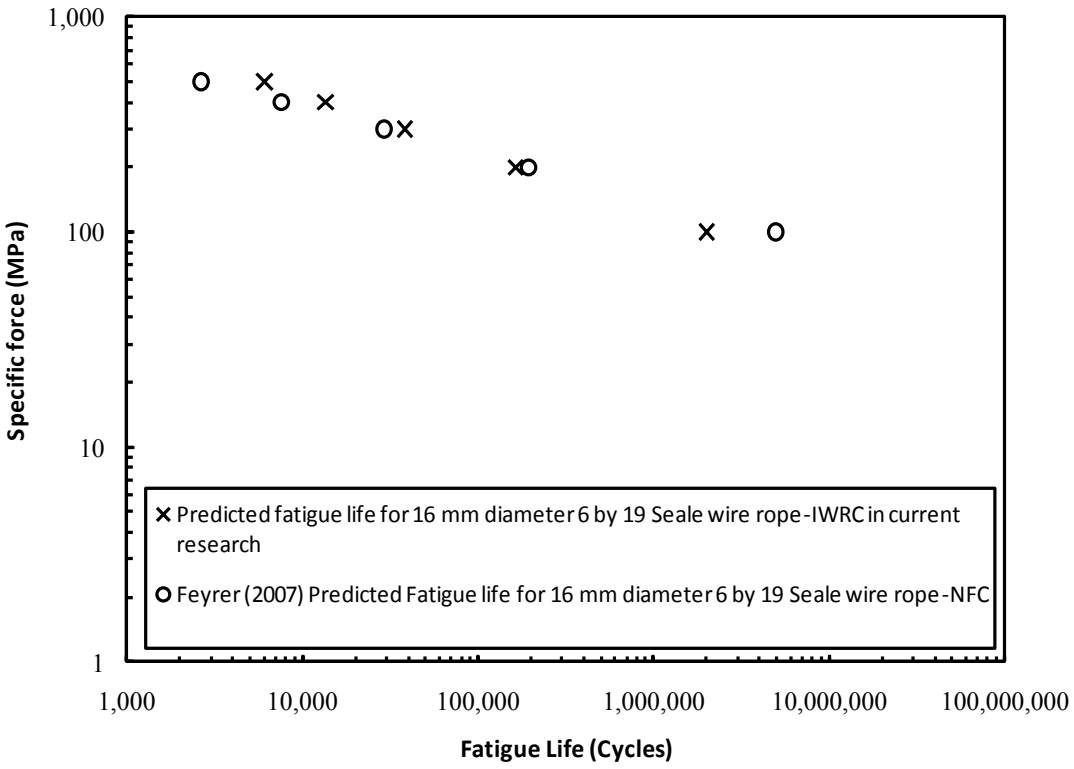

Figure 4-33: Comparison of predicted fatigue life for 6×19 Seale with different cores

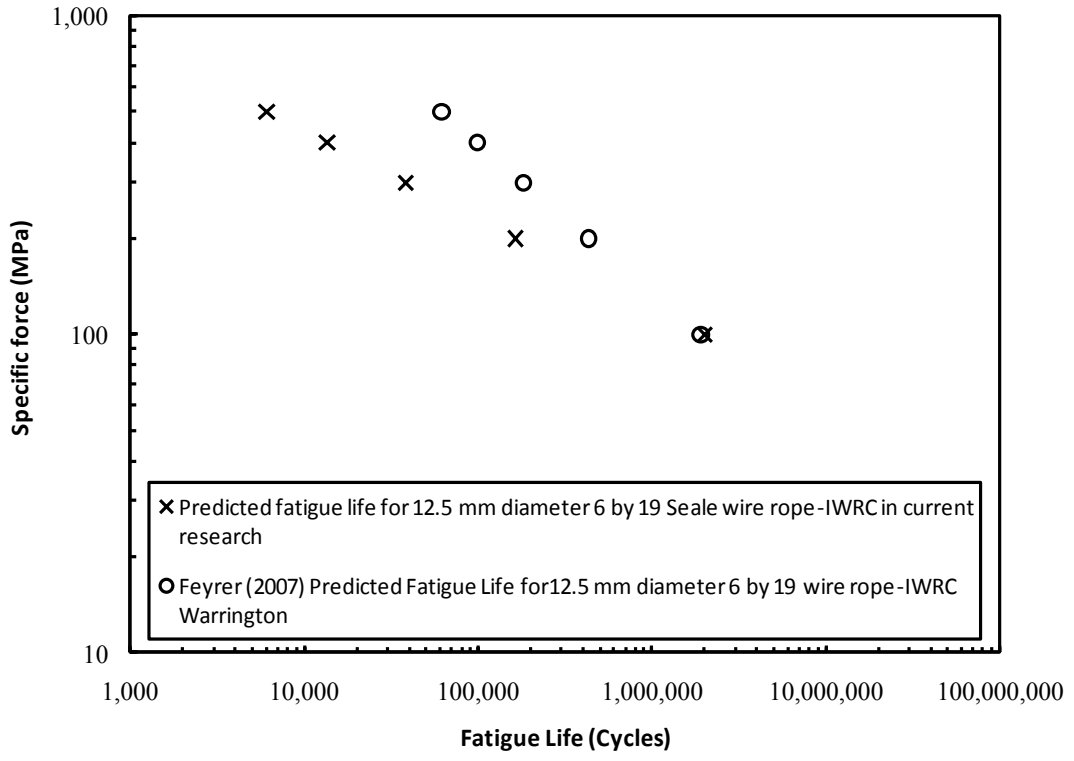

Figure 4-34: Comparison of predicted fatigue life for 6×19 Seale and Warrington Seale ropes

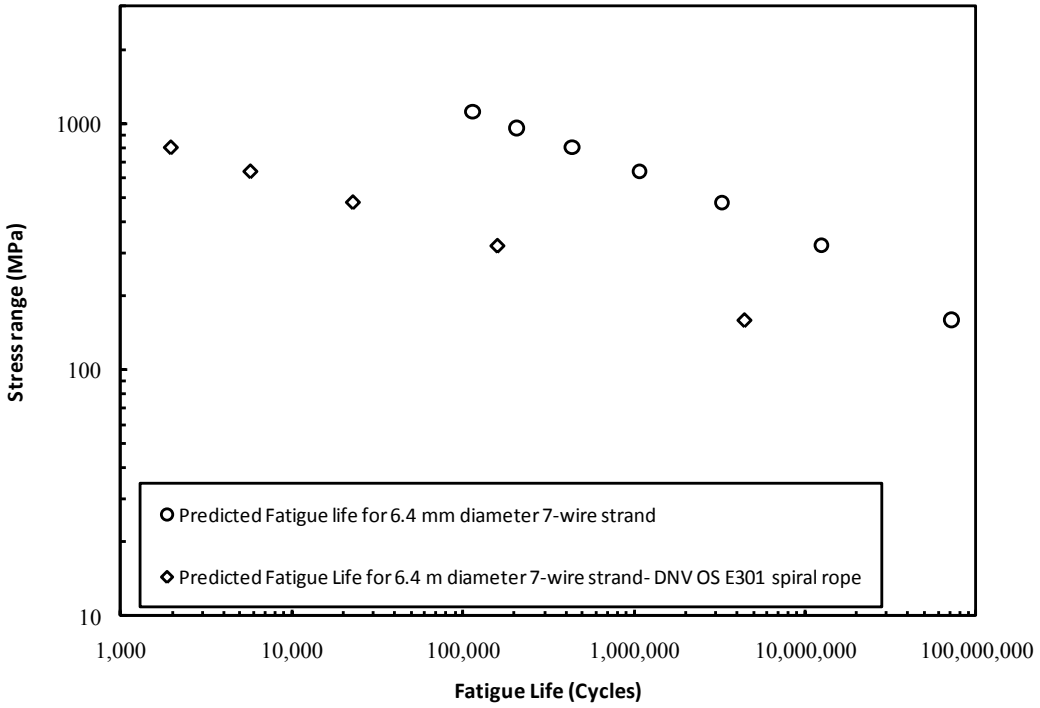

Figure 4-35: Comparison of predicted fatigue life for 7-wire strand and DNV-OS-E301 spiral strand

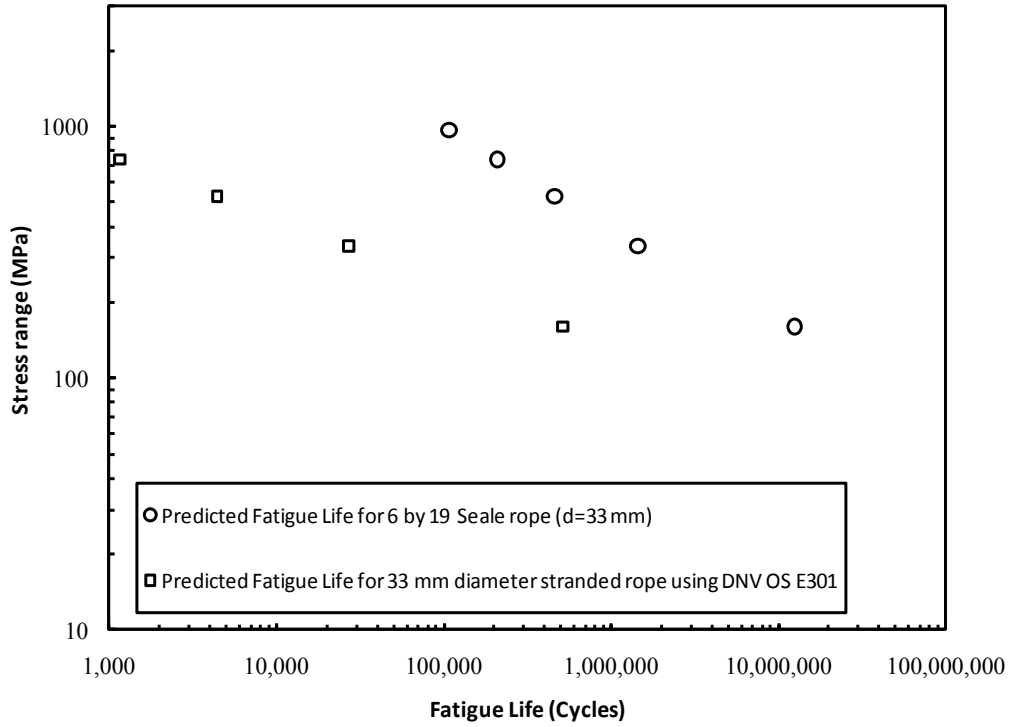

Figure 4-36: Comparison of predicted fatigue life for 6×19 Seale and DNV-OS-E301 stranded rope

CHAPTER 5

FINITE ELEMENT AND FATIGUE LIFE RESULTS FOR STRANDS BENT OVER SHEAVE

5.1 INTRODUCTION

The 'bend over' sheave behaviour of two types of cables was investigated. A model was developed using the finite element method described in Chapter 3. The first strand modeled consisted of a 7-wire strand with a diameter of 15.5 mm and nominal cross section area of 145.55 mm^2, and the second strand was a 19-wire strand with a diameter of 3.3 mm, and nominal cross section are of 6.3 mm^2. These strands were previously investigated by Costello (1997) and Knapp (2004), respectively, and were chosen for comparison due to the availability of experimental and/or analytical results. The stresses obtained from the finite element will vary based on the angle of wrap of the cables on the sheave based on the work of researchers like Muller (1961), who reported an investigation involving several angle of wrap, and from his investigation, the fatigue life is reduced for angle of wraps less than 40 degrees, at about 30 degrees the fatigue life is lowest, but for angle of wrap greater than 40 degrees the fatigue life remains almost the same and definitely it will be higher than at lower wrap angles. Scoble (1930) also observed a similar behaviour; hence a constant angle of wrap was adopted for this research on cables bent over sheaves of 180 degrees, since beyond an angle of wrap of 40 degrees, the fatigue life remains constant from their investigation. Also in shovels, elevators, and cranes where running cables are used, an angle of wrap greater than 40 degrees will typically be used. The maximum von Mises stress is obtained for a configuration when the cable is subjected to bending over the sheave as well as simultaneously being subjected to tension, otherwise known as tension bending configuration. It is assumed that the maximum von Mises stress obtained in such a configuration should give the maximum stress condition if the cables are actually subjected to fatigue, although the bending stresses will be very small given that very small part of cross section of the cable will be in bending.

5.2 COMPARISON BETWEEN KNAPP TEST AND CURRENT STRESS BASED APPROACH PREDICTED FATIGUE LIFE FOR STRAND BENT OVER SHEAVE

In the previous chapter, a proposed stress based approach was used to predict the fatigue life for strands and wire ropes in tension, where this approach was observed to produce reasonably good predicted fatigue life when compared to test results. This work is now expanded to compare the fatigue life predicted from finite element analysis stresses and a stress based fatigue life model, to the test results reported by Knapp (2004) for a strand bent over a sheave.

The strand tested by Knapp had a diameter of 3.3 mm and was made of 19 wires. The test was conducted on a sheave with a diameter D=300 mm and the groove radius was 6.34 mm (obtained from CABLECAD User manual). Table 5-1 tabulates stresses obtained from the finite element analysis for different load levels. Although the maximum calculated von Mises stress is the stress used for the fatigue life prediction, other stresses such as the maximum contact stress and the maximum principal stress have also been tabulated for comparison. The von Mises stress can be observed to be greater than the contact and maximum principal stresses, indicating that it should be a more conservative stress for fatigue life computations. The table also shows the nominal stress concentration factor, SCF_{nom}, obtained by dividing the maximum von Mises stress by the strand nominal stress (i.e. the reaction force divided by the nominal cross sectional area).

Figure 5-1(a) shows the strand after it has been bent over a sheave, where the location of the maximum von Mises stress can be seen near the top of the sheave, when it was subjected to a load of 9.49 kN. In Figure 5-19(b) a cross section of the model shows the location of the wire in which the maximum von Mises stress was observed. The point of maximum stress is located where the wire is in contact with the sheave groove. Feyrer (2007) based on analytical formulations of the bending stresses on a rope, predicted that for wire ropes bent over sheaves made of steel, it is possible that the first wire break could shift from the central wire to any of the wires that are in direct contact with a sheave groove for stranded ropes. He attributed this behaviour to high contact stresses in wires. This is supported by the results of the finite element analysis. Figure 5-1(c) shows the maximum von Mises stress where some of the wires are removed, showing that the maximum stress was in layer 3 of the strand (a wire in contact with the sheave), at the interface between layers 3 and 2.

The contact surface is elliptical as was previously observed in strands and wire ropes subjected to tension outlined in the previous chapter. Table 5-2 shows the predicted fatigue life for different loads, obtained using the stress based approach at different load levels. Figure 5-2 shows the plot of the fatigue test results generated by Knapp (2004) and the predicted fatigue life. The predicted fatigue life for the strand using the stress based approach proposed here shows good agreement with the Knapp's test results. Figure 5-3 shows the mean predicted S-N regression line, where the slope of the mean predicted fatigue relationship is 1.93 and the intercept is 10.14. A standard deviation of 0.051 was obtained in the regression analysis for Knapp`s test results (Appendix B). The lines located 2 standard deviations from the mean regression are also indicated; since the crack initiation life for such strands or wire ropes bent over a sheave is expected to be very small compared to the total rope life, there is little variability in the test data as also reflected by Knapp's test.

5.3 FINITE ELEMENT ANALYSIS RESULTS FOR 7-WIRE STRAND

5.3.1 EFFECT OF LOAD AMPLITUDE AND DIAMETER OF SHEAVE TO DIAMETER OF STRAND RATIO

The 7-wire strand (Costello, 1997) described in Chapter 3 was used to investigate the effect of change in load amplitude and D/d ratio on the maximum stress and SCF_{nom}. All groove sizes analysed were kept constant at a groove radius $r = 0.53d$, since normally this is the groove radius used (Feyrer, 2007). For a D/d ratio of 12, the load was varied from 17.91 kN to 172.91 kN, these loads are obtained from the reaction force on the sheaves. Table 5-3 shows the stresses and stress parameters output required for the calculation of the fatigue life of the 7-wire strand. The von Mises stresses are again higher than the contact and maximum principal stresses. Figure 5-4 (a) shows the strand bent over a sheave where the maximum von Mises stress for this case at a load of 172.91 kN is 7,823 MPa. This maximum stress occurred directly above the centre of the sheave, it has been observed in the industries that use running ropes that failures have typically occurred in the sections of the rope that runs off and on the sheaves and not in lengths of the rope free from contact with the sheaves. Figure 5-4 (b) shows that the location of the wire with a maximum von Mises stress occurs where it is in direct contact with the sheave. Figure 5-4 (c) shows that the maximum von Mises stress in the critical wire where the wire

directly rests on the sheave and specifically at the interface between one of the wires (the layer with 6 wires) and the central straight wire. The stress concentration zone exhibited isolated elliptical contact patches. These contact patches would eventually form wear scars under fretting fatigue loading. Wear scars of the same shape as the contact patches have also been reported by Urchegui *et al.* (2008).

Table 5-4 shows the results of the analysis for a D/d ratio of 15, where the load was increased from 17.44 kN to 177.19 kN. At the maximum load, the maximum von Mises stress was 7,605 MPa, as shown in Figure 5-5 (a). Again the location of the critically stressed wire is exactly the same as indicated by the Costello strand described previously for a D/d ratio of 12 above. Figure 5-5 (b) shows a close-up view of the interior of the exterior six wires directly on the sheave, where again the generation of elliptical contact patches are observed.

The maximum load and maximum von Mises stress for a $D/d = 20$ was 90.71 kN and 4,610 MPa, respectively. Figure 5-6 (a) shows the magnitude and location of the maximum von Mises stress, while the other stress parameters are shown in Table 5-5 and the contact patches are shown in Figure 5-6 (b).

For a $D/d = 40$ the stress parameters are shown in Table 5-6, where again the maximum von Mises stress of 4,111 MPa at a load of 74.3 kN occurred at the portion of the strand directly at the top centre of the sheave as shown in Figure 5-7 (a), commensurate with a single elliptical contact patch. The single contact patch is considered due to an increased sheave size, which had reduced the stresses in the strand. Basically fretting will be reduced in such cases where the sheave is large.

Finally, for the 7-wire strand, the effect of change in load was investigated for a D/d ratio of 60. This ratio would be commensurate with the types of sheave that are typically found in cranes, draglines and mining shovels, and are recommended for installations were safety of the rope system is a very high priority. Table 5-7 shows the stresses generated as the load was increased, and Figure 5-8 (a) shows the magnitude and location of the maximum von Mises stress. As seen here, the maximum von Mises stress occurred at the part of the strand directly over the top centre of the sheave. Figure 5-8 (b) shows the contact patch formed in the six exterior wires that rest over the sheave, again in isolation. In all cases of D/d ratio investigated,

the maximum von Mises stress occurred in the layer with six wires and between that layer and the central wire. The strand models with D/d ratios of 20, 40 and 60 exhibited the maximum von Mises stress at the wires directly in contact with the sheave as described previously for D/d of 12.

Figure 5-9 shows the plot of von Mises stress versus the nominal stress for D/d ratios of 12, 15, 20, 40 and 60. The trend here seems to be that as the load increased, the von Mises stress in the strands increased linearly. Also, as suggested by researchers such as Feyrer (2007), and as can be seen in Figure 5-9, as the D/d ratio increased, the slope of the von Mises stress versus the strand nominal stress decreased. That is, there exist an inverse relationship between the von Mises stress and the D/d ratio. From the same plot, it is evident that an increase in D/d ratio reduced the stress developed in the strands. In fact, in Figure 5-10, the effect of the curvature of the strands as they bend over the sheave can be seen. At a D/d ratio of 60, the slope of the von Mises stress versus the product of the D/d ratio and nominal stress, $((D/d)\times\sigma_{nom})$, is less than 5%. The highest slope at about 12.43% was evident for a D/d ratio of 12. Figure 5-11 shows the plot of SCF_{nom} versus the $D/d\times(\sigma_{nom}/E)$ dimensionless parameter, established by Costello (1997), where he observed a large decrease in SCF_{nom} as the dimensionless parameter increased in magnitude. Costello (1997) observed that at some point, the SCF_{nom} became asymptotic to a constant SCF_{nom} value. The same trend was observed here, for which the SCF_{nom} decreased with an increase in the dimensionless parameter prior to remaining constant at a SCF_{nom} range of 5 to 8. Nabijou and Hobbs (1995) investigated the relative movements within cables bent over sheave, and it was observed that the location of the wire failure was also the position with the highest relative movement (slip) for cables bent over sheaves. In the current research information about the relative movements in the wires as they bend over sheaves was not requested from the finite element analysis output database, but by visually observing the maximum displacements of the wires, it was observed that for all 7-wire strands bent over sheave in the current work the location of maximum displacement was within the external wires of the 7-wire strand. It was also noticed that the shear stresses were maximum in the external wires of the 7-wire strands as it is subjected to combined tension and bending. It must be recognised that using the maximum von Mises stress for obtaining the fatigue life

implicitly accounts for the normal, tangential and slip behaviours as discussed previously, since the von Mises stress is a stress obtained by the combination of all multi-axial stresses acting on the cable. Also a fatigue failure is a shear type failure and this is a further justification for the use of the von Mises stress for obtaining the fatigue life.

To investigate the effect of change in strand diameter on fatigue life, two sizes of strand at 7.8 and 11.62 mm diameter were used. A D/d ratio of 12 and 15 were investigated per diameter. Tables 5-8 through 5-11 shows the resulting stress parametric studies. For the same D/d ratio either 12 or 15, the von Mises stress was higher for 11.62 mm over 7.8 mm diameter strands. This behaviour was previously reported by Feyrer (2007) and other researchers, commensurate with an increase in D/d ratio.

5.3.2 EFFECT OF GROOVE SIZE ON THE STRESSES IN 7-WIRE STRANDS BENT OVER SHEAVE

For the 7-wire strands, four groove sizes were investigated, $r = 0.53d$, $r = 0.8d$, $r = 1.0d$ and a groove size with an infinite radius (a flat groove), all at a constant D/d ratio of 12. Tables 5-12 through 5-14 show the finite element stress results by groove size. To observe the impact of the groove geometry as the D/d was increased, the effect of the groove size for a D/d ratio of 15 was also investigated. For this case the groove sizes investigated were $r = 0.53d$, $r = 0.8d$ and $r = 1.0d$. Tables 5-15 and 5-16 show the stress parameters from the finite element analysis for a groove size of $r = 0.8d$ and $r = 1.0d$ respectively. The strand analysed was kept the same as used by Costello (1997), described in Chapter 3. Figure 5-12 shows the plot of the von Mises stress versus nominal stress, from which we can observe that the stress in the strand bent over a sheave increase with an increase in groove radius. In the case where the groove is flat, the stress is highest, but at very high nominal stresses (above 1,000 MPa) the groove sizes tend to exhibit the same von Mises stress. This means that at very high loads the stresses in the strands or wire rope will no longer be a function of the groove dimensions. Cables used for steel construction and crane stay ropes typically will have a factor of safety of 2.2 and 3.2, respectively (Feyrer, 2007); hence the groove dimensions will be pertinent to the stress in the cable and by association to the fatigue life.

5.4 FINITE ELEMENT ANALYSIS RESULTS FOR 19-WIRE STRAND

5.4.1 EFFECT OF LOAD AMPLITUDE, DIAMETER OF SHEAVE TO DIAMETER OF STRAND RATIO FOR 19-WIRE STRAND

The effect of an increase in load and D/d ratio was investigated using the model tested by Knapp (2004), where the dimensions, boundary conditions and loads were previously described in Chapter 3. The D/d ratios investigated were 10, 15, 30, 60 and 90.9. The D/d ratio of 90.9 with $r = 1.92d$ was discussed early in this chapter, chosen because the fatigue test results reported by Knapp (2004) used these dimensions, permitting the fatigue life predicted using finite element results to be compared with these earlier fatigue test results. Except for a D/d ratio of 90.9 (predicted fatigue has been presented earlier in this chapter), all other D/d ratios investigated in this section had $r = 0.53d$.

The first D/d ratio considered here was 10. Figure 5-13 (a) shows a maximum von Mises stress of 9,823 MPa at a load of 9.29 kN located as shown at the top centre of the sheave as was the case for the 7-wire strand described in section 5.2.1. The location of the critical wire with respect to the sheave is effectively the same as for Knapp's model with a D/d ratio of 90.9 described previously, located in one of the twelve external wires that were directly in contact with the sheave. Figure 5-13 (b) shows the wire with the maximum von Mises stress when some of the internal wires were removed for clarity; where again the maximum stress location is shown to occur in one of the 12 exterior wires that rest directly on the sheave, between layers 3 and 2. Table 5-17 shows the changes in all the stress and stress parameters as the load was increased.

With a D/d ratio of 15, Figure 5-14 (a) shows that the location of the maximum von Mises stress has moved away from the top centre of the sheave, to the left side of the sheave, but still very close to the top centre. The value of the von Mises stress here was 8,582 MPa at a load of 10.79 kN. Table 5-18 provides the variation in the stress parameters by load. Figure 5-14 (b) shows again that the maximum von Mises stress occurs at the 12 exterior wires that rest directly on the sheave as described in the Knapp's model for a D/d ratio of 90.9. Similarly, for D/d ratios of 30 and 60, the maximum von Mises stress had values of 6,310 MPa and 4,715 MPa respectively. Tables 5-19 and 5-20 provide the changes in stress and stress parameters with changing load.

Figures 5-15 (a) and 5-16 (a) show the location of maximum von Mises stress for D/d ratios of 30 and 60, respectively, which as before, occurred at the part of the strand on the top of the centre of the sheave. Figures 5-15 (b) and 5-16 (b) show that the contact patches are still located on one of the wires in the 12 exterior wires (layer 3) that rest on the sheave, where the intensity of the contact patches on the wires in the strands decreased as the D/d ratio increased. For a D/d ratio of 90.9 and $r = 1.92d$ the stresses were seen to be very high as shown earlier in Table 5-1, due to the impact of groove size.

Figure 5-17 shows the plot of von Mises stress versus nominal stress for Knapp's model at D/d ratios of 10, 15, 30, 60 and 90.9. It can be seen that as the D/d ratio and the load increased, the von Mises stress in the strands also increased. The effect of using a groove size of $r = 1.92d$ was seen to endorse the notion that a larger groove size has the tendency to increase stress and the stress concentration factor in the cables, and hence reduce the fatigue life of the cables. To clearly see the effect of the von Mises stress or SCF_{nom}, Figure 5-18 was plotted. As previously noted for the case of the 7-wire strand, in the case of the 19-wire strand at a D/d ratio of 60, the rate of increase in the von Mises stress to the $(D/d)\times\sigma_{nom}$ parameter was less than 3%, as shown in Figure 5-18. At a D/d ratio of 10 the rate was almost 19%. So again, for cranes, and mining equipment such as shovels, a large D/d ratio of 60 or higher is recommended based on the high stresses observed when smaller D/d ratio is used. Figure 5-19 shows the variation of SCF_{nom} versus $(D/d)\times\sigma_{nom}/E$, where again the same trend was evident as observed for the 7-wire strand discussed previously, to which Costello (1997) had observed similar trends for large diameter 6×19 Seale ropes. The SCF_{nom} effectively decreased with an increase in the dimensionless parameter, but thereafter remained constant at 2.5 to 3.5. That is, for a very high D/d ratio, typically greater than 60, the increase in stress or SCF_{nom} in a strand or wire rope becomes very small notwithstanding the load in the cable.

To investigate the effect of change in the strand diameter on fatigue life, two sizes of strand at 4.95 mm and 6.60 mm were used. For each diameter of strand the impact of a change in D/d ratio from 10 and 15 were investigated. Tables 5-21 through 5-24 show the stress parameters for these parametric studies, where it was observed that the von Mises stress are

higher for 6.60 mm strands compared to 4.95 mm strands. Therefore, this also supports the notion that an increase in D/d decreased the stress in the strands.

5.4.2 EFFECT OF GROOVE SIZE ON THE STRESSES IN 19-WIRE STRANDS BENT OVER SHEAVES

Three groove sizes were investigated: $r = 0.53d$, $r = 0.8d$, and $r = 1.0d$ for a constant D/d ratio of 10. Tables 5-25 and 5-26 show the stress results for a finite element analysis for groove sizes of $r = 0.8d$ and $r = 1.0d$ respectively. Figure 5-20 shows the plot of von Mises stress versus nominal stress for the different groove sizes. The stress was observed to be highest for $r = 0.53d$ at low loads, and lowest for $r = 1.0d$. But as the load was further increased, the reverse was the case, although an overall difference in groove size on stress concentration was considered negligible within the range investigated. The reason for this non-typical behaviour may be due to the number of wires in a strand or wire rope increasing. For smaller grooves, the stresses due to the adjacent wires are more than for cases when the groove is larger (effectively separating the adjacent wires), and this shows the importance of using sheaves with very small groove radii for equipment using strands or wire rope that will be subjected to very high fluctuating loads as may be seen in the present study commensurate with mining shovels. Figure 5-20 showed that there is a point where the effect of groove is minimal for the 19-wire strand bent over sheave, again this is at higher loads as observed in the 7-wire strands and this behaviour will be the same for a particular D/d ratio and strand or wire rope construction.

5.5 FATIGUE ANALYSIS RESULTS

5.5.1 FATIGUE ANALYSIS RESULTS FOR 7-WIRE STRANDS BENT OVER A SHEAVE

The fatigue resistance of the 7-wire strand bent over a sheave was evaluated using finite element analysis. The fatigue life and corresponding stress amplitude were shown in Tables 5-27 through 5-35. Figures 5-21 through 5-29 show the S-N plots and the mean predicted regression relationships. The fatigue life was shown to increase with an increase in D/d ratio and a decrease in stress amplitude. Tables 5-36 through 5-40 show the effect of an increase in groove radius for D/d ratios of 12 and 15, and Figures 5-30 through 5-34 show the S-N diagrams for the effect of groove geometry on the fatigue life. Between the groove sizes of $r = 0.53d$,

$r = 0.8d$, and $r = 1.0d$ little significant difference was observed in the predicted fatigue life especially a higher stress amplitudes or loads, but became more noticeable for the groove size $r = Infinity$ such that if the groove geometry is continuously increased the fatigue life may potentially be significantly reduced.

5.5.2 FATIGUE ANALYSIS RESULTS FOR 19-WIRE STRANDS BENT OVER A SHEAVE

The fatigue behaviour of the 19-wire strand bent over a sheave was obtained using the finite element and fatigue life analyses for their corresponding stress amplitudes as shown in Tables 5-41 through 5-48. Figures 5-35 through 5-42 show the S-N plots and the mean predicted regressions. The fatigue life, as previously observed for the 7-wire strand bent over a sheave increased with an increase in D/d ratio and decrease in stress amplitude. Tables 5-49 and 5-50 show the effect of an increase in groove radius for a D/d ratio of 10. Figures 5-43 and 5-44 show the S-N diagrams for the effect of groove geometry on fatigue life. Between the groove sizes of $r = 0.53d$, $r = 0.8d$, and $r = 1.0d$ little significant difference was observed in the predicted fatigue life, especially at higher load levels or stress amplitude.

5.5.3 FATIGUE REGRESSION MODEL AND COEFFICIENTS FOR 7-WIRE AND 19-WIRE STRANDS OVER SHEAVES

Multiple linear regression analysis was carried out for the parameters outlined by Feyrer (2007) for cables bent over sheaves. Regression analysis performed in the research reported in this thesis only determines the coefficients of the model for 7 and 19-wire strands. Its applicability to strands with a greater number of wires should be investigated before using these coefficients. The Feyrer's model given in Equation 5-1:

$$LogN = b_0 + b_1\left[\log\left(\frac{S}{d^2}\right) - 0.4\log\left(\frac{R_0}{1770}\right)\right] + b_2\log\left(\frac{D}{d}\right)\left[\log\left(\frac{S}{d^2}\right) - 0.4\log\left(\frac{R_0}{1770}\right)\right]$$
$$+ b_3\log\frac{D}{d} + b_4\log d + \frac{b_5}{1+\log\frac{l}{d}} \qquad (5\text{-}1)$$

Table 5-51 shows the regression coefficients for Equation 5-1 for 7 and 19-wire strands. An additional regression analysis was carried out by combining the results for the 7-wire and the 19-wire strands. The number of wires in the strand was added to the model as $b_6 \log z$, where the coefficients are also indicated in Table 5-51.

Comparison between the predicted tension bending fatigue life of a 3.3 mm diameter 19-wire strand in the current research using Equation 5-1 and a 8×19 seale wire rope of the same diameter was carried out and the result is shown in Figure 5-45. From the figure it can be seen that the predictions from the current research is less conservative but is significantly close (bearing in mind that failure is considered as first wire fracture) compared to the predicted fatigue life from Feyrer (2007). There is very little basis for comparison since both cables are substantially different in type and construction. This only reinforces the notion that when cables are subjected to bending over sheaves, cable construction is not of predominating influence on the fatigue life compared to parameters such as the D/d ratio, and the stress amplitude. A similarly good comparison was also found when comparing the predicted fatigue life for a 15.5 mm diameter strand and a 8×19 seale wire rope of the same diameter in tension bending fatigue as can be seen in Figure 5-46. Both comparisons had a D/d ratio of 60. Again the cables are different in construction, but the predictions did not seem to suggest any significant dependence of the fatigue life on the rope construction or type.

5.6 DISCUSSION

In Chapter 4, the fatigue of cables in tension was investigated and comparison between the predicted fatigue life and experimentally obtained fatigue life was carried out, but in bending of cables over sheaves we have a situation where the cable is subjected to tension bending fatigue. So it is necessary to compare the predicted fatigue life obtained using the stress based method to fatigue test results for a tension bending scenario. One of the very few test results was by Knapp (2004), and it involved the tension bending fatigue test of a 19-wire strand. A model of the 19-wire strand was created using finite element analysis where it was subjected to tension and bending to simulate the tension bending fatigue load. The stress based approach was used to obtain the predicted fatigue life and there was good agreement between the test fatigue life and the predicted fatigue life.

Using the 19-wire strand by Knapp, and the 7-wire strand by Costello (1997) subjected to bending over sheave, a parametric study was carried out. The von Mises stress was observed to decrease with increase in D/d ratio, also there exist a direct relationship between the von Mises stress and the stress or load amplitude.

The effect of groove radius and diameter of cable on the stress condition on strands bent over sheave was also investigated, and it was observed that an increase in the diameter of strand, for both the 7 and 19-wire strands increases the von Mises stress in the strands. For the groove sizes investigated, of $r = 0.53d$ to $r = 1.0d$ the effect of groove seems very minimal, but for groove sizes above this range as in the case of Knapp (2004) model, the von Mises stresses were observed to be significantly higher.

The fatigue life was predicted using the stress based approach from the linear elastic stress concentration factor, SCF_{nom}, and using the predicted fatigue life obtained from the parametric study, a multiple regression analysis was carried out using the Feyrer (2007) model as the basis for the analysis, and hence regression coefficients were proposed for the slightly different form of the Feyrer's model. The predicted fatigue life increases with an increase in D/d ratio and decrease in the stress amplitude. Feyrer (2007) and other researchers have observed this trend, Nabijou and Hobbs (1995) also observed and predicted that the fatigue life was directly proportional to the D/d ratio, although they confirmed that slip increases with increasing lay length to diameter of rope ratio, and decreasing D/d ratio. They observed that the highest wire slip correlates well with the experimental locations of wire failure when they are subjected to tension bending fatigue. The current research did not obtain relative movements of wires, although implicitly the relative movement is accounted for in the use of the maximum von Mises stress for obtaining the fatigue life. In all cases investigated, the location of the maximum von Mises stress was on the external wires that were in contact with the sheaves.

Table 5-1: Effect of strand force on various stress parameters for 19-wire strand, D/d=90.9

Strand force (kN)	**Max. von Mises stress (MPa)**	**Max. principal stress (MPa)**	**Max. Contact stress (MPa)**	SCF_{nom}
3.27	4,710	4,669	5,352	9.06
3.97	5,449	5,247	5,123	8.65
6.12	5,068	4,467	5,453	5.22
6.61	6,115	5,994	5,334	5.83
7.90	5,484	5,470	6,105	4.38
9.01	6,198	6,184	5,755	4.33
9.49	6,122	6,004	6,609	4.06

Table 5-2: Predicted fatigue life for 19-wire strand using finite element analysis results (D/d=90.9)

Strand force (kN)	S_N **(MPa)**	N **(Cycles)**
3.27	302.57	207,784
3.97	380.24	143,983
6.12	659.92	56,238
6.61	733.82	45,859
7.90	950.15	25,350
9.01	1,169.64	16,042
9.49	1,275.13	12,741

Table 5-3: Effect of strand force on various stress parameters for 7-wire strand, D/d=12

Strand force (kN)	**Max. von Mises stress (MPa)**	**Max. principal stress (MPa)**	**Max. Contact stress (MPa)**	SCF_{nom}
17.91	6,235	6,141	4,534	50.66
68.36	6,774	6,664	5,069	14.42
118.21	7,281	7,156	5,548	8.97
172.91	7,823	7,664	5,984	6.59

Table 5-4: Effect of strand force on various stress parameters for 7-wire strand, D/d=15

Strand force (kN)	**Max. von Mises stress (MPa)**	**Max. principal stress (MPa)**	**Max. Contact stress (MPa)**	SCF_{nom}
17.44	5,825	5,825	3,433	48.61
46.84	6,204	6,115	3,793	19.28
84.64	6,664	6,435	4,233	11.46
130.04	7,158	6,794	4,340	8.01
177.19	7,605	7,168	4,597	6.25

Table 5-5: Effect of strand force on various stress parameters for 7-wire strand, D/d=20

Strand force (kN)	**Max. von Mises stress (MPa)**	**Max. principal stress (MPa)**	**Max. Contact stress (MPa)**	SCF_{nom}
10.21	3,787	3,775	2,572	54.01
27.01	3,980	3,948	2,959	21.45
40.91	4,109	4,068	3,141	14.62
59.31	4,316	4,236	3,385	10.59
76.11	4,479	4,373	3,462	8.57
85.71	4,561	4,443	3,567	7.75
90.71	4,610	4,484	3,639	7.40

Table 5-6: Effect of strand force on various stress parameters for 7-wire strand, D/d=40

Strand force (kN)	**Max. von Mises stress (MPa)**	**Max. principal stress (MPa)**	**Max. Contact stress (MPa)**	SCF_{nom}
3.33	3,225	3,230	4,316	140.80
10.70	3,323	3,327	4,386	45.21
17.75	3,431	3,437	4,496	28.14
21.60	3,484	3,492	4,588	23.48
28.20	3,527	3,532	4,641	18.20
39.10	3,706	3,690	4,946	13.80
43.25	3,708	3,682	4,908	12.48
55.05	3,858	3,798	4,994	10.20
67.90	4,061	3,936	5,144	8.71
74.30	4,111	3,945	5,215	8.05

Table 5-7: Effect of strand force on various stress parameters for 7-wire strand, D/d=60

Strand force (kN)	**Max. von Mises stress (MPa)**	**Max. principal stress (MPa)**	**Max. Contact stress (MPa)**	SCF_{nom}
4.91	2,031	2,026	2,050	60.21
10.74	2,171	2,164	2,048	29.42
21.13	2,341	2,325	2,204	16.13
47.68	2,779	2,762	2,584	8.48
70.63	3,111	3,054	2,993	6.41
74.53	3,209	3,140	3,121	6.27

Table 5-8: Effect of strand force on various stress parameters for 7-wire strand, D/d=12 (d=7.80 mm)

Strand force (kN)	**Max. von Mises stress (MPa)**	**Max. principal stress (MPa)**	**Max. Contact stress (MPa)**	SCF_{nom}
3.01	6,230	6,113	3,998	75.35
14.91	6,687	6,565	4,361	16.32
27.17	7,160	7,038	4,645	9.59
40.70	7,687	7,550	5,210	6.87
54.50	8,246	8,053	6,179	5.51
68.55	8,857	8,538	6,506	4.70

Table 5-9: Effect of strand force on various stress parameters for 7-wire strand, D/d=15 (d=7.80 mm)

Strand force (kN)	**Max. von Mises stress (MPa)**	**Max. principal stress (MPa)**	**Max. Contact stress (MPa)**	SCF_{nom}
3.06	5,821	5,778	3,196	69.32
10.27	6,167	6,131	3,741	21.86
19.70	6,513	6,478	4,107	12.03
31.21	6,934	6,887	4,158	8.08
42.86	7,374	7,273	4,524	6.26
54.61	7,821	7,682	4,689	5.21

Table 5-10: Effect of strand force on various stress parameters for 7-wire strand, D/d=12 (d=11.62 mm)

Strand force (kN)	**Max. von Mises stress (MPa)**	**Max. principal stress (MPa)**	**Max. Contact stress (MPa)**	SCF_{nom}
1.91	6,018	5,908	3,810	258.70
13.56	6,186	6,077	4,051	37.36
31.31	6,512	6,413	4,456	17.03
49.31	6,816	6,715	4,723	11.32
68.56	7,170	7,070	5,103	8.56
88.81	7,530	7,421	5,422	6.94

Table 5-11: Effect of strand force on various stress parameters for 7-wire strand, D/d=15 (d=11.62 mm)

Strand force (kN)	**Max. von Mises stress (MPa)**	**Max. principal stress (MPa)**	**Max. Contact stress (MPa)**	SCF_{nom}
4.32	5,928	5,926	3,489	112.29
15.05	6,119	6,107	3,661	33.30
28.15	6,395	6,331	3,871	18.61
44.00	6,728	6,564	3,980	12.52
60.35	7,019	6,801	4,120	9.53
78.40	7,356	7,060	4,352	7.68

Table 5-12: Effect of strand force on various stress parameters for 7-wire strand, D/d=12 ($r = 0.8d$)

Strand force (kN)	**Max. von Mises stress (MPa)**	**Max. principal stress (MPa)**	**Max. Contact stress (MPa)**	SCF_{nom}
10.73	6,197	6,134	3,604	84.06
35.38	6,674	6,658	3,811	27.45
68.58	7,067	7,043	4,001	15.00
114.58	7,449	7,454	4,461	9.46
164.98	7,861	7,867	5,474	6.94
197.18	8,145	8,120	5,714	6.01

Table 5-13: Effect of strand force on various stress parameters for 7-wire strand, D/d=12 ($r = 1.0d$)

Strand force (kN)	Max. von Mises stress (MPa)	Max. principal stress (MPa)	Max. Contact stress (MPa)	SCF_{nom}
13.67	6,346	6,283	2,767	67.58
28.65	6,459	6,438	3,442	32.82
54.95	6,914	6,862	3,362	18.31
92.40	7,384	7,348	3,895	11.63
137.15	7,820	7,793	4,455	8.30
167.95	8,161	8,109	4,826	7.07

Table 5-14: Effect of strand force on various stress parameters for 7-wire strand, D/d=12 ($r = Infinity$)

Strand force (kN)	Max. von Mises stress (MPa)	Max. principal stress (MPa)	Max. Contact stress (MPa)	SCF_{nom}
6.28	6,046	6,016	5,104	140.03
16.12	6,373	6,325	5,226	57.53
29.12	6,925	6,839	5,778	34.61
47.77	7,248	7,232	7,032	22.08
72.12	7,644	7,601	6,124	15.43
90.77	7,804	7,791	6,100	12.51

Table 5-15: Effect of strand force on various stress parameters for 7-wire strand, D/d=15 ($r = 0.8d$)

Strand force (kN)	Max. von Mises stress (MPa)	Max. principal stress (MPa)	Max. Contact stress (MPa)	SCF_{nom}
8.39	6,177	6,107	3,605	107.20
27.14	6,563	6,539	3,707	35.20
53.89	6,853	6,750	4,127	18.51
90.49	7,156	7,054	4,364	11.51
132.64	7,514	7,408	4,361	8.25

Table 5-16: Effect of strand force on various stress parameters for 7-wire strand, D/d=15 ($r = 1.0d$)

Strand force (kN)	Max. von Mises stress (MPa)	Max. principal stress (MPa)	Max. Contact stress (MPa)	SCF_{nom}
8.46	6,184	6,145	3,855	106.43
26.91	6,410	6,347	4,038	34.67
53.96	6,710	6,583	4,612	18.10
85.71	7,051	6,944	4,889	11.97
125.96	7,394	7,261	5,201	8.54

Table 5-17: Effect of strand force on various stress parameters for 19-wire strand, D/d=10

Strand force (kN)	Max. von Mises stress (MPa)	Max. principal stress (MPa)	Max. Contact stress (MPa)	SCF_{nom}
1.71	7,561	7,468	4,345	27.82
3.95	8,318	8,190	5,219	13.28
6.37	9,067	8,893	6,007	8.97
9.29	9,823	9,632	6,943	6.66

Table 5-18: Effect of strand force on various stress parameters for 19-wire strand, D/d=15

Strand force (kN)	Max. von Mises stress (MPa)	Max. principal stress (MPa)	Max. Contact stress (MPa)	SCF_{nom}
1.33	4,761	4,177	4,643	22.61
2.58	5,304	4,800	4,986	12.94
4.71	6,196	5,626	5,649	8.28
6.45	6,896	6,129	5,937	6.73
8.49	7,850	6,702	6,240	5.83
10.79	8,582	7,187	6,872	5.01

Table 5-19: Effect of strand force on various stress parameters for 19-wire strand, D/d=30

Strand force (kN)	Max. von Mises stress (MPa)	Max. principal stress (MPa)	Max. Contact stress (MPa)	SCF_{nom}
1.01	3,391	3,147	3,621	21.08
3.29	4,342	3,692	4,117	8.31
5.05	4,574	4,781	4,794	5.71
7.58	5,630	5,400	5,629	4.68
9.30	6,310	5,838	6,166	4.28

Table 5-20: Effect of strand force on various stress parameters for 19-wire strand, D/d=60

Strand force (kN)	Max. von Mises stress (MPa)	Max. principal stress (MPa)	Max. Contact stress (MPa)	SCF_{nom}
3.91	3,148	2,905	3,072	5.07
4.60	3,503	3,945	3,003	4.80
6.09	3,727	3,923	3,389	3.86
7.25	3,894	4,366	3,590	3.39
8.33	4,226	4,631	3,757	3.20
9.89	4,715	4,830	4,906	3.00
10.76	4,819	5,367	6,268	2.82

Table 5-21: Effect of strand force on various stress parameters for 19-wire strand, D/d=10 (d=4.95 mm)

Strand force (kN)	**Max. von Mises stress (MPa)**	**Max. principal stress (MPa)**	**Max. Contact stress (MPa)**	SCF_{nom}
5.08	8,324	8,202	5,262	23.21
11.49	9,359	9,239	5,869	11.55
19.29	10,370	10,180	8,485	7.62

Table 5-22: Effect of strand force on various stress parameters for 19-wire strand, D/d=15 (d=4.95 mm)

Strand force (kN)	**Max. von Mises stress (MPa)**	**Max. principal stress (MPa)**	**Max. Contact stress (MPa)**	SCF_{nom}
3.57	4,597	4,256	4,387	18.23
7.57	5,275	4,963	5,025	9.87
13.75	6,488	5,871	5,629	6.69

Table 5-23: Effect of strand force on various stress parameters for 19- wire strand, D/d=10 (d=6.6 mm)

Strand force (kN)	**Max. von Mises stress (MPa)**	**Max. principal stress (MPa)**	**Max. Contact stress (MPa)**	SCF_{nom}
6.68	8,047	7,956	4,804	30.36
15.00	8,981	8,893	5,326	15.08
24.62	9,796	9,680	11,040	10.03

Table 5-24: Effect of strand force on various stress parameters for 19-wire strand, D/d=15 (d=6.6 mm)

Strand force (kN)	**Max. von Mises stress (MPa)**	**Max. principal stress (MPa)**	**Max. Contact stress (MPa)**	SCF_{nom}
4.34	3,888	3,641	4,761	5.65
10.69	4,833	4,350	5,180	2.85
16.47	5,224	4,902	6,768	2.00
24.47	6,061	5,518	5,603	1.56

Table 5-25: Effect of strand force on various stress parameters for 19-wire strand, D/d=10 ($r = 0.8d$)

Strand force (kN)	Max. von Mises stress (MPa)	Max. principal stress (MPa)	Max. Contact stress (MPa)	SCF_{nom}
1.67	7,270	7,172	5,941	27.39
3.50	7,851	7,597	6,900	14.14
6.04	8,538	8,440	8,232	8.91
8.69	9,605	9,181	8,555	6.97

Table 5-26: Effect of strand force on various stress parameters for 19-wire strand, D/d=10 ($r = 1.0d$)

Strand force (kN)	Max. von Mises stress (MPa)	Max. principal stress (MPa)	Max. Contact stress (MPa)	SCF_{nom}
0.732	5,319	4,901	4,248	45.79
2.22	5,798	5,587	4,546	16.43
3.90	6,577	6,330	5,535	10.63
6.25	7,547	7,034	6,402	7.61
8.80	8,705	7,564	7,648	6.24

Table 5-27: Predicted fatigue results for 7-wire strand using finite element analysis results (D/d=12)

Strand force (kN)	S_N **(MPa)**	N **(Cycles)**
17.91	63.67	670,916
68.36	269.21	202,249
118.21	521.1	83,297
172.91	877.18	33,924

Table 5-28: Predicted fatigue results for 7-wire strand using finite element analysis results (D/d=15)

Strand force (kN)	S_N **(MPa)**	N **(Cycles)**
17.44	61.93	705,252
46.84	176.33	321,199
84.64	345.33	150,989
130.04	589.95	68,471
177.19	909.6	31,418

Table 5-29: Predicted fatigue results for 7-wire strand using finite element analysis results (D/d=20)

Strand force (kN)	S_N **(MPa)**	N **(Cycles)**
27.01	97.69	651,243
40.91	152.14	448,993
59.31	229.09	290,481
76.11	304.74	202,349
85.71	350.50	166,171
90.71	375.12	150,174

Table 5-30: Predicted fatigue results for 7-wire strand using finite element analysis results (D/d=40)

Strand force (kN)	S_N **(MPa)**	N **(Cycles)**
21.60	77.32	827,015
28.20	102.25	678,335
39.10	144.89	497,353
43.25	161.62	450,188
55.05	210.77	336,834
67.90	267.11	249,486
74.30	296.34	217,369

Table 5-31: Predicted fatigue results for 7-wire strand using finite element analysis results (D/d=60)

Strand force (kN)	S_N **(MPa)**	N **(Cycles)**
21.13	75.57	1,110,089
47.68	179.8	485,177
70.63	279.49	268,313
74.53	297.41	242,436

Table 5-32: Predicted fatigue results for 7-wire strand using finite element analysis results (D/d=12, d=7.80 mm)

Strand force (kN)	S_N **(MPa)**	N **(Cycles)**
3.01	42.29	872,788
14.91	230.60	248,641
27.17	468.42	99,433
40.70	803.50	39,432

Table 5-33: Predicted fatigue results for 7-wire strand using finite element analysis results (D/d=15, d=7.80 mm)

Strand force (kN)	S_N **(MPa)**	N **(Cycles)**
3.06	42.97	897,361
10.27	152.77	381,522
19.70	317.29	173,931
31.21	559.16	75,429
42.86	866.12	33,747

Table 5-34: Predicted fatigue results for 7-wire strand using finite element analysis results (D/d=12, d=11.62 mm)

Strand force (kN)	S_N **(MPa)**	N **(Cycles)**
1.91	11.71	1,410,867
13.56	86.70	565,363
31.31	213.34	265,308
49.31	359.98	143,327
68.56	541.89	78,699
88.81	768.83	43,104

Table 5-35: Predicted fatigue results for 7-wire strand using finite element analysis results (D/d=15, d=11.62 mm)

Strand force (kN)	S_N **(MPa)**	N **(Cycles)**
4.32	26.78	1,060,645
15.05	96.71	528,143
28.15	189.57	299,951
44.00	314.57	170,533
60.35	460.74	101,149
78.40	647.00	58,619

Table 5-36: Predicted fatigue results for 7-wire strand using finite element analysis results ($d = 15.5mm, D/d = 12, r = 0.8d$)

Strand force (kN)	S_N **(MPa)**	N **(Cycles)**
10.73	37.61	925,079
35.38	130.14	419,771
68.58	270.18	204,951
114.58	500.73	89,317
164.98	819.02	38,131

Table 5-37: Predicted fatigue results for 7-wire strand using finite element analysis results ($d = 15.5mm, D/d = 12, r = 1.0d$)

Strand force (kN)	S_N **(MPa)**	N **(Cycles)**
13.67	48.18	810,257
28.65	103.97	504,701
54.95	210.34	269,650
92.40	383.58	131,277
137.15	633.29	60,811
167.95	840.48	36,497

Table 5-38: Predicted fatigue results for 7-wire strand using finite element analysis results ($d = 15.5mm, D/d = 12, r = Infinity$)

Strand force (kN)	S_N **(MPa)**	N **(Cycles)**
6.28	21.84	1,175,732
16.12	57.11	739,031
29.12	105.78	482,100
47.77	180.17	306,769
72.12	286.30	186,948
90.77	375.44	133,300

Table 5-39: Predicted fatigue results for 7-wire strand using finite element analysis results ($d = 15.5mm, D/d = 15, r = 0.8d$)

Strand force (kN)	S_N **(MPa)**	N **(Cycles)**
8.39	29.27	1,034,934
27.14	98.20	521,321
53.89	205.82	276,511
90.49	374.03	136,833
132.64	605.61	65,666

Table 5-40: Predicted fatigue results for 7-wires strand using finite element analysis results ($d = 15.5mm, D/d = 15, r = 1.0d$)

Strand force (kN)	S_N **(MPa)**	N **(Cycles)**
8.46	29.52	1,030,662
26.91	97.32	530,687
53.96	206.12	278,495
85.71	350.51	149,627
125.96	565.73	73,621

Table 5-41: Predicted fatigue results for 19-wire strand using finite element analysis results (D/d=10)

Strand force (kN)	S_N **(MPa)**	N **(Cycles)**
1.71	146.71	360,335
3.95	377.53	130,391
6.37	696.63	51,823

Table 5-42: Predicted fatigue results for 19-wire strand using finite element analysis results (D/d=15)

Strand force (kN)	S_N **(MPa)**	N **(Cycles)**
1.33	111.71	561,712
2.58	230.60	273,793
4.71	469.36	101,630
6.45	709.52	49,435

Table 5-43: Predicted fatigue results for 19-wire strand using finite element analysis results (D/d=30)

Strand force (kN)	S_N **(MPa)**	N **(Cycles)**
1.01	84.16	847,048
3.29	304.51	213,112
5.05	511.89	92,590
7.58	893.47	29,555

Table 5-44: Predicted fatigue results for 19-wire strand using finite element analysis results (D/d=60)

Strand force (kN)	S_N **(MPa)**	N **(Cycles)**
3.91	373.16	180,680
4.60	455.45	122,080
6.09	655.53	56,727
7.25	836.36	31,229

Table 5-45: Predicted fatigue results for 19-wire strand using finite element analysis results (D/d=10, d=4.95 mm)

Strand force (kN)	S_N **(MPa)**	N **(Cycles)**
5.08	198.70	265,291
11.49	519.61	82,302
19.29	1079.86	23,749

Table 5-46: Predicted fatigue results for 19-wire strand using finite element analysis results (D/d=15, d=4.95 mm)

Strand force (kN)	S_N **(MPa)**	N **(Cycles)**
3.57	135.34	491,671
7.57	312.54	190,606
13.75	658.55	56,702

Table 5-47: Predicted fatigue results for 19-wire strand using finite element analysis results (D/d=10, d=6.6 mm)

Strand force (kN)	S_N **(MPa)**	N **(Cycles)**
6.68	142.81	358,767
15.00	355.16	138,359
24.62	665.02	56,108

Table 5-48: Predicted fatigue results for 19-wire strand using finite element analysis results (D/d=15, d=6.6 mm)

Strand force (kN)	S_N **(MPa)**	N **(Cycles)**
4.34	90.23	739,201
10.69	239.74	273,382
16.47	397.36	136,567
24.47	659.55	56,480

Table 5-49: Predicted fatigue results for 19-wire strand using finite element analysis results ($d = 3.3mm, D/d = 10, r = 0.8d$)

Strand force (kN)	S_N **(MPa)**	N **(Cycles)**
1.67	143.01	374,289
3.50	326.84	158,581
6.04	647.82	58,508

Table 5-50: Predicted fatigue results for 19-wire strand using finite element analysis results ($d = 3.3mm, D/d = 10, r = 1.0d$)

Strand force (kN)	S_N **(MPa)**	N **(Cycles)**
0.732	59.99	791,461
2.22	195.24	312,922
3.90	372.12	140,826
6.25	679.11	53,806

Table 5-51: Mean fatigue life prediction regression coefficients for strands bent over sheaves

Strand or wire rope type	b_0	b_1	b_2	b_3	b_4	b_5	b_6
7-wire	13.31	-0.74	-0.28	-0.57	0.087	-11.80	-
19-wire	18.11	-1.36	-0.051	-2.17	-0.11	-16.19	-
7 &19-wire	13.29	-0.37	-0.67	-0.023	0.16	-13.42	0.24

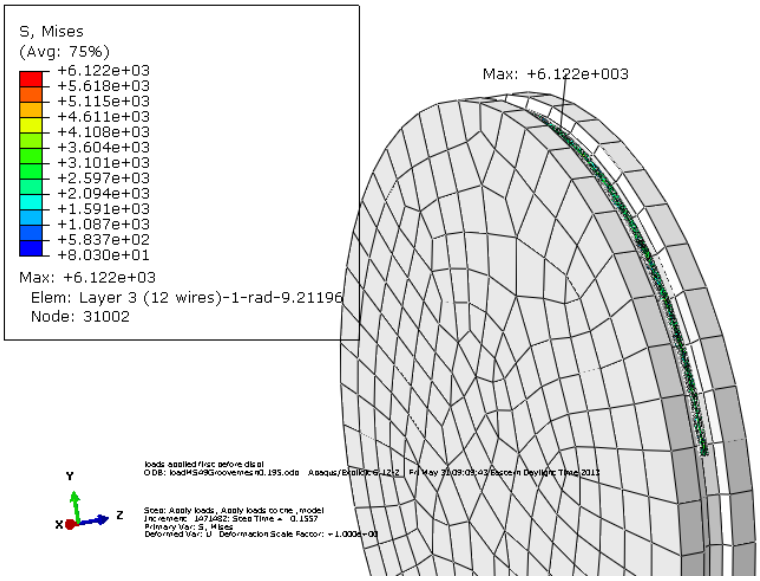

(a) Knapp model bent over sheave showing location of maximum von Mises stress

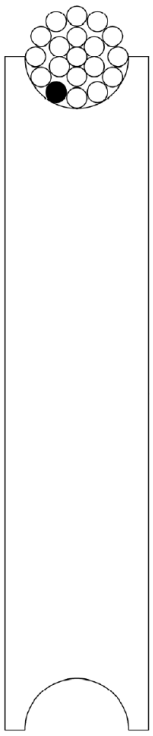

(b) Diagram of Knapp's strand cross section on sheave showing the critical wire

Figure 5-1: FEA model of strand tested by Knapp (D/d=90.9; strand force = 9.49 kN)

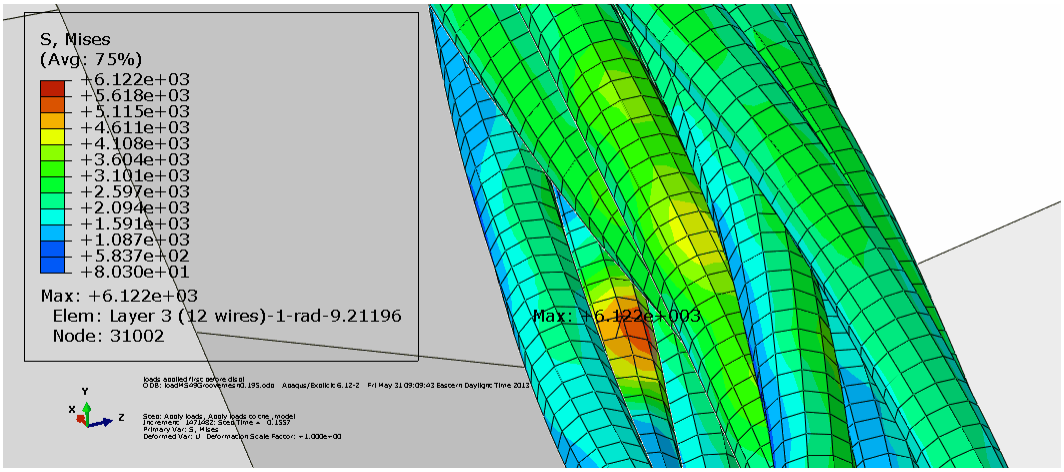

(c) Close-up of Knapp model bent over sheave showing location of maximum von Mises stress for a strand force of 9.49 kN

Figure 5-1: (Cont'd)

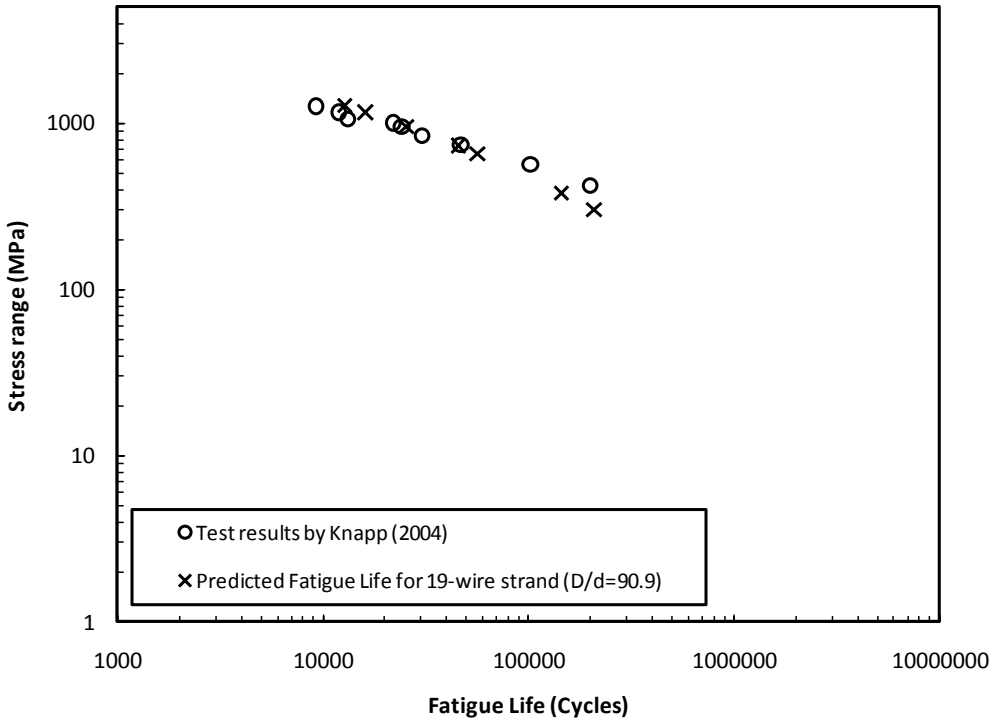

Figure 5-2: Comparison between test results and prediction for 19-wire strand

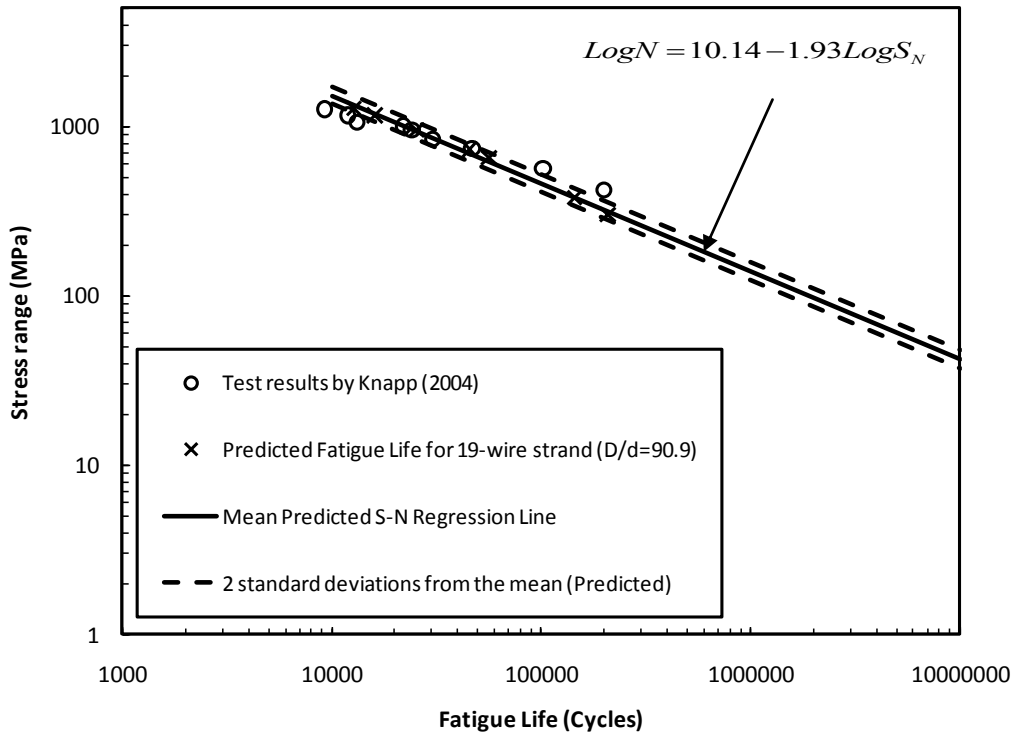

Figure 5-3: Comparison between test results and prediction for 19-wire strand

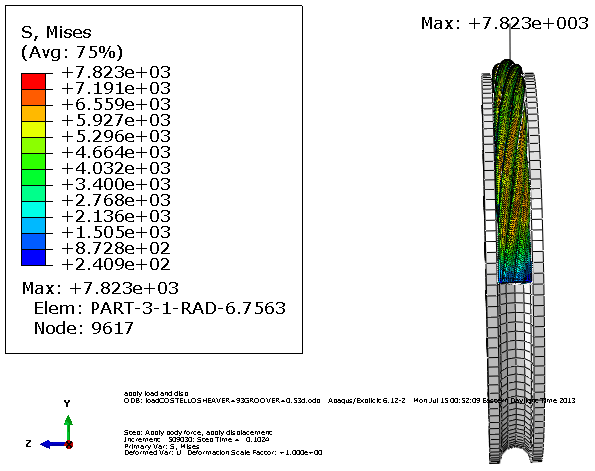

(a) Costello 7-wire strand model showing location of maximum von Mises stress

Figure 5-4: Costello model for D/d=12 bent over sheave for a strand force of 172.91 kN

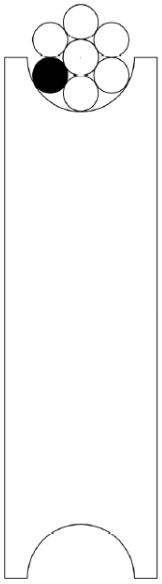

(b) Diagram of Costello's strand cross section on sheave showing the critical wire

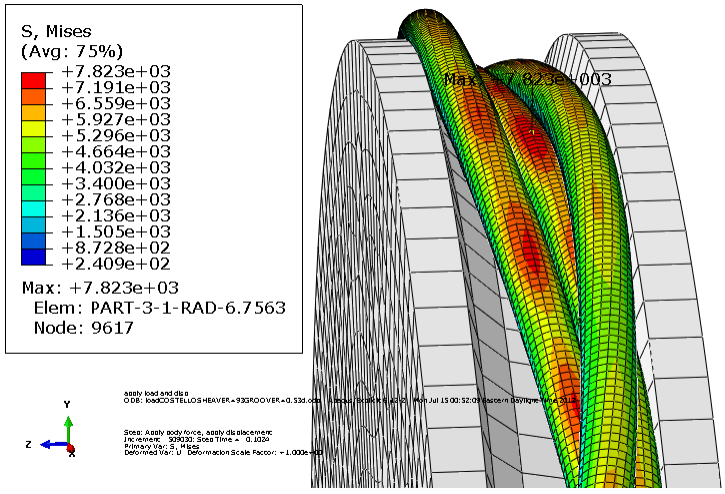

(c) Close-up of Costello 7-wire strand bent over sheave showing location of maximum von Mises stress

Figure 5-4: (Cont'd)

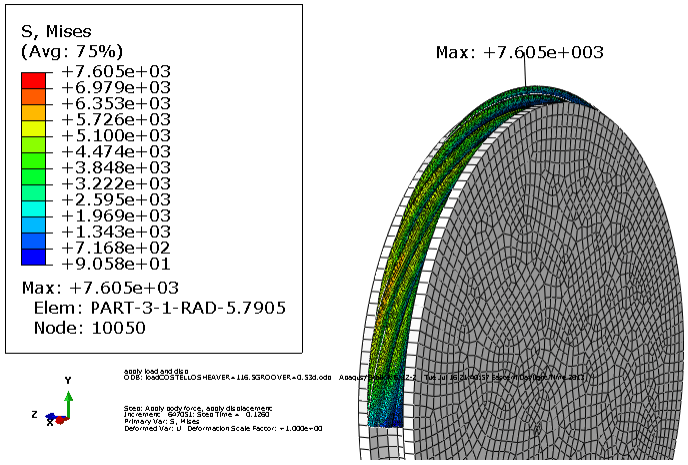

(a) Costello 7-wire strand model showing location of maximum von Mises stress

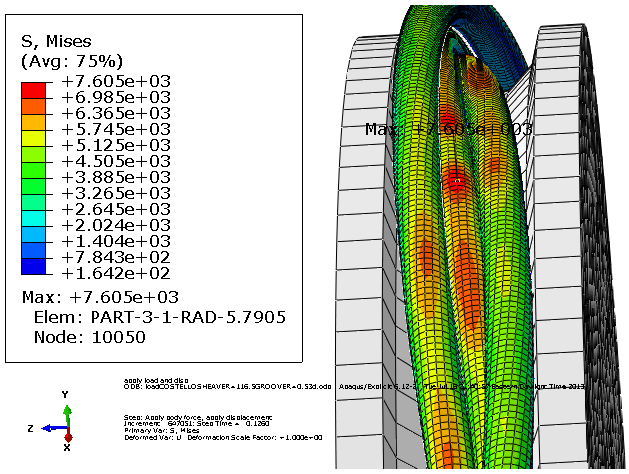

(b) Close-up of Costello 7-wire strand bent over sheave showing location of maximum von Mises stress

Figure 5-5: Costello 7-wire strand for D/d=15 bent over sheave for a strand force of 177.19 kN

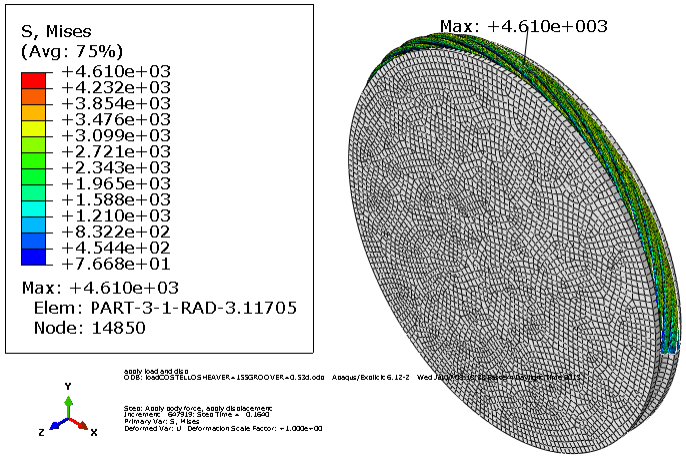

(a) Costello 7-wire strand model showing location of maximum von Mises stress

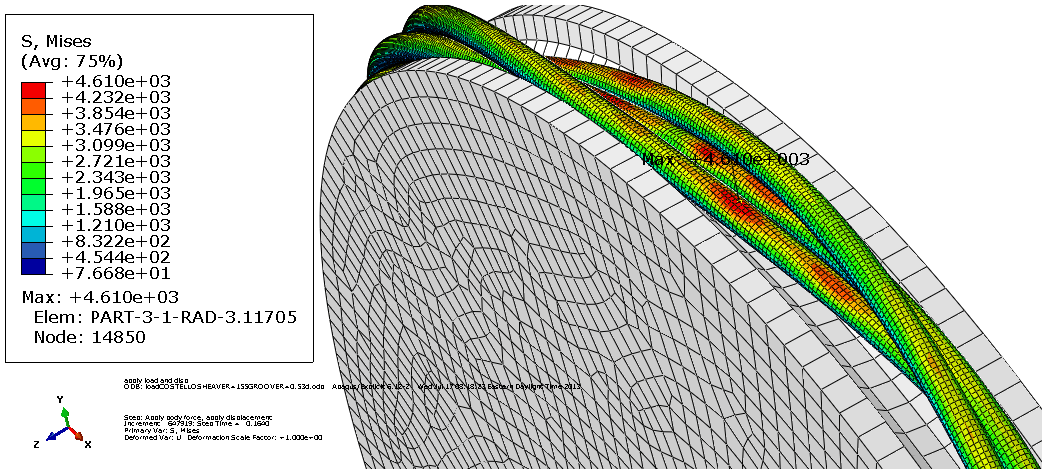

(b) Close-up of Costello 7-wire strand bent over sheave showing location of maximum von Mises stress

Figure 5-6: Costello model for D/d=20 bent over sheave for a strand force of 90.71 kN

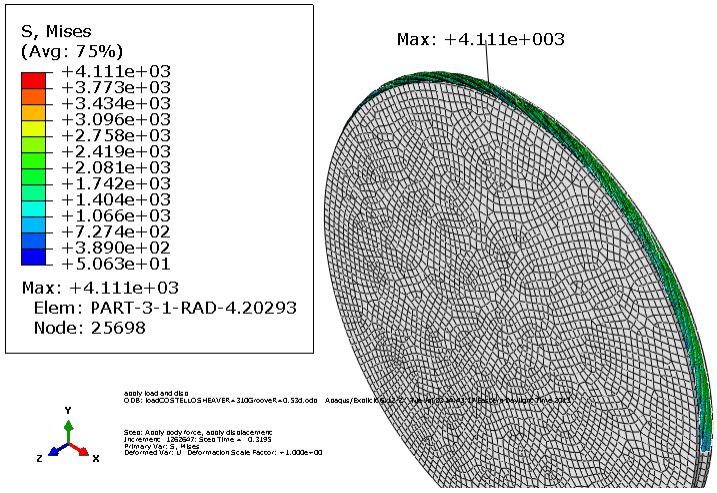

(a) Costello 7-wire strand showing location of maximum von Mises stress

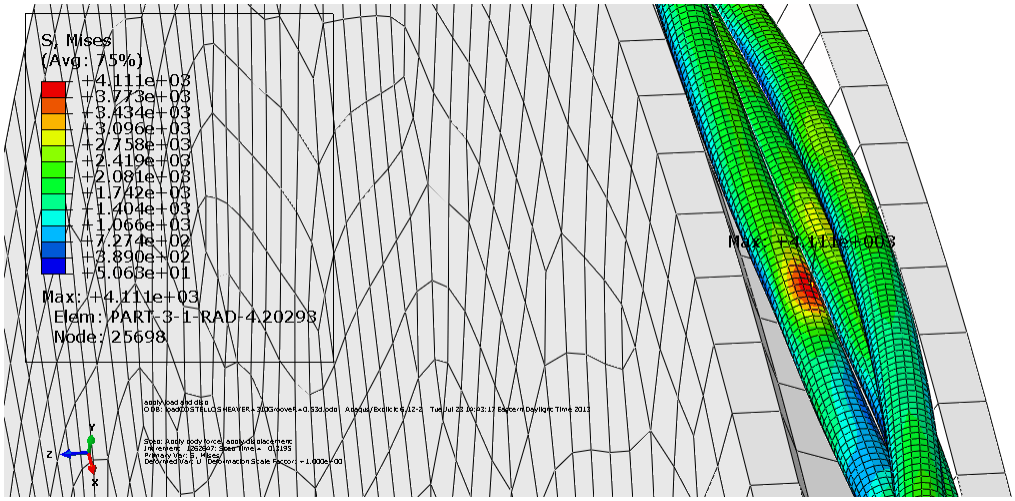

(b) Close-up of Costello 7-wire strand bent over sheave showing location of maximum von Mises stress

Figure 5-7: Costello 7-wire strand for D/d=40 bent over sheave for a strand force of 74.30 kN

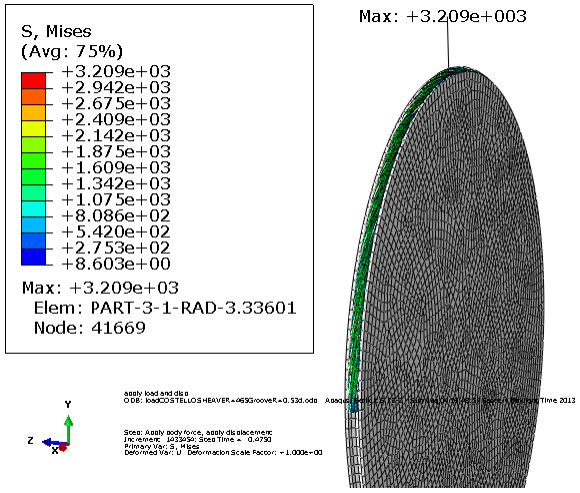

(a) Costello 7-wire strand model showing location of maximum von Mises stress

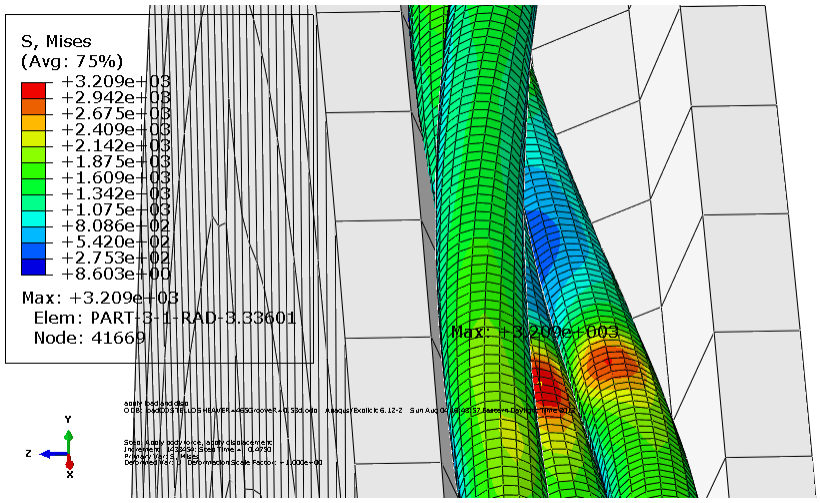

(b) Close-up of Costello 7-wire strand bent over sheave showing location of maximum von Mises stress

Figure 5-8: Costello 7-wire strand for D/d=60 bent over sheave for a strand force of 74.53 kN

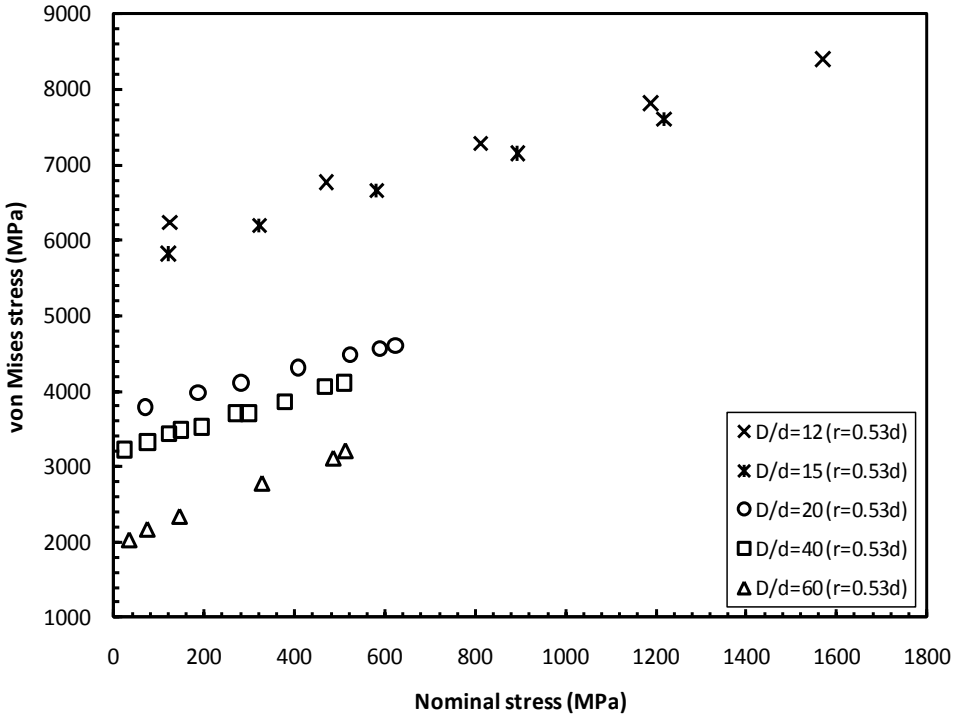

Figure 5-9: von Mises stress versus strand applied stress for 7-wire strand for various D/d and constant sheave radius of 0.53d

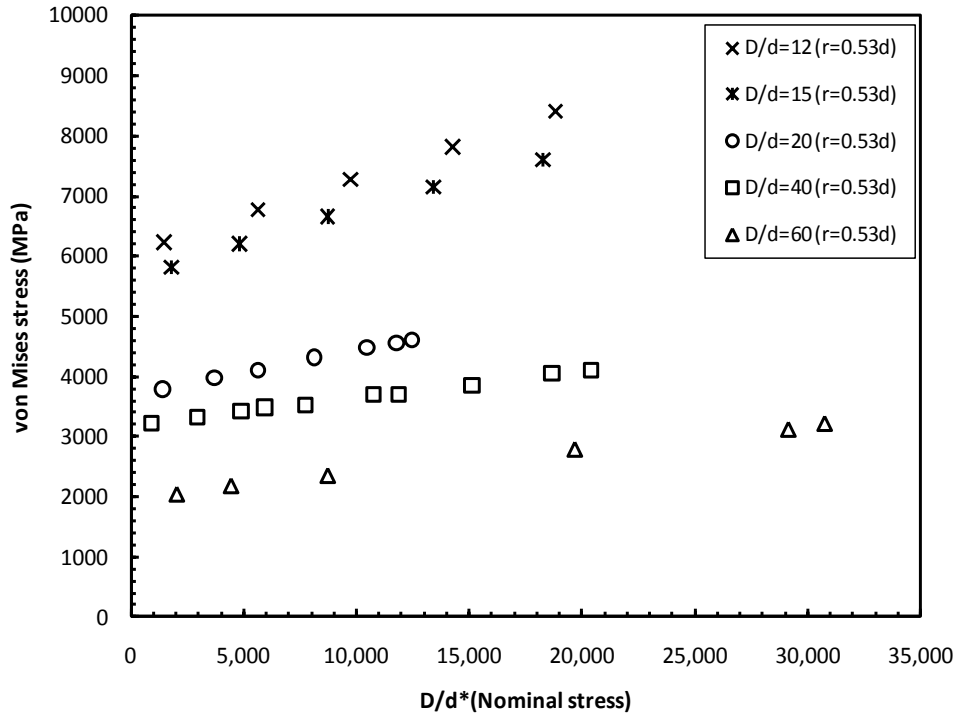

Figure 5-10: von Mises stress versus strand dimensional parameter for 7-wire strand for various D/d and constant sheave radius of 0.53d

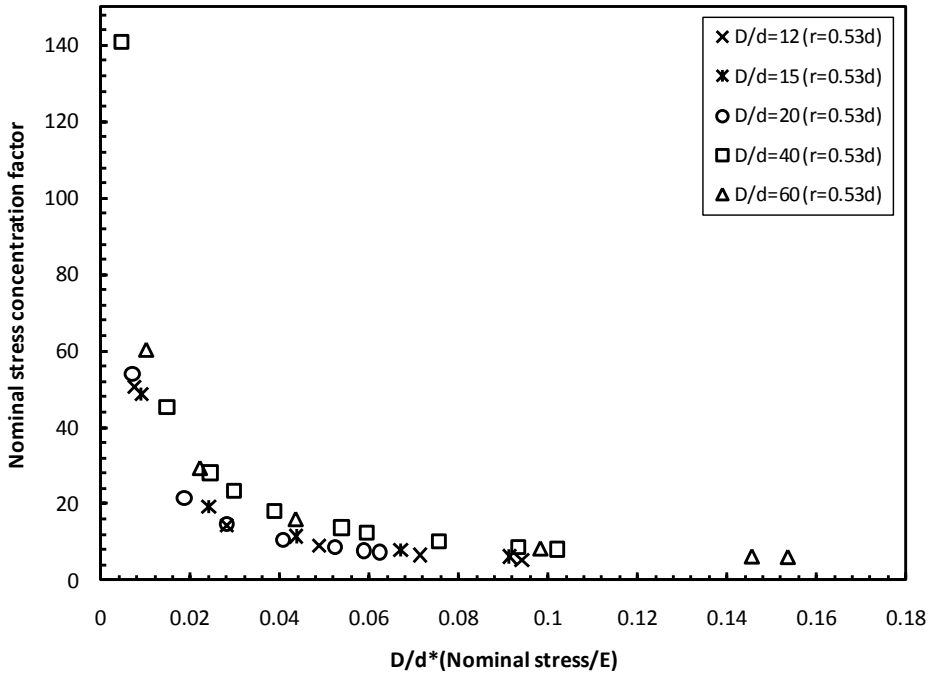

Figure 5-11: SCF_{nom} versus dimensionless parameter for 7-wire strand various D/d and constant groove radius

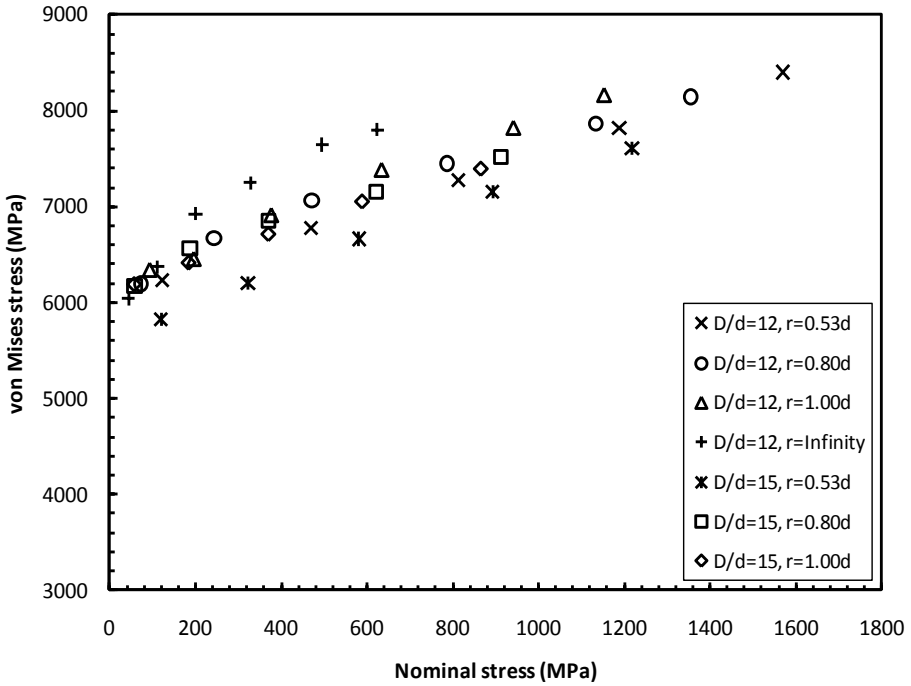

Figure 5-12: Effect of groove size for 7-wire strand various D/d and constant groove radius

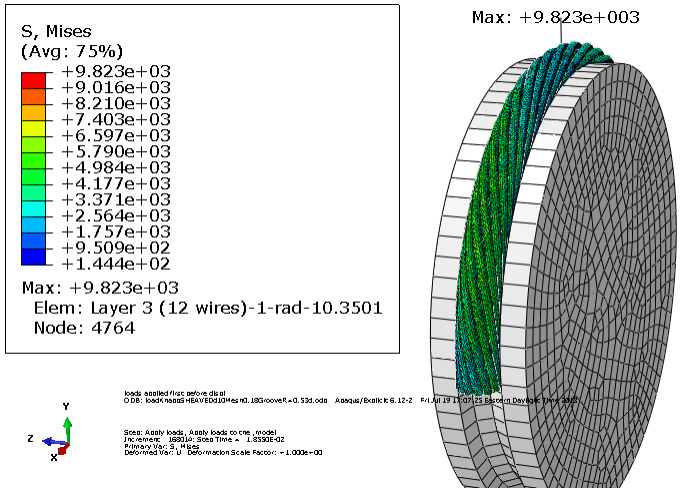

(a) Knapp 19-wire strand model showing location of maximum von Mises stress

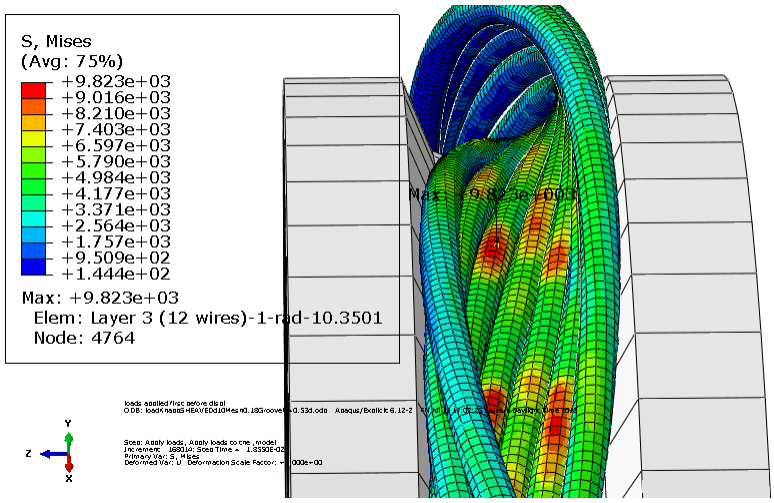

(b) Close-up of Knapp 19-wire strand bent over sheave showing location of maximum von Mises stress

Figure 5-13: Knapp 19-wire strand for D/d=10 bent over sheave for a strand force of 9.29 kN

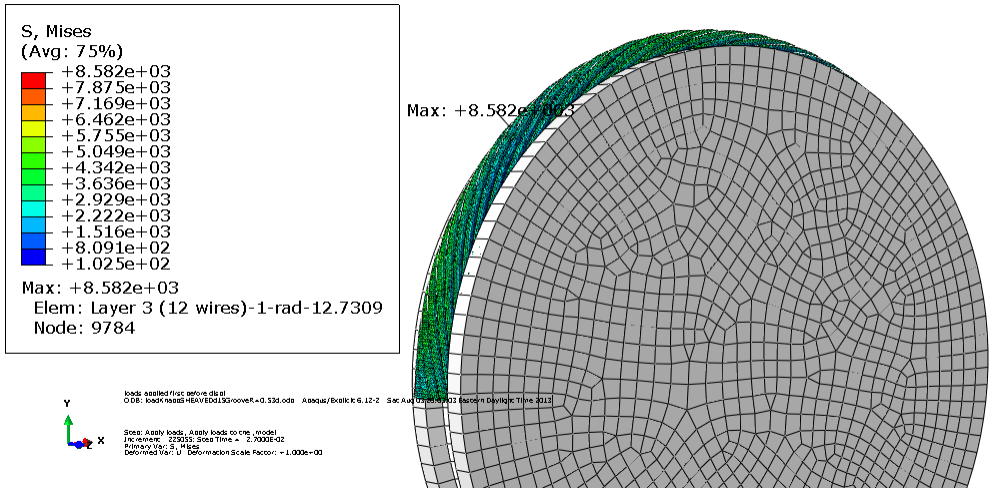

(a) Knapp 19-wire strand model showing location of maximum von Mises stress

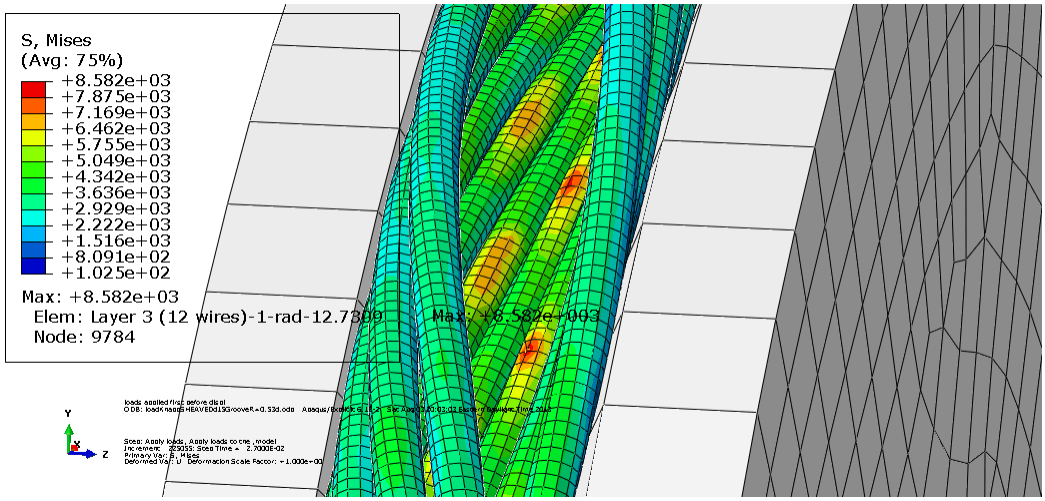

(b) Close-up of Knapp 19-wire strand bent over sheave showing location of maximum von Mises stress

Figure 5-14: Knapp 19-wire strand for D/d=15 bent over sheave for a strand force of 10.79 kN

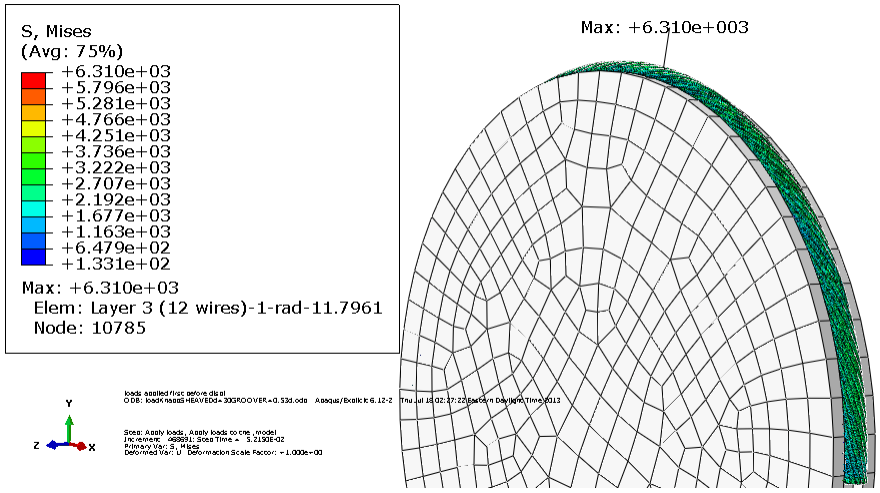

(a) Knapp 19-wire strand model showing location of maximum von Mises stress

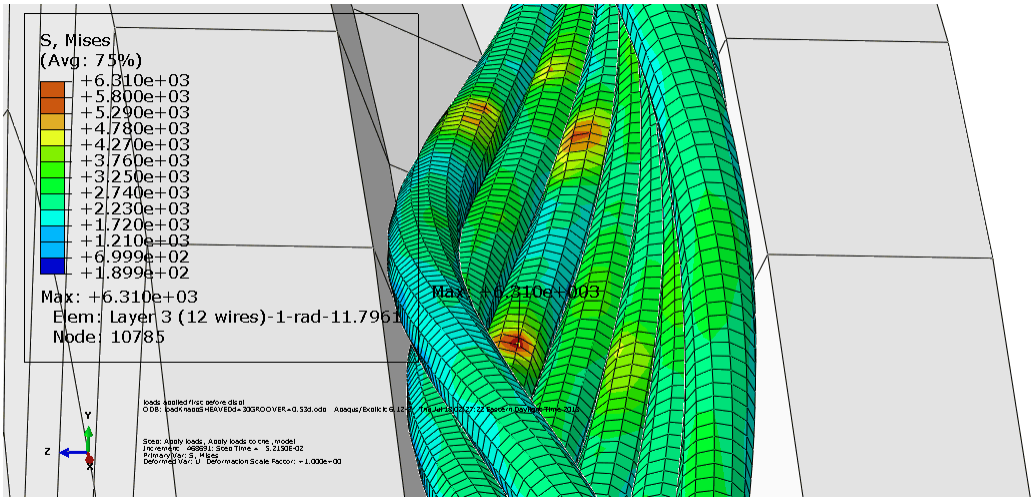

(b) Close-up of Knapp 19-wire strand bent over sheave showing location of maximum von Mises stress

Figure 5-15: Knapp 19-wire strand for D/d=30 bent over sheave for a strand force of 9.30 kN

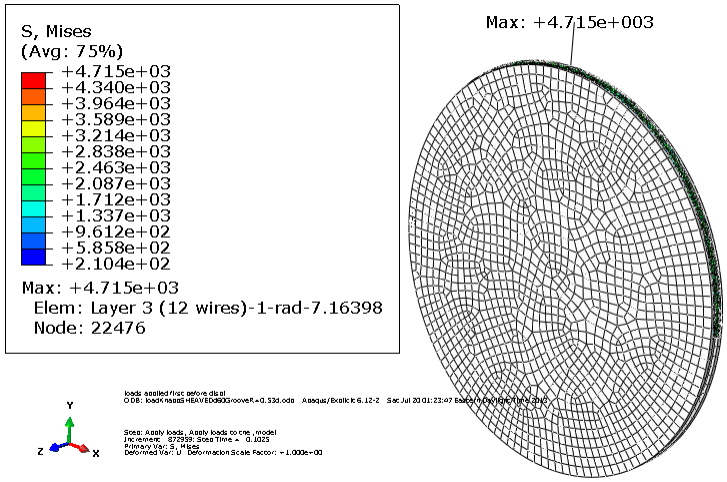

(a) Knapp 19-wire strand model showing location of maximum von Mises stress

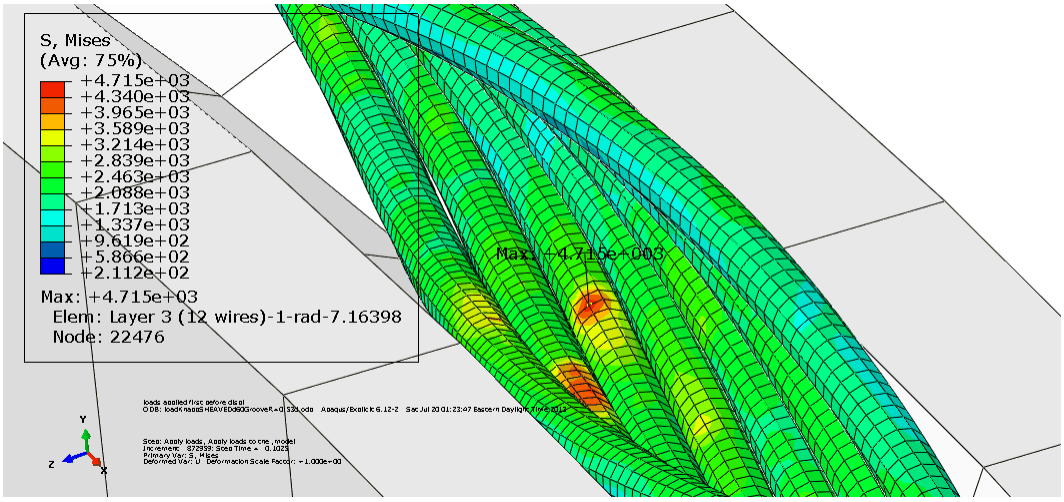

(b) Close-up of Knapp 19-wire strand bent over sheave showing location of maximum von Mises stress

Figure 5-16: Knapp 19-wire strand for D/d=60 bent over sheave for a strand force of 9.89 kN

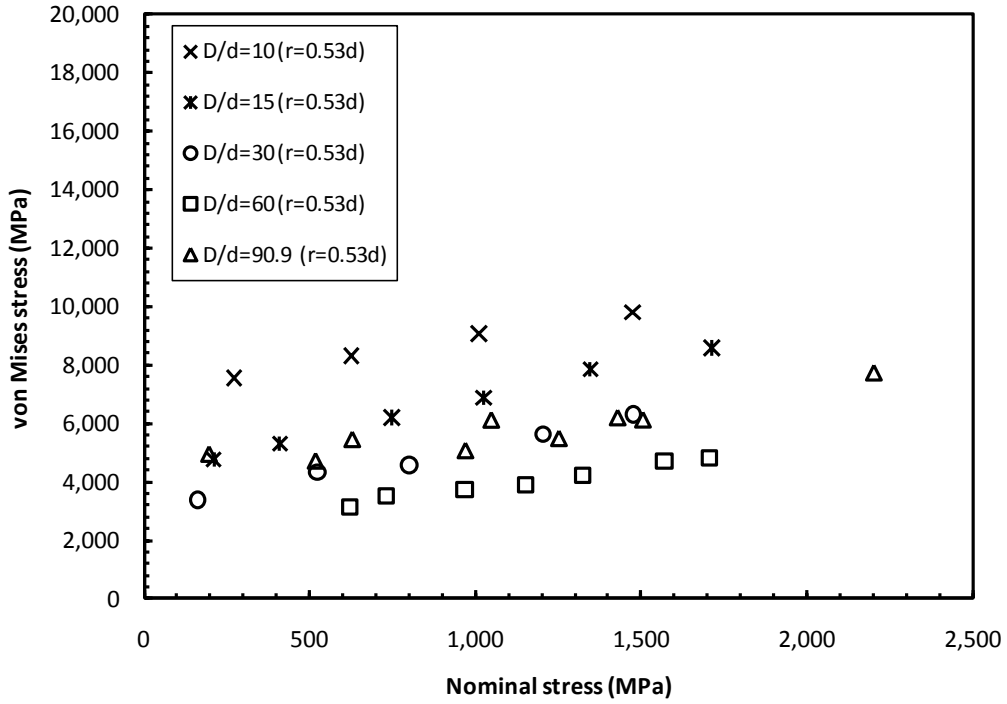

Figure 5-17: von Mises stress versus strand stress for 19-wire strand for various D/d and constant groove radius

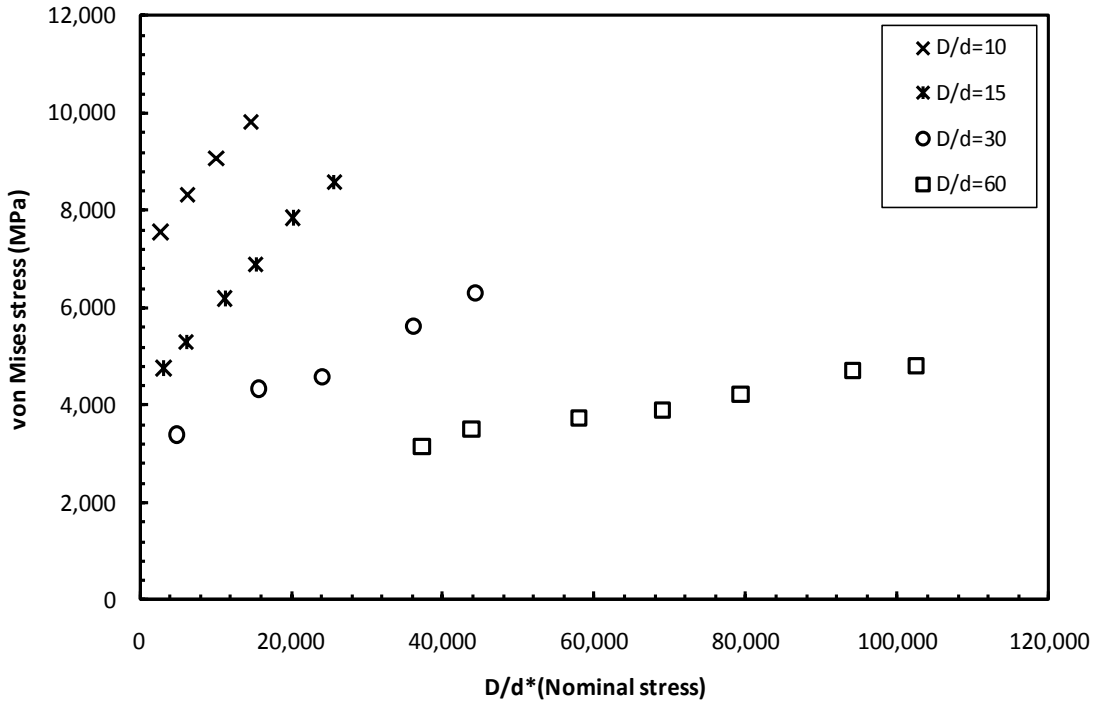

Figure 5-18: von Mises stress versus stress parameter for 19-wire strand for various D/d and constant groove radius

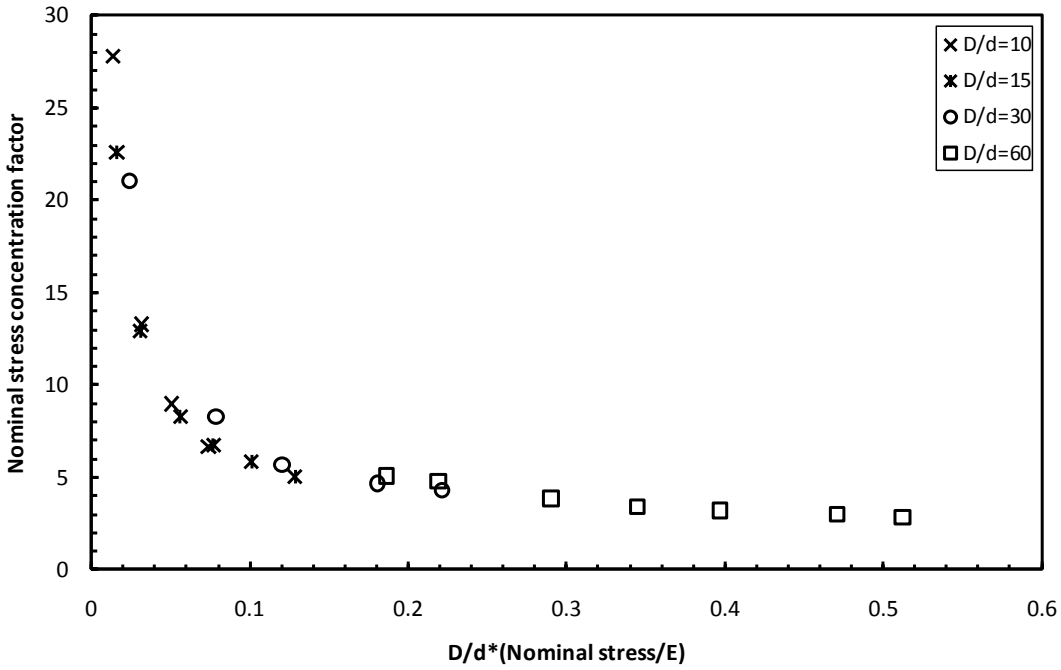

Figure 5-19: SCF_{nom} versus dimensionless parameter for 19-wire strand for various D/d and constant groove radius

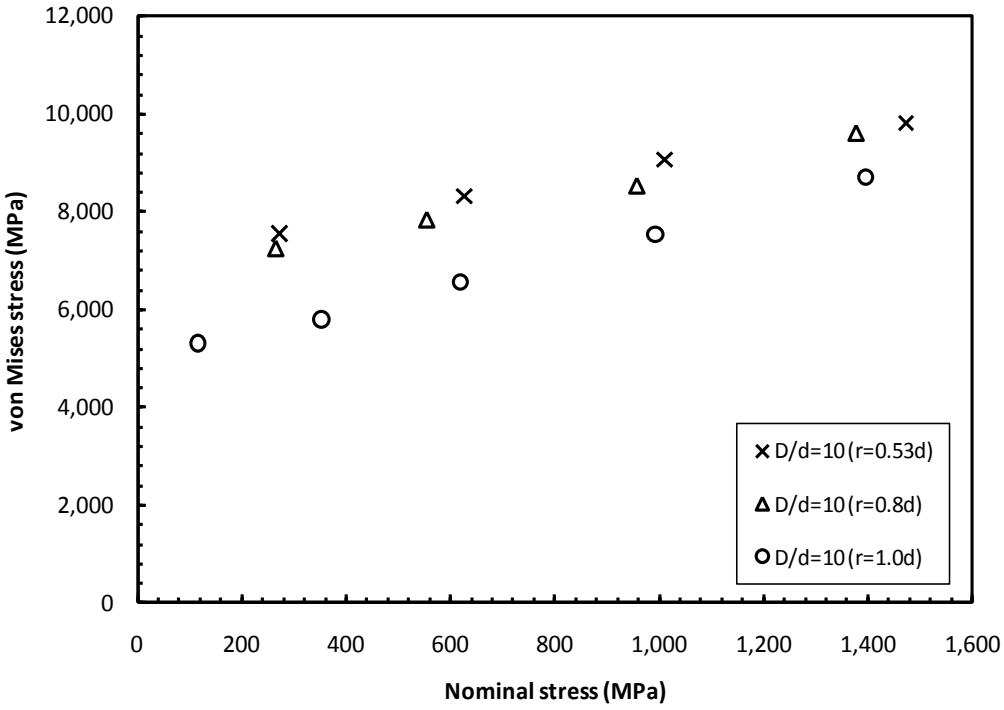

Figure 5-20: Effect of groove size for 19-wire strand for various D/d and constant groove radius

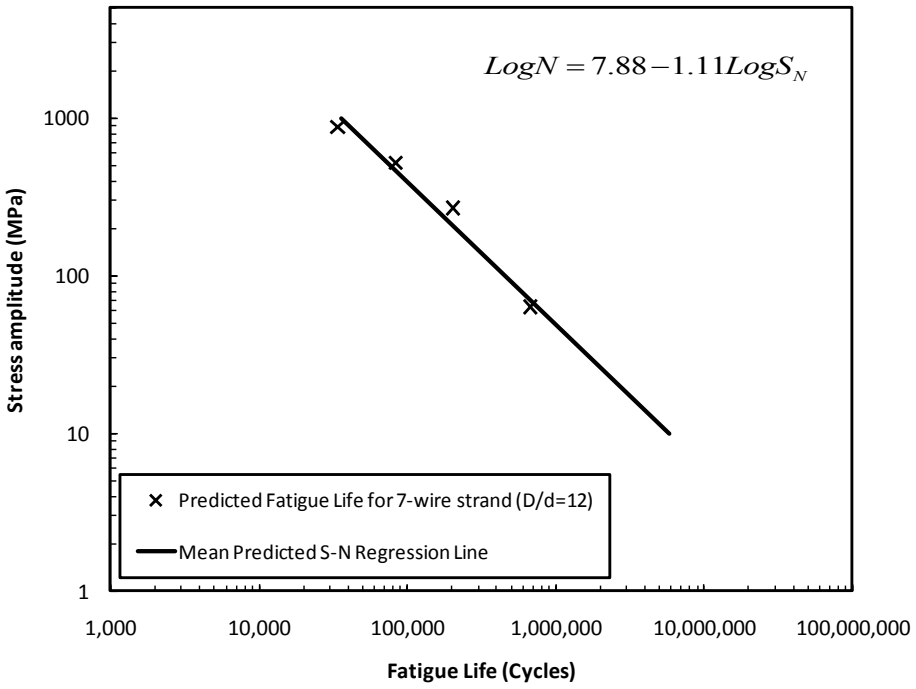

Figure 5-21: Fatigue life for 7-wire strand bent over sheave with D/d=12

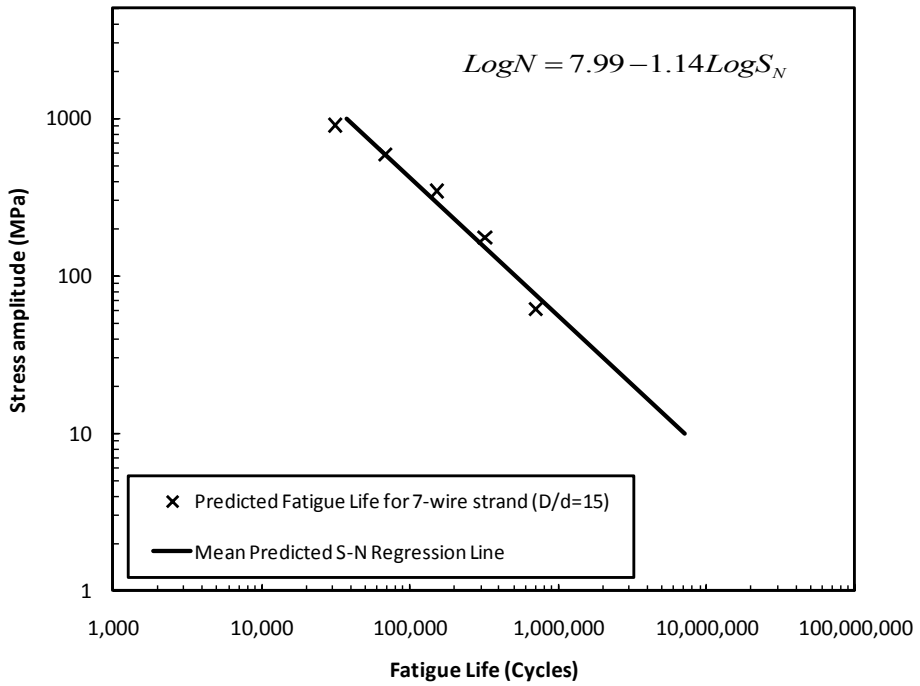

Figure 5-22: Fatigue life for 7-wire strand bent over sheave with D/d=15

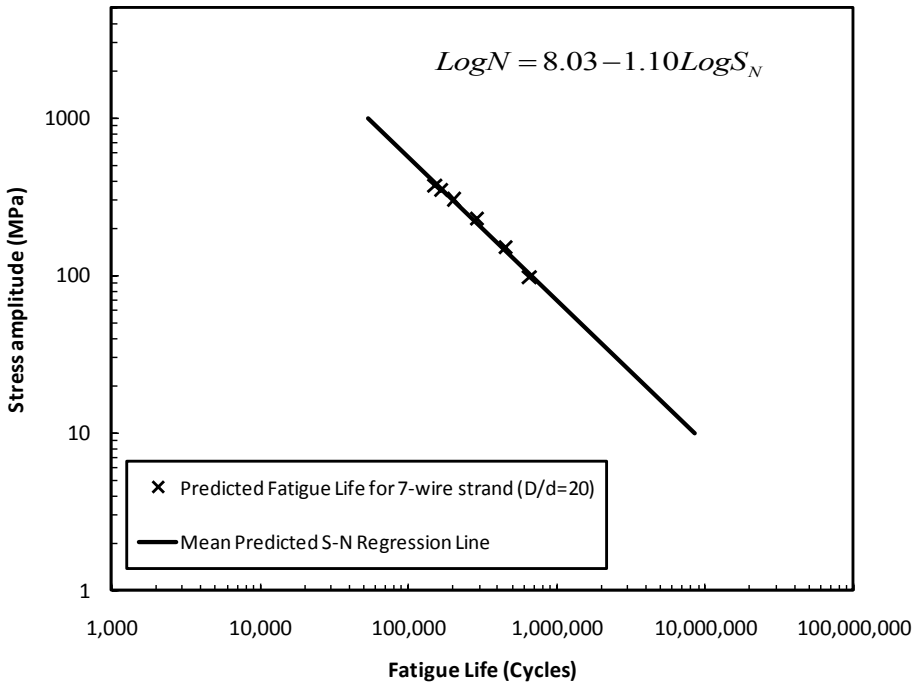

Figure 5-23: Fatigue life for 7-wire strand bent over sheave with D/d=20

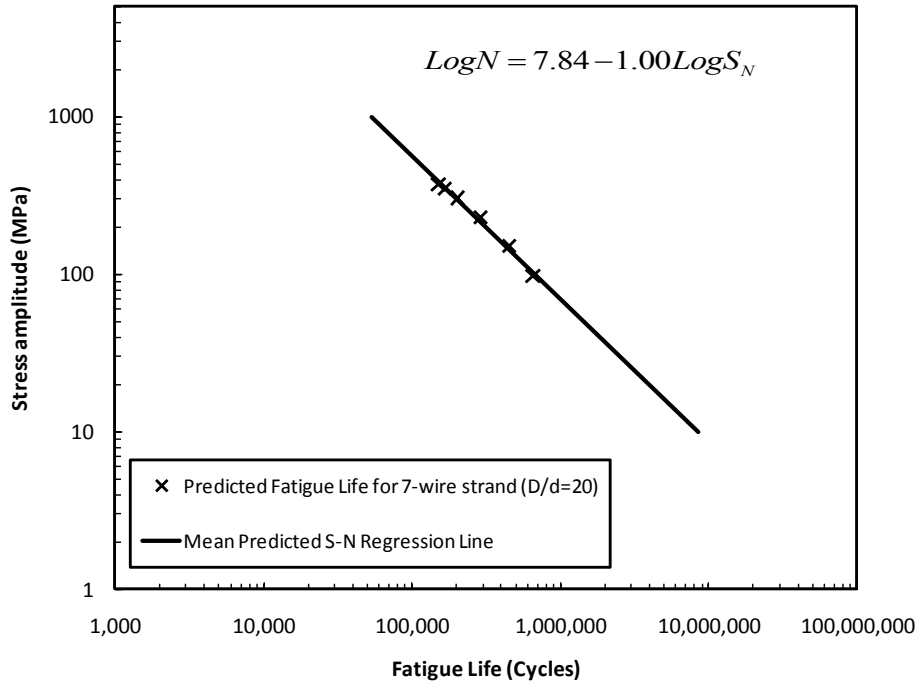

Figure 5-24: Fatigue life for 7-wire strand bent over sheave with D/d=40

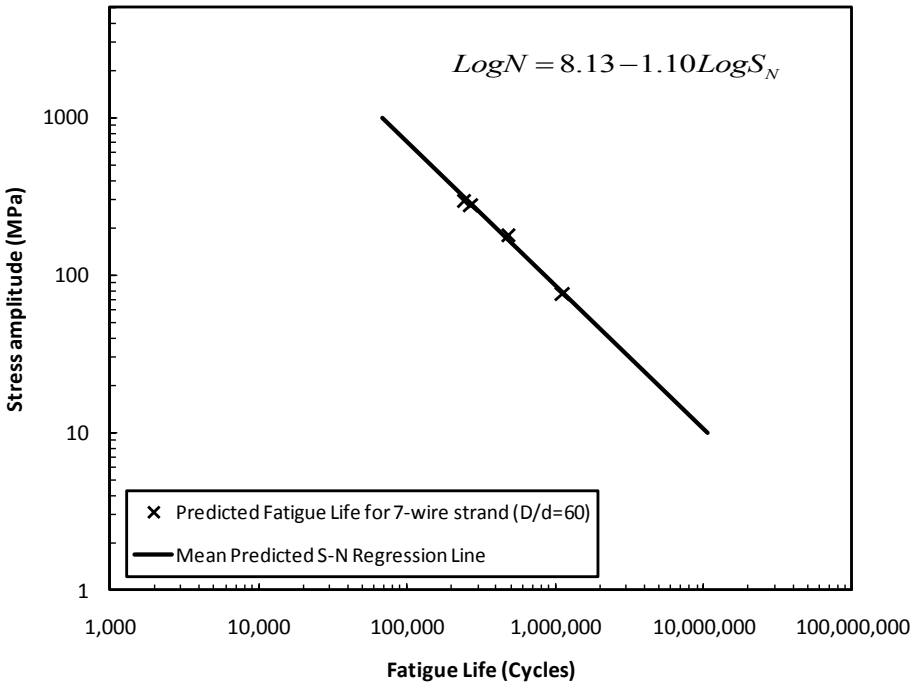

Figure 5-25: Fatigue life for 7-wire strand bent over sheave with D/d=60

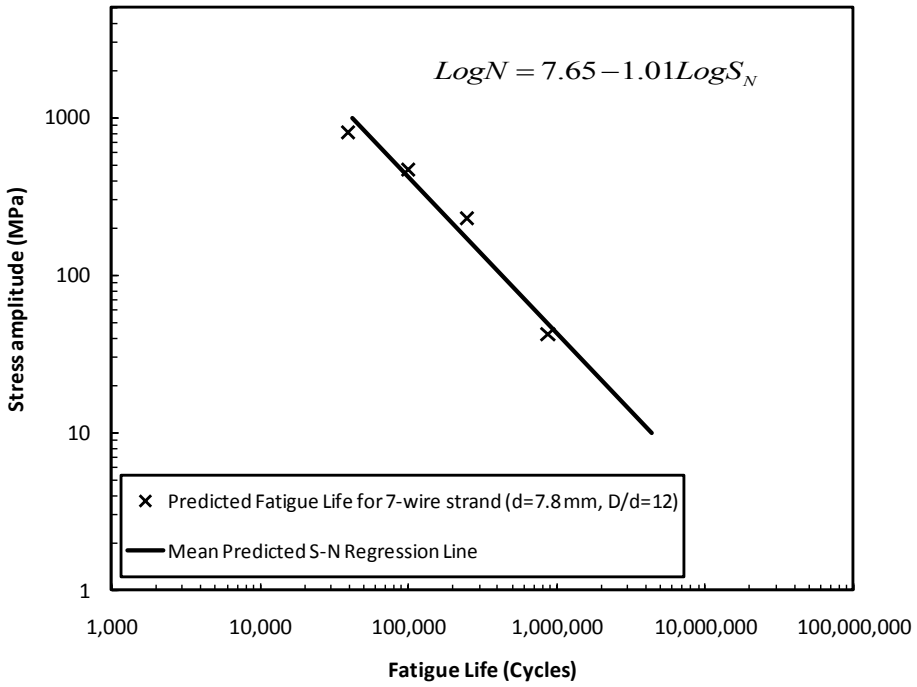

Figure 5-26: Fatigue life for 7-wire strand bent over sheave with d=7.8 mm, D/d=12

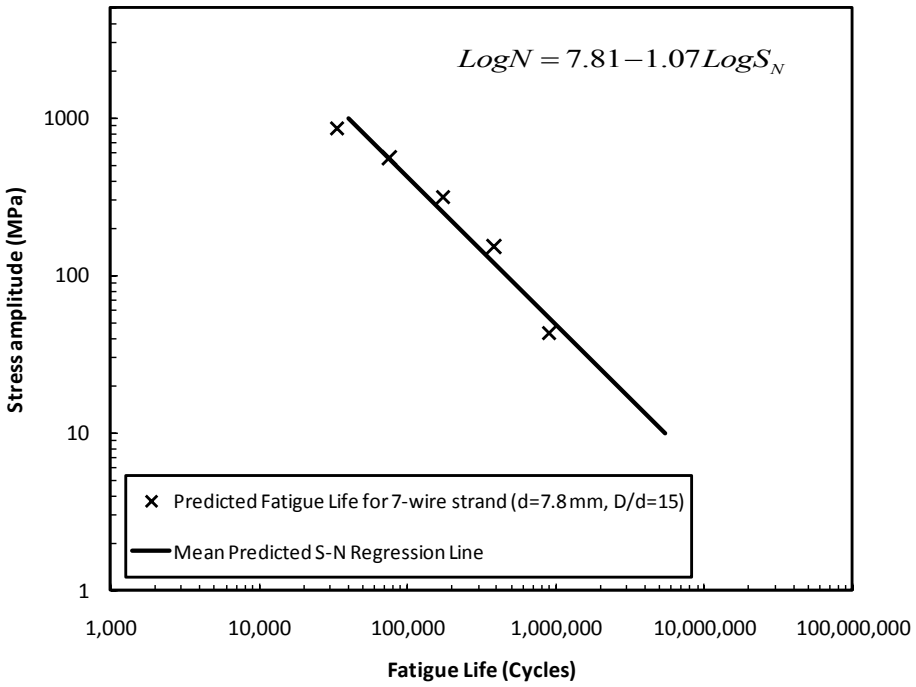

Figure 5-27: Fatigue life for 7-wire strand bent over sheave with d=7.8 mm, D/d=15

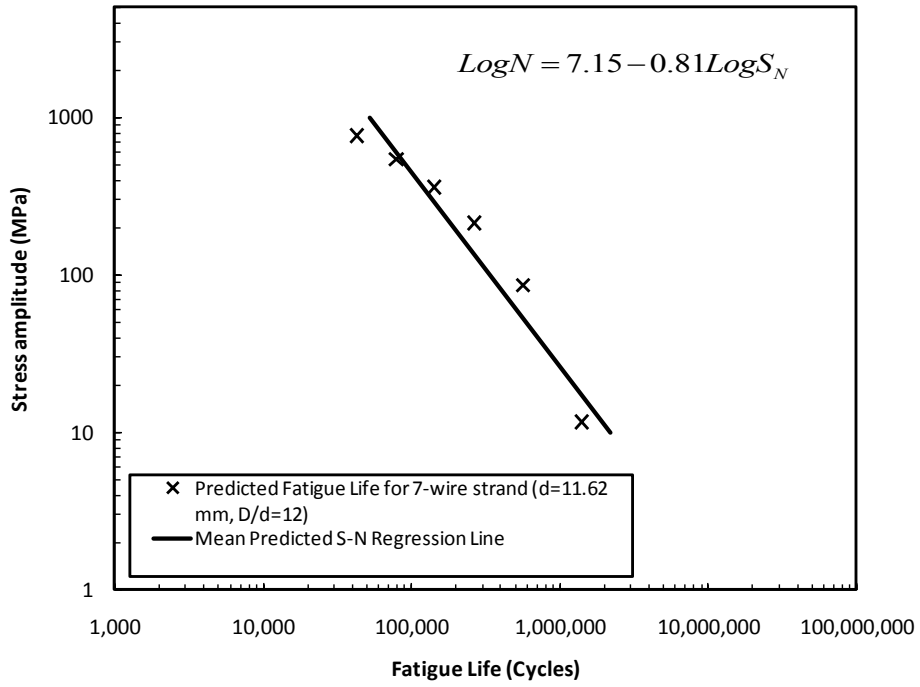

Figure 5-28: Fatigue life for 7-wire strand bent over sheave with d=11.62 mm, D/d=12

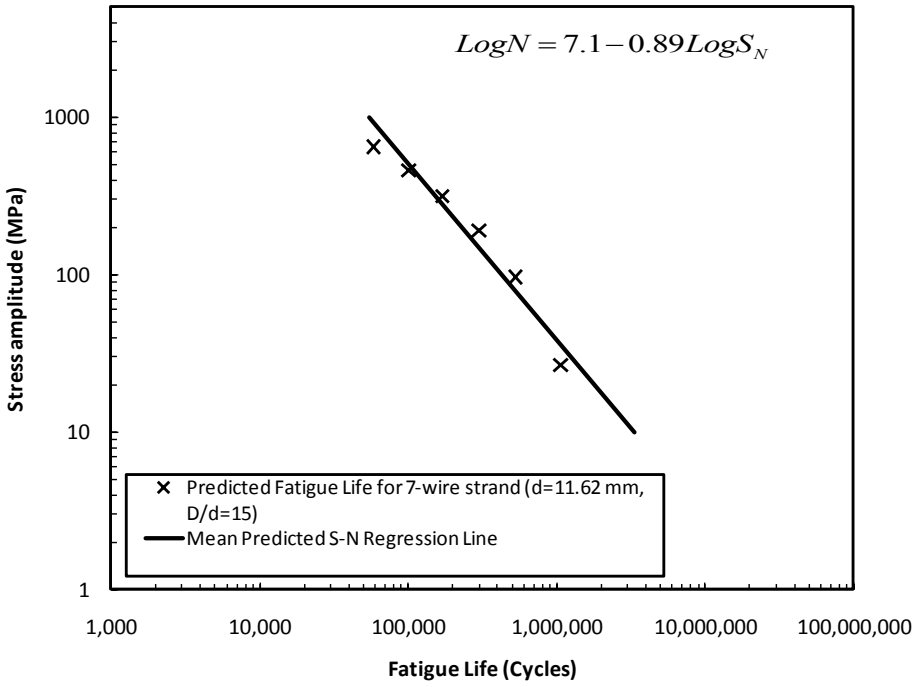

Figure 5-29: Fatigue life for 7-wire strand bent over sheave with d=11.62 mm, D/d=15

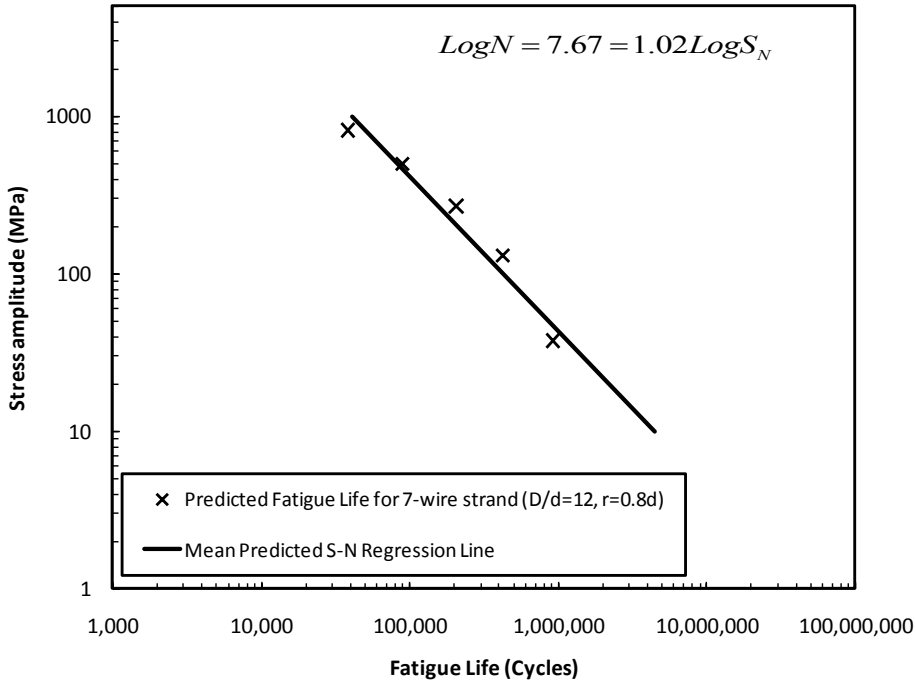

Figure 5-30: Fatigue life for 7-wire strand bent over sheave with D/d=12, r=0.8d

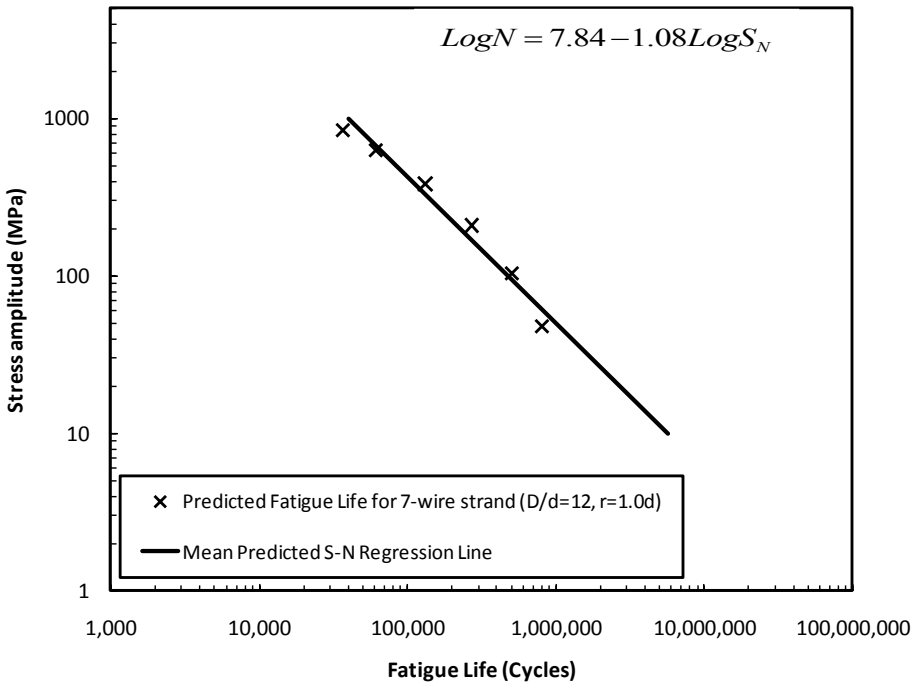

Figure 5-31: Fatigue life for 7-wire strand bent over sheave with D/d=12, r=1.0d

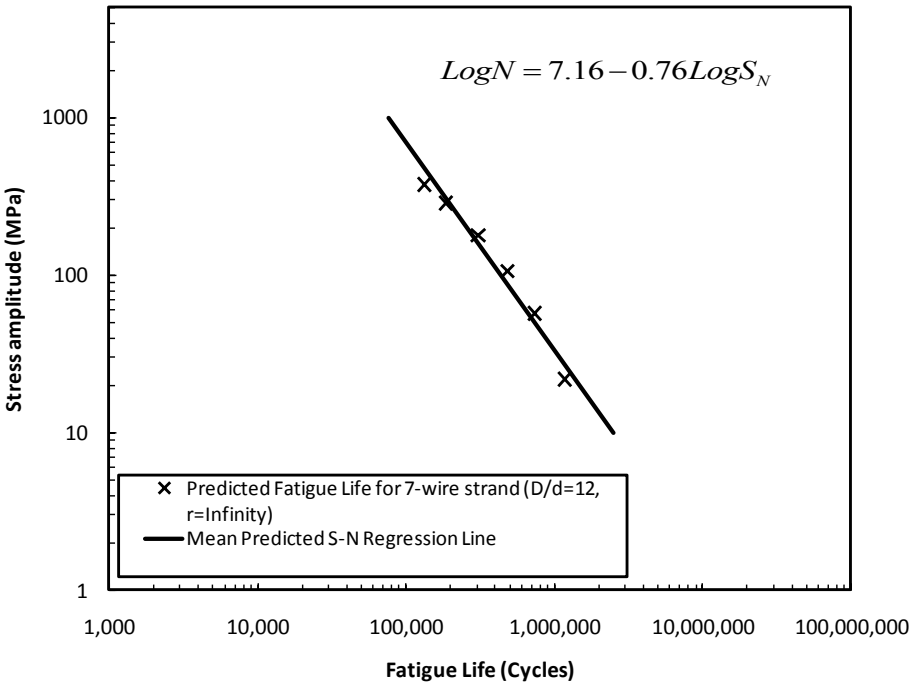

Figure 5-32: Fatigue life for 7-wire strand bent over sheave with D/d=12, r=Infinity

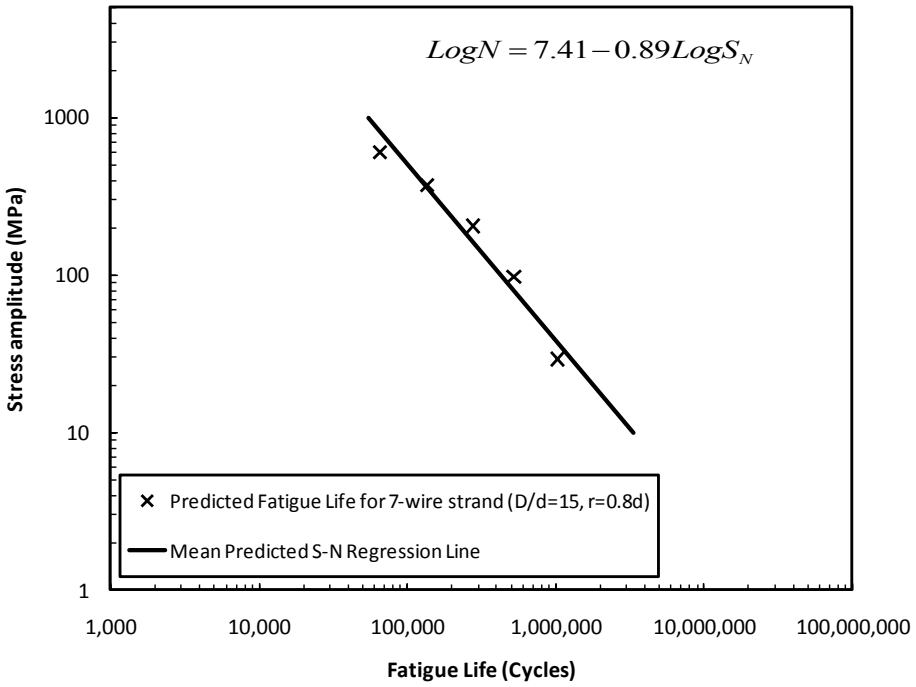

Figure 5-33: Fatigue life for 7-wire strand bent over sheave with D/d=15, r=0.8d

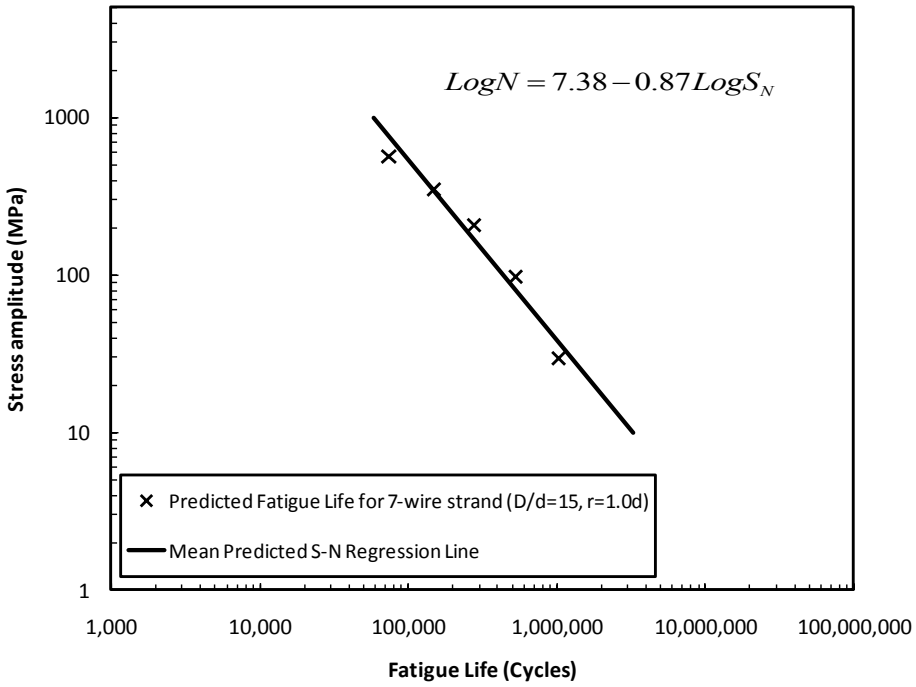

Figure 5-34: Fatigue life for 7-wire strand bent over sheave with D/d=15, r=1.0d

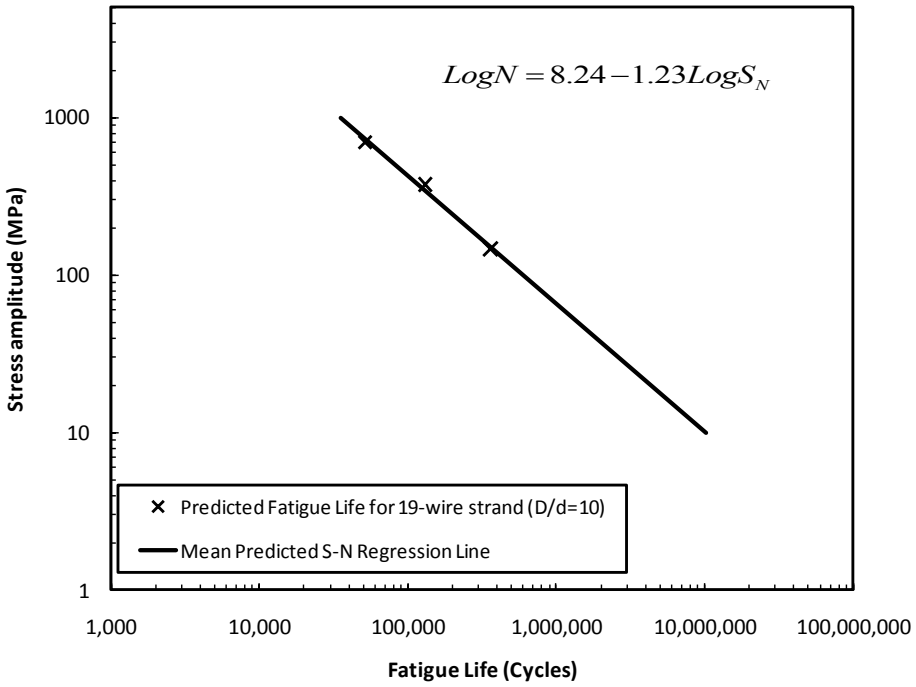

Figure 5-35: Fatigue life for 19-wire strand bent over sheave with D/d=10

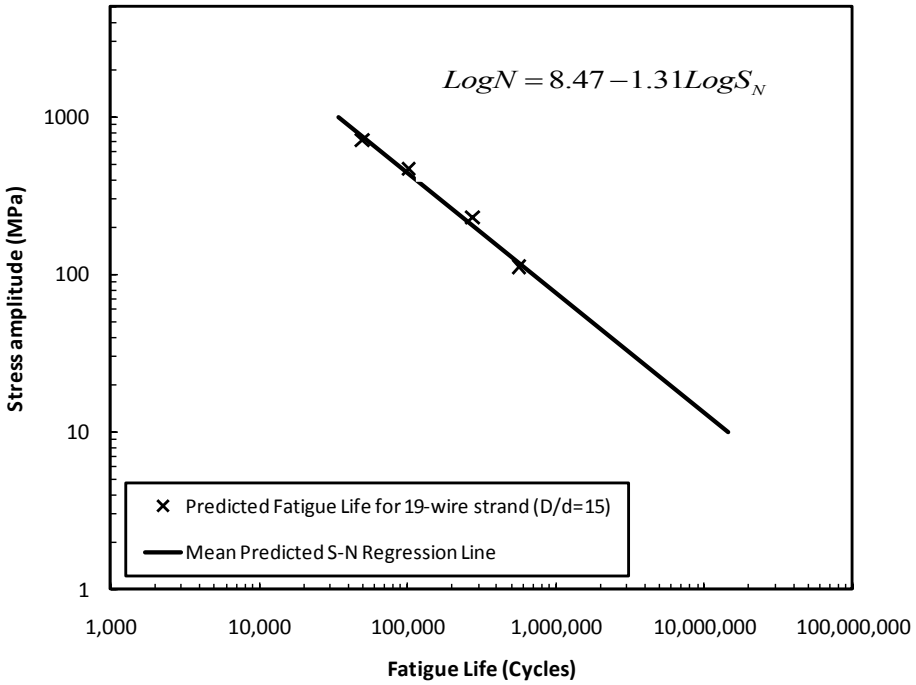

Figure 5-36: Fatigue life for 19-wire strand bent over sheave with D/d=15

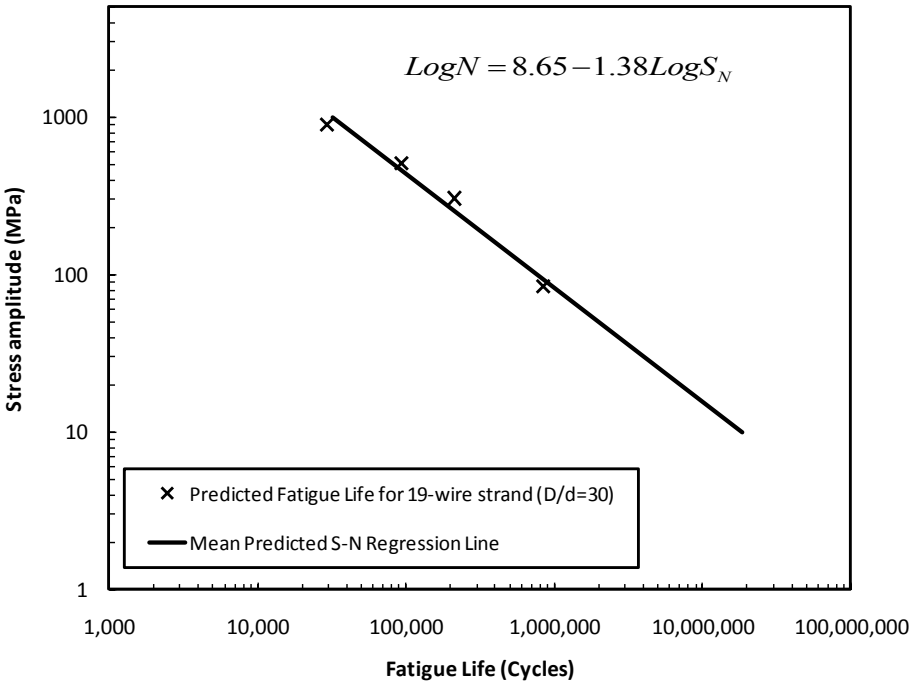

Figure 5-37: Fatigue life for 19-wire strand bent over sheave with D/d=30

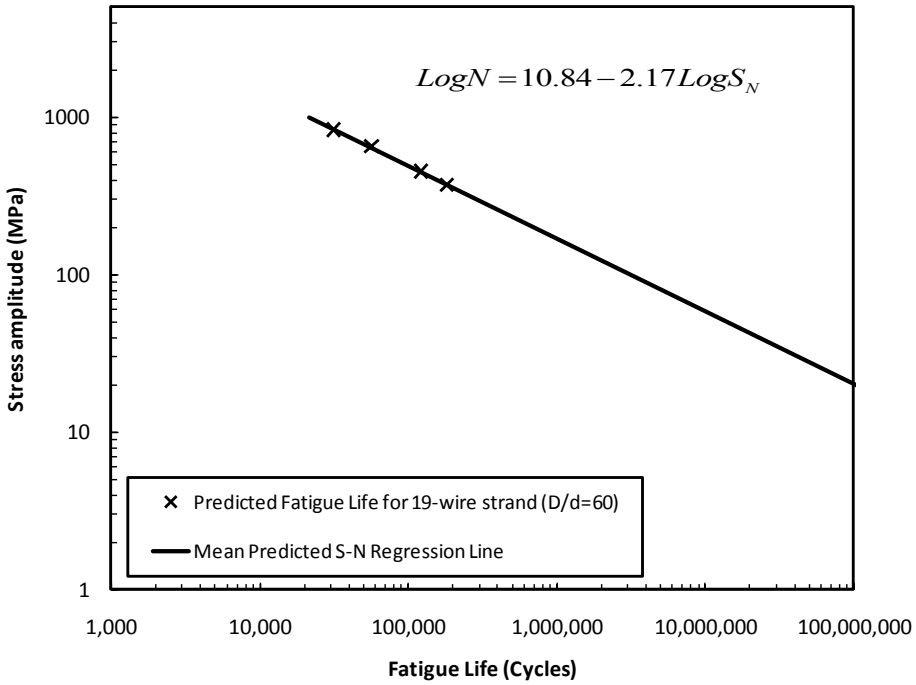

Figure 5-38: Fatigue life for 19-wire strand bent over sheave with D/d=60

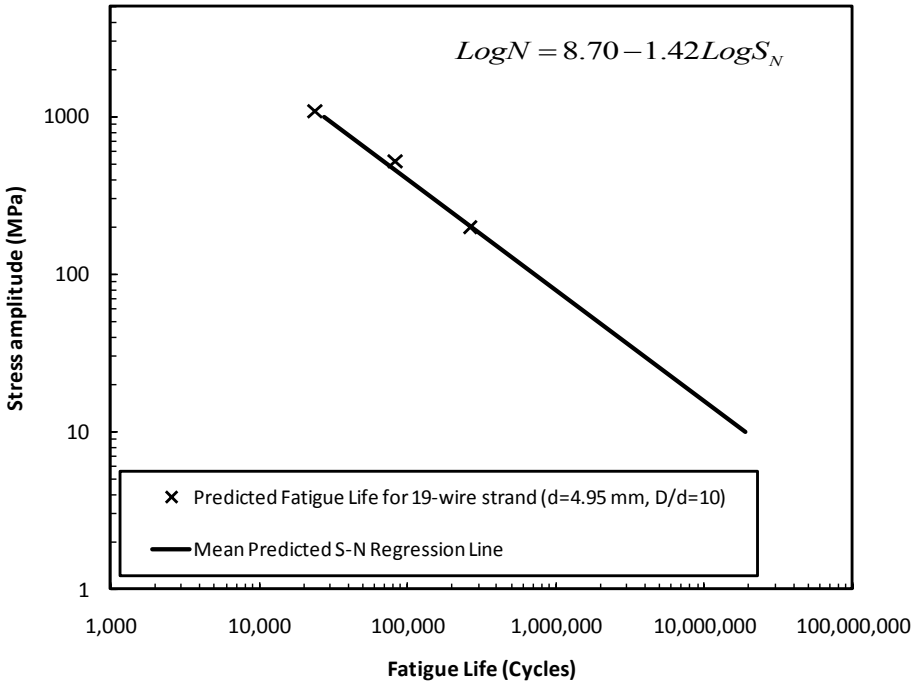

Figure 5-39: Fatigue life for 19-wire strand bent over sheave with d=4.95 mm, D/d=10

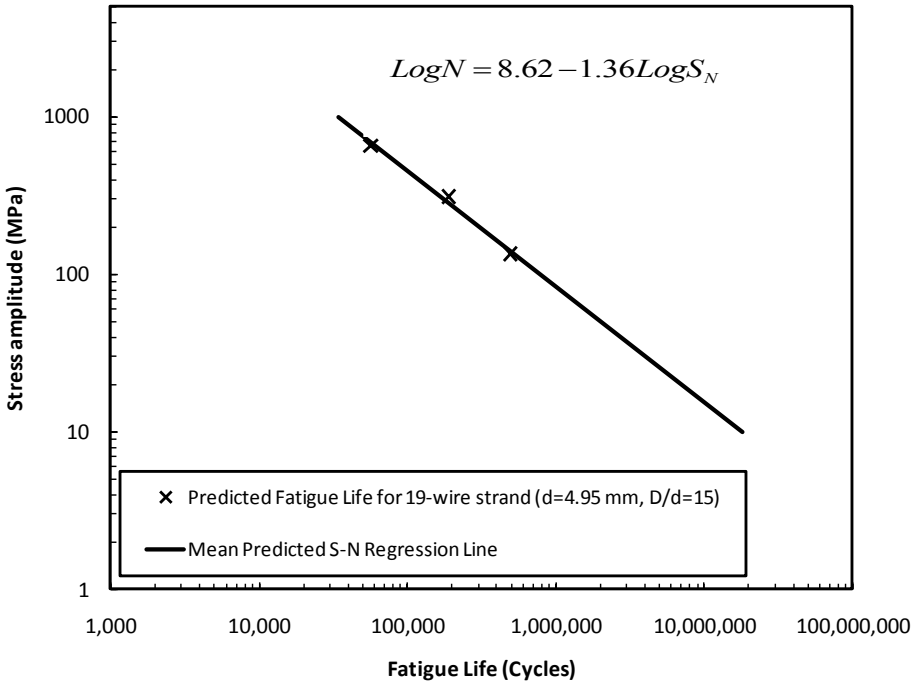

Figure 5-40: Fatigue life for 19-wire strand bent over sheave with d=4.95 mm, D/d=15

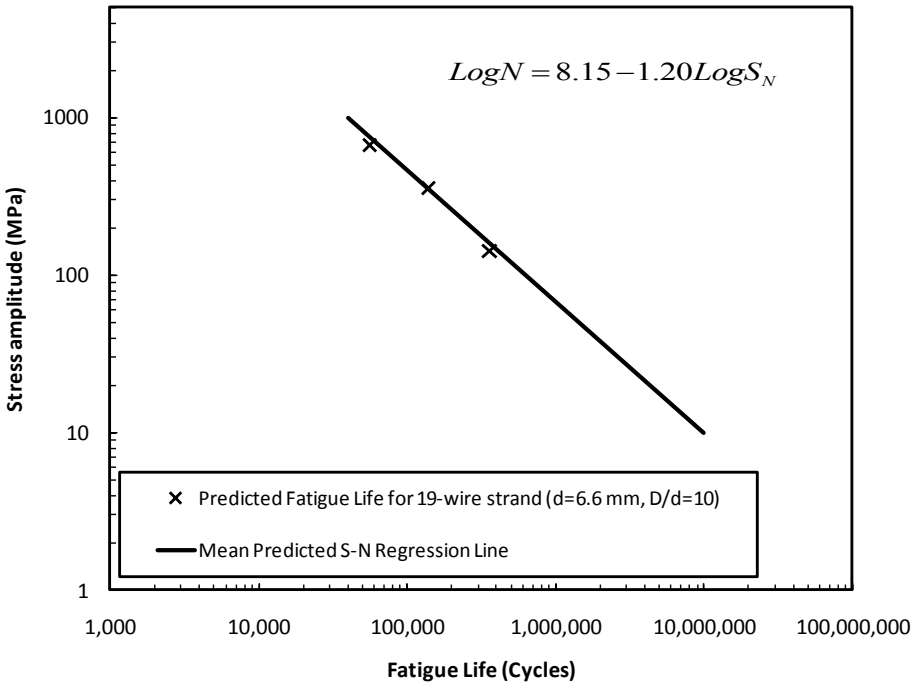

Figure 5-41: Fatigue life for 19-wire strand bent over sheave with d=6.6 mm, D/d=10

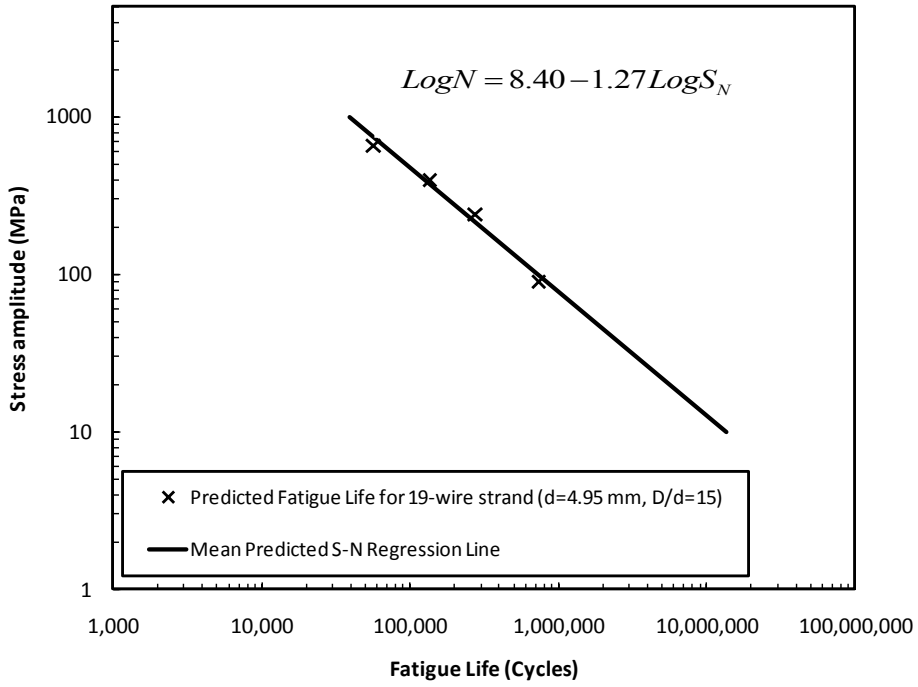

Figure 5-42: Fatigue life for 19-wire strand bent over sheave with d=6.6 mm, D/d=15

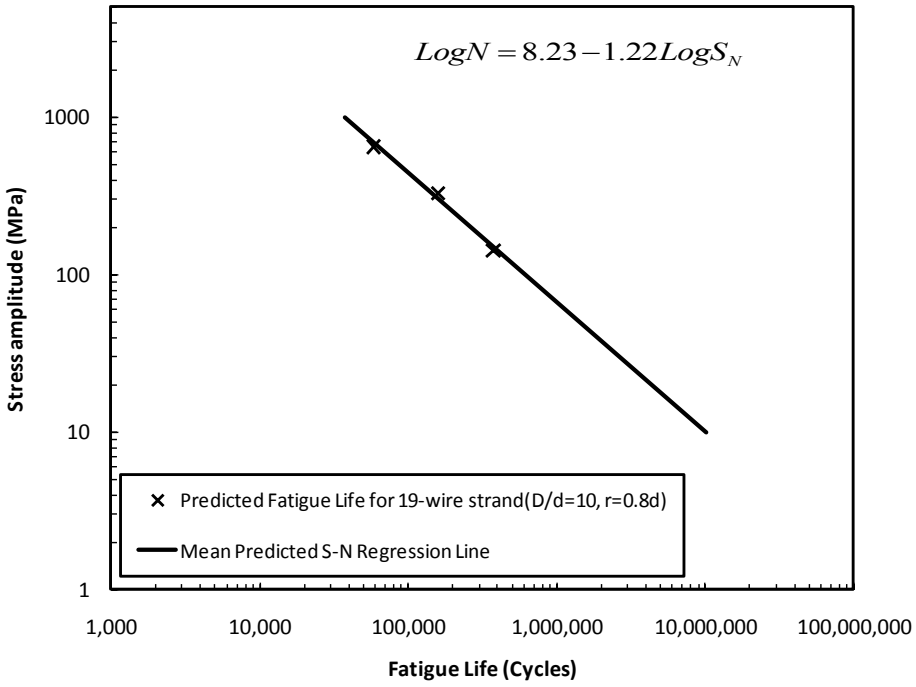

Figure 5-43: Fatigue life for 19-wire strand bent over sheave with D/d=10, r=0.8d

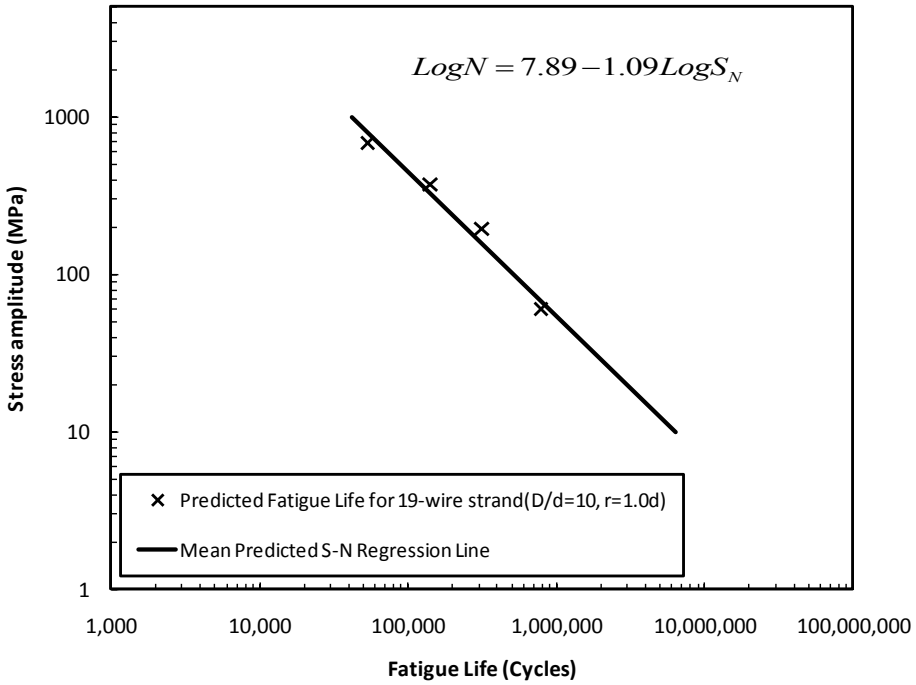

Figure 5-44: Fatigue life for 19-wire strand bent over sheave with D/d=10, r=1.0d

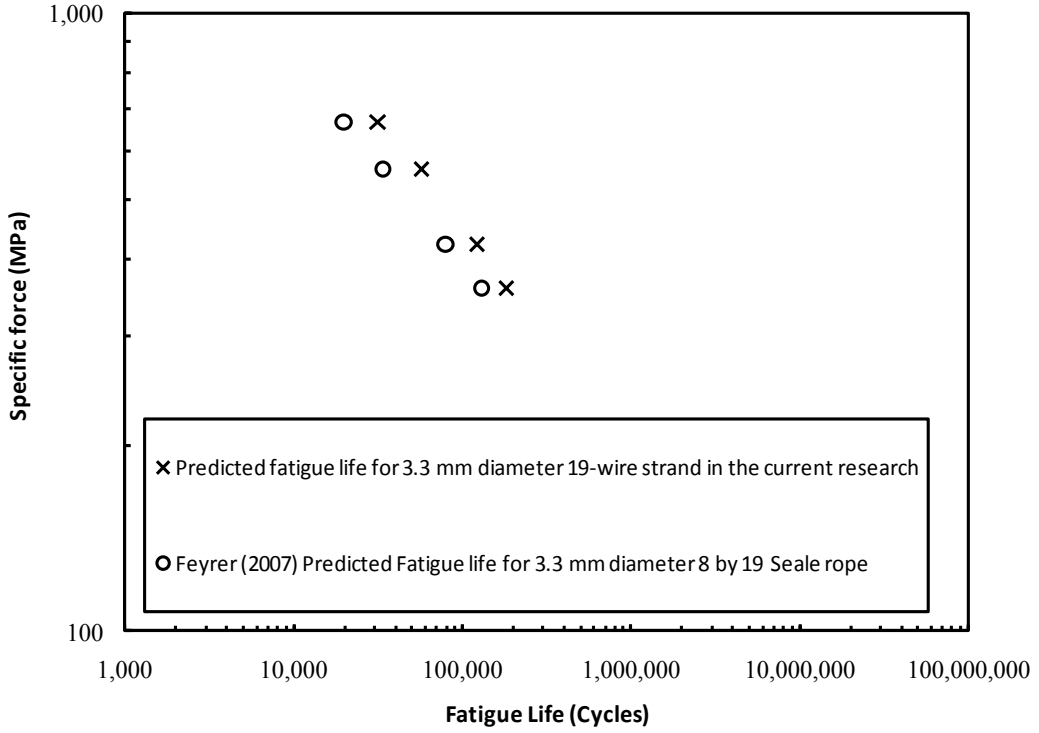

Figure 5-45: Comparison of predicted fatigue life to Feyrer (2007) prediction

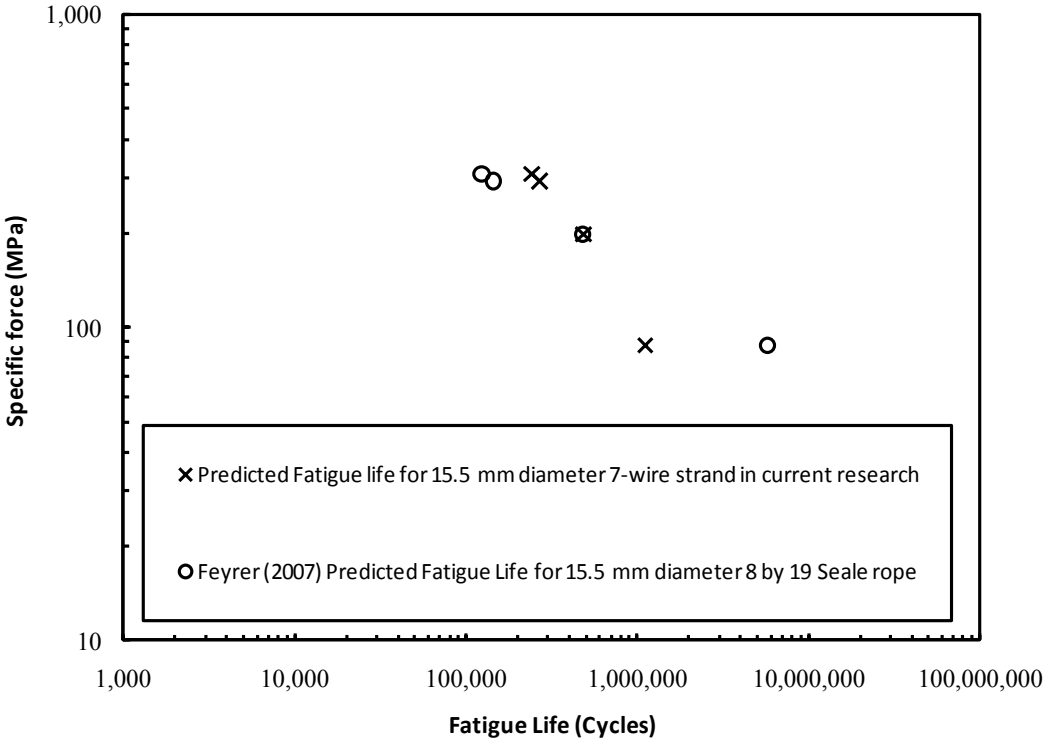

Figure 5-46: Comparison of predicted fatigue life to Feyrer (2007) prediction

CHAPTER 6

SUMMARY, CONCLUSIONS AND RECOMMENDATIONS

6.1 SUMMARY

Fatigue of cables (strands and wire ropes) has been extensively investigated as reflected by the literature review in Chapter 2, however little progress into the prediction of the fatigue life has been achieved. The principal research to date in predicting the fatigue life of cables was performed by Feyrer (2007), who developed fatigue models for predicting the life of cables in cyclic tension, and cables bent over sheaves. The coefficients of regression for strands in cyclic tension presented by Feyrer were not however exhaustive, with 7 and 19-wire strand coefficients including bending over sheave fatigue behaviour remaining yet to be investigated. The cyclic tension fatigue behaviour of IWRC or 6×19 Seale wire rope with IWRC, representing fundamental wire rope categories for larger size wire ropes, representing two categories in high industrial use mining and hoisting equipment, had also not been investigated. Limited research was identified focusing on investigating or accounting for parameters such as lay length, and groove size related to fatigue resistance of cables in cyclic tension and bending over sheaves. It is these deficiencies in the knowledge base of cable behaviour that was targeted as the focus of this research thesis.

A total of 213 finite element analyses were conducted here to obtain elastic stresses for selected cables. The stress based approach applied to the resulting parameters was similar to that previously used by Knapp (2004) and Raoof (1990), accounting for the different methodologies that Knapp and Raoof had previously adopted to predict fatigue life as stress based approaches.

This research proposed two means of estimating fatigue life that accounts for the effect of lay length and/or proximity of wires to each other. The first approach uses a stress concentration factor, while the second approach uses a stress correction factor, applied to cables subjected to tension. As a consequence of the extent of modeling performed here, this thesis also substantially increases the database of knowledge on parameters that affect the fatigue life of cables, such as d, D/d, stress range, and groove size.

6.2 CONCLUSIONS

Six ASTM A416 prestressing strands were numerically analysed in tension to estimate their fatigue life. The strands of different diameters were analysed at different load levels, such that it was observed that within the range of lay length investigated, the lay length had a negligible influence on the fatigue life for 7-wire ASTM prestressing strands, it was surmised that this was because the lay angle or lay length of these strands are substantially small (less than 9 degrees), that it looks like an almost straight wire over the core straight wire. The reduced lay angle reduces the contact pressure, but multiple contact points, which may still produce high stress concentrations will exist in such cases because of the reduced lay length. Conversely, for 19, 91, 92-wire strands, the 6×7 wire rope and 6×19 Seale wire rope in tension, the lay length had an appreciable influence on fatigue life. It was observed that for fatigue life predictions for multi-layer strands or wire ropes, the most critical layer can be known from the summation of the lay angle at two consecutive layers, with layers with opposite lay directions being most critical than layers with same lay directions. The higher the values obtained from the summation of lay angles in two contacting layers (or lay lengths) the lower the von Mises stress and the higher the fatigue life. The increased lay angle yielded higher isolated stresses, but when the reduced lay angle yielded lower point contact stresses, but more contact points along the length of the cable effectively yielding a more critically stressed configuration and reduced fatigue life. Similarly, the lay length was shown to be insignificant for 7- and 19-wire strands bent over sheaves, shown with good prediction and correlation, when the nominal stress concentration was used to compute the fatigue life for strands previously tested and reported by Knapp (2004). Stress amplitude was shown to have a significant effect on the fatigue life for 19, 91, and 92-wire strands, IWRC and the 6×19 Seale wire ropes subjected to tension.

Two approaches to obtain the fatigue life of cables were proposed. The first approach uses the SCF_{nom} parameter obtained using the nominal stress, while the second approach uses the $CF_{\text{int}.stress}$ parameter obtained using the maximum internal axial stress. It was consequently shown that if an initial contact between wires that make up a strand or wire rope; related to lay length; is expected, then the estimate of fatigue life using either approach yields a similar result. However in all cases the fatigue life obtained using the SCF_{nom} is invariably more conservative.

Simultaneously, it was also observed that the length of a sample is insignificant in obtaining stresses in strands or wire ropes in tension.

In bending over sheaves, the effect of the D/d ratio exhibited the most significant impact on fatigue life estimate. The fatigue life was observed to increase with increase the D/d ratio. The stress amplitude had less of an effect on fatigue life, while still remaining a significant consideration and the fatigue life was observed to decrease with increase in the stress amplitude. The effect of groove size was shown to be essentially negligible within the range investigated, but as groove radius increased the induced stresses in strands increased, effectively reducing the fatigue life. As such, as the groove radius approaches a radius of infinity stresses become higher as also reflected by both Knapp's model with D/d ratio of 90.9 and $r = 1.92d$ and by Costello's model with D/d ratio of 12 and $r = Infinity$ (representing a flat groove). From the statistical analyses performed, it is evident that fatigue lives of strands bent over sheaves, extended to also imply wire ropes, are not strongly dependent on lay length.

In progressing the application of Feyrer (2007) model, the following coefficients were clarified to permit mean predicted fatigue regression relationships for strands and wire ropes in tension, via using either the nominal stress or the maximum internal stress as reflected by Equations 4-20 and 4-21:

Table 4-30: Mean fatigue life prediction regression coefficients using the maximum internal axial stress

Strand or wire rope type	a_0	a_1	a_2	a_3	a_4	a_5
7-wire	10.14	-0.99	0.012	1.32E-05	0.211	-
19-wire	-27.32	17.50	0.18	0.00044	5.20	-
7 &19-wire	3.58	2.73	0.029	3.37E-05	0.80	-1.62
7,19,91,92-wire	7.42	0.54	0.017	1.78E-05	0.52	-1.05
IWRC	11.80	-2.65	-0.0021	-1.1E-06	-0.11	-
6×19 Seale	13.64	-3.60	-0.0076	-1.3E-05	-0.12	-

Table 4-31: Mean fatigue life prediction regression coefficients using the nominal stress

Strand or wire rope type	a_0	a_1	a_2	a_3	a_4	a_5
7-wire	10.00	-0.83	0.013	1.47E-05	0.01	-
19-wire	-6.35	5.75	0.069	0.00016	3.32	-
7 &19-wire	4.21	2.58	0.027	3.12E-05	0.68	-1.94
7,19,91,92-wire	5.64	1.48	0.020	1.96E-05	0.50	-1.26
IWRC	8.38	-1.23	0.00086	1.23E-06	-0.036	-
6×19 Seale	8.80	-1.42	-2.5E-06	-7.8E-07	-0.045	-

Similarly, for strands in bending over sheaves to fatigue, the following coefficients were discerned to be used with Equation 5-1:

Table 5-51: Mean fatigue life prediction regression coefficients for strands bent over sheaves

Strand or wire rope type	b_0	b_1	b_2	b_3	b_4	b_5	b_6
7-wire	13.31	-0.74	-0.28	-0.57	0.087	-11.80	-
19-wire	18.11	-1.36	-0.051	-2.17	-0.11	-16.19	-
7 &19-wire	13.29	-0.37	-0.67	-0.023	0.16	-13.42	0.24

6.3 RECOMMENDATIONS

Design recommendations and recommendations for future work will be discussed in this section.

6.3.1 DESIGN RECOMMENDATIONS

The fatigue life of 7-wire ASTM prestressing strands, 19, 91, and 92-wire strands or IWRC and 6×19 Seale wire rope and any other wire rope may be modeled in Abaqus/CAE. The results from such analyses may be then used to predict such strands' and ropes', cyclic tension and bending over sheaves, fatigue life via a stress based approach developed here. Confidence in this procedure has been built through this research thesis, where such predictions have been shown with good correlation to independently documented experimental tests on strands and wire ropes from other earlier research.

The mean predicted regression relationships as described by Equations 4-20 and 4-21, and their corresponding coefficients reported in Tables 4-30 and 4-31 to 2 standard deviations may reliably be used to predict fatigue resistance of strands ranging from 7 to 92 wires in tension, and for IWRC or 6×19 Seale wire ropes in cyclic tension. The coefficients identified and quantified here are a function of the level of accuracy desired by the user, reflected in the regression analysis of Appendix C.

The mean predicted regression relationship described by Equation 5-1, with corresponding coefficients given in Table 5-51 to 2 standard deviations, should be used for predicting the fatigue life of 7 and 19-wire strands bent over sheaves; however, the applicability of the model and its coefficients beyond 19-wire strands should be further investigated before such an extrapolation should be employed.

From the analysis of various D/d ratios for strands subjected to bending over sheave fatigue, it is recommended that the higher D/d ratios, typically over 60 are recommended for high risk structures. The effect of groove geometry within the range $r = 0.53d$ to $r = 1.00d$ show little variance in fatigue behaviour, but for groove geometries beyond this range a thorough investigation should be conducted, as there exists the potential for a significant reduction in fatigue life due to increased contact stress.

6.3.2 RECOMMENDATIONS FOR FUTURE WORK

Many questions are yet to be answered beyond this work, which creates significant scope for future research study. Such considerations might include:

1. Mining shovel, dragline and crane cyclic loads as experienced in the field are highly variable. These are dependent on a complex set of inter-related external factors such as the geology associated with an excavation medium, excavation ground moisture content, weather conditions, face release (exhibited as a sudden release of energy in the hoist ropes as a shovel dipper or dragline bucket is released from the excavation face post digging trajectory) and operator skill. An investigation of an acceptable simplification of such cyclic loading activity to a more model manageable equivalent constant amplitude loading, generating similar damage, prior to input into a fatigue prediction model needs further investigation and verification.

2. As most heavy equipment employing tensile hoisting functions are designed with more than one sheave commensurate with multiple hoist ropes that may or may not be synchronous, the application of the fatigue models outlined in this work for bending over sheaves needs both implication consideration and further investigation that may undoubtedly lead to a more complex expansive fatigue modelling approach.

3. Although this work did add to the parameter knowledge base improving the scope of predictive models; many other strand and rope configurations specific to other industrial application remain unaccounted for in fatigue prediction analysis. The principles of

analysis outlined here should be extended to include additional widely used strand and rope configurations.

4. The research outlined in this thesis solely considered the "dry" strand and rope condition. In actual practice, lubrication plays a huge role from friction reduction and cooling actions to acting as a medium within which abrasive dusts and particles may be moved away from the contact surfaces. Both the consideration of the inclusion of contaminant particles of mismatched hardness of such particles to the steel wires raises implications of abrasion and corrosion which should be considered. The effect of lubrication on the fatigue life of cables within the context of industrial application raises a huge research area as yet barely tapped; although Feyrer (2007) presented basic modifications for fatigue models to account for simple lubrication.

5. Consideration of probability and consequence of failure leads to the notion of fatigue prediction via stochastic models rather than deterministic models. Such considerations would lead predictive modeling to establish the level of risk as a function of fatigue. This area of research calls for a greater consideration of qualitative parameters, that generate quantitative equivalency questions related to capturing magnitude and impact knowledge associated with application circumstance. Such thoughts are essentially foreign in a structural analysis world and give rise to the considerations of the value of such knowledge in the overall analysis.

It is evident that the scope surrounding this research is far reaching, but generates the potential for a large array of future direction. It is hoped that the knowledge additions associated with this work will create the opportunity for further work of a both expansive and novel nature to continue in this research area.

References

ABAQUS (2012) “ABAQUS Documentation” , Dassault Systemes, Providence, RI, USA.

ASTM A 416/A416 M-99, (1999), Standard Specification for Steel Strand, Uncoated Seven-Wire for Prestressed Concrete, American Society for Testing and Materials, West Conshohocken, Pennsylvania.

ASTM A586-86, (1986), Standard Specification for Zinc-coated parallel and helical steel wire structural strand, American Society for Testing and Materials, Philadelphia.

Argatov, I. I., Gómez, X., Tato, W., and Urchegui, M. A. (2011). Wear evolution in a stranded rope under cyclic bending: Implications to fatigue life estimation. *Wear,* 271(11–12), 2857-2867.

Bannantine, J. A., Comer, J. J., and Handrock, J. L. (1990). Fundamentals of metal fatigue analysis. Upper Saddle River, NJ: Prentice- Hall.

CABLECAD (1998) “CCAD User Manual”, Knapp Engineering, Inc, USA.

Cappa, P. (1988). Experimental study of wire strains in an undamaged and damaged steel strand subjected to tensile load. *Experimental Mechanics,* 28(4), 346-349.

Casey, N. F., and Waters, D. (1988). Fatigue behaviour of large diameter wire ropes. *Wire Industry,* 55(653), 371-378.

Casey, N. F. (1988). Fatigue testing of wire ropes. *Wire Industry,* 55(659), 758-761.

Casey, N. F., and Lee, W. K. (1989). The fatigue failure of large diameter six strand wire rope. *International Journal of Fatigue,* 11(2), 78-84.

Casey, N. F., Wedlake, D., Taylor, J. L., and Holford, K. M. (1985). Acoustic detection of wire ropes failure. *Wire Industry,* 52(617), 307-309.

Casey, N. F., Holford, K. M., and Taylor, J. L. (1988).Wire break detection during the tensile fatigue testing of 40 mm diameter wire rope. *British Journal of Non-Destructive Testing,* 30(5), 338-341.

Chen, J., and Gage, P. (1981). Improved wire rope endurance life with nylon sheaves. OTC 4001, 1, 443-452.

Costello, G. A. (1997). *Theory of wire rope* (2nd Ed.). New York: Springer-Verlag.

Cruzado, A., Hartelt, M., Wäsche, R., Urchegui, M. A., and Gómez, X. (2010).Fretting wear of thin steel wires.Part 1: Influence of contact pressure. *Wear,* 268(11–12), 1409-1416.

Cruzado, A., Hartelt, M., Wäsche, R., Urchegui, M. A., and Gómez, X. (2011).Fretting wear of thin steel wires.Part 2: Influence of crossing angle. *Wear,* 273(1), 60-69.

Cullimore, M. S. G. (1972). The fatigue strength of high tensile steel wire cable subjected to stress fluctuations of small amplitude. *International Association of Bridge and Structural Engineers*. pp 49-56.

de Silva, A. R. T., and Fong, L. W. (2002). Effect of abrasive wear on the tensile strength of steel wire rope. *Engineering Failure Analysis,* 9(3), 349-358.

DNV-OS-E301, Position Mooring, October 2013.

Drucker, D.C.A., and Tachau, H. (1945). A new design criterion for the wire rope. *Journal of Applied Mechanics*, 12, A33-A38

Erdönmez C., and İmrak C. E. (2009). Modeling and numerical analysis of the wire strand. *Journal of Naval Science and Engineering*, 5(1), 30-38.

Erdönmez C., and İmrak C. E. (2011). Modeling techniques of nested helical structure based geometry for numerical analysis. *Journal of Mechanical Engineering*, 57(2011)4, 283-292.

Edward, N. S. (1988). Degradation of wire rope. Wire Industry, 55(657), 642-644.

Evans, J. J., Ridge, I. M. L., and Chaplin, C. R. (2001). Wire failures in ropes and their influence on local wire strain behaviour in tension-tension fatigue. *Journal of Strain Analysis for Engineering Design,* 36(2), 231-244.

Feyrer, K. (1981a). Statistical evaluation of results of wire rope bending tests, part I. *Wire,* 31(3), 118-121.

Feyrer, K. (1981b). Statistical evaluation of results of wire rope bending tests, part II. *Wire,* 31(4), 158-162.

Feyrer, K. (2007). *Wire ropes: Tension, endurance, reliability.* (1st Ed.). Germany: Springer.

Feyrer, K. (1981c). Effect of bending length on endurance of wire ropes. Wire World Int., 23(4) 115-119.

Fisher, J. W., and Viest, I. M. (1961). Fatigue tests of bridge materials of AASHO road test. Special Report No. 66, pp 132-147.

Giglio, M., and Manes, A. (2005). Life prediction of a wire rope subjected to axial and bending loads. *Engineering Failure Analysis,* 12(4), 549-568.

Giglio, M., and Manes, A. (2003). Bending fatigue tests on a metallic wire rope for aircraft rescue hoists. *Engineering Failure Analysis,* 10(2), 223-235.

Gorbatov, E. K., Klekovkina, N. A., Saltuk, V. N., Fogel, V., Barsukov, V. K., Barsukov, E. V., Kadochnikov, N. P., Makarova, E. V., Kurashov, D. A. (2007). Steel rope with longer service life and improved quality. *Metallurgist,* 51(5-6), 279-283.

Hansel, J., and Oleksy, W. (1986). Life of wire ropes based on stresses in wires. Wire Industry, 53(629), 391-394.

Hanzawa, M., Yokota, H., Toda, Y., and Yokoyama, k. (1981).Fatigue behaviour of large-diameter wire ropes. *Proceedings of the Annual Offshore Technology Conference,* OTC 3999, Vol. 1, pp. 435-442.

Heller, B. E. (2003). Fatigue response of pretensioned concrete beams. MSc *Thesis.* Faculty of Graduate School. The University of Texas at Austin, Austin, TX, USA.

Hobbs, R. E., and Ghavami, K. (1982).Fatigue of structural wire strands. Int. J. Fatigue, 4(2), 69-72.

Hobbs, R. E., and Raoof, M. (1996). Behaviour of cables under dynamic or repeated loading. *J. Construct. Steel Res*., 39(1), 31-50.

Hobbs, R. E., and Smith, B. W. (1983). Fatigue performance of socketed terminations to structural strands. Proc. Inst. Civ. Engrs., Part 2, Vol 75, pp. 35-48.

İmrak C. E., and Erdönmez C. (2010). On the problem of wire rope model generation with axial loading. *Mathematical and Computational Applications*, Association for Scientific Research. 15(2), pp. 259-268.

Jiang, W.G. (2012). A concise finite element model for pure bending analysis of simple wire strand. *International Journal of Mechanical Sciences,* 54(1), 69-73.

Knapp, R. H. (1987). Axial fatigue model for wire rope strand. Materials and member behavior*, Proceedings of the Sessions at Structures Congress'87,* ASCE, New York, USA. Pp 347-359

Knapp, R. H. (1988). Helical wire stresses in bent cables. *Journal of Offshore Mechanics and Arctic Engineering,* 110(1), 55-61.

Knapp, R. H. (2004). Tension and bending fatigue modeling of cables. *Proceedings of the International Offshore and Polar Engineering Conference,* Toulon, France. pp. 289-295.

Krause, H., and Neumann, P. (1984). Effect on the life time of wire ropes. Wireworld international, 26(4), 150-152.

Kuruppu, M. D., Tytko, A., and Golosinski, T. S. (2000). Loss of metallic area in winder ropes subject to external wear. *Engineering Failure Analysis,* 7(3), 199-207.

Little, R. E., and Jebe, E. H. (1975). Statistical design of fatigue experiments. Applied Science Publishers Ltd., Essex, England.

Llorca J., Varona J.M., Sanchez V., Sanchez-Galvez,V., and Gutierrez Solana F. (1989). Fatigue behaviour of wire ropes. *Materials and Structures,* 22(132), 411-419.

Metcalf, J. T., and Matanzo, F. (1980).Wire rope terminations, section, and replacement criteria. *Proceedings of the Annual Offshore Technology Conference*, OTC 3853, pp. 517-524.

Muller, F., and Zeller, W. (1975). Zulassungsprufungen and Spanndrahtlitzen T 12.4 mm, St 160/180 und T 15.2 mm, St 160/180: heir: Dauerschwingversuche. Prufungsbreicht, Institut fur Beton und Stahlbeton, Universitat Karlsruhe.

Müller, H. (1961). The properties of wire rope under alternating stresses. *Wire World International,* 3(5), 249-258.

Nabijou, S., and Hobbs, R. E. (1995). Relative movements within wire ropes bent over sheaves. *Journal of strain analysis,* 30(2), 155-165.

Nabijou, S., and Hobbs, R. E. (1994). Fatigue of wire ropes bent over small sheaves. *International Journal of Fatigue,* 16(7), 453-460.

Neuber, H. (1961). Theory of notch stress, U.S. Office of Technical Services, Washington, DC.

Onur, Y. A., and Imrak, C. E. (2012). Experimental and theoretical investigation of bending over sheave fatigue life of stranded steel wire rope. *Indian Journal of Engineering & Materials Sciences ,* 19(3), 189-95.

Papanikolas, P. (1995). Axial Fatigue of Multi-layered Wire Strands. *PhD Thesis*. Dep. of Civil and Environmental Engineering. University of Alberta, Canada.

Paulson, C. Jr., Frank, K. H., and Breen, J. E. (1983). A fatigue study of Prestressing strand. Research Report 300-1, Centre for Transportation Research, Bureau of Engineering Research, The University of Texas at Austin, Austin, TX, USA.

Pilkey, W. D. (1997). Peterson's Stress Concentration Factors. (2nd Ed.). New York : John Wiley & Sons.

Raoof, M. (1990). Axial fatigue of multilayered strands. *Journal of Engineering Mechanics,* ASCE, 116(10), 2083-2099.

Raoof, M. (1990a). Comparison between the performance of newly manufactured and well-used spiral strand. Proc. Inst. Civ. Eng. Part 2 Res. Theory, 89. pp. 103-120.

Raoof, M., and Hobbs, R. E. (1988). Torsion tests on large spiral strands. *Journal of Strain Analysis for Engineering Design,* 23(2), 97-104.

Raoof, M., and Huang, Y. P. (1992). Wire stress calculations in helical strands undergoing bending. *Journal of Offshore Mechanics and Arctic Engineering,* 114(3), 212-219.

Ridge, I. M. L., Chaplin, C. R., and Zheng, J. (2001). Effect of degradation and impaired quality on wire rope bending over sheave fatigue endurance. *Engineering Failure Analysis,* 8(2001), 173-187.

Ridge, I. M. L., Zheng, J., and Chaplin, C. R. (2000). Measurement of cyclic bending strains in steel wire rope. *Journal of Strain Analysis for Engineering Design,* 35(6), 545-558.

Sasaki Koji, Iwakura Shota, Takahashi Tatsuhiko, Moriya Toshiyuki, and Furukawa Ippei. (2007). Estimating the fatigue life of wire rope with a stochastic approach. Journal of Solid Mechanics and Materials Engineering, The Japan Society of Mechanical Engineers 1(8), 1052-1062.

Scoble, W. A. (1930). Fourth report of the wire ropes research commitee. Proc. Inst. Mech. Eng., Issue 2.

Shigley, J. E., and Mitchell, L. D. (1983). Mechanical Engineering Design. (4th ed.). New York: McGraw-Hill.

Smith, H. L., Stonesifer, F. R., and Seibert, E. R. (1978). Increased fatigue life of wire rope through periodic overloads. *Proceedings of the Annual Offshore Technology Conference,* OTC 3256, pp. 1771-1778.

Stephens, R. I., Fatemi A., Stephens, R. R., and Fuchs, H. O. (2001). Metal fatigue in engineering. (2nd Ed.). New York: John Wiley & Sons Inc.

Stonesifer, F. R., and Smith, H. L. (1979).Tensile fatigue in wire rope. *Proceedings of the Annual Offshore Technology Conference*, OTC 3419, pp. 539-545.

Suh, J., and Chang, S. P. (2000). Experimental study on fatigue behaviour of wire ropes. *International Journal of Fatigue, 22*(4), 339-347.

Sumiden Wire Products Corporation. (n.d.). SWPC Specification Sheets. Retrieved from http://www.sumidenwire.com/prod/pc/tech-data/index.html.

Thomas, H. R., and Hoersh, V. A. (1930).Stresses due to pressure of one elastic solid upon another. *Bulletin no. 212, Engrg. Exp. Sta., Univ. of Illinois, 26*(46), Urbana, Ill.

Thorpe, T. W., and Rance, A. (1983).The tensile fatigue of wire rope: A new approach. *Proceedings of the Annual Offshore Technology Conference*, OTC 4638, pp. 483-490.

Thorpe, T. W., Rance, A., and Silvester, D. R. V. (1985).The fatigue of electrogalvanised wire used in the manufacture of wire ropes. *Report by Materials Development Div., Atomic Energy Research Establishment (AERE),* Harwell, U.K. Jan.

Urchegui, M. A., Tato, W., and Gómez, X. (2008). Wear evolution in a stranded rope subjected to cyclic bending. *Journal of Materials Engineering and Performance,* ASM International, *17*(4), 550-560.

Utting, W. S., and Jones, N. (1985). Tensile testing of a wire rope strand. *I.Mech.E, Journal of Strain Analysis for Engineering Design, 20*(3), 151-164.

Vennemann, O., Törnqvist, R., Ernst, B., Winter, S., and Fraser, I. (2008). Bending fatigue tests using a suitable NDT method to determine lifetime of large diameter wire ropes for offshore lifting applications. *, vol 1 Proceedings of the 27th International Conference on Offshore Mechanics and Arctic Engineering, OMAE 2008.*pp. 155-161.

Velinsky, S. A. (1981). Analysis of wire ropes with complex cross sections. Ph.D. Thesis, Department of Theoretical and Applied Mechanics, University of Illinois at Urbana-Champaign.

Velinsky, S. A., and Schmidt, J. D. (1988). Simplified treatise on the effect of wear in cables. *Journal of Offshore Mechanics and Arctic Engineering, 110*(1), 32-37.

Wang, D., Zhang, D., Wang, S., and Ge, S. (2013). Finite element analysis of hoisting rope and fretting wear evolution and fatigue life estimation of steel wires. *Engineering Failure Analysis, vol 27*, 173-193.

Warner, R. F., and Hulsbos, C. L. (1966). Fatigue properties of prestressing strand. Prestressed Concrete Institute Journal, 11(1), pp 32-52.

Waters, D. M. (1985). Fatigue testing of large wire ropes. Wire Industry, *52*(620), 493-496.

Wiek, L. (1973). Facts and figures of stresses in ropes. OIPEEC Round Table Milano, S94-111.

Wokem, C., and Grondin, G. Y. (2010). Effect of stress concentration on fatigue of built-up I-shaped members. *Structural Engineering Rep.* No. 292. Dep. of Civil and Environmental Engineering, University of Alberta, Edmonton, Canada.

Yeung, Y., and Walton, J. (1986).Accelerated fatigue testing of wire ropes. Wire Industry, *53*(631), 490-493.

Zhang, D. K., Ge, S. R., and Qiang, Y. H. (2003).Research on the fatigue and fracture behavior due to the fretting wear of steel wire in hoisting rope. *Wear, 255*(7–12), 1233-1237.

Appendix A

PARAMETRIC EQUATIONS FOR 6×19 SEALE WIRE ROPE

PARAMETRIC EQUATIONS FOR 6×19 SEALE WIRE ROPE

This appendix contains the parametric equations used to create a model of the 6×19 Seale wire rope. The dimensions of each of the ropes were discussed in Chapter 3. The general forms of these parametric equations were originally reported by Feyrer (2007) and Erdonmez and Imrak (2011):

The coordinates of the centreline of a single helix wire are given by:

$$X_{sh} = r_{sh}\cos\theta_{sh}$$

$$Y_{sh} = r_{sh}\sin\theta_{sh}$$

$$Z_{sh} = r_{sh}\tan(\alpha_{sh})\theta_{sh}$$

where r_{sh} is the radius of a single helix strand, α_{sh} is the single helix lay angle, and $\theta_{sh} = \theta_{sh0} + \theta$, and θ_{sh0} is the single helix phase angle, where θ is the free angle rotated about the rope axis.

The coordinates of the centreline of a double wire in a wire rope are given by:

$$X_{dh} = X_{sh} + r_{dh}\cos\theta_{dh}\cos\theta_{sh} - r_{dh}\sin\theta_{dh}\sin\theta_{sh}\sin\alpha_{sh}$$

$$Y_{dh} = Y_{sh} + r_{dh}\cos\theta_{dh}\sin\theta_{sh} + r_{dh}\sin\theta_{dh}\cos\theta_{sh}\sin\alpha_{sh}$$

$$Z_{dh} = Z_{sh} - r_{dh}\sin\theta_{dh}\cos\alpha_{sh}$$

where $\theta_{dh} = \theta_{dh0} + m\theta_{sh}$,

$m = r_{sh} / (r_{dh}\tan\alpha_{dh}\cos\alpha_{sh})$,

r_{dh} is the double helix radius representing the distance along the double helix wire centreline for the single helix strand centreline.

and θ_{dh0} is the double helix wire phase angle.

6× 19 Seale wire rope (33 mm) coordinates

Strand 1 wire radius = 0.735 mm

H11.

$$X_{sh} = 1.536*\cos(t)$$

$$Y_{sh} = 1.536*\sin(t)$$

$$Z_{sh} = 5.255*t$$

H12.

$$X_{sh} = 1.536*\cos(t+1.0476)$$

$$Y_{sh} = 1.536*\sin(t+1.0476)$$

$$Z_{sh} = 5.255*t$$

H13.

$$X_{sh} = 1.536*\cos(t+2.0952)$$

$$Y_{sh} = 1.536*\sin(t+2.0952)$$

$$Z_{sh} = 5.255*t$$

H14.

$$X_{sh} = 1.536*\cos(t+3.1429)$$

$$Y_{sh} = 1.536*\sin(t+3.1429)$$

$$Z_{sh} = 5.255*t$$

H15.

$X_{sh} = 1.536*\cos(t+4.1905)$

$Y_{sh} = 1.536*\sin(t+4.1905)$

$Z_{sh} = 5.255*t$

H16.

$X_{sh} = 1.536*\cos(t+5.2381)$

$Y_{sh} = 1.536*\sin(t+5.2381)$

$Z_{sh} = 5.255*t$

Strand 2 Single helix, wire radius = 0.704 mm

H20.

$$X_{sh} = 4.287*\cos(t)$$

$$Y_{sh} = 4.287*\sin(t)$$

$$Z_{sh} = 12.331*t$$

Strand 2 Double helix, wire radius = 0.656 mm

H21.

$$X_{dh} = 4.287*\cos(t)+1.360*\cos(1.5087*t)*\cos(t)-1.360*\sin(1.5087*t)*\sin(t)*\sin(1.2362)$$

$$Y_{dh} = 4.287*\sin(t)+1.360*\cos(1.5087*t)*\sin(t)+1.360*\sin(1.5087*t)*\cos(t)*\sin(1.2362)$$

$$Z_{dh} = 12.331*t-1.360*\sin(1.5087*t)*\cos(1.2362)$$

H22

$$X_{dh} = 4.287*\cos(t)+1.360*\cos(1.5087*t+1.0476)*\cos(t)-1.360*\sin(1.5087*t+1.0476)*\sin(t)*\sin(1.2362)$$

$$Y_{dh} = 4.287*\sin(t)+1.360*\cos(1.5087*t+1.0476)*\sin(t)+1.360*\sin(1.5087*t+1.0476)*\cos(t)*\sin(1.2362)$$

$$Z_{dh} = 12.331*t-1.360*\sin(1.5087*t+1.0476)*\cos(1.2362)$$

H23

$$X_{dh} = 4.287*\cos(t)+1.360*\cos(1.5087*t+2.0952)*\cos(t)-1.360*\sin(1.5087*t+2.0952)*\sin(t)*\sin(1.2362)$$

$$Y_{dh} = 4.287*\sin(t)+1.360*\cos(1.5087*t+2.0952)*\sin(t)+1.360*\sin(1.5087*t+2.0952)*\cos(t)*\sin(1.2362)$$

$$Z_{dh} = 12.331*t-1.360*\sin(1.5087*t+2.0952)*\cos(1.2362)$$

H24

X_{dh} = 4.287*cos(t)+1.360*cos(1.5087*t+3.1429)*cos(t)-1.360*sin(1.5087*t+3.1429)*sin(t)*sin(1.2362)

Y_{dh} = 4.287*sin(t)+1.360*cos(1.5087*t+3.1429)*sin(t)+1.360*sin(1.5087*t+3.1429)*cos(t)*sin(1.2362)

Z_{dh} = 12.331*t-1.360*sin(1.5087*t+3.1429)*cos(1.2362)

H25

X_{dh} = 4.287*cos(t)+1.360*cos(1.5087*t+4.1905)*cos(t)-1.360*sin(1.5087*t+4.1905)*sin(t)*sin(1.2362)

Y_{dh} = 4.287*sin(t)+1.360*cos(1.5087*t+4.1905)*sin(t)+1.360*sin(1.5087*t+4.1905)*cos(t)*sin(1.2362)

Z_{dh} = 12.331*t-1.360*sin(1.5087*t+4.1905)*cos(1.2362)

H26

X_{dh} = 4.287*cos(t)+1.360*cos(1.5087*t+5.2381)*cos(t)-1.360*sin(1.5087*t+5.2381)*sin(t)*sin(1.2362)

Y_{dh} = 4.287*sin(t)+1.360*cos(1.5087*t+5.2381)*sin(t)+1.360*sin(1.5087*t+5.2381)*cos(t)*sin(1.2362)

Z_{dh} = 12.331*t-1.360*sin(1.5087*t+5.2381)*cos(1.2362)

Strand 3 Single helix, wire radius = 1.456 mm

H30.

X_{sh} = -11.413*cos(t)

Y_{sh} = 11.413*sin(t)

Z_{sh} = 31.72*t

Stand 3 Double helix, wire radius = 0.712 mm

H31.

X_{dh} = -(11.413*cos(t)+2.168*cos(-3.3855*t+0.3492)*cos(t)-2.168*sin(-3.3855*t+0.3492)*sin(t)*sin(1.2259))

Y_{dh} = 11.413*sin(t)+2.168*cos(-3.3855*t+0.3492)*sin(t)+2.168*sin(-3.3855*t+0.3492)*cos(t)*sin(1.2259)

Z_{dh} = 31.72*t-2.168*sin(-3.3855*t+0.3492)*cos(1.2259)

H32

X_{dh} = - (11.413*cos(t)+2.168*cos(-3.3855*t+1.0476)*cos(t)-2.168*sin(-3.3855*t+1.0476)*sin(t)*sin(1.2259))

Y_{dh} = 11.413*sin(t)+2.168*cos(-3.3855*t+1.0476)*sin(t)+2.168*sin(-3.3855*t+1.0476)*cos(t)*sin(1.2259)

Z_{dh} = 31.72*t-2.168*sin(-3.3855*t+1.0476)*cos(1.2259)

H33

X_{dh} = - (11.413*cos(t)+2.168*cos(-3.3855*t+1.7460)*cos(t)-2.168*sin(-3.3855*t+1.7460)*sin(t)*sin(1.2259))

Y_{dh} = 11.413*sin(t)+2.168*cos(-3.3855*t+1.7460)*sin(t)+2.168*sin(-3.3855*t+1.7460)*cos(t)*sin(1.2259)

Z_{dh} = 31.72*t-2.168*sin(-3.3855*t+1.7460)*cos(1.2259)

H34

X_{dh} = - (11.413*cos(t)+2.168*cos(-3.3855*t+2.4444)*cos(t)-2.168*sin(-3.3855*t+2.4444)*sin(t)*sin(1.2259))

Y_{dh} = 11.413*sin(t)+2.168*cos(-3.3855*t+2.4444)*sin(t)+2.168*sin(-3.3855*t+2.4444)*cos(t)*sin(1.2259)

Z_{dh} = 31.72*t-2.168*sin(-3.3855*t+2.4444)*cos(1.2259)

H35

X_{dh} = - (11.413*cos(t)+2.168*cos(-3.3855*t+3.1429)*cos(t)-2.168*sin(-3.3855*t+3.1429)*sin(t)*sin(1.2259))

Y_{dh} = 11.413*sin(t)+2.168*cos(-3.3855*t+3.1429)*sin(t)+2.168*sin(-3.3855*t+3.1429)*cos(t)*sin(1.2259)

Z_{dh} = 31.72*t-2.168*sin(-3.3855*t+3.1429)*cos(1.2259)

H36

X_{dh} = - (11.413*cos(t)+2.168*cos(-3.3855*t+3.8413)*cos(t)-2.168*sin(-3.3855*t+3.8413)*sin(t)*sin(1.2259))

Y_{dh} = 11.413*sin(t)+2.168*cos(-3.3855*t+3.8413)*sin(t)+2.168*sin(-3.3855*t+3.8413)*cos(t)*sin(1.2259)

Z_{dh} = 31.72*t-2.168*sin(-3.3855*t+3.8413)*cos(1.2259)

H37

X_{dh} = - (11.413*cos(t)+2.168*cos(-3.3855*t+4.5397)*cos(t)-2.168*sin(-3.3855*t+4.5397)*sin(t)*sin(1.2259))

Y_{dh} = 11.413*sin(t)+2.168*cos(-3.3855*t+4.5397)*sin(t)+2.168*sin(-3.3855*t+4.5397)*cos(t)*sin(1.2259)

Z_{dh} = 31.72*t-2.168*sin(-3.3855*t+4.5397)*cos(1.2259)

H38

X_{dh} = - (11.413*cos(t)+2.168*cos(-3.3855*t+5.2381)*cos(t)-2.168*sin(-3.3855*t+5.2381)*sin(t)*sin(1.2259))

Y_{dh} = 11.413*sin(t)+2.168*cos(-3.3855*t+5.2381)*sin(t)+2.168*sin(-3.3855*t+5.2381)*cos(t)*sin(1.2259)

Z_{dh} = 31.72*t-2.168*sin(-3.3855*t+5.2381)*cos(1.2259)

H39

X_{dh} = - (11.413*cos(t)+2.168*cos(-3.3855*t+5.9365)*cos(t)-2.168*sin(-3.3855*t+5.9365)*sin(t)*sin(1.2259))

Y_{dh} = 11.413*sin(t)+2.168*cos(-3.3855*t+5.9365)*sin(t)+2.168*sin(-3.3855*t+5.9365)*cos(t)*sin(1.2259)

Z_{dh} = 31.72*t-2.168*sin(-3.3855*t+5.9365)*cos(1.2259)

Strand 3 Double helix, wire radius = 1.243 mm

H41

X_{dh} = - (11.413*cos(t)+ 3.867*cos(-3.3855*t)*cos(t)- 3.867*sin(-3.3855*t)*sin(t)*sin(1.2259))

Y_{dh} = 11.413*sin(t)+ 3.867*cos(-3.3855*t)*sin(t)+ 3.867*sin(-3.3855*t)*cos(t)*sin(1.2259)

Z_{dh} = 31.72*t-3.867*sin(-3.3855*t)*cos(1.2259)

H42

X_{dh} = - (11.413*cos(t)+ 3.867*cos(-3.3855*t+0.6984)*cos(t)- 3.867*sin(-3.3855*t+0.6984)*sin(t)*sin(1.2259))

Y_{dh} = 11.413*sin(t)+ 3.867*cos(-3.3855*t+0.6984)*sin(t)+ 3.867*sin(-3.3855*t+0.6984)*cos(t)*sin(1.2259)

Z_{dh} = 31.72*t-3.867*sin(-3.3855*t+0.6984)*cos(1.2259)

H43

X_{dh} = - (11.413*cos(t)+ 3.867*cos(-3.3855*t+1.3968)*cos(t)- 3.867*sin(-3.3855*t+1.3968)*sin(t)*sin(1.2259))

Y_{dh} = 11.413*sin(t)+ 3.867*cos(-3.3855*t+1.3968)*sin(t)+ 3.867*sin(-3.3855*t+1.3968)*cos(t)*sin(1.2259)

Z_{dh} = 31.72*t-3.867*sin(-3.3855*t+1.3968)*cos(1.2259)

H44

X_{dh} = - (11.413*cos(t)+ 3.867*cos(-3.3855*t+2.0952)*cos(t)- 3.867*sin(-3.3855*t+2.0952)*sin(t)*sin(1.2259))

Y_{dh} = 11.413*sin(t)+ 3.867*cos(-3.3855*t+2.0952)*sin(t)+ 3.867*sin(-3.3855*t+2.0952)*cos(t)*sin(1.2259)

Z_{dh} = 31.72*t-3.867*sin(-3.3855*t+2.0952)*cos(1.2259)

H45

X_{dh} = - (11.413*cos(t)+ 3.867*cos(-3.3855*t+2.7937)*cos(t)- 3.867*sin(-3.3855*t+2.7937)*sin(t)*sin(1.2259))

Y_{dh} = 11.413*sin(t)+ 3.867*cos(-3.3855*t+2.7937)*sin(t)+ 3.867*sin(-3.3855*t+2.7937)*cos(t)*sin(1.2259)

Z_{dh} = 31.72*t-3.867*sin(-3.3855*t+2.7937)*cos(1.2259)

H46

X_{dh} = - (11.413*cos(t)+ 3.867*cos(-3.3855*t+3.4921)*cos(t)- 3.867*sin(-3.3855*t+3.4921)*sin(t)*sin(1.2259))

Y_{dh} = 11.413*sin(t)+ 3.867*cos(-3.3855*t+3.4921)*sin(t)+ 3.867*sin(-3.3855*t+3.4921)*cos(t)*sin(1.2259)

Z_{dh} = 31.72*t-3.867*sin(-3.3855*t+3.4921)*cos(1.2259)

H47

X_{dh} = - (11.413*cos(t)+ 3.867*cos(-3.3855*t+4.1905)*cos(t)- 3.867*sin(-3.3855*t+4.1905)*sin(t)*sin(1.2259))

Y_{dh} = 11.413*sin(t)+ 3.867*cos(-3.3855*t+4.1905)*sin(t)+ 3.867*sin(-3.3855*t+4.1905)*cos(t)*sin(1.2259)

Z_{dh} = 31.72*t-3.867*sin(-3.3855*t+4.1905)*cos(1.2259)

H48

X_{dh} = - (11.413*cos(t)+ 3.867*cos(-3.3855*t+4.8888)*cos(t)- 3.867*sin(-3.3855*t+4.8888)*sin(t)*sin(1.2259))

Y_{dh} = 11.413*sin(t)+ 3.867*cos(-3.3855*t+4.8888)*sin(t)+ 3.867*sin(-3.3855*t+4.8888)*cos(t)*sin(1.2259)

Z_{dh} = 31.72*t-3.867*sin(-3.3855*t+4.8888)*cos(1.2259)

H49

X_{dh} = - (11.413*cos(t)+ 3.867*cos(-3.3855*t+5.5872)*cos(t)- 3.867*sin(-3.3855*t+5.5872)*sin(t)*sin(1.2259))

Y_{dh} = 11.413*sin(t)+ 3.867*cos(-3.3855*t+5.5872)*sin(t)+ 3.867*sin(-3.3855*t+5.5872)*cos(t)*sin(1.2259)

Z_{dh} = 31.72*t-3.867*sin(-3.3855*t+5.5872)*cos(1.2259)

Appendix B

FINITE ELEMENT RESULT FOR SHORTER AND LONGER 7-WIRE PRESTRESSING STRANDS AND LOCATION OF MAXIMUM STRESS FOR CABLES IN TENSION

FINITE ELEMENT AND FATIGUE RESULT FOR SHORTER AND LONGER 7-WIRE PRESTRESSING STRANDS AND LOCATION OF MAXIMUM STRESS FOR CABLES IN TENSION

This Appendix shows the von Mises stresses in the 7-wire strand models, and the finite element analysis results for the short models ($1/6^{th}$ of lay length) and long models (300 mm for all 7-wire strands) in terms of the magnitude and location of the maximum von Mises stresses in the 7-wire strands. The comparison of the fatigue life for the short and long models is also presented in this Appendix. Figures B-1 to B-6 show the von Mises stresses on the surface of the wires for several load levels for the short model. Tables B-1 to B-6 show the magnitude and the location of the maximum von Mises stresses at different load levels for the short and long strand models. In these tables "E.Helix" means that the location of the maximum von Mises stress is at the end of one of the 6 helix wires that wrap around the core, "I.Core" means that the location of the maximum von Mises stress is on the core wire, and finally "I.Helix" means that the location of the maximum von Mises stress is on one of the 6 helix wires that wrap around the core, at some distance from the ends. Figure B-7 shows the distribution of von Mises stress across the length of various 7-wire strand at the maximum applied loads. Figures B-8 to B-13 are showing the distribution of von Mises stresses and the maximum von Mises stresses in the long strand model of the 7-wire prestressing strands, when one external wire is removed. By visual inspection of Figures B-8 to B-13, it can be seen that the maximum von Mises stress or any other internal maximum von Mises stress away from the ends will not be significantly different, and noting that the load is applied in tension only. From the ratio of the maximum von Mises stress for the short model to the maximum von Mises stress of the long model $(\sigma_{mv(short)}/\sigma_{mv(long)})$, a maximum difference between the magnitudes of the maximum von Mises stress is 10%.

A plot showing the fatigue life for the short and long model is shown in Figure B-14, and by visual inspection it can be observed the difference in fatigue life between the long and short model is insignificant. Table B-7 gives the fatigue life for the long model at different load levels. The S-N plot for 6.4 mm prestressing strand gives a mean fatigue regression equation as follows:

$$LogN = 16.92 - 4.31 LogS_N \qquad \text{(C-1)}$$

Figure B-15 shows the the S-N plot for long and short 7.9 prestressing strand, Table B-8 shows the Fatigue life at various load levels, again by visual inpection of the plot, it can be concluded there isn't any significant difference in fatigue life between the long and short model. The mean fatigue regression equation is given by:

$$LogN = 16.99 - 4.33 LogS_N \tag{C-2}$$

In Figures B-16 through B-19 the S-N plot for the 9.5 to 15.24 mm strands are compared for the long and short models. For these plots it can be seen that there is not significant difference between the predicted fatigue life between the long and short model. Tables B-9 to B-12 show the fatigue life values for the long models. The mean fatigue regression equations for the 9.5, 11.11, 12.7 and 15.24 mm prestressing strands are given in Equations C-3, C-4, C-5, and C-6, respectively as follows:

$$LogN = 16.29 - 4.08 LogS_N \tag{C-3}$$

$$LogN = 14.81 - 3.53 LogS_N \tag{C-4}$$

$$LogN = 15.01 - 3.62 LogS_N \tag{C-5}$$

$$LogN = 15.91 - 3.95 LogS_N \tag{C-6}$$

The difference in magnitude of the slope of the mean fatigue regression equations between the short and long models is 0.05, 0.07, 0.2, 0.24, 0.02 and 0.15 for the 6.4, 7.9, 9.5, 11.11, 12.7 and 15.24 mm strands, respectively. Also the difference in the magnitude of the intercept of the mean fatigue regression equations between the short and long models is 0.17, 0.24, 0.57, 0.57, 0.08 and 0.44 for the 6.4, 7.9, 9.5, 11.11, 12.7 and 15.24 mm strands, respectively. Little and Jebe (1975) proposed methods for checking if two or more mean regression fatigue curve are identical, but it is was concluded in the current research that such statistical checks does not seem to be necessary, since visual examination of the fatigue plots for the long and short models were pretty conclusive in accessing whether there was any significant difference between their predictions. In the author's opinion there is insignificant difference in the slopes and intercepts of the short and long models. In this appendix the location of the maximum von Mises stress for all other cables subjected to tension only at different load levels is indicated in Tables B-13 to B-18. In

these tables the layers where the maximum von Mises stress occurred is indicated, as examples, “I.Lay2-3” means that the maximum von Mises stress occurred internally (not at the ends of the model), in one of the wires in Layer 2, but at the interface between Layer 2 and Layer 3. “I.H10-H11” means that the location of the maximum von Mises stress occurred internally, in the core wire (H10), but at the interface between the core wire and the next layer comprised of H11 wires.

Table B-1: Comparison of the magnitude and location of maximum von Mises stress for a 6.4 mm ASTM A416 prestressing strand

Applied Load (kN)	Short model		Long model		$\frac{\sigma_{mv(short)}}{\sigma_{mv(long)}}$
	Maximum von Mises stress (MPa)	Location of maximum von Mises stress	Maximum von Mises stress (MPa)	Location of maximum von Mises stress	
8.00	450	E.Helix	500	I.Core	0.90
10.00	556	E.Helix	536	I.Core	1.04
12.00	664	E.Helix	649	I.Core	1.02
14.00	774	E.Helix	777	I.Core	1.00
16.00	880	E.Helix	844	I.Core	1.04
18.00	989	E.Helix	980	I.Core	1.01
20.00	1,098	E.Helix	1,137	I.Core	0.96

Table B-2: Comparison of the magnitude and location of maximum von Mises stress for a 7.9 mm ASTM A416 prestressing strand

Applied Load (kN)	Short model		Long model		$\frac{\sigma_{mv(short)}}{\sigma_{mv(long)}}$
	Maximum von Mises stress (MPa)	Location of maximum von Mises stress	Maximum von Mises stress (MPa)	Location of maximum von Mises stress	
12.90	479	I.Helix	517	I.Core	0.93
16.13	588	E.Helix	571	E.Helix	1.03
19.35	700	E.Helix	678	E.Helix	1.03
22.58	813	E.Helix	780	I.Core	1.04
25.80	925	E.Helix	890	E.Helix	1.04
29.03	1,040	E.Helix	1,015	E.Helix	1.03
32.25	1,150	E.Helix	1,103	I.Core	1.04

Table B-3: Comparison of the magnitude and location of maximum von Mises stress for a 9.5 mm ASTM A416 prestressing strand

Applied Load (kN)	Short model		Long model		$\frac{\sigma_{mv(short)}}{\sigma_{mv(long)}}$
	Maximum von Mises stress (MPa)	Location of maximum von Mises stress	Maximum von Mises stress (MPa)	Location of maximum von Mises stress	
18.00	476	I.Helix	501	I.Core	0.95
22.50	580	I.Helix	550	I.Core	1.05
27.00	674	I.Helix	660	I.Core	1.02
31.50	775	E.Helix	781	I.Core	0.99
36.00	884	E.Helix	858	I.Core	1.03
40.50	989	E.Helix	1,000	I.Core	0.99
45.00	1,093	E.Helix	1,040	E.Helix	1.05

Table B-4: Comparison of the magnitude and location of maximum von Mises stress for an 11.11 mm ASTM A416 prestressing strand

Applied Load (kN)	Short model		Long model		$\frac{\sigma_{mv(short)}}{\sigma_{mv(long)}}$
	Maximum von Mises stress (MPa)	Location of maximum von Mises stress	Maximum von Mises stress (MPa)	Location of maximum von Mises stress	
18.00	374	E.Helix	376	I.Core	0.99
24.00	475	E.Helix	531	I.Core	0.90
30.00	589	E.Helix	582	I.Core	1.01
36.00	691	E.Helix	684	I.Core	1.01
42.00	803	E.Helix	797	I.Core	1.01
48.00	901	E.Helix	846	I.Core	1.07
54.00	1,008	E.Helix	993	I.Core	1.02
60.00	1,112	E.Helix	1,024	I.Core	1.09

Table B-5: Comparison of the magnitude and location of maximum von Mises stress for a 12.7 mm ASTM A416 prestressing strand

Applied Load (kN)	Short model		Long model		$\frac{\sigma_{mv(short)}}{\sigma_{mv(long)}}$
	Maximum von Mises stress (MPa)	Location of maximum von Mises stress	Maximum von Mises stress (MPa)	Location of maximum von Mises stress	
25.10	379	I.Helix	363	I.Core	1.04
33.46	484	I.Helix	510	I.Core	0.95
41.82	592	E.Helix	562	I.Core	1.05
50.19	702	E.Helix	678	I.Core	1.04
58.55	815	E.Helix	829	E.Helix	0.98
66.92	926	E.Helix	923	E.Helix	1.00
75.28	1,042	E.Helix	1,045	E.Helix	1.00
83.64	1,158	E.Helix	1,160	E.Helix	1.00

Table B-6: Comparison of the magnitude and location of maximum von Mises stress for a 15.24 mm ASTM A416 prestressing strand

Applied Load (kN)	Short model		Long model		$\frac{\sigma_{mv(short)}}{\sigma_{mv(long)}}$
	Maximum von Mises stress (MPa)	Location of maximum von Mises stress	Maximum von Mises stress (MPa)	Location of maximum von Mises stress	
42.67	453	I.Helix	442	I.Core	1.03
53.33	547	I.Helix	550	I.Core	1.00
64.00	640	I.Helix	633	I.Core	1.01
74.67	737	I.Helix	750	I.Core	0.98
85.33	827	I.Helix	822	I.Core	1.01
96.00	915	I.Helix	910	I.Core	1.01
106.70	1,012	E.Helix	1,011	I.Core	1.00
117.30	1,108	E.Helix	1,081	I.Core	1.03
128.00	1,205	E.Helix	1,186	I.Core	1.15

Table B-7: Predicted fatigue results for a 6.4 mm prestressing strand using finite element analysis results (Long Model)

Applied Load (kN)	**Axial Wire Strain**	$N_{\text{int}.stress}$ **(Cycles)**
8.00	0.001830	10,852,695
10.00	0.002077	4,592,972
12.00	0.002557	1,890,118
14.00	0.003069	830,483
16.00	0.003301	390,106
18.00	0.003980	209,114
20.00	0.004210	105,652

Table B-8: Predicted fatigue results for a 7.9 mm prestressing strand using finite element analysis results (Long Model)

Applied Load (kN)	**Axial Wire Strain**	$N_{\text{int}.stress}$ **(Cycles)**
12.90	0.001935	11,969,543
16.13	0.002188	4,396,484
19.35	0.002702	1,954,573
22.58	0.003238	935,348
25.80	0.003483	389,974
29.03	0.004200	213,162
32.25	0.004397	109,593

Table B-9: Predicted fatigue results for a 9.5 mm prestressing strand using finite element analysis results (Long Model)

Applied Load (kN)	**Axial Wire Strain**	$N_{\text{int.}stress}$ **(Cycles)**
18.00	0.001877	11,088,942
22.50	0.002124	4,437,353
27.00	0.002607	1,971,855
31.50	0.003137	946,326
36.00	0.003367	452,413
40.50	0.004057	253,022
45.00	0.004233	141,053

Table B-10: Predicted fatigue results for an 11.11 mm prestressing strand using finite element analysis results (Long Model)

Applied Load (kN)	**Axial Wire Strain**	$N_{\text{int.}stress}$ **(Cycles)**
18.00	0.001141	13,541,862
24.00	0.001838	6,894,281
30.00	0.002061	2,775,050
36.00	0.002536	1,356,587
42.00	0.003044	681,398
48.00	0.003263	349,330
54.00	0.003953	193,238
60.00	0.004093	107,295

Table B-11 Predicted fatigue results for a 12.7 mm prestressing strand using finite element analysis results (UTS = 1860 MPa) (Long Model)

Applied Load (kN)	**Axial Wire Strain**	$N_{\text{int}.stress}$ **(Cycles)**
25.10	0.001237	14,612,266
33.46	0.001946	7,016,875
41.82	0.002207	2,914,038
50.19	0.002716	1,346,086
58.55	0.003257	628,227
66.92	0.003507	318,317
75.28	0.004220	191,400
83.64	0.004413	108,144

Table B-12: Predicted fatigue results for a 15.24 mm prestressing strand using finite element analysis results (Long Model)

Applied Load (kN)	**Axial Wire Strain**	$N_{\text{int}.stress}$ **(Cycles)**
42.67	0.001621	13,062,217
53.33	0.002037	5,048,275
64.00	0.002377	2,304,117
74.67	0.002854	1,155,513
85.33	0.003197	628,862
96.00	0.003607	356,239
106.70	0.004050	206,356
117.30	0.004377	123,845
128.00	0.004843	75,713

Table B-13: Locations of maximum von Mises stress for a 19-wire strand by Raoof (1990)

Applied Load (kN)	Max. von Mises stress (MPa)	Location of maximum von Mises stress
23.42	1,081	I.Lay2-1
46.77	2,015	I.Lay2-1
70.19	3,011	I.Lay2-1
81.90	3,395	I.Lay2-1

Table B-14: Locations of maximum von Mises stress for a 19-wire strand by Papanikolas (1995)

Applied Load (kN)	Max. von Mises stress (MPa)	Location of maximum von Mises stress
45.00	304	I.Lay2-3
60.00	407	I.Lay2-3
75.00	509	I.Lay2-3
90.00	593	I.Lay2-3
105.00	673	I.Lay2-3
120.00	792	I.CORE
135.00	924	I.CORE
150.00	1,048	I.CORE

Table B-15: Locations of maximum von Mises stress for a 39 mm strand (92 wires)

Applied Load (kN)	Max. von Mises stress (MPa)	Location of maximum von Mises stress
61.50	2,122	I.Lay3-2
123.00	3,092	I.Lay2-3
184.50	4,179	I.Lay3-4
246.00	5,227	I.Lay3-4
307.50	5,872	I.Lay4-3
369.00	6,962	I.Lay4-3

Table B-16: Locations of maximum von Mises stress for a 45 mm strand (91 wires)

Applied Load (kN)	Maximum von Mises stress (MPa)	Location of maximum von Mises stress
140.00	2,046	I.Lay2-3
280.00	2,902	I.Lay2-3
420.00	3,430	I.Lay3-4
560.00	4,246	I.Lay3-4
700.00	4,905	I.Lay3-4

Table B-17: Locations of maximum von Mises stress for a 6×7 wire rope (d=12.60 mm)

Applied Load (kN)	Max. von Mises stress (MPa)	Location of maximum von Mises stress
10.00	2,035	I.H10-H11
20.00	3,702	I.H11-H10
30.00	5,115	I.H11-H10
40.00	5,950	I.H10-H11
50.00	6,843	I.H10-H11

Table B-18: Locations of maximum von Mises stress for a 6×19 Seale wire rope (d=33.02 mm)

Applied Load (kN)	Max. von Mises stress (MPa)	Location of maximum von Mises stress
72.00	1,710	I.H10-H11
144.00	3,253	I.H11-H10
216.00	4,702	I.H10-H11
288.00	6,001	I.H10-H11
360.00	7,934	I.H11-H10

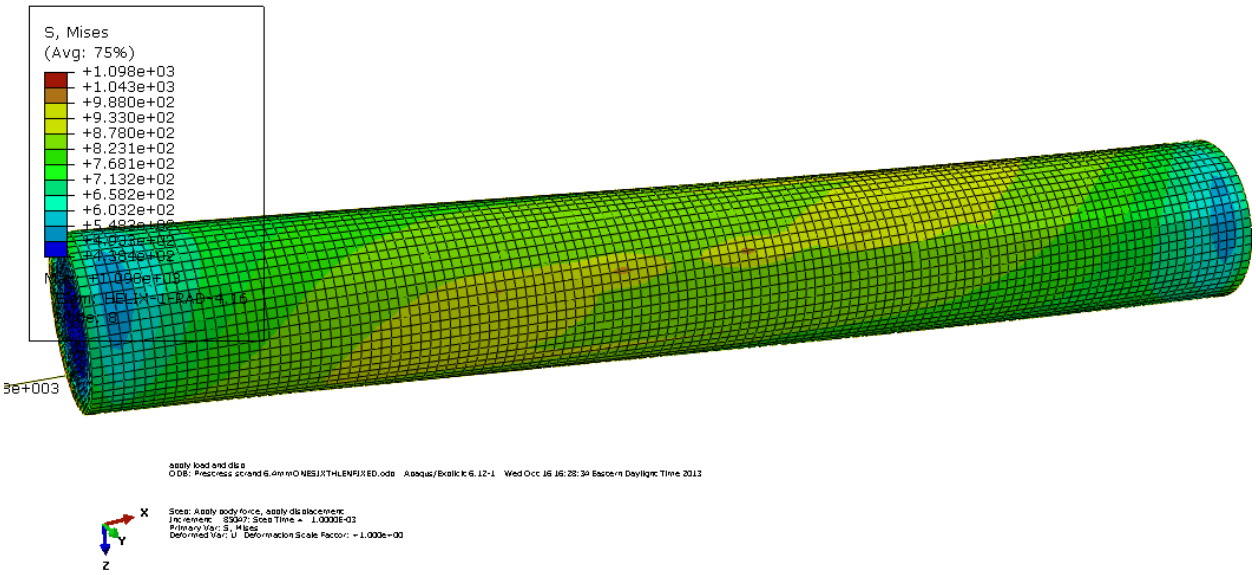

Figure B-1: von Mises stresses in the 6.4 mm ASTM A416 7-wire prestressing strand subjected to a tensile force of 20 kN

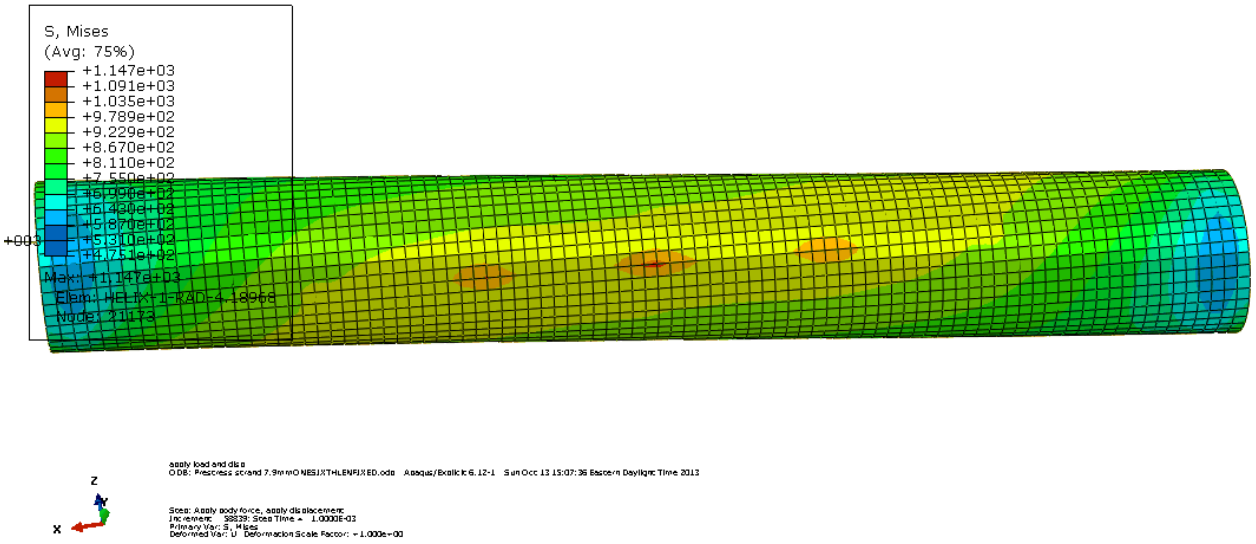

Figure B-2: von Mises stresses in 7.9 mm ASTM A416 7-wire prestressing strand subjected to a tensile force of 32.25 kN

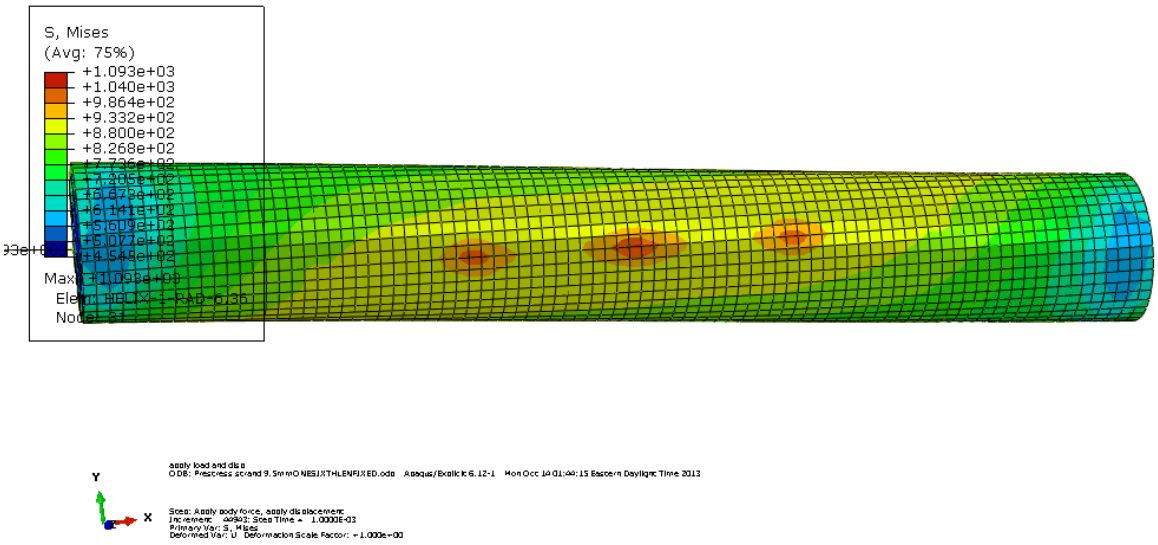

Figure B-3: von Mises stresses in 9.5 mm ASTM A416 7-wire prestressing strand subjected to a tensile force of 45 kN

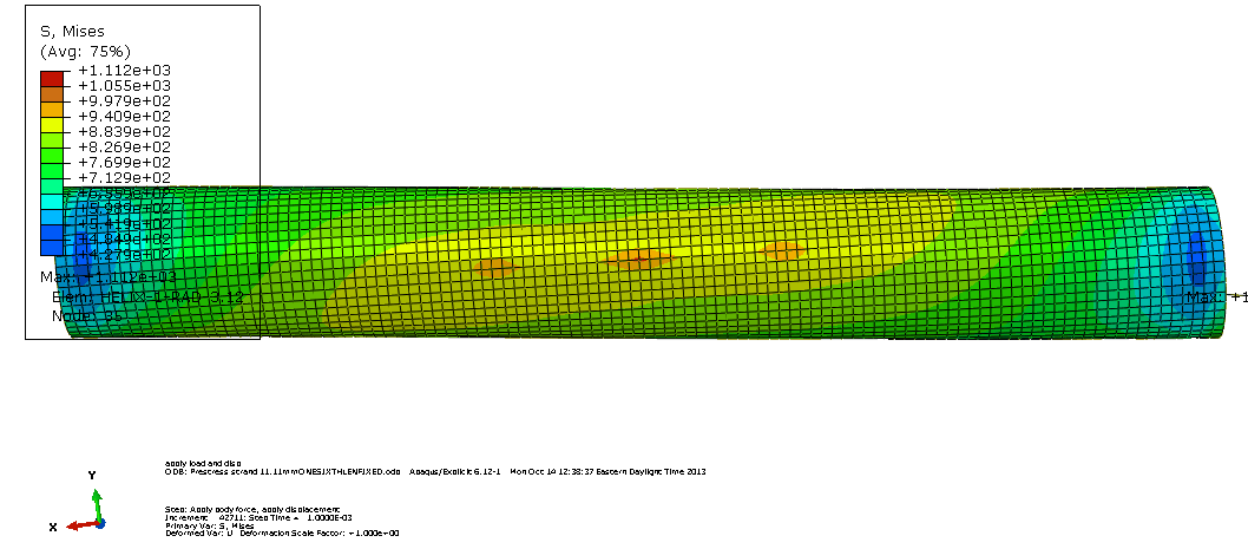

Figure B-4: von Mises stresses in 11.11 mm ASTM A416 7-wire prestressing strand subjected to a tensile force of 60 kN

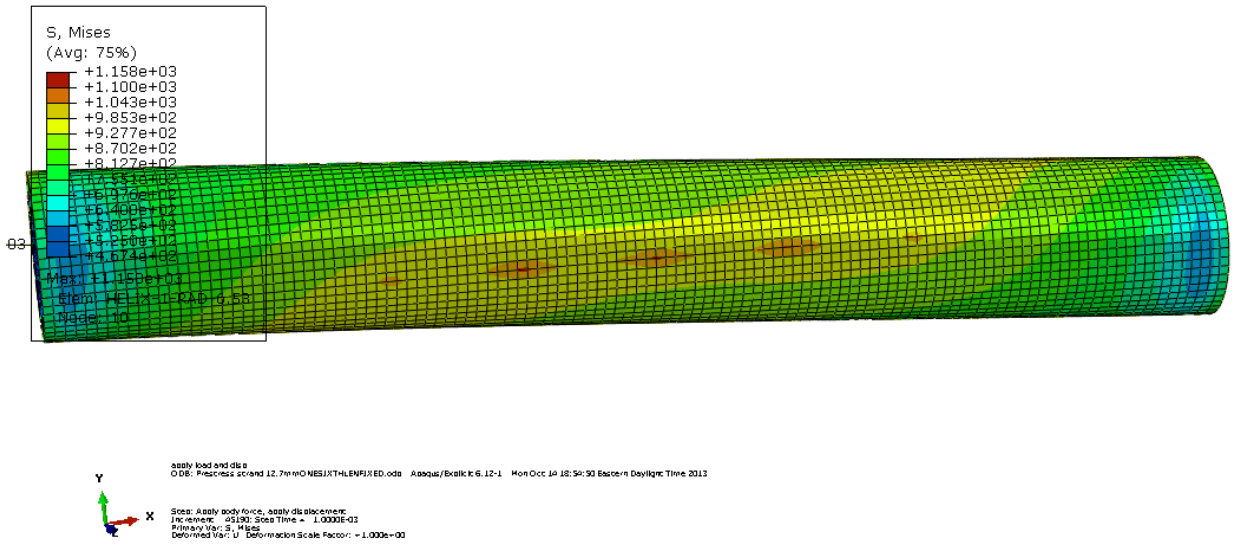

Figure B-5: von Mises stresses in 12.7 mm ASTM A416 7-wire prestressing strand subjected to a tensile force of 83.64 kN

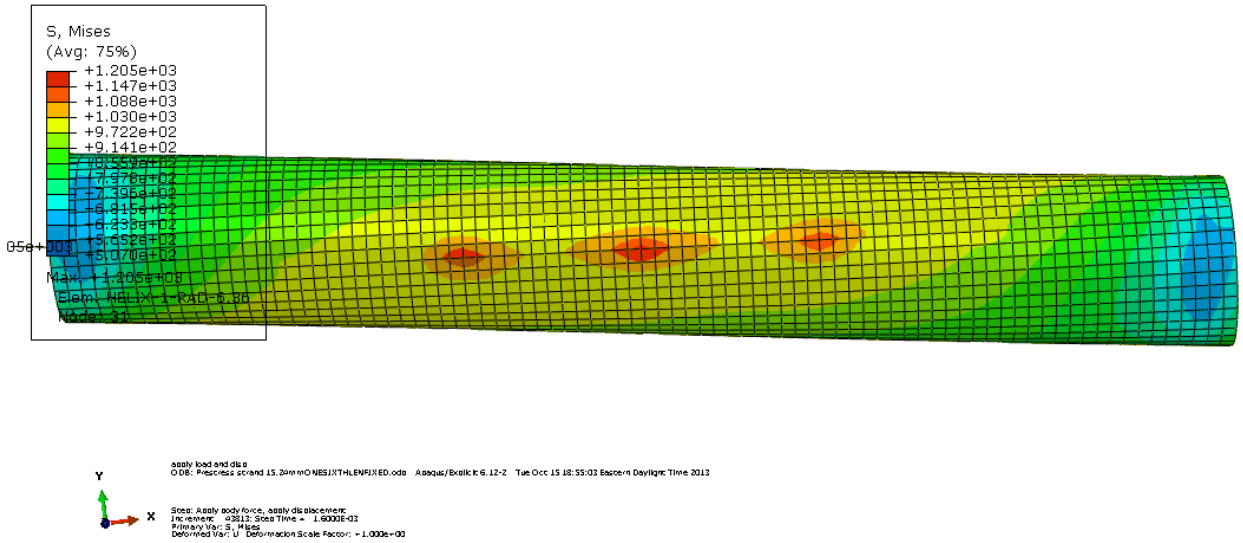

Figure B-6: von Mises stresses in 15.24 mm ASTM A416 7-wire prestressing strand subjected to a tensile force of 128 kN

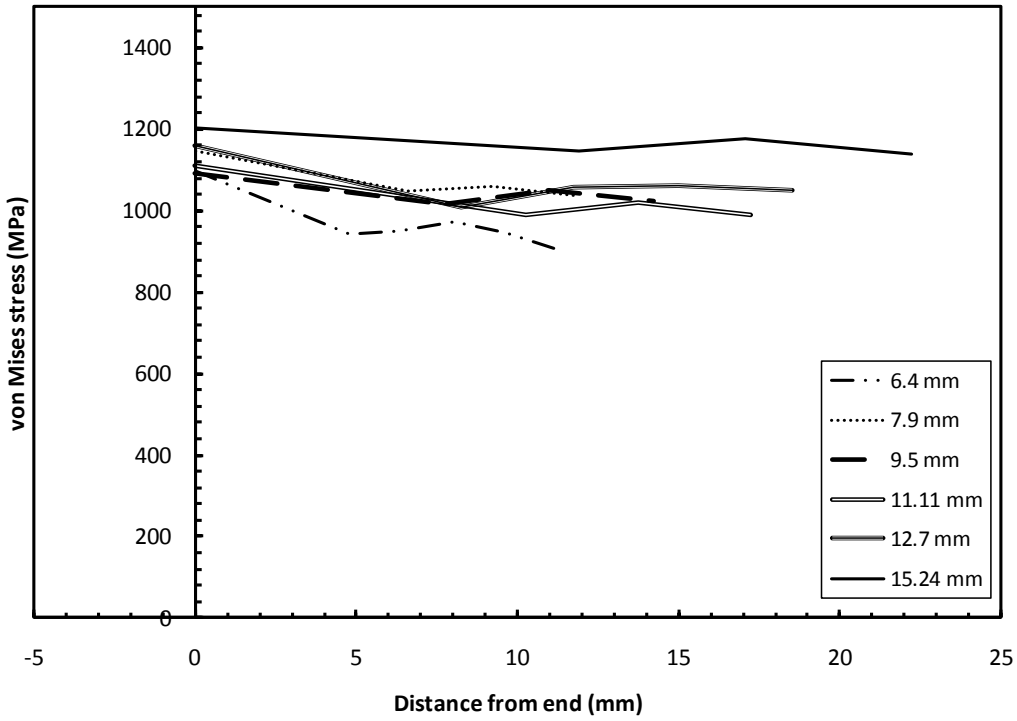

Figure B-7: Variation of von Mises stress along the length of the critical wire for 7-wire strands at 50% of the tensile strength (short model)

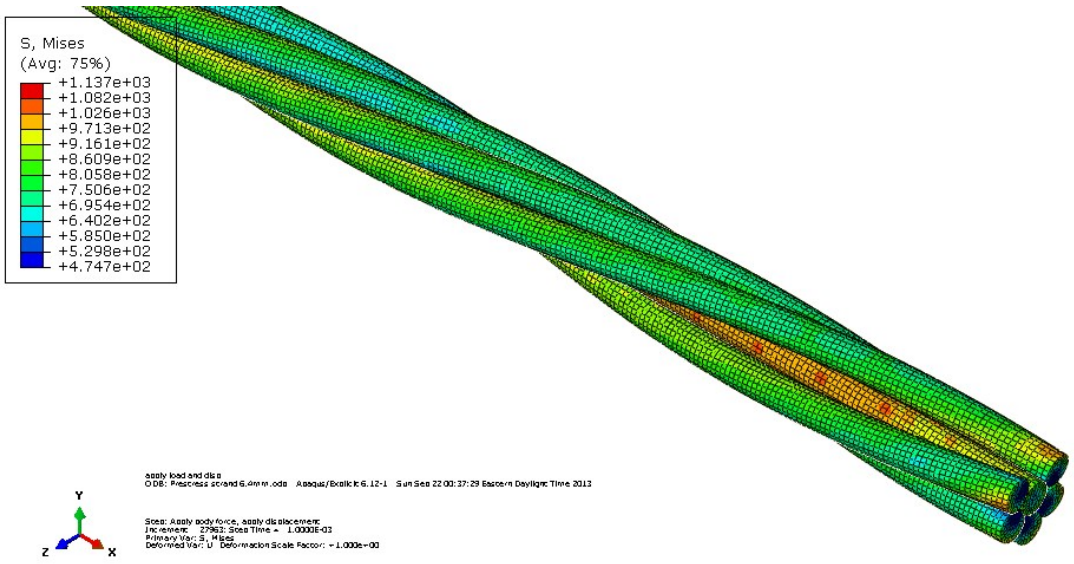

Figure B-8: von Mises stresses in 6.4 mm ASTM A416 7-wire prestressing strand subjected to tensile force of 20 kN

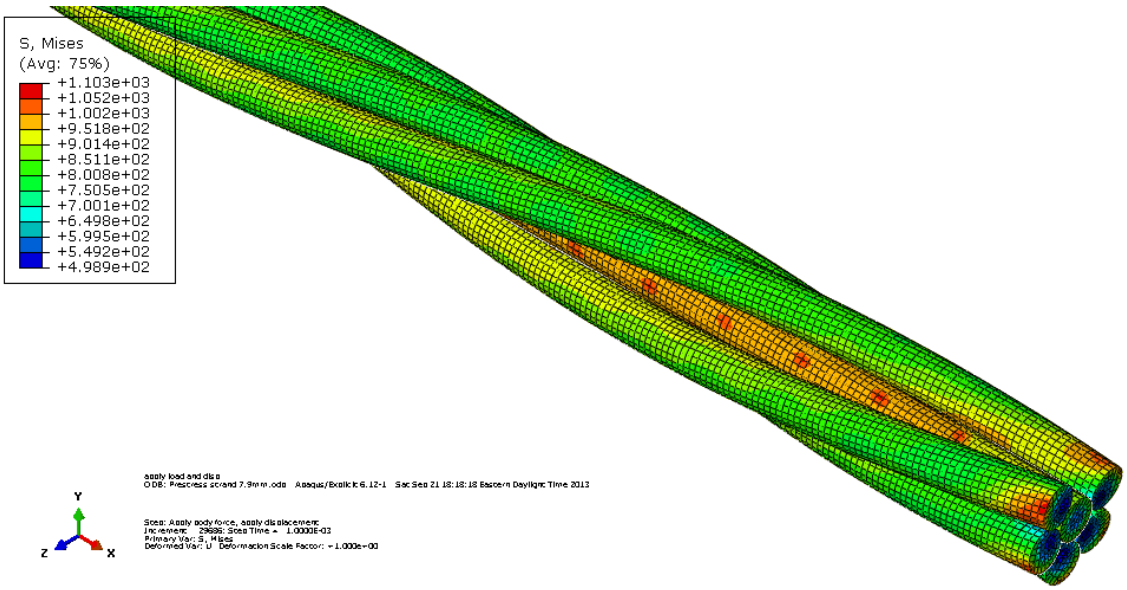

Figure B-9: von Mises stresses in 7.9 mm ASTM A416 7-wire prestressing strand subjected to a tensile force of 32.25 kN

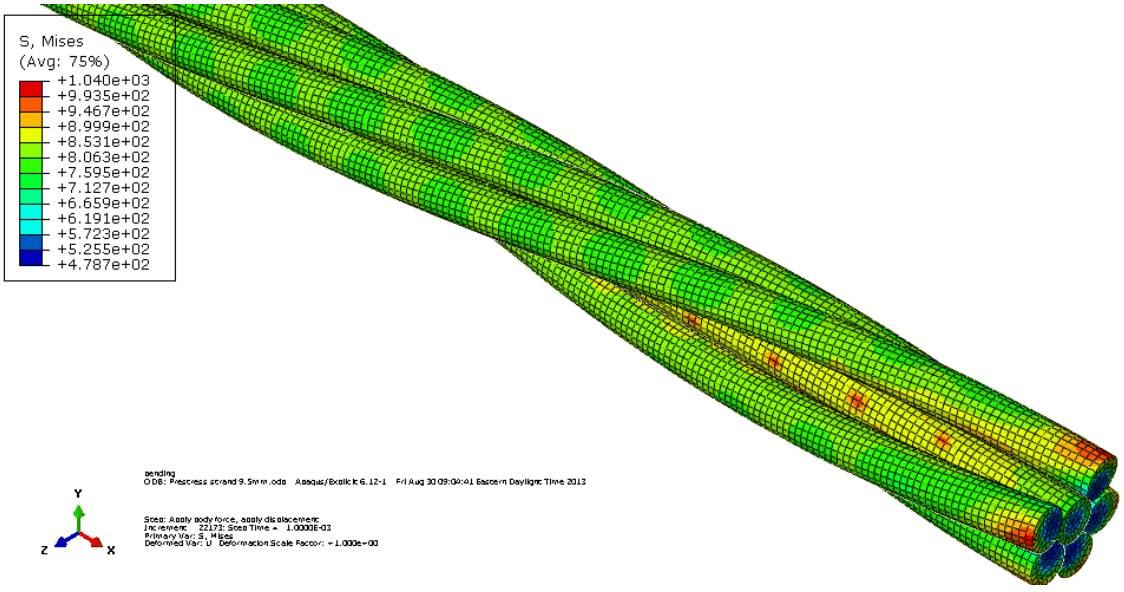

Figure B-10: von Mises stresses in 9.5 mm ASTM A416 7-wire prestressing strand subjected to a tensile force of 45 kN

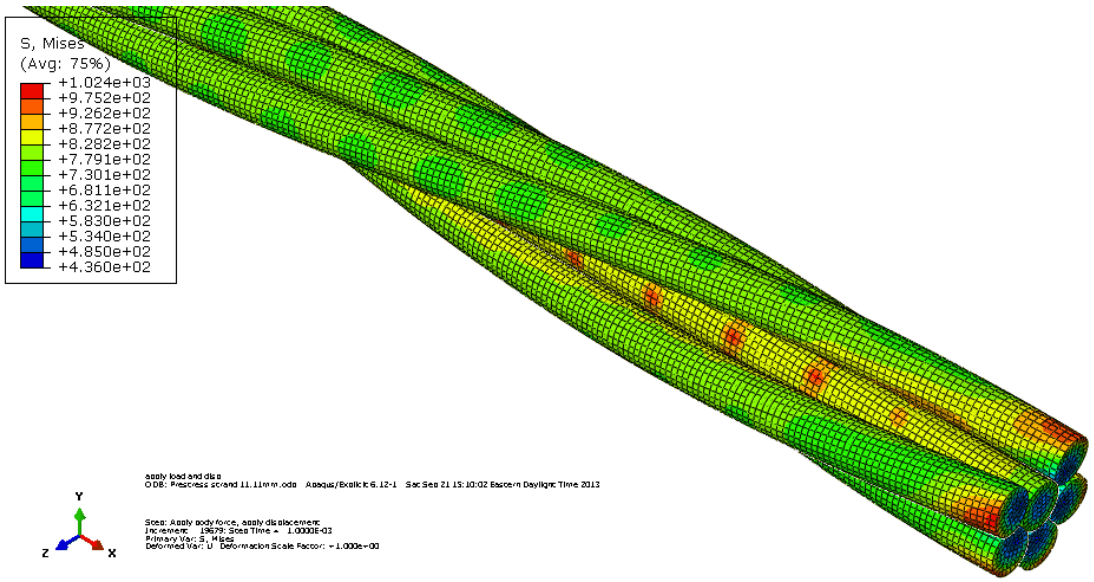

Figure B-11: von Mises stresses in 11.11 mm ASTM A416 7-wire prestressing strand subjected to a tensile force of 60 kN

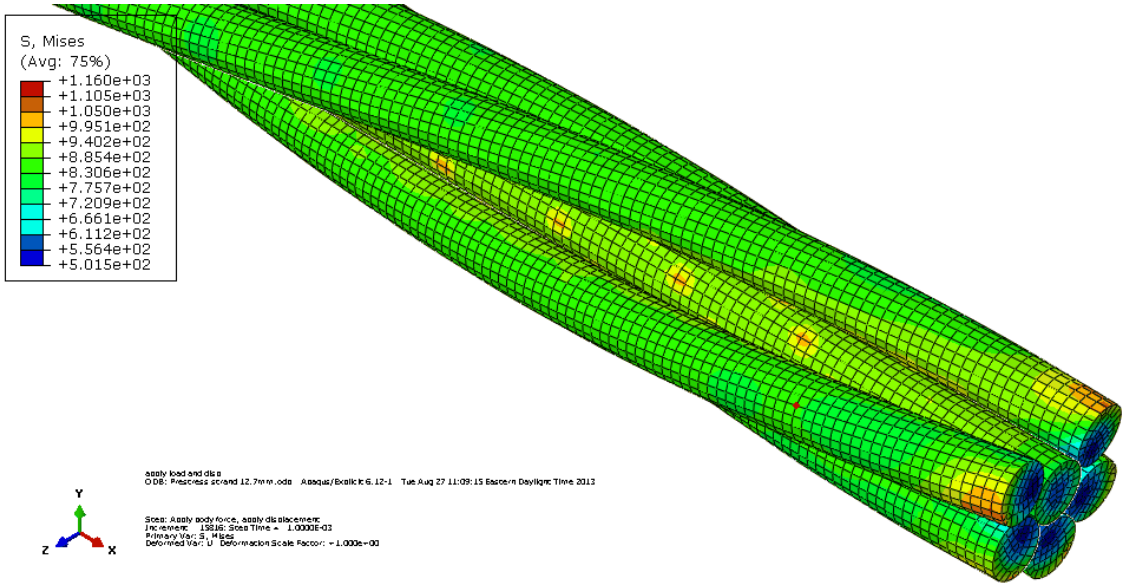

Figure B-12: von Mises stresses in 12.7 mm ASTM A416 7-wire prestressing strand subjected to a tensile force of 83.64 kN

Figure B-13: von Mises stresses in 15.24 mm ASTM A416 7-wire prestressing strand subjected to a tensile force of 128 kN

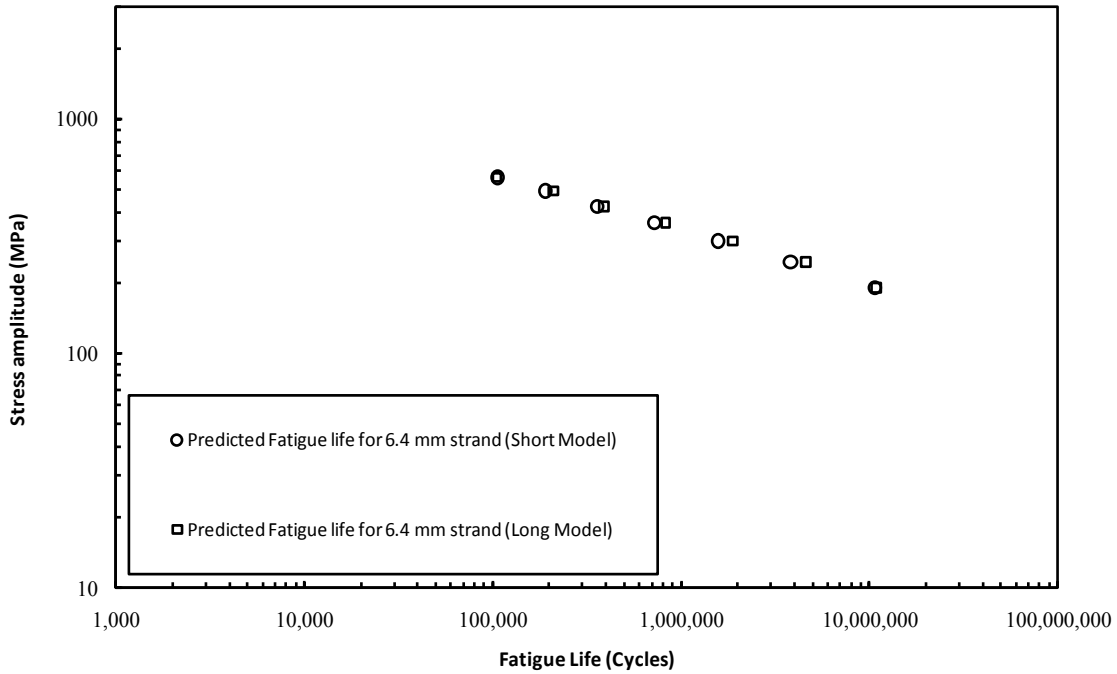

Figure B-14: Comparison of fatigue Life for long and short model 6.4 mm ASTM A416 7-wire prestressing strand

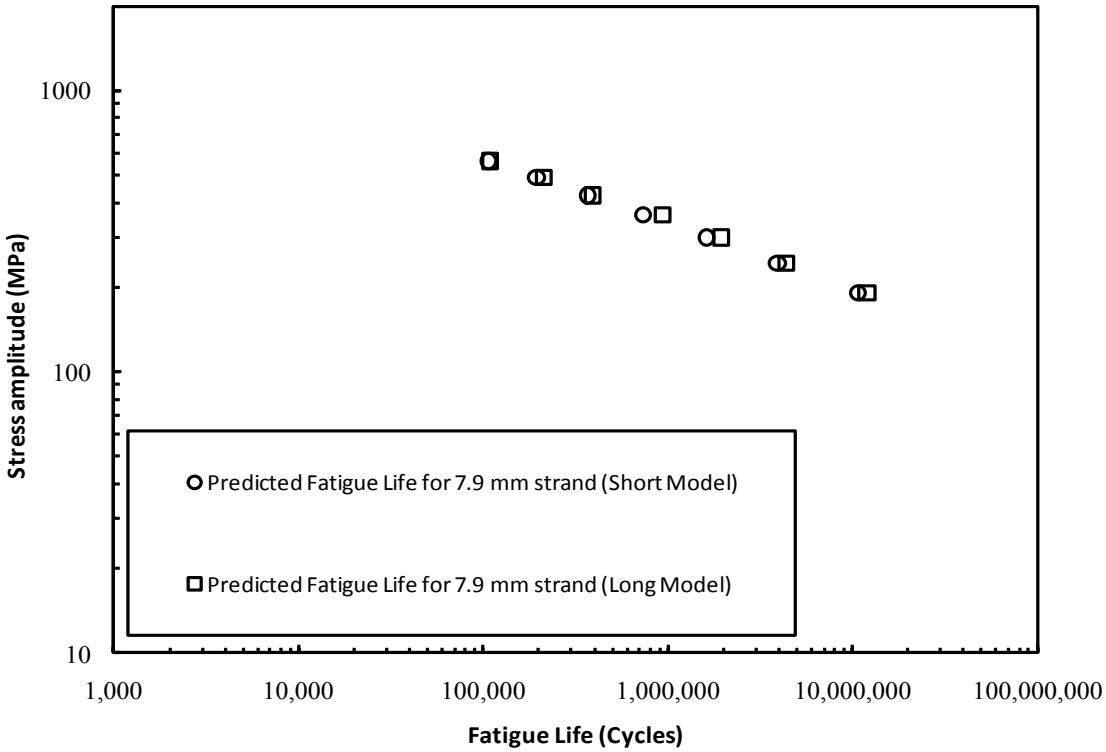

Figure B-15: Comparison of fatigue Life for long and short model 7.9 mm ASTM A416 7-wire prestressing strand

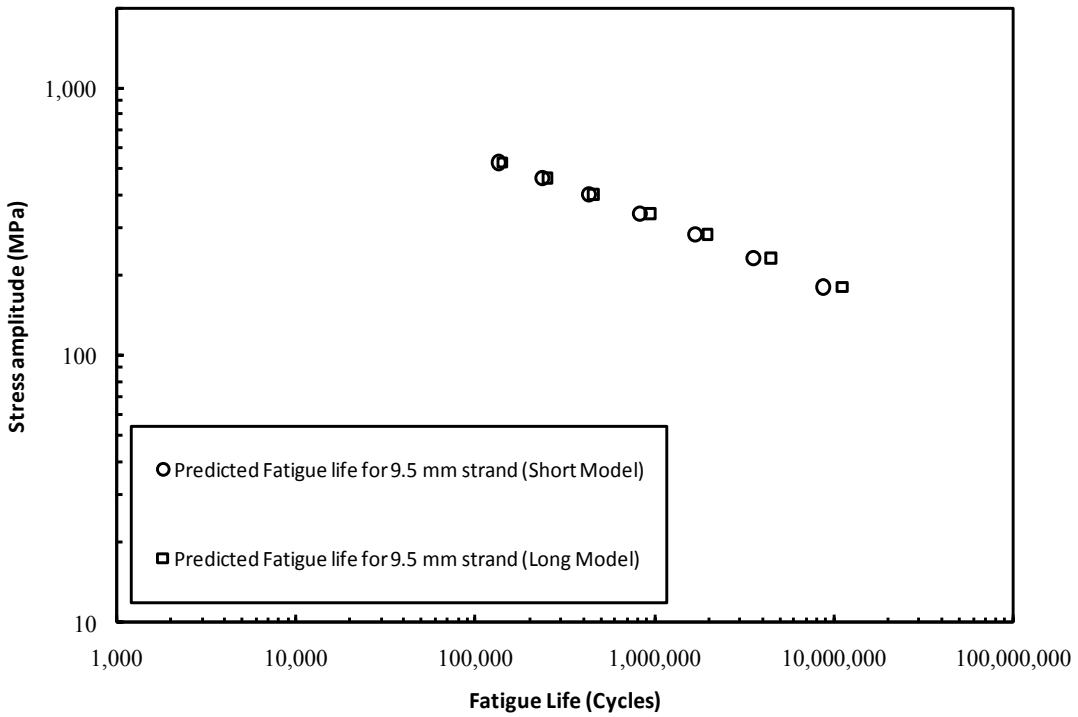

Figure B-16: Comparison of fatigue Life for long and short model 9.5 mm ASTM A416 7-wire prestressing strand

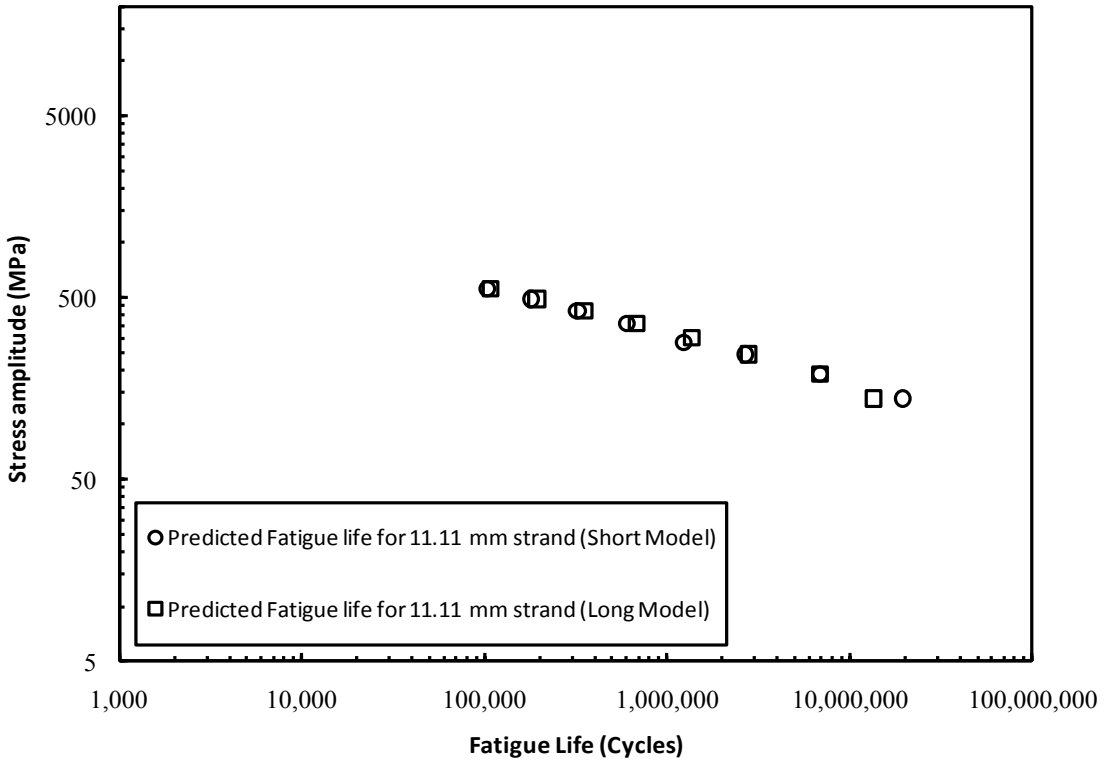

Figure B-17: Comparison of fatigue Life for long and short model 11.11 mm ASTM A416 7-wire prestressing strand

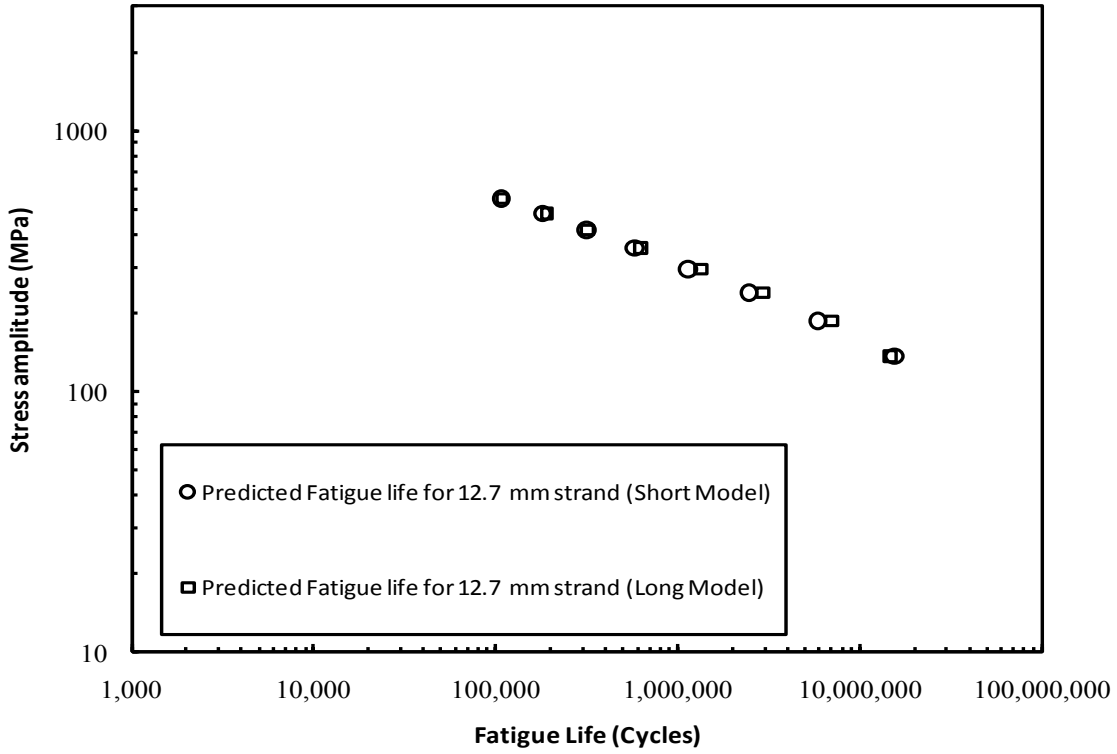

Figure B-18: Comparison of fatigue Life for long and short model 12.7 mm ASTM A416 7-wire prestressing strand

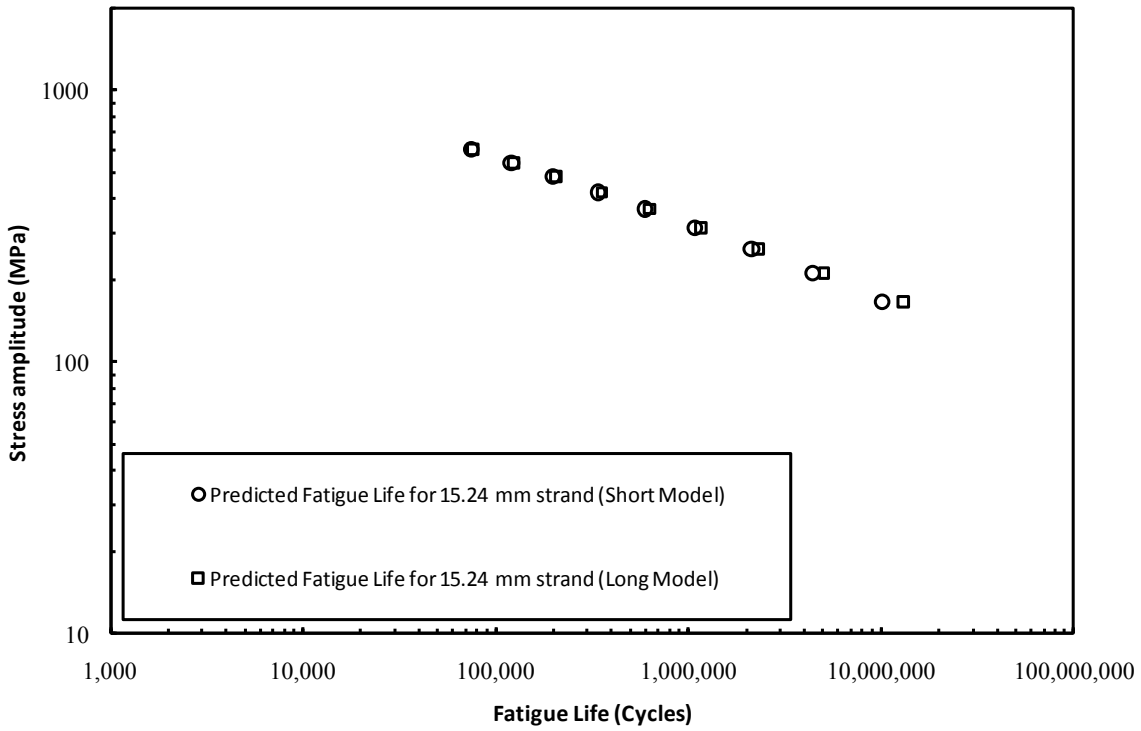

Figure B-19: Comparison of fatigue Life for long and short model 15.24 mm ASTM A416 7-wire prestressing strand

Appendix C

STATISTICAL ANALYSIS OF FATIGUE TEST RESULTS

STATISTICAL ANALYSIS OF FATIGUE TEST RESULTS

The regression analyses conducted on the test results reported by Thorpe *et al*. (1985) is provided in this appendix. Table C-1 shows the results, which reveals that 11 data points were used for the regression. The mean stress for the fatigue test was taken at 50% of the ultimate tensile strength (UTS=1840 MPa). The data obtained from their S-N plot had the following mean regression fatigue life:

$$LogN = 56.88 - 18.5LogS_N \tag{C-1}$$

The standard error of the estimate for the test data is 0.36. For all the test data by various researchers fatigue run-off were not presented in this Appendix.

The only test on 19-wire strands bent over a sheave was that reported by Knapp (2004), where the 19-wire test data (obtained by a digitization of the plot from Knapp (2004)) is presented in Table C-2. These points were obtained by digitizing. The mean regression relationship for the test results is:

$$LogN = 12.82 - 2.85LogS_a \tag{C-2}$$

The standard error for the test data is 0.051.

The test results reported by Cullimore (1972) on 15.24 mm strands under tension are shown in Table C-3 and had the following mean regression fatigue life:

$$LogN = 14.85 - 3.60LogS_{eq} \tag{C-3}$$

The standard error for the test data is 0.36.

The test results of Muller and Zeller (1975) on 15.24 mm strands in tension are shown in Table C-4 and had the following mean fatigue S-N curve:

$$LogN = 16.91 - 4.48LogS_{eq} \tag{C-4}$$

The standard error for the test data is 0.21.

The test results of Muller and Zeller (1975) on 12.7 mm (Grade 250) strands in tension are shown in Table C-5 and had the following mean fatigue S-N curve:

$$LogN = 13.61 - 3.28 LogS_{eq} \quad \text{(C-5)}$$

The standard error for the test data is 0.25.

The 12.7 mm Grade 270 strand results, tested in tension by Heller (2003) are presented in Table C-6. The mean regression relationship for the experimental results is:

$$LogN = 15.0 - 3.64 LogS_{eq} \quad \text{(C-6)}$$

The standard error for the test data is 0.18.

Warner and Hulsbos (1966) tested 11.11 mm strands in tension where the results are shown in Table C-7. The experimental results from Warner and Hulsbos (1966) had a mean regression line of:

$$LogN = 12.63 - 2.69 LogS_{eq} \quad \text{(C-7)}$$

The standard error for the test data is 0.23.

Although Paulson *et al*. (1983) tested 11.11 mm prestressing strands in tension, shown in Table C-8, at only two stress ranges and probably insufficient to fit an S-N regression, the data did yield a mean regression indication of:

$$LogN = 9.50 - 1.58 LogS_{eq} \quad \text{(C-8)}$$

The standard error for the test data is 0.24.

Fisher and Viest (1961) performed tension fatigue tests on 9.5 mm ASTM A416 prestressing strands. The test results are shown in Table C-9.The mean regression S-N relationship for their data was:

$$LogN = 15.87 - 3.81 LogS_{eq} \quad \text{(C-9)}$$

The standard error for the test data is 0.22.

Table C-1: Results of fatigue test on single wire by Thorpe *et al*. (1985)

	S_r	**Fatigue Life**
1	690.42	74469
2	633.84	59738
3	633.73	65780
4	629.01	97940
5	641.64	117500
6	603.58	155360
7	590.81	295690
8	548.57	1930000
9	523.41	4310000
10	506.34	2030000
11	492.06	50130000

Table C-2: Results of fatigue test on 19-wire strand bent over sheave by Knapp (2004)

	S_a	**Fatigue Life**
1	423.62	200282
2	564.83	102415
3	741.33	46735
4	847.24	30285
5	953.14	24158
6	1006.10	21976
7	1059.05	13153
8	1164.95	11862
9	1270.86	9270

Table C-3: Results of fatigue test on 15.24 mm prestressing strand by Cullimore (1972)

Group	$S_{\min}$	$S_{\max}$	S_r	S_{eq}	**Fatigue Life**
501	499.18	714.3	215.12	164.15	6620000
"	499.18	714.3	"	"	4200000
502	459.19	753.6	294.41	224.58	3070000
"	459.19	753.6	"	"	2120000
"	459.19	753.6	"	"	1370000
503	438.5	774.97	336.46	256.74	1230000
"	438.5	774.97	"	"	2560000
"	438.5	774.97	"	"	4370000
"	438.5	774.97	"	"	706000
"	438.5	774.97	"	"	8020000
504	417.13	796.35	379.21	289.37	1200000
"	417.13	796.35	"	"	670000
"	417.13	796.35	"	"	814000
"	417.13	796.35	"	"	539000
"	417.13	796.35	"	"	314000
"	417.13	796.35	"	"	4990000
505	397.14	815.65	418.51	319.25	382000
"	397.14	815.65	"	"	821000
"	397.14	815.65	"	"	3160000
"	397.14	815.65	"	"	347000
"	397.14	815.65	"	"	354000
506	376.45	837.02	461.26	351.44	412000
"	376.45	837.02	"	"	1330000
"	376.45	837.02	"	"	283000
"	376.45	837.02	"	"	142000
"	376.45	837.02	"	"	429000

Table C-4: Results of fatigue test on 15.24 mm prestressing strand by Muller and Zeller (1975)

Group	$S_{\min}$	$S_{\max}$	S_r	S_{eq}	**Fatigue Life**
712	666.72	970.78	304.06	284.27	1439000
713	647.42	970.78	323.36	299.25	644000
714	608.12	970.78	362.66	328.83	317000
715	578.47	970.78	392.31	350.36	234000
716	559.17	970.78	411.62	364.03	219000
717	529.52	970.78	441.27	384.52	145000
718	500.56	970.78	470.91	403.97	170000
719	480.57	970.78	490.22	417.07	330000

Table C-5: Results of fatigue test on 12.7 mm prestressing strand by Muller and Zeller (1975), Ultimate strength of 1760 MPa

Group	$S_{\min}$	$S_{\max}$	S_r	S_{eq}	**Fatigue Life**
703	647.42	970.78	323.36	299.25	1095000
704	627.42	970.78	343.36	314.45	612000
705	617.77	970.78	353.01	321.67	443000
706	608.12	970.78	362.66	328.82	625000
707	598.47	970.78	373.01	335.90	303000
708	588.1	970.78	382.66	343.44	1293000
709	578.47	970.78	392.31	350.36	320000

Table C-6: Results of fatigue test on 12.7 mm prestressing strand by Heller (2003), Ultimate tensile strength of 1860 MPa

Strand Number	S_{m}	S_r	S_{eq}	**Fatigue Life**
A15	1054.9	330.95	382.29	181668
A16	1054.9	330.95	382.29	561414
A17	1054.9	330.95	382.29	720707
A18	1054.9	330.95	382.29	464364
A19	1034.21	448.16	504.72	137283
A20	1034.21	448.16	504.72	124005
A24	1034.21	448.16	504.72	157755
A25	1034.21	448.16	504.72	132489
A26	1034.21	551.58	621.19	88824
A27	1034.21	551.58	621.19	97706
A28	1034.21	551.58	621.19	91763
5L	1034.21	551.58	621.19	38914

Table C-7: Results of fatigue test on 11.11 mm prestressing strand by Warner and Hulsbos (1966)

Group	$S_{\min}$	$S_{\max}$	S_r	S_{eq}	**Fatigue Life**
302	729.47	1048	319.23	310.93	1246000
“	729.47	1048	319.23	310.93	1159600
“	729.47	1048	319.23	310.93	1082000
“	729.47	1048	319.23	310.93	561000
“	729.47	1048	319.23	310.93	591000
“	729.47	1048	319.23	310.93	715000
303	729.47	1093.51	364.73	364.24	287400
“	729.47	1093.51	364.73	364.24	308400
“	729.47	1093.51	364.73	364.24	344100
“	729.47	1093.51	364.73	364.24	274000
“	729.47	1093.51	364.73	364.24	573000
“	729.47	1093.51	364.73	364.24	359000
304	729.47	1185.21	455.74	480.17	175500
“	729.47	1185.21	455.74	480.17	152600
“	729.47	1185.21	455.74	480.17	168000
“	729.47	1185.21	455.74	480.17	116000
“	729.47	1185.21	455.74	480.17	126000
“	729.47	1185.21	455.74	480.17	174000
305	729.47	1276.22	546.75	608.05	90400
“	729.47	1276.22	546.75	608.05	92000
“	729.47	1276.22	546.75	608.05	105200
“	729.47	1276.22	546.75	608.05	100400
“	729.47	1276.22	546.75	608.05	71000
“	729.47	1276.22	546.75	608.05	76000
306	729.47	1367.23	637.77	750.99	36500
“	729.47	1367.23	637.77	750.99	54000

Table C-7: Results of fatigue test on 11.11 mm prestressing strand by Warner and Hulsbos (1966) (continued)

Group	$S_{\min}$	$S_{\max}$	S_r	S_{eq}	**Fatigue Life**
307	729.47	1458.24	729.47	911.78	37800
308	1093.51	1276.22	182.02	261.25	3306000
309	1093.51	1312.76	218.56	322.75	652800
“	1093.51	1312.76	218.56	322.75	1873500
311	1093.51	1367.23	273.72	421.48	425500
“	1093.51	1367.23	273.72	421.48	304800
“	1093.51	1367.23	273.72	421.48	777000
“	1093.51	1367.23	273.72	421.48	863000
“	1093.51	1367.23	273.72	421.48	768500
“	1093.51	1367.23	273.72	421.48	300600
	1093.51	1367.23	273.72	421.48	1500000
312	1093.51	1458.24	364.73	608.41	234400
“	1093.51	1458.24	364.73	608.41	211000
“	1093.51	1458.24	364.73	608.41	160000
“	1093.51	1458.24	364.73	608.41	170600
“	1093.51	1458.24	364.73	608.41	121000
“	1093.51	1458.24	364.73	608.41	159000
“	1093.51	1458.24	364.73	608.41	222000
“	1093.51	1458.24	364.73	608.41	95500
“	1093.51	1458.24	364.73	608.41	155000
“	1093.51	1458.24	364.73	608.41	235800
“	1093.51	1458.24	364.73	608.41	271800
“	1093.51	1458.24	364.73	608.41	191300
“	1093.51	1458.24	364.73	608.41	176000
“	1093.51	1458.24	364.73	608.41	162400
“	1093.51	1458.24	364.73	608.41	208400

Table C-7: Results of fatigue test on 11.11 mm prestressing strand by Warner and Hulsbos (1966) (continued)

Group	$S_{\min}$	$S_{\max}$	S_r	S_{eq}	**Fatigue Life**
312	1093.51	1458.24	364.73	608.41	214500
“	1093.51	1458.24	364.73	608.41	147600
“	1093.51	1458.24	364.73	608.41	40900
“	1093.51	1458.24	364.73	608.41	164500
“	1093.51	1458.24	364.73	608.41	220600
313	1093.51	1549.25	455.74	829.33	103000
“	1093.51	1549.25	455.74	829.33	70000
“	1093.51	1549.25	455.74	829.33	88300
“	1093.51	1549.25	455.74	829.33	73000
“	1093.51	1549.25	455.74	829.33	88500
“	1093.51	1549.25	455.74	829.33	68600

Table C-8: Results of fatigue test on 11.11 mm prestressing strand by Paulson *et al.* (1983)

Sample	$S_{\min}$	$S_{\max}$	S_r	S_{eq}	**Fatigue Life**
A	1116.95	1582.35	465.40	897.60	45800
	1116.95	1582.35	465.40	897.60	65200
	1116.95	1582.35	465.40	897.60	58300
	1116.95	1582.35	465.40	897.60	72900
	558.48	884.60	326.12	269.97	725000
	558.48	884.60	326.12	269.97	190400
	558.48	884.60	326.12	269.97	653000
B	1116.95	1582.35	465.40	897.60	78200
	1116.95	1582.35	465.40	897.60	120000
	1116.95	1582.35	465.40	897.60	78600
	558.48	884.60	326.12	269.97	284000
	558.48	884.60	326.12	269.97	607000
	558.48	884.60	326.12	269.97	908000
C	1116.95	1582.35	465.40	897.60	61600
	558.48	884.60	326.12	269.97	351000
	558.48	884.60	326.12	269.97	270000
	558.48	884.60	326.12	269.97	734000
D	558.48	884.60	326.12	269.97	167800
	558.48	884.60	326.12	269.97	163700
E	1116.95	1582.35	465.40	897.60	44100
	558.48	884.60	326.12	269.97	591000
	558.48	884.60	326.12	269.97	254000
	558.48	884.60	326.12	269.97	342000
F	1116.95	1582.35	465.40	897.60	41100
	1116.95	1582.35	465.40	897.60	53400
	1116.95	1582.35	465.40	897.60	76600
	1116.95	1582.35	465.40	897.60	69900
	558.48	884.60	326.12	269.97	270000
	558.48	884.60	326.12	269.97	956000
	558.48	884.60	326.12	269.97	199100

Table C-8: Results of fatigue test on 11.11 mm prestressing strand by Paulson *et al.* (1983) (Continued)

Group	$S_{\min}$	$S_{\max}$	S_r	S_{eq}	**Fatigue Life**
G	1116.95	1582.35	465.40	897.60	67700
	1116.95	1582.35	465.40	897.60	103900
	1116.95	1582.35	465.40	897.60	88100
	558.48	884.60	326.12	269.97	792000
	558.48	884.60	326.12	269.97	434000
	558.48	884.60	326.12	269.97	272000
	558.48	884.60	326.12	269.97	821000
H	1116.95	1582.35	465.40	897.60	117800
	1116.95	1582.35	465.40	897.60	74800
	1116.95	1582.35	465.40	897.60	99900
	558.48	884.60	326.12	269.97	1500000
	558.48	884.60	326.12	269.97	593000
	558.48	884.60	326.12	269.97	468000
J	1016.98	1482.37	465.40	740.79	91600
	1016.98	1482.37	465.40	740.79	88600
	1016.98	1482.37	465.40	740.79	92100
	504.70	830.82	326.12	257.39	2626900

Table C-9: Results of fatigue test on 9.5 mm prestressing strand by Fisher and Viest. (1961)

Group	$S_{\min}$	$S_{\max}$	S_r	S_{eq}	**Fatigue Life**
251	932.17	1265.88	333.71	406.57	1236000
	932.17	1265.88	333.71	406.57	909200
	932.17	1265.88	333.71	406.57	579000
252	932.17	1360.34	428.17	555.98	560700
	932.17	1360.34	428.17	555.98	152700
	932.17	1360.34	428.17	555.98	174000
253	932.17	1454.10	521.93	725.09	68100
	932.17	1454.10	521.93	725.09	48700
	932.17	1454.10	521.93	725.09	38200
254	1120.40	1360.34	239.94	358.58	1351400
255	1120.40	1454.10	333.71	539.24	512800
	1120.40	1454.10	333.71	539.24	422000
	1120.40	1454.10	333.71	539.24	199100
256	1120.40	1548.56	428.17	753.60	213400
	1120.40	1548.56	428.17	753.60	90600
	1120.40	1548.56	428.17	753.60	159000

Appendix D

STATISTICAL ANALYSIS OF PREDICTED FATIGUE RESULTS

STATISTICAL ANALYSIS OF FATIGUE TEST RESULTS

In this appendix the regression analysis for strands and wire ropes subjected to tension and bending over sheaves will be presented. Tables D-1 through D-6 presents the regression analyses for the fatigue life of strands and wire ropes in tension using the stress correction factor; calculated from using the maximum internal axial stress. Tables D-7 through D-12 show the regression analysis for strands and wire ropes in tension, obtained using the nominal stress correction factor. Tables D-13 through D-15 show the regression results for the fatigue of 7 and 19-wire strands bent over sheaves.

Table D-1: Regression analysis for 7-wire strands fatigue life in tension

(a) Regression statistics

REGRESSION STATISTICS	
Multiple R	0.996
R^2	0.992
Adjusted R^2	0.991
Standard error	0.065
Number of observations	54

(b) ANOVA-1

	df	SS	MS	F	Significance F
Regression	4	25.75	6.44	1507	1.29E-50
Residual	49	0.21	0.0043		
Total	53	25.96			

(c) ANOVA-2

	Coefficients (a_i)	Standard error	t Stat	P-value
Intercept	10.14	1.48	6.85	1.15E-08
$\log 2S_a/d^2$	-0.99	0.72	-1.38	0.18
S_{lower}/d^2	0.012	0.0033	3.58	0.00078
$\left(S_{lower}/d^2\right)^2$	1.32E-05	4.22E-06	3.12	0.0030
$\log d$	0.107	0.109	0.98	0.333

Table D-2: Regression analysis for 19-wire strands fatigue life in tension

(a) Regression statistics

REGRESSION STATISTICS	
Multiple R	0.978
R^2	0.956
Adjusted R^2	0.912
Standard error	0.18
Number of observations	9

(b) ANOVA-1

	df	SS	MS	F	Significance F
Regression	4	2.82	0.705	21.84	0.00558
Residual	4	0.129	0.032		
Total	8	2.95			

(c) ANOVA-2

	Coefficients (a_i)	Standard error	t Stat	P-value
Intercept	-27.32	13.88	-1.97	0.12
$\log 2S_a/d^2$	17.50	8.30	2.11	0.103
S_{lower}/d^2	0.181	0.077	2.36	0.078
$\left(S_{lower}/d^2\right)^2$	0.00044	0.00019	2.31	0.082
$\log d$	5.20	0.93	5.58	0.0051

Table D-3: Regression analysis for 7 and 19-wire strands fatigue life in tension

(a) Regression statistics

REGRESSION STATISTICS	
Multiple R	0.977
R^2	0.955
Adjusted R^2	0.951
Standard error	0.153
Number of observations	63

(b) ANOVA-1

	df	SS	MS	F	Significance F
Regression	5	28.23	5.65	239	6.68E-37
Residual	57	1.347	0.024		
Total	62	29.57			

(c) ANOVA-2

	Coefficients (a_i)	Standard error	t Stat	P-value
Intercept	3.58	1.91	1.88	0.066
$\log 2S_a/d^2$	2.73	0.95	2.88	0.0057
S_{lower}/d^2	0.029	0.0050	5.78	3.24E-07
$\left(S_{lower}/d^2\right)^2$	3.37E-05	7.12E-06	4.74	1.46E-05
$\log d$	0.804	0.186	4.32	6.28E-05
$\log z$	-1.62	0.181	-8.91	2.19E-12

Table D-4: Regression analysis for 7, 19, 91 and 92-wire strands fatigue life in tension

(a) Regression statistics

REGRESSION STATISTICS	
Multiple R	0.970
R^2	0.94
Adjusted R^2	0.931
Standard error	0.176
Number of observations	74

(b) ANOVA-1

	df	SS	MS	F	Significance F
Regression	5	30.52	6.10	196.64	5.29E-39
Residual	68	2.11	0.031		
Total	73	32.63			

(c) ANOVA-2

	Coefficients (a_i)	Standard error	t Stat	P-value
Intercept	7.42	0.96	7.73	6.83E-11
$\log 2S_a/d^2$	0.54	0.51	1.07	0.289
S_{lower}/d^2	0.017	0.0034	4.93	5.67E-06
$\left(S_{lower}/d^2\right)^2$	1.78E-05	5.74E-06	3.10	0.00278
$\log d$	0.52	0.189	2.75	0.00755
$\log z$	-1.05	0.118	-8.95	4.18E-13

Table D-5: Regression analysis for IWRC fatigue life in tension

(a) Regression statistics

REGRESSION STATISTICS	
Multiple R	0.9994
R^2	0.9989
Adjusted R^2	0.9984
Standard error	0.025
Number of observations	15

(b) ANOVA-1

	df	SS	MS	F	Significance F
Regression	4	5.785	1.446	2237.81	1.04E-14
Residual	10	0.0065	0.000646		
Total	14	5.792			

(c) ANOVA-2

	Coefficients (a_i)	Standard error	t Stat	P-value
Intercept	11.80	0.51	23.15	5.11E-10
$\log 2S_a/d^2$	-2.65	0.316	-8.38	7.79E-06
S_{lower}/d^2	-0.00209	0.0032	-0.655	0.53
$\left(S_{lower}/d^2\right)^2$	-1.1E-06	7.88E-06	-0.14	0.89
$\log d$	-0.112	0.0244	-4.60	0.00098

Table D-6: Regression analysis for 6×19 Seale wire rope fatigue life in tension

(a) Regression statistics

REGRESSION STATISTICS	
Multiple R	0.9998
R^2	0.9997
Adjusted R^2	0.9996
Standard error	0.0151
Number of observations	15

(b) ANOVA-1

	df	SS	MS	F	Significance F
Regression	4	7.60	1.90	8361.19	1.43E-17
Residual	10	0.0023	0.00023		
Total	14	7.60			

(c) ANOVA-2

	Coefficients (a_i)	Standard error	t Stat	P-value
Intercept	13.64	0.314	43.44	1.0E-12
$\log 2S_a / d^2$	-3.60	0.197	-18.30	5.11E-09
S_{lower} / d^2	-0.0076	0.0019	-4.02	0.0025
$\left(S_{lower} / d^2\right)^2$	-1.3E-05	4.37E-06	-2.87	0.017
$\log d$	-0.121	0.0292	-4.16	0.0020

Table D-7: Regression analysis for 7-wire strands fatigue life in tension

(a) Regression statistics

REGRESSION STATISTICS	
Multiple R	0.997
R^2	0.994
Adjusted R^2	0.994
Standard error	0.055
Number of observations	54

(b) ANOVA-1

	df	SS	MS	F	Significance F
Regression	4	26.32	6.58	2150.51	2.27E-54
Residual	49	0.15	0.0031		
Total	53	26.47			

(c) ANOVA-2

	Coefficients (a_i)	Standard error	t Stat	P-value
Intercept	10.00	1.25	7.97	2.12E-10
$\log 2S_a/d^2$	-0.834	0.61	-1.37	0.176
S_{lower}/d^2	0.013	0.0028	4.62	2.78E-05
$\left(S_{lower}/d^2\right)^2$	1.47E-05	3.57E-06	4.13	0.00014
$\log d$	0.01	0.0927	0.11	0.915

Table D-8: Regression analysis for 19-wire strands fatigue life in tension

(a) Regression statistics

REGRESSION STATISTICS	
Multiple R	0.994
R^2	0.989
Adjusted R^2	0.977
Standard error	0.066
Number of observations	9

(b) ANOVA-1

	df	SS	MS	F	Significance F
Regression	4	1.53	0.383	86.93	0.000385
Residual	4	0.018	0.0044		
Total	8	1.551			

(c) ANOVA-2

	Coefficients (a_i)	Standard error	t Stat	P-value
Intercept	-6.35	5.13	-1.23	0.28
$\log 2S_a/d^2$	5.75	3.07	1.87	0.13
S_{lower}/d^2	0.069	0.028	2.42	0.072
$\left(S_{lower}/d^2\right)^2$	0.00016	7.01E-05	2.34	0.080
$\log d$	3.32	0.344	9.64	0.00065

Table D-9: Regression analysis for 7 and 19-wire strands fatigue life in tension

(a) Regression statistics

REGRESSION STATISTICS	
Multiple R	0.988
R^2	0.976
Adjusted R^2	0.974
Standard error	0.107
Number of observations	63

(b) ANOVA-1

	df	SS	MS	F	Significance F
Regression	5	26.95	5.37	470.16	5.47E-45
Residual	57	0.653	0.0115		
Total	62	27.60			

(c) ANOVA-2

	Coefficients (a_i)	Standard error	t Stat	P-value
Intercept	4.21	1.331	3.16	9.41E-06
$\log 2S_a/d^2$	2.58	0.662	3.90	0.0644
S_{lower}/d^2	0.027	0.00345	7.88	1.44E-07
$\left(S_{lower}/d^2\right)^2$	3.12E-05	4.96E-06	6.30	3.3E-05
$\log d$	0.68	0.130	5.25	3.23E-07
$\log z$	-1.941	0.126	-15.37	4.1E-16

Table D-10: Regression analysis for 7, 19, 91 and 92-wire strands fatigue life in tension

(a) Regression statistics

REGRESSION STATISTICS	
Multiple R	0.971
R^2	0.943
Adjusted R^2	0.939
Standard error	0.157
Number of observations	74

(b) ANOVA-1

	df	SS	MS	F	Significance F
Regression	5	27.81	5.56	225.12	7.11E-41
Residual	68	1.68	0.025		
Total	73	29.49			

(c) ANOVA-2

	Coefficients (a_i)	Standard error	t Stat	P-value
Intercept	5.64	0.857	6.59	7.82E-09
$\log 2S_a/d^2$	1.48	0.452	3.25	0.00175
S_{lower}/d^2	0.020	0.00305	6.39	1.76E-08
$\left(S_{lower}/d^2\right)^2$	1.96E-05	5.12E-06	3.83	0.00028
$\log d$	0.500	0.168	2.97	0.00415
$\log z$	-1.256	0.105	-11.96	2.19E-18

Table D-11: Regression analysis for IWRC fatigue life in tension

(a) Regression statistics

REGRESSION STATISTICS	
Multiple R	0.9998
R^2	0.9997
Adjusted R^2	0.9996
Standard error	0.0085
Number of observations	15

(b) ANOVA-1

	df	SS	MS	F	Significance F
Regression	4	2.03	0.509	7130.29	3.17E-17
Residual	10	0.000713	7.13E-05		
Total	14	2.035			

(c) ANOVA-2

	Coefficients (a_i)	Standard error	t Stat	P-value
Intercept	8.38	0.169	49.49	2.74E-13
$\log 2S_a/d^2$	-1.23	0.105	-11.69	3.73E-07
S_{lower}/d^2	0.000856	0.00106	0.81	0.437
$\left(S_{lower}/d^2\right)^2$	1.23E-06	2.62E-06	0..47	0.65
$\log d$	-0.0364	0.00812	-4.48	0.0012

Table D-12: Regression analysis for 6×19 Seale wire rope fatigue life in tension

(a) Regression statistics

REGRESSION STATISTICS	
Multiple R	1.0000
R^2	0.9999
Adjusted R^2	0.9999
Standard error	0.0045
Number of observations	15

(b) ANOVA-1

	df	SS	MS	F	Significance F
Regression	4	2.43	0.61	29839.48	2.48E-20
Residual	10	0.0002	2.04E-05		
Total	14	2.43			

(c) ANOVA-2

	Coefficients (a_i)	Standard error	t Stat	P-value
Intercept	8.80	0.094	93.58	4.75E-16
$\log 2S_a/d^2$	-1.42	0.059	-24.15	3.38E-10
S_{lower}/d^2	-2.5E-06	0.00057	-0.00434	0.997
$\left(S_{lower}/d^2\right)^2$	-7.8E-07	1.31E-06	-0.596	0.564
$\log d$	-0.045	0.0088	-5.18	0.000411

Table D-13: Regression analysis for 7-wire strands fatigue life in BOS

(a) Regression statistics

REGRESSION STATISTICS	
Multiple R	0.963
R^2	0.926
Adjusted R^2	0.917
Standard error	0.128
Number of observations	47

(b) ANOVA-1

	df	SS	MS	F	Significance F
Regression	5	8.48	1.70	103.23	4.03E-22
Residual	41	0.67	0.016		
Total	46	9.15			

(c) ANOVA-2

	Coefficients (b_i)	Standard error	t Stat	P-value
Intercept	13.31	6.38	2.09	0.043
$\log\left(\frac{S}{d^2}\right)-0.4\log\left(\frac{R_0}{1770}\right)$	-0.74	0.39	-1.89	0.066
$\log\left(\frac{D}{d}\right)\left[\log\left(\frac{S}{d^2}\right)-0.4\log\left(\frac{R_0}{1770}\right)\right]$	-0.28	0.33	-0.83	0.41
$\log\left(\frac{D}{d}\right)$	-0.57	1.68	-0.34	0.73
$\log d$	0.087	0.19	0.45	0.65
$\frac{1}{1.0+\log\left(\frac{l}{d}\right)}$	-11.80	10.82	-1.09	0.28

Table D-14: Regression analysis for 19-wire strands fatigue life in BOS

(a) Regression statistics

REGRESSION STATISTICS	
Multiple R	0.977
R^2	0.955
Adjusted R^2	0.945
Standard error	0.101
Number of observations	28

(b) ANOVA-1

	df	SS	MS	F	Significance F
Regression	5	4.80	0.96	93.49	4.58E-14
Residual	22	0.226	0.010		
Total	27	5.03			

(c) ANOVA-2

	Coefficients (b_i)	Standard error	t Stat	P-value
Intercept	18.11	4.65	3.89	0.0008
$\log\left(\frac{S}{d^2}\right)-0.4\log\left(\frac{R_0}{1770}\right)$	-1.36	0.44	-3.12	0.005
$\log\left(\frac{D}{d}\right)\left[\log\left(\frac{S}{d^2}\right)-0.4\log\left(\frac{R_0}{1770}\right)\right]$	-0.051	0.35	-0.145	0.886
$\log\left(\frac{D}{d}\right)$	-2.17	1.54	-1.404	0.174
$\log d$	-0.11	0.17	-0.65	0.052
$\frac{1}{1.0+\log\left(\frac{l}{d}\right)}$	-16.19	7.28	-2.22	0.037

Table D-15: Regression analysis for 7 and 19-wire strands fatigue life in BOS

(a) Regression statistics

REGRESSION STATISTICS	
Multiple R	0.961
R^2	0.923
Adjusted R^2	0.916
Standard error	0.131
Number of observations	75

(b) ANOVA-1

	df	SS	MS	F	Significance F
Regression	6	14.01	2.33	135.39	8.29E-36
Residual	68	1.17	0.017		
Total	74	15.18			

(c) ANOVA-2

	Coefficients (b_i)	Standard error	t Stat	P-value
Intercept	13.29	4.07	3.27	0.0017
$\log\left(\frac{S}{d^2}\right)-0.4\log\left(\frac{R_0}{1770}\right)$	-0.37	0.27	-1.36	0.18
$\log\left(\frac{D}{d}\right)\left[\log\left(\frac{S}{d^2}\right)-0.4\log\left(\frac{R_0}{1770}\right)\right]$	-0.67	0.22	-2.99	0.0039
$\log\left(\frac{D}{d}\right)$	-0.023	1.12	-0.02	0.98
$\log d$	0.16	0.13	1.20	0.23
$\frac{1}{1.0+\log\left(\frac{l}{d}\right)}$	-13.42	6.89	-1.95	0.055
$\log z$	0.23	0.16	1.48	0.14